PL-TR-91-2117(I)

AD-A256 692

RMS Lg as a Yield Estimator in Eurasia

Hans Israelsson
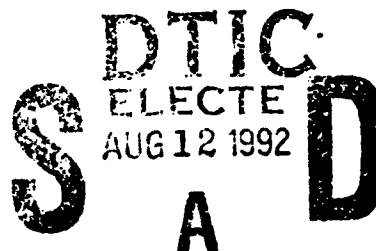
DTIC
ELECTE
AUG 12 1992
S
A
D

Science Applications International Corporation
Center for Seismic Studies
1300 N. 17th Street, Suite 1450
Arlington, VA 22209

April 1992

Final Report: Part I
October 1990 - March 1992

APPROVED FOR PUBLIC RELEASE; DISTRIBUTION UNLIMITED

PHILLIPS LABORATORY
AIR FORCE SYSTEMS COMMAND
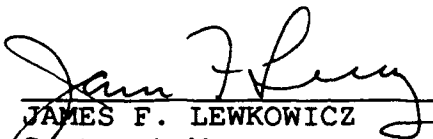HANSCOM AIR FORCE BASE, MASSACHUSETTS 01731-5000

92-22625

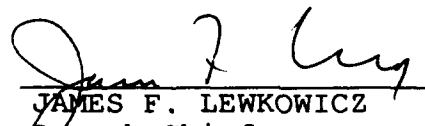**92** 8 10 107

The views and conclusions contained in this document are those of the authors and should not be interpreted as representing the official policies, either expressed or implied, of the Defense Advanced Research Projects Agency or the U.S. Government.

This technical report has been reviewed and is approved for publication.

JAMES F. LEWKOWICZ
Contract Manager
Solid Earth Geophysics Branch
Earth Sciences Division

JAMES F. LEWKOWICZ
Branch Chief
Solid Earth Geophysics Branch
Earth Sciences Division

DONALD H. ECKHARDT, Director
Earth Sciences Division

REPORT DOCUMENTATION PAGE

Public reporting burden for this collection of information is estimated to average 1 hour per response, including the time for reviewing instructions, searching existing data sources, gathering and maintaining the data needed, and completing and reviewing the collection of information. Send comments regarding this burden estimate or any other aspect of this collection of information, including suggestions for reducing this burden to Washington Headquarters Services, Directorate for Information Operations and Reports, 1215 Jefferson Davis Highway, Suite 1204, Arlington, VA 22202-4302, and to the Office of Management and Budget, Paperwork Reduction Project (0704-0188), Washington, DC 20503

1. AGENCY USE ONLY (Leave blank)	2. REPORT DATE April 1992	3. REPORT TYPE AND DATES COVERED Final Part I (Oct 1990–March 1992)

4. TITLE AND SUBTITLE	5. FUNDING NUMBERS
RMS Lg as a Yield Estimator in Eurasia	PE 62714E
	PR 9A10 TA DA WU BI
6. AUTHOR(S)	Contract F19628-89-C-0203
Hans Israelsson	

7. PERFORMING ORGANIZATION NAME(S) AND ADDRESS(ES)	8. PERFORMING ORGANIZATION REPORT NUMBER
Science Applications International Corporation Center for Seismic Studies 1300 N. 17th Street, Suite 1450 Arlington, VA 22209	

9. SPONSORING/MONITORING AGENCY NAME(S) AND ADDRESS(ES)	10. SPONSORING/MONITORING AGENCY REPORT NUMBER
Phillips Laboratory Hanscom AFB, MA 01731-5000 Contract Manager: James Lewkowicz/GPEH	PL-TR-92-2117 (I)

11. SUPPLEMENTARY NOTES

12a. DISTRIBUTION/AVAILABILITY STATEMENT	12b. DISTRIBUTION CODE
Approved for public release; distribution unlimited	

13. ABSTRACT (Maximum 200 words)

This report has been divided into two parts. The first part is devoted entirely to a description of, and research performed on, the hand digitized waveforms of Soviet regional data that were obtained by Dr Alan Ryall of DARPA and Sgt Mike Berry of AFTAC as part of the bilateral Nuclear Testing Talks between the US and the former USSR. Digitized by ENSCO Inc at Indian Harbour Beach, FL., the data were subsequently compiled by Dr Herron and her staff at AFTAC and are now available at the Center for Seismic Studies. The first paper of Part I is a description of the data. This is followed by two papers that analyzed the RMS Lg magnitudes at Novaya Zemlya and Semipalatinsk, respectively. The Semipalatinsk report also compares the RMS Lg measurements and the Bocharov yields as well as exploring the effects of depth on the magnitude measurement. The fourth paper combines the data from the two test sites with data from underground nuclear explosions elsewhere in the former Soviet Union in a decomposition of the RMS Lg measurement into source, path, and station terms. The last paper in Part I examines the RMS Lg measurement as a function of frequency in order to explain the variability of the mb (Lg) – yield scale among stations.

14. SUBJECT TERMS			15. NUMBER OF PAGES
RMS Lg Yield estimation Novaya Zemlya Semipalatinsk m_b (Lg)			188
			16. PRICE CODE

17. SECURITY CLASSIFICATION OF REPORT	18. SECURITY CLASSIFICATION OF THIS PAGE	19. SECURITY CLASSIFICATION OF ABSTRACT	20. LIMITATION OF ABSTRACT
Unclassified	Unclassified	Unclassified	SAR

Table of Contents

RMS Lg Magnitudes and Path Corrections for U.S.S.R. Explosions

A Spectral Decomposition of *Lg* Waves from Explosions and Scaling of RMS Magnitudes

List of Figures

Analysis Of RMS Magnitudes For Explosions At Novaya Zemlya Based On Recordings At Soviet Stations

Analysis of Historical Seismograms - RMS Lg Magnitudes, Yields, and Depths of Explosions at the Semipalatinsk Test Range

RMS Lg Magnitudes and Path Corrections for U.S.S.R. Explosions

A Spectral Decomposition of *Lg* Waves from Explosions and Scaling of RMS Magnitudes

List of Tables

Foreword

Jerry A. Carter

This is the final report of a multi-year effort by the researchers at the Center for Seismic Studies under contract # F19628-89-C-0203. The papers presented within are not a complete description of all of the work that was performed under this contract; rather, they represent the research that was performed in the last 15 months of the contract. Previous work is described in PL-TR-91-2127, *Nuclear Monitoring Research at the Center for Seismic Studies*.

The report has been divided into two parts. The first part is devoted entirely to a description of, and research performed on, the hand digitized waveforms of Soviet regional data that were obtained by Dr. Alan Ryall of DARPA and Sgt. Mike Berry of AFTAC as part of the bi-lateral Nuclear Testing Talks between the U.S. and the former U.S.S.R. Digitized by ENSCO Inc. at Indian Harbour Beach, FL., the data were subsequently compiled by Dr. Herron and her staff at AFTAC and are now available at the Center for Seismic Studies. The first paper of Part I is a description of the data. This is followed by two papers that analyze the RMS Lg magnitudes at Novaya Zemlya and Semipalatinsk, respectively. The Semipalatinsk report also compares the RMS Lg measurements and the Bocharov yields as well as exploring the effects of depth on the magnitude measurement. The fourth paper combines the data from the two test sites with data from underground nuclear explosions elsewhere in the former Soviet Union in a decomposition of the RMS Lg measurement into source, path, and station terms. The last paper in Part I examines the RMS Lg measurement as a function of frequency in order to explain the variability of the $m_b(Lg)$ - yield scale among stations.

Part II contains reports primarily focused on regional monitoring of underground nuclear explosions. A broad spectrum of issues is addressed; from improving automatic processing to an assessment of monitoring capability using certain network configurations. The first two papers examine the use of three-component seismic data for phase identification; one applies discriminant analysis to the three-component IRIS/IDA stations in the former USSR in anticipation of those stations being added to the Intelligent Monitoring System (IMS), and the other applies the same techniques to the three component stations of ARCESS and NORESS in a comparison with newly-developed neural network techniques. The third report uses travel-time information from long range refraction profiles that is independent of the IMS to derive an average travel-time curve for Fennoscandia. In addition, regional variations in the *Pn* travel times are defined and used to relocate a small

set of events. This type of regional knowledge, when incorporated into event location routines, should reduce location errors. The fourth report is the result of work performed on a Deep Seismic Sounding profile that was obtained by the USGS. A reinterpretation of this data has been made by the USGS and the results were reported at various meetings. The Centers contribution was to determine the validity of the preliminary interpretation of the data. H.Benz, J. Unger, and W. Leith, though not funded under this contract were co-authors of this report. The final two reports in Part II deal with monitoring networks. One presents the results of network simulation of the GSE Network using empirical noise calculations from the recent technical test. This research was funded primarily by the Center for Seismic Studies Contract and was co-authored by Steve Bratt and David Corely. Because the research is germane to this contract, some of the effort was funded under the research contract and we include it in this final report. The final report is a summary note on starting and improving a regional network. It summarizes and integrates the results of our research related to the way the US would proceed to monitor with an in-country regional network of three-component (3-C) stations and arrays.

Hand Digitized Waveforms of Seismic Recordings from Soviet Stations for Nuclear Explosions in the U.S.S.R.

Hans Israelsson

Abstract

A large number of analog seismic recordings from Soviet stations for underground nuclear explosions in the U.S.S.R. has become available. This note presents and reviews basic information for 476 of these recordings that have been hand digitized. The data include waveforms from 11 stations throughout the Western and Central U.S.S.R for 114 explosions at the Semipalatinsk and Novaya Zemlya test ranges and a few other sites. Four large suites of events at distinctly separate areas - Balapan NE, Balapan SW, Degelen, and Matochkin Shar - constitute almost 90% of all explosions in the data set. Three of the suites consist essentially of large magnitude events, whereas the fourth, at Degelen, includes events with a fairly large magnitude range $m_b = 4.8 - 6.0$. The waveforms were recorded almost uniformly with the same type of vertical component short period seismometer, SKM-3, although with different instrument parameters adjusted to local geology and ambient noise conditions at the stations. The waveforms appeared to have been recorded with a high degree of operational consistency despite being obtained over a long period of time, 1964-1988, and they were, for most of the stations, accompanied with comprehensive instrument calibrations. Thus, obtained over the course of more than 20 years, the instrument calibrations reflect fluctuations in seismometer characteristics that correspond to standard deviations of no more than 7% of the amplitude response in the short period frequency band, 0.5-4 Hz. Comparisons with modern high quality digital recordings from the JVE explosion suggest that the hand-digitization method, sampling the data to 20 Hz, provided satisfactory results in the frequency band from about 0.2 to about 4 Hz.

Introduction

Until the late 1980's information on Soviet underground nuclear explosions, let alone seismic recordings on Soviet soil, were not generally available to the seismological community. The dramatic changes since then have resulted in access to a wide variety of seismic data from Soviet explosions. In this note we present a data set, unique to the field of seismic verification, that became available in 1991 as a result of the bi-lateral Nuclear Testing Talks. The data include a large number of waveforms from in-country seismological stations for Soviet nuclear explosions, some with announced yields. The 476 waveforms were hand digitized from copies of traditional analog recordings obtained at 11 stations

broadly distributed throughout the Western and Central U.S.S.R from a total of 114 explosions. Primarily for explosions at the two main testing sites near Semipalatinsk and Novaya Zemlya, the data also include some waveforms from explosions at Azghir, two locations in Central Siberia, and one location near Lake Baikal.

In this note we have summarized and reviewed information on the explosions, seismological stations, and waveforms in this data set, which contains recordings obtained over the course of more than 20 years. As the characteristics of recording instruments at some stations changed during this period of time due perhaps to temporal drift in the instrumentation or to deliberate alterations by station operators, available information on instrument calibrations is also described and reviewed. All the basic data - waveforms and instrument calibrations - were collected at the Obninsk Data Center by Dr. Alan Ryall at DARPA and Sgt. Steve Berry at AFTAC. Digitized by ENSCO Inc. at Indian Harbour Beach, FL., the data were subsequently compiled by Dr. Herron and her staff at AFTAC.

Explosions

The map in Figure 1 shows the relative locations of the explosion sites (asterisks) and the seismological stations (station codes). Each explosion site - station pair for which at least one waveform was available is connected with solid lines approximating great circle paths between explosion site and station. The boundaries of the major tectonic elements of the U.S.S.R. (after Zonenschain *et al.*, 1991) are portrayed with dotted lines in Figure 1 showing that the paths traverse a diversity of tectonic structures.

Information on time, location, and body wave magnitude, $m_b(P)$, reported for the explosions by ISC, is compiled in Table 1. Precise locations and times, ostensibly based on non-seismological information, have been published by Bocharov *et al.* (1989) for some of the explosions at Semipalatinsk. Joint epicenter determinations, JED by Marshall *et al.* (1985) and by Lilwal and Marshall (1986) are also available for many of the explosions at Semipalatinsk and at Novaya Zemlya.

The epicenter estimates entered in Table 1 are limited to those of ISC as they are the only type of determination consistently applied to all the explosions, with two exceptions: on 77/10/14 at Azghir and on 84/06/28 at Matochkin Shar, the locations of which were obtained at the Center for Seismic Studies.

There are three "double" events among the Semipalatinsk explosions in Table 1, so called because each of these events consists of two explosions set off within 5 to 10 seconds at locations about 50 km apart. Although not reported as a double event by ISC or other International Seismological Services, the Novaya Zemlya event on 80/10/11 too is presumed to be a double event according to Stewart and Marshall (1988), who suggested that

2
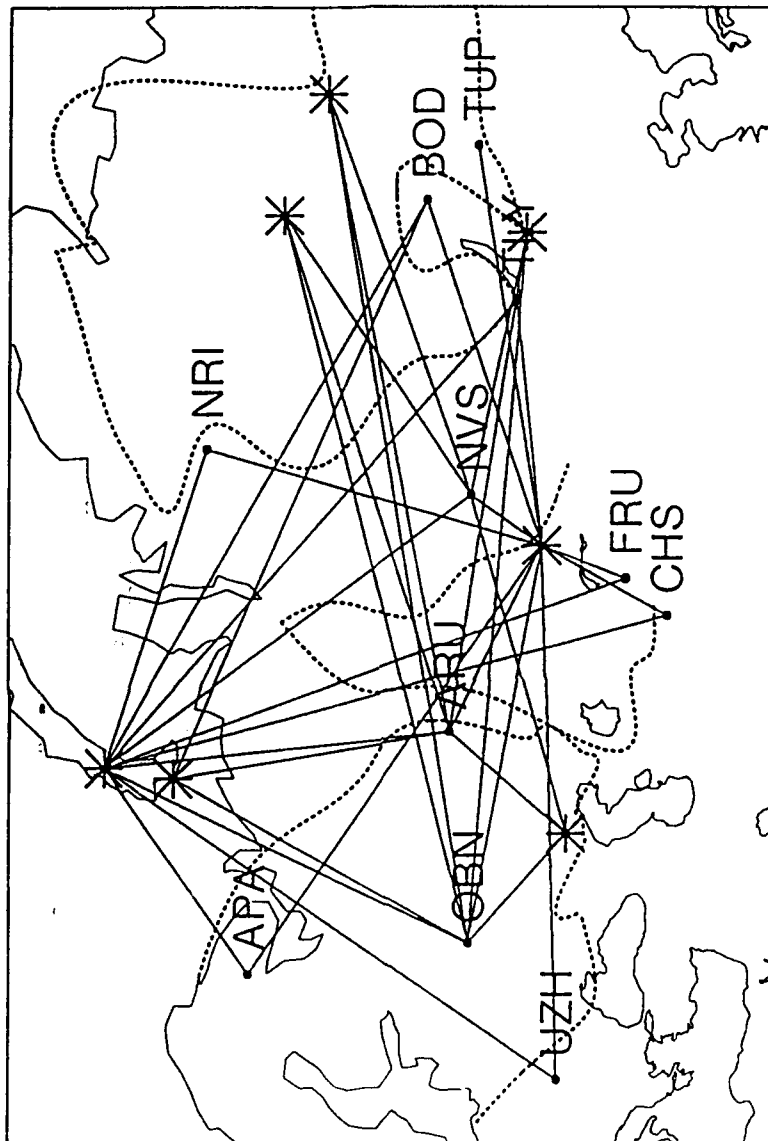
Figure 1:   Map showing pairs of explosion sites (asterisks) and stations (marked codes) for which at least one waveform is available. Such pairs are connected with straight lines. The dotted contours outline the major tectonic elements of the Western and Central U.S.S.R. (after Zonenshain, 1991).

Table 1: Explosions

Data	Time	Lat.(N)	Long.(E)	$m_b(ISC)$	Site
64/10/25	07:59:58.3	73.390	53.900	5.0	Matochkin Shar
65/11/21	04:57:58.2	49.860	78.040	5.6	Degelen
66/02/13	04:58:00.0	50.000	78.000	0.0	Degelen
66/03/20	05:49:57.8	49.720	78.070	6.0	Degelen
66/05/07	03:57:58.2	49.740	77.950	4.8	Degelen
67/09/22	05:03:57.8	50.020	77.720	5.2	Murzhik
67/10/21	04:59:58.4	73.400	54.420	5.9	Matochkin Shar
68/09/29	03:42:57.8	49.820	78.180	5.8	Degelen
68/11/07	10:02:07.0	73.500	55.000	0.0	Matochkin Shar
69/07/23	02:46:58.0	49.880	78.230	5.4	Degelen
69/11/30	03:32:57.3	49.940	78.980	6.0	Balapan SW
69/12/28	03:46:57.8	49.980	77.790	5.7	Murzhik
71/04/25	03:32:57.9	49.766	78.081	5.9	Degelen
71/06/06	04:02:57.3	49.977	77.740	5.5	Murzhik
71/06/19	04:03:57.7	49.966	77.724	5.4	Murzhik
71/10/09	06:02:57.2	49.986	77.687	5.3	Murzhik
71/10/21	06:02:57.5	50.004	77.631	5.5	Murzhik
71/12/22	06:59:56.5	47.903	48.067	6.0	Azghir
71/12/30	06:20:57.9	49.750	78.100	5.7	Degelen
72/02/10	05:02:57.6	50.024	78.942	5.4	Balapan NE
72/03/28	04:21:57.4	49.738	78.160	5.1	Degelen
72/08/16	03:16:57.5	49.774	78.132	5.0	Degelen
72/09/02	08:56:57.3	49.884	77.603	4.9	Murzhik
72/11/02	01:26:57.8	49.914	78.848	6.1	Balapan SW
72/12/10	04:27:07.6	49.966	78.946	6.0	Balapan NE

Table 1: Explosions

Data	Time	Lat.(N)	Long.(E)	$m_b(ISC)$	Site
73/07/23	01:22:57.7	49.936	78.854	6.1	Balapan NE
73/09/27	06:59:58.5	70.804	53.419	5.9	Krasino
73/12/14	07:46:57.1	50.026	79.016	5.8	Balapan NE
74/12/27	05:46:56.8	49.908	79.053	5.6	Balapan NE
75/02/20	05:32:57.7	49.756	78.094	5.7	Degelen
75/06/08	03:26:57.6	49.752	78.080	5.5	Degelen
75/12/25	05:16:57.2	50.018	78.863	5.7	Balapan NE
76/07/29	04:59:58.0	47.812	48.101	5.9	Azghir
76/08/28	02:56:57.6	49.948	78.980	5.8	Balapan NE
76/09/29	02:59:57.7	73.406	54.503	5.8	Matochkin Shar
76/10/20	07:59:57.8	73.402	54.472	5.1	Matochkin Shar
77/03/29	03:56:57.8	49.790	78.154	5.4	Degelen
77/08/10	22:00:01.8	50.948	110.782	5.0	Lake Baikal
77/09/01	02:59:57.8	73.374	54.411	5.7	Matochkin Shar
77/09/05	03:02:57.8	50.048	78.929	5.8	Balapan NE
77/09/30	06:59:55.9	47.849	48.127	5.0	Azghir
77/10/09	10:59:58.8	73.469	53.977	4.6	Matochkin Shar
77/10/14	07:00:00.0	47.800	48.100	0.0	Azghir
77/10/29	03:07:03.0	50.056	78.866	5.6	Balapan NE
77/11/30	04:06:57.6	49.934	78.894	6.0	Balapan NE
78/03/26	03:56:57.7	49.713	78.065	5.6	Degelen
78/06/11	02:56:57.8	49.879	78.814	5.9	Balapan SW
78/07/28	02:46:57.8	49.732	78.152	5.7	Degelen
78/08/09	17:59:58.1	63.653	125.345	5.6	Central Siberia
78/08/10	07:59:57.7	73.314	54.697	5.9	Matochkin Shar

5

Table 1: Explosions

Data	Time	Lat.(N)	Long.(E)	$m_b(ISC)$	Site
78/08/24	18:00:03.9	65.866	112.563	5.1	Central Siberia
78/08/29	02:37:06.4	49.984	79.017	5.9	Balapan NE
78/09/27	02:04:58.4	73.382	54.441	5.6	Matochkin Shar
78/11/04	05:05:57.5	50.028	78.976	5.6	Balapan NE
79/06/23	02:56:59.0	49.886	78.916	6.2	Balapan SW
79/07/07	03:46:57.5	50.048	79.063	5.8	Balapan NE
79/07/14	04:59:55.2	47.813	48.067	5.6	Azghir
79/08/04	03:56:57.2	49.860	78.942	6.1	Balapan SW
79/08/18	02:51:57.3	49.928	78.981	6.1	Balapan SW
79/09/24	03:29:58.4	73.372	54.578	5.7	Matochkin Shar
79/10/18	07:09:58.5	73.341	54.733	5.8	Matochkin Shar
79/10/28	03:16:57.0	49.961	79.068	6.0	Balapan NE
79/12/23	04:56:57.6	49.925	78.796	6.2	Balapan SW
80/05/22	03:56:57.8	49.750	78.107	5.5	Degelen
80/06/12	03:26:57.7	49.954	79.055	5.6	Balapan NE
80/09/14	02:42:39.3	49.936	78.863	6.2	Balapan SW
80/10/11	07:09:57.2	73.361	54.820	5.7	Matochkin Shar
80/10/12	03:34:14.2	49.937	79.104	5.9	Balapan NE
80/12/14	03:47:06.5	49.867	78.967	5.9	Balapan SW
80/12/27	04:09:08.5	50.008	79.026	5.9	Balapan NE
81/03/29	04:03:50.1	49.979	79.016	5.6	Balapan NE
81/04/22	01:17:11.4	49.870	78.896	6.0	Balapan SW
81/09/13	02:17:18.4	49.890	78.976	6.1	Balapan SW
81/10/01	12:14:56.9	73.323	54.554	6.0	Matochkin Shar
81/10/18	03:57:02.7	49.876	78.885	6.1	Balapan SW

Table 1: Explosions

Data	Time	Lat.(N)	Long.(E)	$m_b(ISC)$	Site
81/11/29	03:35:08.8	49.848	78.850	5.7	Balapan NE
81/12/27	03:43:14.2	49.895	78.859	6.2	Balapan SW
82/02/19	03:56:11.1	49.826	78.125	5.4	Degelen
82/04/25	03:23:05.5	49.871	78.917	6.1	Balapan SW
82/07/04	01:17:14.5	49.968	78.857	6.1	Balapan SW
82/10/11	07:14:58.4	73.371	54.342	5.6	Matochkin Shar
82/12/05	03:37:12.7	49.890	78.860	6.1	Balapan SW
82/12/26	03:35:14.4	50.061	79.049	5.7	Balapan NE
83/06/12	02:36:43.7	49.905	78.967	6.1	Balapan SW
83/08/18	16:09:58.6	73.377	54.868	5.9	Matochkin Shar
83/09/25	13:09:57.9	73.349	54.377	5.8	Matochkin Shar
83/10/06	01:47:06.8	49.909	78.827	6.0	Balapan SW
83/10/26	01:55:05.0	49.887	78.901	6.1	Balapan SW
83/12/26	04:29:07.0	49.835	78.205	5.6	Degelen
84/03/07	02:39:06.4	49.999	78.987	5.7	Balapan NE
84/04/15	03:17:09.3	49.686	78.141	5.7	Degelen
84/04/25	01:09:03.7	49.911	78.913	6.0	Balapan SW
84/05/26	03:13:12.5	49.925	79.030	6.1	Balapan NE
84/07/14	01:09:10.5	49.852	78.921	6.2	Balapan SW
84/08/26	03:30:00.0	73.380	54.800	0.0	Matochkin Shar
84/10/25	06:29:58.1	73.369	54.842	5.8	Matochkin Shar
84/10/27	01:50:10.7	49.917	78.829	6.2	Balapan SW
84/12/02	03:19:06.5	49.946	79.032	5.9	Balapan NE
84/12/16	03:55:02.8	49.884	78.824	6.1	Balapan SW
84/12/28	03:50:10.9	49.826	78.710	6.0	Balapan SW

Table 1: Explosions

Data	Time	Lat.(N)	Long.(E)	$m_b(ISC)$	Site
85/02/10	03:27:07.7	49.865	78.839	5.9	Balapan SW
85/07/20	00:53:14.8	49.916	78.803	6.0	Balapan SW
87/02/26	04:58:22.1	49.800	78.104	5.4	Degelen
87/04/03	01:17:08.1	49.874	78.812	6.2	Balapan SW
87/05/06	04:02:05.8	49.803	78.110	5.6	Degelen
87/06/06	02:37:07.1	49.803	78.089	5.4	Degelen
87/07/17	01:17:07.1	49.769	78.100	5.8	Degelen
87/08/02	02:00:00.1	73.346	54.578	5.8	Matochkin Shar
87/12/13	03:21:04.9	49.930	78.820	6.1	Balapan SW
87/12/27	03:05:04.9	49.820	78.730	6.1	Balapan SW
88/02/13	03:05:06.0	49.930	78.910	6.1	Balapan SW
88/04/03	01:33:05.9	49.870	78.920	6.0	Balapan SW
88/05/04	00:57:06.8	49.890	78.760	6.1	Balapan SW
88/05/07	22:49:58.3	73.350	54.430	5.9	Matochkin Shar
88/09/14	03:59:57.6	49.810	78.800	6.1	Balapan SW
88/12/04	05:19:53.2	73.380	54.960	5.9	Matochkin Shar

it consisted of two simultaneous explosions about 7 km apart. Because of the spatial and temporal closeness, waves recorded from the two explosions of a double event will interfere except possibly for the initial P wave. For the sake of simplicity, we will, therefore, treat recordings from double events as one waveform and list only the larger of the two explosions in Table 1.

Table 2 summarizes the distribution of explosions over test sites and the distribution of waveforms over stations as well as test sites. The stations are described in the following section. About three quarters of the explosions (86) were carried out at the Semipalatinsk test range, which in Table 2 has been divided into four sub regions, Balapan NE, Balapan SW, Degelen, and Murzhik. The epicenters of the events within each subregion are confined to areas with diameters of about 10 km or less (Figure 2). The distance between Degelen and Balapan, and between Degelen and Murzhik are about 70 and 30 km respec-

8
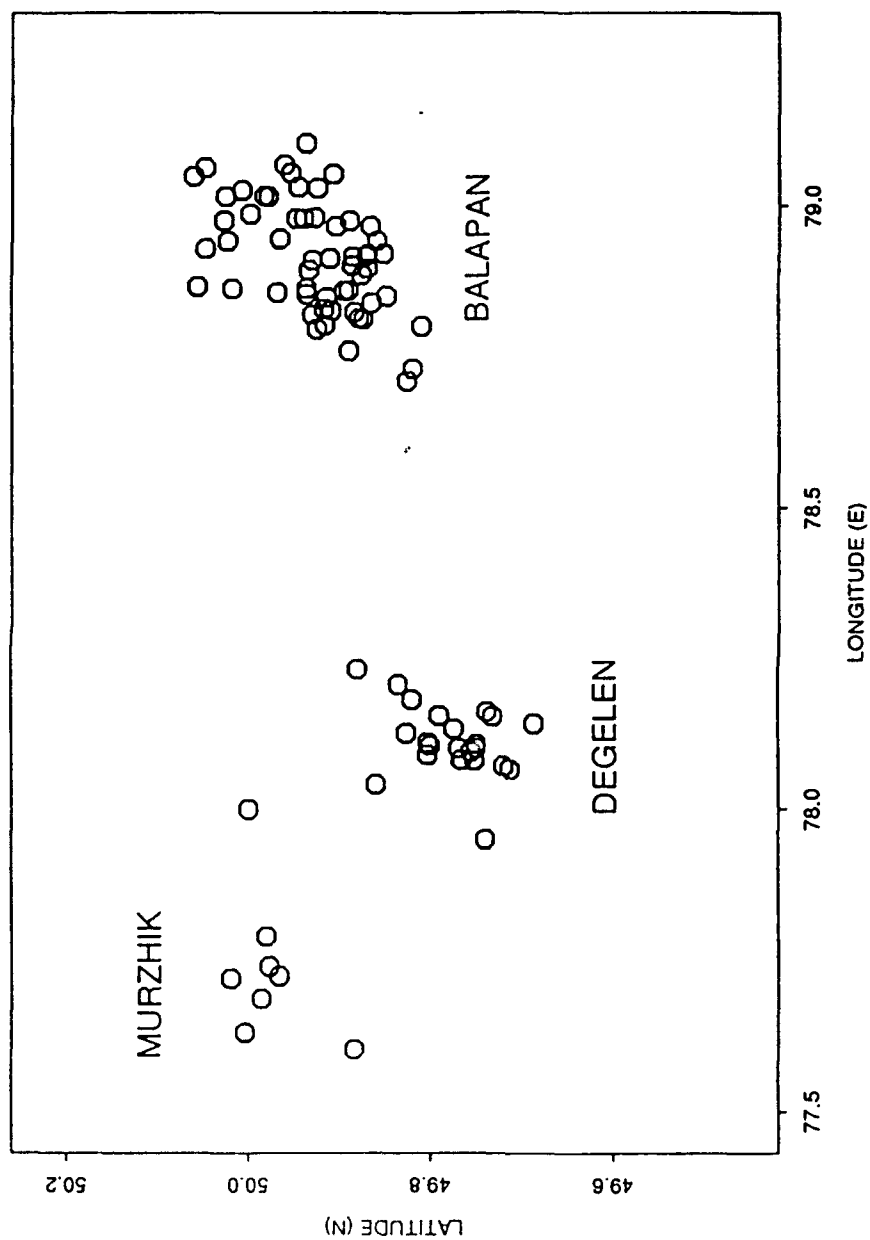
Figure 2: Relative locations of explosions at the Semipalatinsk test range.

Table 2: Summary of Explosions and Waveforms

TEST SITE		No. of explo	No.of waveforms												Total
			APA	ARU	BOD	CHS	FRU	NRI	NVS	OBN	TLY	TUP	UZH	
Semipalatinsk	Balapan NE	23	1	19	4	1	4	2	13	22	3	1	12	82
	Balapan SW	33	1	24	3		19	4	27	32	12	5	24	151
	Degelen	23	2	12	4	2	8	3	17	21	6		11	86
	Murzhik	7		2	1		2	4	5	7			1	22
Novaya Zemlya	Krasino	1		1	1					1				3
	Matochkin	21	20	15	14	9	1	3	16	16	5		12	111
Azghir		5		4					4	4				12
C. Siberia		2		2					2	2				6
Lake Baikal		1		1					1	1				3
Total		114	24	80	27	12	16	34	16	106	26	6	60	476

tively. The explosions at Semipalatinsk have generally large magnitudes; only about 10% of the events, all at Degelen and Murzhik, have $m_b(P) < 5.4$ and all Balapan SW events have $m_b(P) > 5.8$ (Figure 3). Yields, depths, and other shot parameters have been published by Bocharov et al. (1989) for 19 of the Semipalatinsk explosions.

All but one of the 22 explosions at Novaya Zemlya occurred near Matochkin Shar, the narrow strait that separates the Southern and Northern Islands. The magnitudes of the Novaya Zemlya explosions too are quite large; there are only two events with $m_b(P) < 5.6$.

Explosions at the remaining sites are few in numbers; 5 at Azghir, 2 at different locations in Central Siberia, and 1 near Lake Baikal. Many of these events also have large magnitudes: only three events have $m_b(P) < 5.2$

In summary, four large suites at distinctly separate areas - Balapan NE, Balapan SW, Degelen, and Matochkin Shar - constitute almost 90% of all explosions in the data set. Three of the suites consist essentially of large magnitude events, whereas the fourth, at Degelen, includes events with a fairly large magnitude range $m_b(P) = 4.8 - 6.0$.

Seismological Stations And Instrument Calibrations

Waveform data are available from the stations listed in Table 3. All stations, except CHS, TLY, and TUP are part of the base network of the Uniform System of Seismic Observations (USSO) in the U.S.S.R. (Kondorskaya and Aronovich, 1979). Their locations are shown in the map of Figure 1. Epicentral distances between stations and explosion sites range between 6 and 35 degrees (see Table 3), thus covering regional, as well as teleseismic distances.

A general and comprehensive review of recording equipment - seismometers and galvanometers - at stations of the USSO has been made by Shishkevish (1974). Typical maximum magnifications of the recording equipment are included in Table 3 and typical instrument responses are shown in Figure 4.

All waveforms were recorded with vertical component instruments and most of them were recorded with short period SKM-3 seismometers, standard short period pendulum instruments with an electromagnetically damped moving coil transducer. The SKM-3 waveforms at ARU and APA were obtained at two maximum magnifications, around 24.7/38.0 k and 5.5/55k respectively. Four waveforms at APA were recorded with a SX seismometer, a short period instrument somewhat older and allegedly less reliable than the SKM-3 (Staravoyt, personal communication, 1991). Finally 8 waveforms, 7 at NVS and 1 at
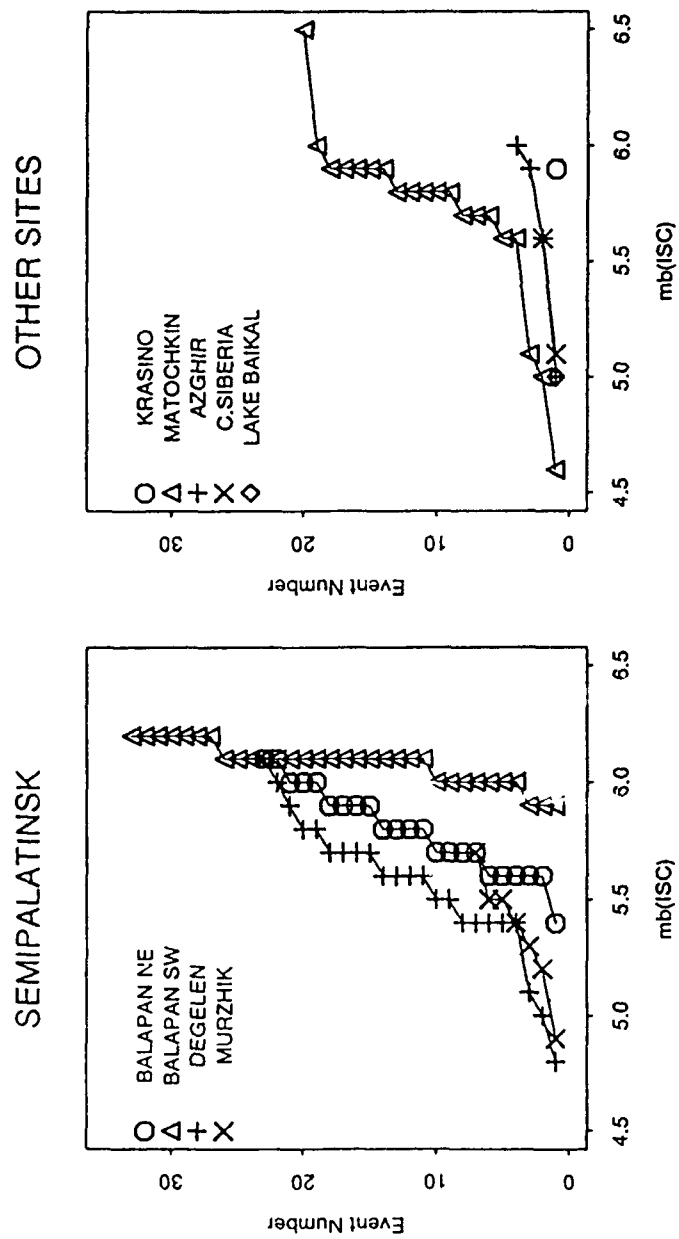
Figure 3: Distribution of magnitudes, $m_b(P)$ determined by ISC, of the explosion sites at the Semipalatinsk test range (to the left) and at other locations in Western and Central U.S.S.R.
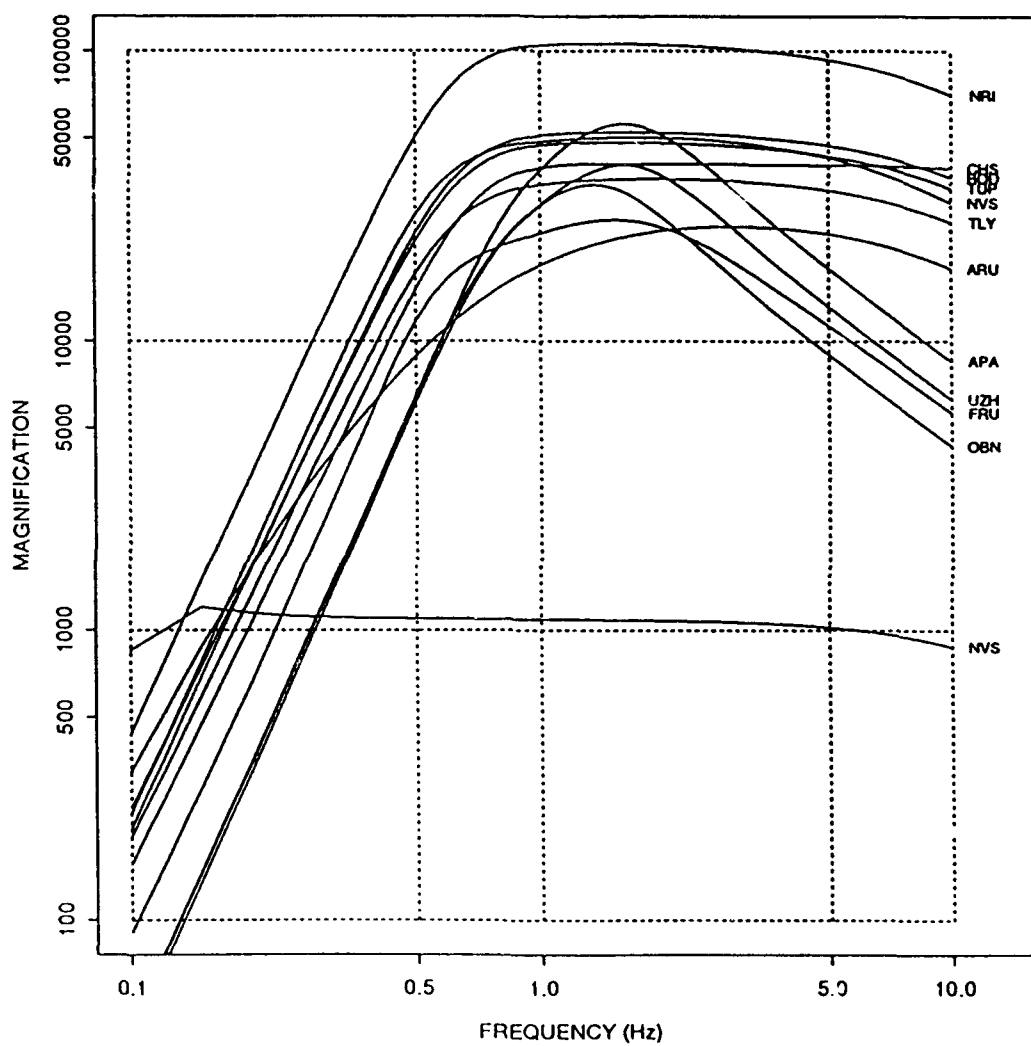
Figure 4:   Typical amplitude response curves of the stations.

Table 3: Seismological Stations

Code	Name	Lat.(N)	Long.(E)	Magnification (k)	Distances (in degrees) to					
					Semi	Matochkin	Azghir	Krasino	Lake Baikal	C.Siberia
APA	Apatity	67.55	33.33	5.5/55	28.4	9.2	(21.1)	(7.8)	(39.8)	(34.9/29.4)
ARU	Arti	56.40	58.60	24.7/38.0	13.4	17.1	10.7	14.6	(30.8)	32.7/26.8
BOD	Bodaybo	57.85	114.18	52.5	22.6	27.4	(39.6)	27.9	(7.2)	(8.0/8.0)
CHS	Chusal	39.10	70.77	40.0	11.9	35.2	(18.6)	(33.0)	(30.3)	(40.2/35.8)
FRU	Fruenze	42.83	74.62	26.0	7.4	32.1	(19.2)	(30.0)	(25.8)	(35.5/31.2)
NRI	Norilsk	69.40	88.10	100.0	20.3	11.2	(29.0)	(11.8)	(21.4)	(15.7/9.9)
NVS	Novosibirsk	54.90	83.30	50.0	6.1	21.9	(22.9)	20.6	17.0	22.8/17.9
OBN	Obninsk	55.10	36.60	36.0	25.5	19.8	10.1	17.4	(42.9)	(42.4/36.6)
TLY	Talaya	51.68	103.63	36.2	16.3	29.8	(35.3)	(29.5)	(4.5)	(16.6/14.9)
TUP	Tupik	54.43	119.90	48.4	25.8	(32.0)	(43.7)	(32.5)	(6.5)	(9.7/12.0)
UZH	Uzhgorod	48.63	22.30	40.0	35.7	28.6	(17.2)	(26.6)	(53.8)	(52.9.47.1)

There is no waveform data for distances within parentheses.

14

OBN, were recorded with SKD seismometers, standard broad-band instruments - with electromagnetic damping as for the SKM-3 - but with low magnification.

As the waveform data for some stations were recorded over a period of more than twenty years, one might expect some variation in the instrument characteristics. This is indeed the case, but the changes with time differ both in type and in degree among the stations. The response curves at some stations change in overall shape and, for a given shape, vary slightly, whereas instrument characteristics at other stations remain the same for all recorded waveforms. Temporal changes in instrument characteristics for the waveform data are described by two kinds of calibrations, daily and annual, made available together with the digitized data.

An annual calibration gives basic parameters - periods and dampings of seismometer and galvanometer, coupling factor, and nominal magnification - that can be used to calculate the amplitude magnification as a function of frequency. In addition, the annual calibrations list the maximum magnification, which is redundant, as it can be derived from the amplitude magnification curve calculated from the basic instrument parameters. For the most commonly used seismometer, SKM-3, the shape of the magnification curves differs among the stations. Some curves are more or less flat above a certain frequency, around 0.7 Hz or so, whereas other curves- such as for APA and OBN - peak between 1 and 2 Hz. Furthermore, the response curves i. some stations, ARU, BOD, NRI, and NVS, have only a single overall shape that stays constant with time, whereas other stations, APA and OBN, have curves with clearly different general shapes for the same instrument over the years - presumably due to deliberate alterations by station operators. The degree to which curves vary around the same overall shape also varies among the stations. The curves for ARU have no variation at all for 10 years of data, whereas curves of similar shape for BOD, NRI and OBN fluctuate as a result of minor changes in the basic instrument parameters. These variations, while minor, still clearly affect the response curves. The standard deviations as a function of frequency of the magnification curves resulting from the variation in instrument parameters are shown in Figure 5 for these three stations. In the short period range, 0.5-5 Hz, this standard deviation varies between 1 and 7% for the three curves.

The data for the annual calibrations are mainly excerpts from the volumes issued by Nauk (1988) for USSO stations. Missing virtually wholly for stations CHS, TLY, and TUP, this information is also missing in some instances for the other stations. The lack of data was either due to the simple fact that annual calibrations were not carried out for all years at all stations or to unavailability of the Nauk annual calibration volumes.

A daily calibration consists of the maximum magnification and a period range, Tm, over

VARIATION IN MAGNIFICATION
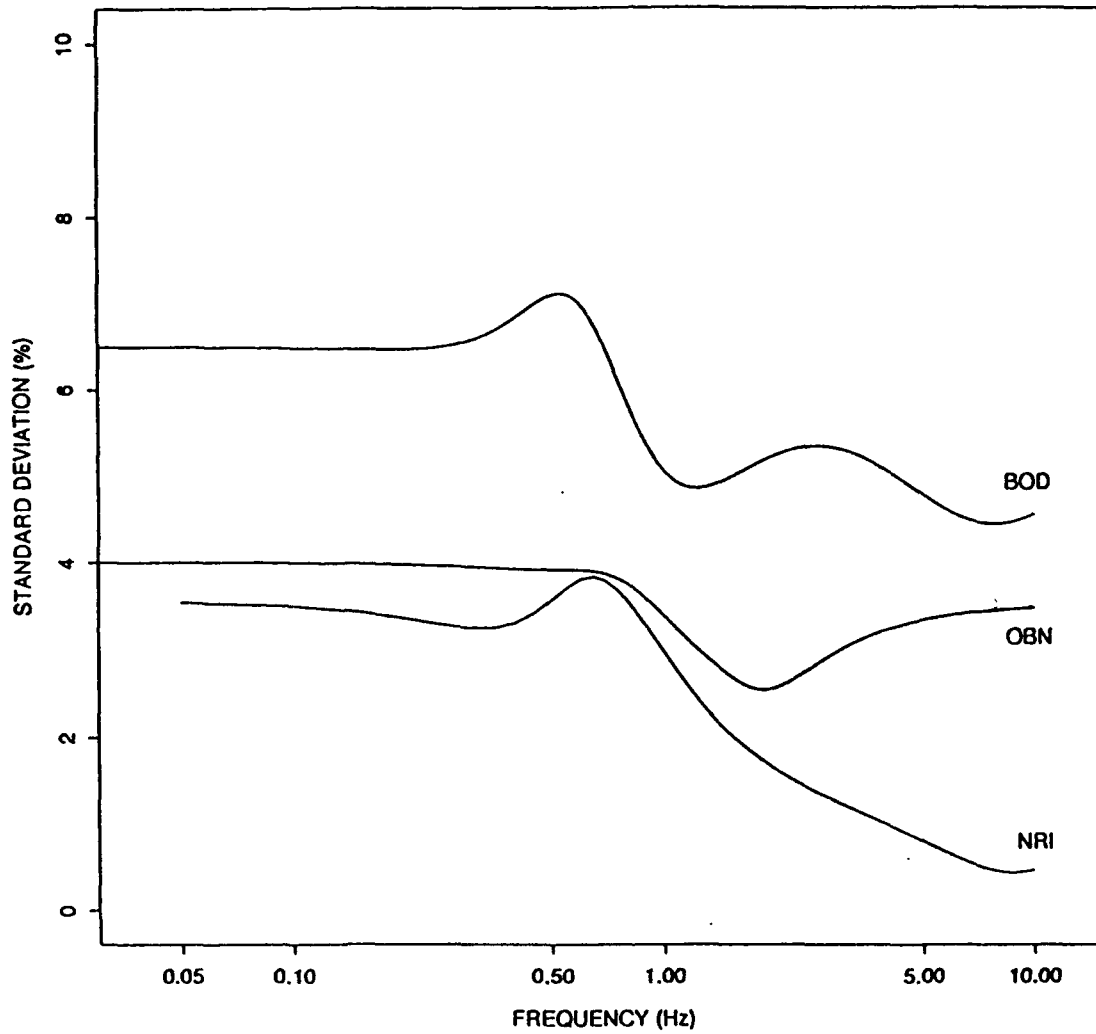
Figure 5:   Standard deviations (in%) as a function of frequency of the instrument mag-
             nifications curves for stations, BOD, NRI, and OBN for similar response
             curves in the period 1965-1988.

16

which the magnification is 90% or more of this maximum. The daily calibrations were based on notations on the original records compiled in part by AFTAC (Heron, personal communication, 1991). Information is not available on the procedure used to determine these parameters or on their accuracy other than that it has been claimed that Tm is determined with an accuracy of 0.05 s when the upper limit of Tm< 1 s, and with an accuracy of up to 0.1 s when the upper limit of Tm< 10 s (Shishkevish, 1974).

The instrument parameters reported in the annual calibrations can be used to correct waveform data for instrument response. In fact, this is the only way to correct for the instrument response when removing the instrument effect of a recorded signal by deconvolution. The magnification and period range noted on original records do not, however, uniquely define the entire instrument response. Conversely, the maximum magnification and the period range, Tm, can be calculated from the basic instrument parameters.

The accuracy of the calibration data, daily and annual, is not known. Soviet seismologists (Staravoyt, personal communication, 1991) quote 5-10% (presumably range of variation) as typical of stations of the USSO, but emphasize that the quality of the calibrations may vary from station to station. The fact that the annual calibrations at some stations show no variation over the years and vary at others (see Figure 5) may be due to differences in the quality of instrument calibrations among stations and, therefore, may not reflect differences in actual changes of instrument characteristics among the stations.

There are also inconsistencies between the annual and daily calibrations. For example, the average daily maximum magnification for a given year is, in some instances, different from the maximum magnification of the annual calibration. Furthermore, the reported maximum magnification of the annual calibration is not always identical with that calculated from the instrument parameters. Figure 6 shows a plot of the ratios of the three types of maximum magnification that can be associated with the instrument for a record: (i) noted on the record, V(daily), (ii) listed in annual reports, V(annual listed), and (iii) calculated from instrument parameters in annual reports, V(annual calculated). A high accuracy of the instrument magnification is desirable for some types of data analysis. For example, magnitudes based on the Lg phase, $m_b(Lg)$, used for yield estimation purposes have in some cases a relative precision of 0.03 magnitude units. This corresponds to a 7% uncertainty in magnification. In Figure 6 we have drawn lines corresponding to 7% discrepancy. We find that for about 10% of the waveforms the ratio V(daily)/V(annual listed) is outside these lines. The inconsistencies are most frequent for stations OBN and UZH. Figure 7 shows the ratios V(daily)/V(annual listed) for these two stations as a function of time. For a given year the ratios are quite consistent although significantly different from one, and the largest deviations occur prior to 1980.
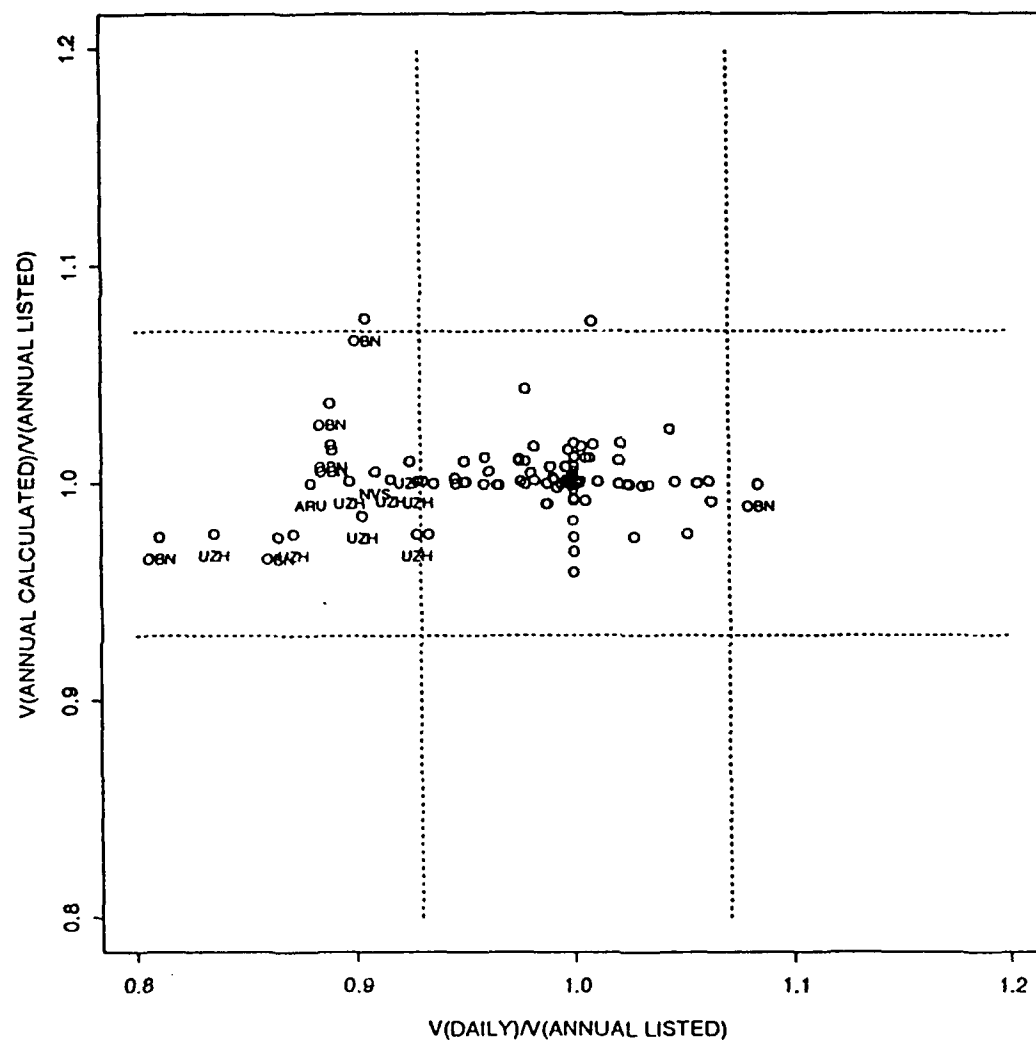
Figure 6: Comparisons of maximum magnification ratios, V(daily), V(annual listed), and V(annual calculated). The dotted lines correspond to a 7% deviation from a ratio of 1.

18
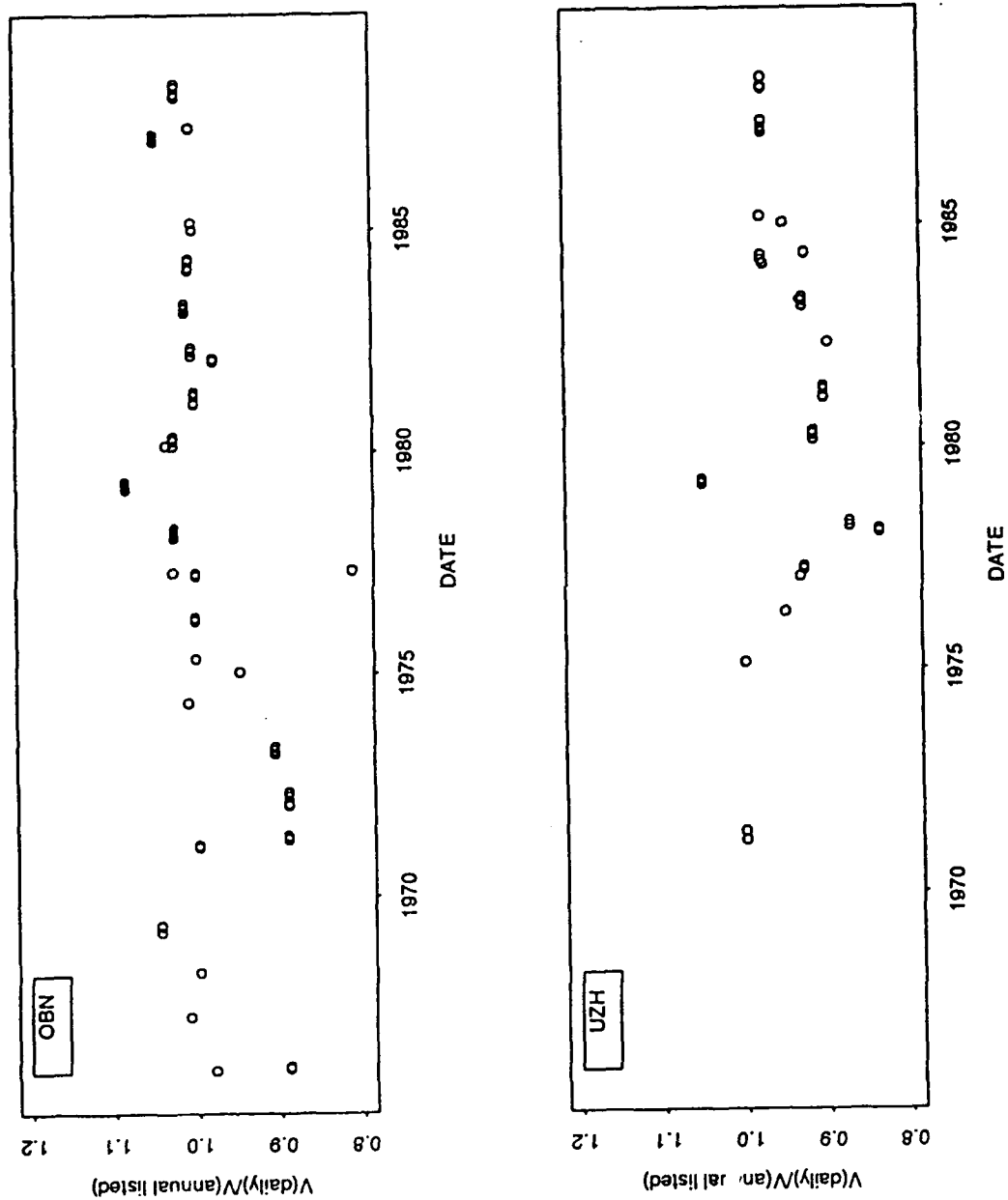
Figure 7:   Maximum magnification ratio, V(daily)/V(annual listed), at stations OBN and UZH as a function of time.

19

The discrepancies between the two types of calibrations raise the issue of which type should be applied to attain the most reliable instrument corrections. As the variations in many cases may be within the limits of measurement errors of the calibration procedures, a third alternative, a single fixed set of instrument parameters for a given station and instrument, may be the most accurate procedure for instrument corrections. Drift or random fluctuations in the actual instrument characteristics may be smaller than those reflected by variations in calibrations at some stations. We compared the consistency of RMS amplitudes of Lg waves at the stations using no instrument correction, the daily calibration, and the annual calibration. The comparison included all of the waveforms from the Novaya Zemlya and Semipalatinsk explosions. Although there were minor differences, the results indicated that either the daily or the annual calibrations could be used.

Waveform Data

The waveform data described here have been digitized from copies of original analog records. Before a trace was digitized it was enlarged by a factor of two, then enhanced, and finally enlarged by another factor of two. The methodology and procedure for the digitization of the analog recordings have been described by Chiburis *et al* (1980).

Each digitized waveform usually consists of 2 minutes of noise prior to the P onset, and extends into the signal coda to a time corresponding to a group velocity of about 3.0 km/s. The sampling rate is 20 Hz and the sampled values, after multiplying with a scaling factor, correspond to the excursion of the original trace in mm. The resolution of the sampling at the digitization table is 0.005 inch or about 0.0125 mm. However, only x-y co-ordinates more than 0.010 inch apart are actually used. A 0.010 inch resolution of the digitization correspond to a time resolution of about 0.06 s, which is somewhat larger than the time increments, 0.05 s, between samples. This means that for waveform segments with little change in amplitude the digitizing table samples at slightly less than 20 Hz. Interpolation routines are used to provide data at a constant rate of 20 samples/s.

Clearly, the hand digitized data is bound to be limited in quality when compared to modern high quality digital recordings. For one thing, they have a narrow frequency band: studying the quality of the digitization, Kemerait *et al.* (1981) found that for 70 mm film chips "it produces good results from dc out to at least 3-4 Hz".

A comparison of the hand digitized and IRIS recordings at the station in Arti (ARU) from the JVE explosion (September 14, 1988 at Semipalatinsk) is shown in Figure 8. Both the Soviet SKM-3 and the IRIS instruments were presumably operating in vaults of the same tunnel system. As can be seen from Figure 9, the amplitude responses are different for the two instruments. The IRIS response peaked around 5 Hz whereas the SKM-3 instrument

COMPARISON OF HAND DIGITIZED AND DIGITAL IRIS RECORDS
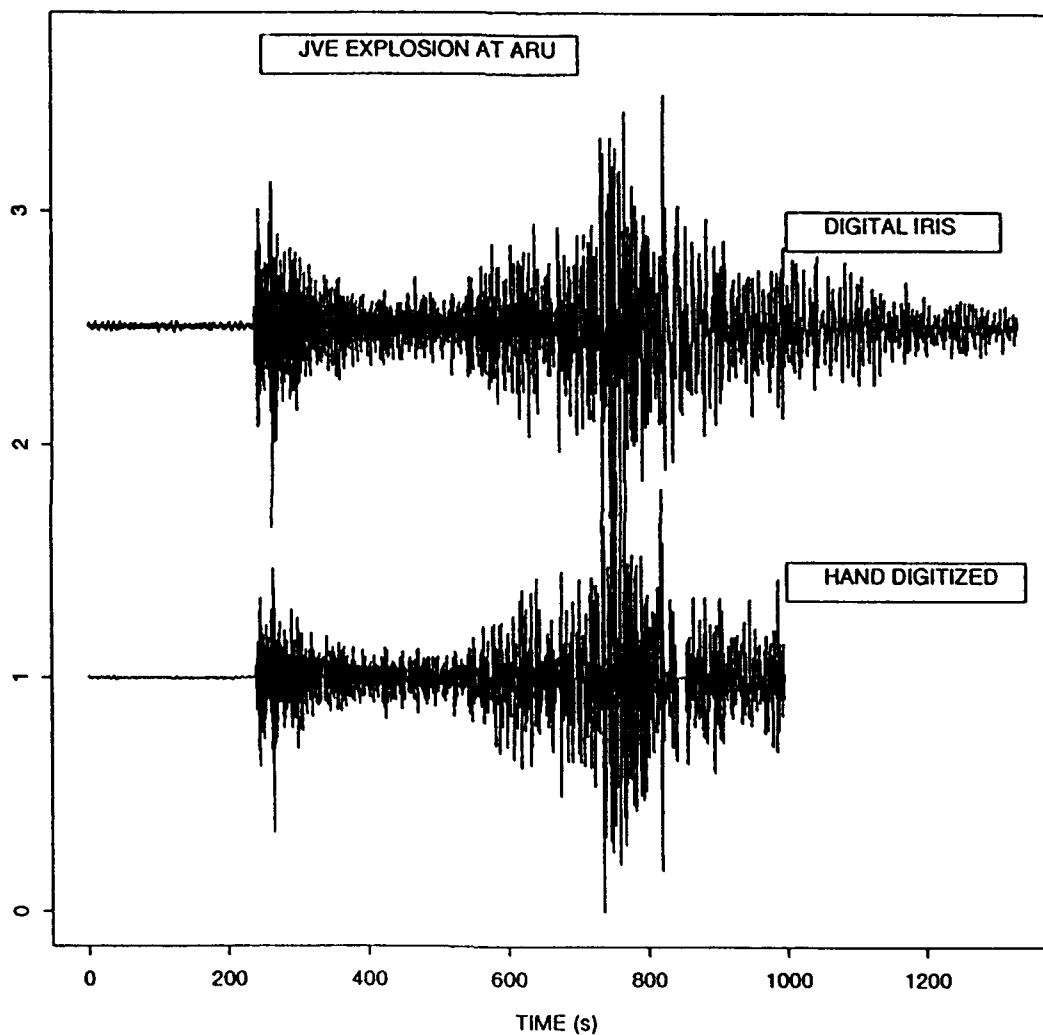
Figure 8: Vertical component recordings of the JVE explosion on Sep, 14, 1988, at IRIS and U.S.S.R. stations at Arti (ARU).

21

has a fairly constant magnification above 1 Hz. The noise spectra in Figure 9 shows that the IRIS instrument appears, perhaps somewhat surprisingly, to have the highest noise level at frequencies just above 1 Hz; the high noise of the IRIS recording is also obvious from the traces in Figure 8. Sharp peaks, at 4 and 5 Hz, of the IRIS noise spectrum indicate that the high level might partly be caused by instrumental or system noise. The NORSAR model for the noise spectrum, equal to f^{-5} nm^2/Hz, is shown for comparison in Figure 9. The two amplitude spectra of the P wave, corrected for noise as well as instrument response, look fairly similar; the ratio is fairly constant in a band from about 0.6 to about 2 Hz. The two Lg spectra have similar general shapes although the ratio varies considerably, about an order of magnitude, in the band from about 0.4 to 1.0 Hz. The spectral ratios for both the P and Lg wave are significantly different at low frequencies, less than 0.2-0.3 Hz. This discrepancy may be due to limited resolution of the hand digitized data at the low frequency end of the short period band. Figure 10 compares the P and Lg waves more in detail. Apart from the original records of the two instruments, a trace representing a transformation of the hand digitized recording into that with a response equivalent to an IRIS instrument response is also included in this comparison. There are apparent shifts between signatures of the Lg wave train along the trace. The first significant amplitude, about 5 s after the beginning of the trace in the figure, appears delayed at the hand digitized data relative to the IRIS trace, whereas he two significant amplitudes around 50 s after the beginning appear to be ahead on the hand digitized records. The reason for this discrepancy is not known at this point in time. Additional analysis of, in particular, the phase responses of the two instruments may explain this issue.

Apart from a narrow frequency range, the hand digitized waveforms also have gaps due to missing data points. In such gaps, sampled values are entered with almost constant values, often close to zero. All waveforms have gaps of 1 second duration at minute marks. What is more, some waveforms also have large gaps of 5 seconds or more in various parts of the record, the initial P, P coda, S or Lg windows, due to the original records being off scale or being difficult to trace. Extensive gaps in the waveforms occurred for 187 records, or almost 40%, of the data. Such gaps in the data are, however, largely limited to a few stations - NVS (64), ARU(36), FRU (31), and UZH (17) - which account for 80% of the waveforms with gaps, but only about half of the total number of waveforms. The gap percentage of station OBN, which has the largest number of waveforms in the data set (106), is only 15%.

Some idea of the accuracy of the time of the data can be obtained from standard deviations of P arrival time residuals, defined as the differences between calculated values and those measured after applying the time corrections annotated on the original records. For this purpose data for explosions at Matochkin Shar (JED events) and at Semipalatinsk (events

22

INSTRUMENTS

NOISE SPECTRA

P-WAVE SPECTRA
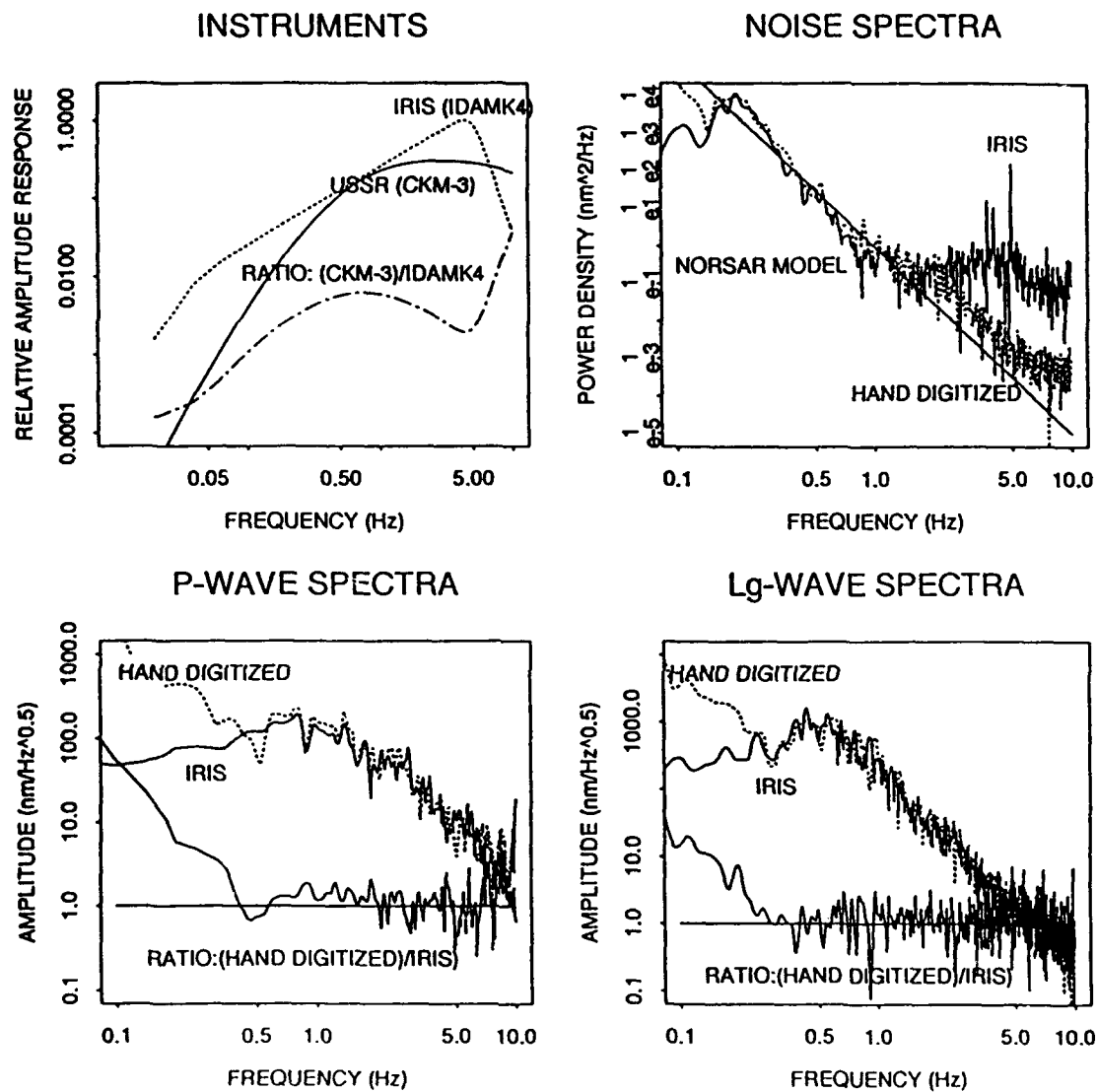
Lg-WAVE SPECTRA

Figure 9: Comparison of instrument response, ambient noise, P-wave and Lg-wave spectra for the JVE explosion by IRIS (IDAMK4) and Soviet SKM-3 instruments at station ARU.

23

P at ARU for JVE Explosion

HAND DIGITIZED

DIGITAL IRIS

HAND DIGITIZED DECONVOLVED TO IRIS

TIME (s)

Lg at ARU for JVE Explosion

HAND DIGITIZED

DIGITAL IRIS

HAND DIGITIZED DECONVOLVED TO IRIS

TIME (s)
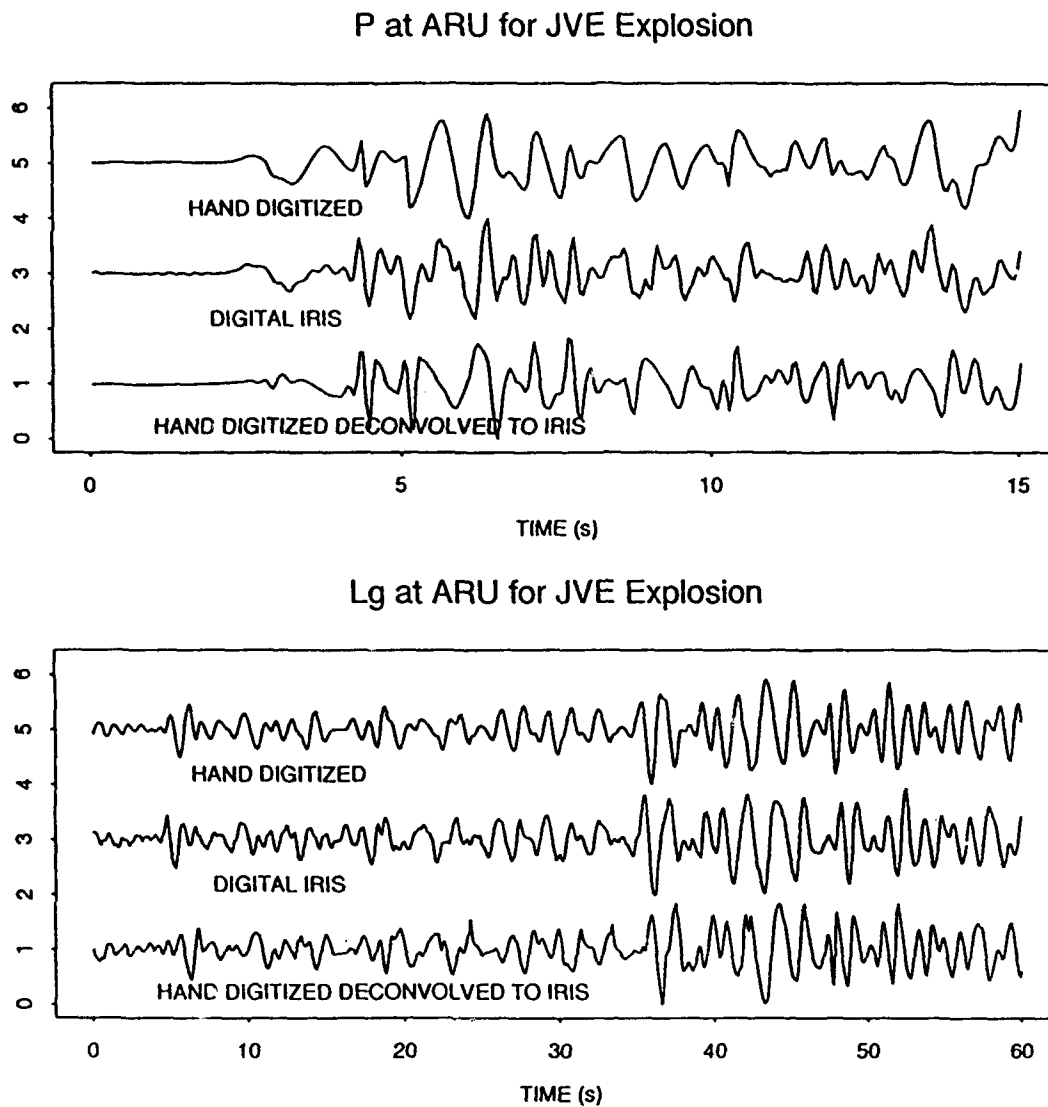
Figure 10: Panels with P-waves and Lg-waves recorded by IRIS and Soviet instruments at Arti (ARU). The Soviet hand-digitized data have been deconvolved with its instrument response and convolved with that of the IRIS instrument (bottom traces in the panels)

24

listed by Bocharov et al (1989)) were used. The standard deviations of the P residuals vary between 0.6-1.4 seconds among the stations. The large value, 1.4 s, for NVS from Semipalatinsk, may be due to short epicentral distance and differences in distances to the subregions of Semipalatinsk.

Typical recordings at all 11 stations from explosions at Semipalatinsk and Novaya Zemlya are plotted as a function of epicentral distance in Figure 11. As there is no explosion with waveforms available at all the stations, the record sections had to be composed of data from several explosions. The repeatability of waveforms at a given station from a given test site is usually high and the composite sections of Figure 11 therefore give a representative picture of the development of various seismic phases along the many paths that are sampled by data. More or less clearly developed Lg phases can be seen for all paths from the explosion sites at Semipalatinsk except for the paths to APA and NRI. The comparatively large Lg waves at TLY from explosions at the Semipalatinsk test range could be an effect of high attenuation of P and S waves relative to that of Lg along the paths to Lake Baikal. S-phases with smaller amplitude than Lg can also be seen in many of the ARU waveforms. For Novaya Zemlya explosions, clear Lg waves can only be seen at station ARU at a distance of 17 degrees. The absence of clear Lg phases could be due to a blockage mechanism of large sediment thickness variations in the Barents and Kara Seas as suggested by Baumgardt (1990). However, clear S-waves can be seen at NRI, APA and ARU and there is an indication of a phase slightly after the expected arrival time of S at stations like BOD, NVS, and OBN.

Concluding Comment

Compared to modern high quality digital recordings the hand digitized data has, as one would expect, a limited frequency range, resolution, and dynamic range. Furthermore, a large percentage of the waveforms had one or more gaps of several seconds or more due to clipping or difficulties in tracing the recorded signatures in the hand digitizing process. These limitations notwithstanding, this data set is of great value for seismic verification research and development. While digital seismic stations mostly have been in operation for a comparatively short time, the 'historical' data described here represent a sample of data over almost the entire period of Soviet underground nuclear testing. Although there is an indication in the data that the reliability of seismometers with associated recording equipment and the quality of instrument calibrations have improved over this time period, the overall consistency in station operation and diligence with calibrations are features that add significantly to the value of this type of historical data for seismic verification research and development.

Figure 11a: Section of typical waveforms for Semipalatinsk explosions.

26

Figure 11b: Section of typical P waveforms for Semipalatinsk explosions.

27

Figure 11c: Section of typical waveforms for Novaya Zemlya explosions.

28

Figure 11d: Section of typical P waveforms for Novaya Zemlya explosions.

Acknowledgements

References

Anderson, J., Farrell, W.E., Garcia, K., Given, J., and H. Swanger (1990), Center for Seismic Studies Version 3 Database: Schema Reference Manual, Center for Seismic Studies, Arlington, VA, Technical Report C90-01

Baumgardt, D.R. (1990), Causes of Lg Amplitude Variations and Scattering in the Eurasian Continental Crust. in Proceedings of the Twelfth Annual DARPA/GL Seismic Research Symposium. (Eds J. Lewkowicz and J. McPhetres), GL-TR-90-0212 Geophysics Laboratory, Hanscom AFB, MA. ADA226635.

Bocharov, V.S., Zelentsoz, S.A., and V.N. Michailov (1989). Characteristics of 96 underground nuclear explosions at the Semipalatinsk test site, Atomic Energy (Atomnaya Energiya), 67.

Chiburis, E.F., R.O. Ahner, E.J. Reinhart (1980), Procedures for Digitizing Seismograms ENSCO Technical Report DCS-STR-80-53

Kemerait, R. C., G. Kraft, J. S. Mott, and E. Dohner (1981), A study of the hand-digitizing process for digitizing short period seismic data. ENSCO Technical Report DCS-SDR-81-57

Kondorskaya, N.V. and Z.I. Aranovich (1979), The uniform system of seismic observations of the U.S.S.R.and prospects for its development, Phys. Earth and Plan. Int., 18, 78-88.

Leith, W., Matzko, J.R., Unger, J. and D.W. Simpson (1990). Geology and Image Analysis of the Soviet Nuclear Test Site at Matochkin Shar, Novaya Zemlya U.S.S.R., in Proceedings of the Twelfth Annual DARPA/GL Seismic Research Symposium. (Eds J. Lewkowicz and J McPhetres), GL-TR-90-0212 Geophysics Laboratory, Hanscom AFB, MA. ADA226635.

Lilwal, R.C. and P.D. Marshall (1986). Body wave magnitudes and locations of Soviet underground explosions at the Novaya Zemlya Test Site, Atomic Weapons Research Establishment, AWRE Report No. O 17/86.

Marshall, P.D., Bache, T.C., and R.C. Lilwal (1985), Body wave magnitudes and locations of Soviet underground explosions at the Semipalatinsk test site, Atomic Weapons Research Establishment, AWRE Report No.O 16/84 (re-issue).

Nauk (1988). Parameters, amplitudes, and phase characteristics of Seismological stations in the U.S.S.R. in 1988. Academie, Nauk, SSSR, Moscow.

Shishkevish, C. (1974), Soviet Seismographic Stations and Seismic Instruments, Part I. Report no. R-1204-ARPA, Rand, Santa Monica, CA 90406.

Stewart, R.C. and P.D. Marshall (1988). Seismic P-waves from Novaya Zemlya explosions: seeing double! Geophys.J.92, 335-338.

Zonenshain, L.P. Verhoef, J. Macnab, R. and H. Meyers (1991), Magnetic Imprints of Continental Accretion in the U.S.S.R EOS, 72, 305.

Analysis Of RMS Magnitudes For Explosions At Novaya Zemlya Based On Recordings At Soviet Stations

Hans Israelsson

Abstract

RMS magnitudes from hand digitized recordings at nine standard seismic stations in the U.S.S.R were analyzed for 21 Novaya Zemlya explosions including a suite of events with magnitudes $m_b(ISC)$ = 5.6 - 6.0. Although there were clearly developed Lg phases at only two stations, APA and ARU, magnitudes calculated from the 3.1-3.7 km/s velocity window were highly consistent among stations. Estimates of the standard deviations of RMS values varied among the stations and had a median of 0.047 magnitude units (m.u.). Least squares network magnitudes based on the RMS values at five stations had estimated standard errors around 0.02 (m.u.). The network magnitudes for twelve of the events were very similar - their standard deviation was less than 0.04 (m.u.). The standard deviation of $m_b(P)$ based on teleseismic P waves recorded at world-wide network stations for the same twelve events was about three time larger.

RMS magnitudes based on windows other than that for Lg, including initial P, P coda, and S with coda, were also analyzed. The results for the S coda and Lg were similar. The RMS amplitude ratios for different phases had small variations from explosion to explosion. The median of the standard deviations for the P coda/Lg and S coda/Lg ratios were 0.08 and 0.04, respectively. The stability of these ratios suggests that work on seismic discrimination problems other than yield estimation might benefit from employing RMS amplitudes rather than traditional maximum amplitudes.

Introduction

Estimating yields of underground nuclear explosions is important for monitoring limited test bans. Significant improvements in the accuracy of seismic yield estimation have been achieved by exploiting Lg waves rather than traditional P and surface waves. For example, a series of studies have demonstrated that RMS Lg magnitudes from explosions at the Semipalatinsk test range are remarkably consistent between stations widely distributed in epicentral distance and azimuth (Ringdal, 1983; Ringdal and Hokland, 1987; Ringdal and Fyen, 1988; Hansen *et al.*, 1990). These magnitudes were based on modern, high quality, digital recordings at the NORSAR array in Norway, the Grafenberg array in Germany, at stations of the IRIS network in the Soviet Union, and of the Chinese Digital Station Network.

A unique set of analog seismic recordings from conventional Soviet stations of a number of underground nuclear explosions at several locations in the U.S.S.R. became available as a result of the bi-lateral Nuclear Testing talks and have subsequently been converted manually into digital form. We have analyzed this data for explosions at Novaya Zemlya. In particular, we examined the stability and consistency of station RMS magnitudes based on Lg time windows for this test site. We calculated network magnitudes from the station magnitudes and estimated their standard errors. In addition, we applied the RMS magnitude concept to time windows other than for Lg, including the initial P phase, the P coda, and the S phase with coda.

Data

The explosion test site near Matochkin Shar (the narrow straight that separates the Northern and Southern Islands of Novaya Zemlya) and the seismic stations are shown in the map of Figure 12. Detailed information on the explosions, the seismic stations and their instruments (with associated calibrations), and the waveform data have been compiled by Israelsson (1992). Here we summarize some of that information relevant to the data analysis.

Source data pertinent to the explosions, which occurred between 1964 and 1988, are listed in Table 4. Data for the three explosions in the 60's were included for the sake of completeness and virtually all of the analysis for this study was focused on waveforms from fifteen explosions between 1976 and 1988 with magnitudes between $m_b(ISC) = 5.6 - 6.0$. RMS magnitudes for waveforms from three smaller explosions, between $m_b = 4$ and 5, were also calculated. The relative locations of the explosions are shown on a map simplified from the digital terrain model for the Matochkin Shar area constructed by Leith et al. (1990). Most of the epicenters were determined by Lilwal and Marshall (1986) using the JED method. The epicenter of the small event on 84/08/26 was obtained at the Center for Seismic Studies. Locations for the last four explosions listed in Table 4 (they occurred after 1983) were estimated by ISC. The epicenters of these four explosions were corrected for the bias between the JED and the ISC epicenters, marked in Figure 13. The epicenters of all the explosions in Figure 13 are limited to an area with a diameter of about 15 km, which is similar to that of the Balapan region at the Semipalatinsk test range. The events cluster on the sides of the mountains separated by the Shumilikha river flowing north into the Matochkin Shar. Stewart and Marshall (1988) suggested that the explosion on Oct 11 1980 was a double event with two simultaneous shots about seven km apart as indicated by the dotted line in Figure 13. From analysis of P-wave seismograms they suggested that the southerly event (marked with an open circle in Figure 13) was about 0.35 the size of the larger explosion.
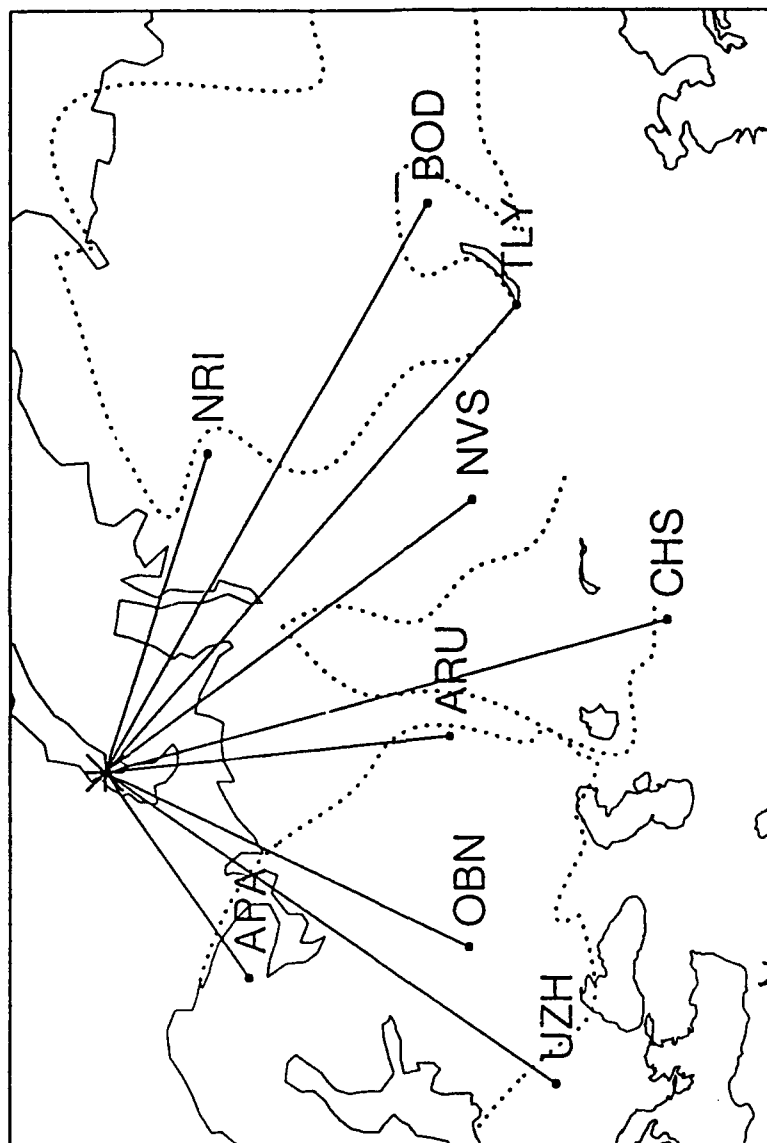
Figure 12: The relative location of the explosion near Matochkin Shar at Novaya Zemlya and the seismological stations. The lines between the explosion site and the stations only approximate great circle paths. The dotted curves outline the major tectonic elements of the U.S.S.R. (after Zonenshain *et al.*, 1991)

35

EXPLOSION EPICENTERS
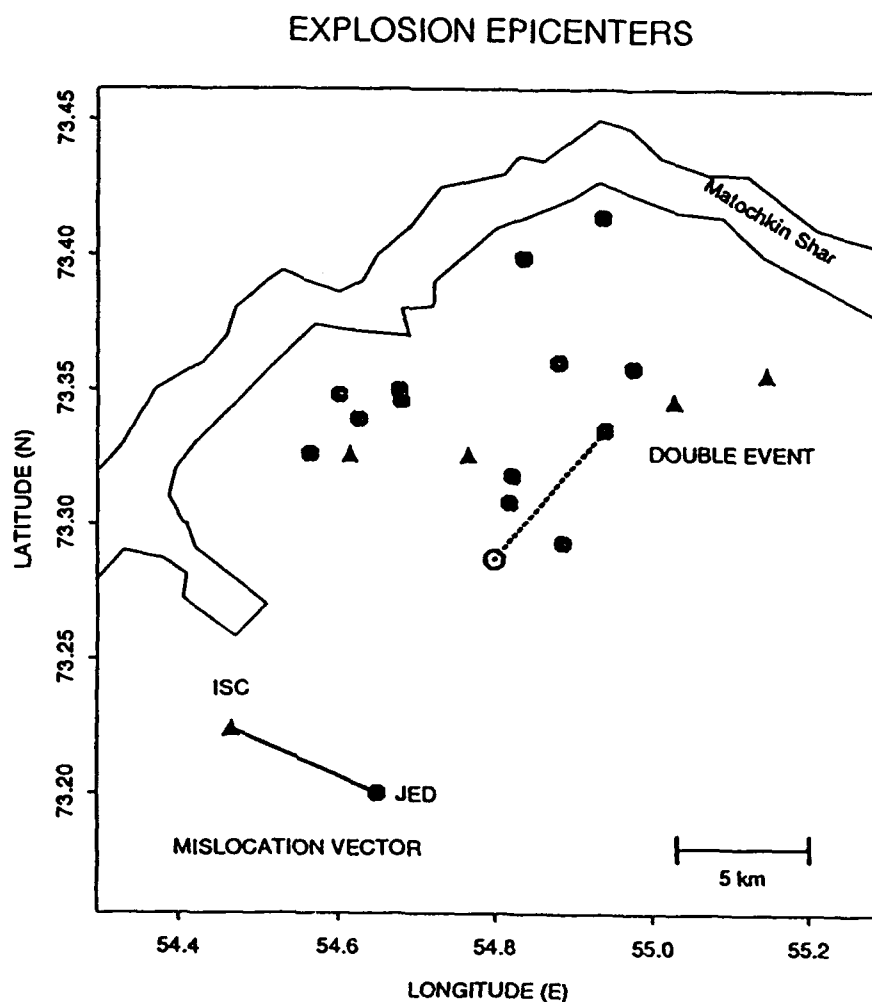
Figure 13: Explosion epicenters near Matochkin Shar. Epicenters determined by Lilwal and Marshall (1986) using the JED method (filled octagons) were used whenever available. For other events, ISC determinations corrected for the systematic difference between ISC and JED locations - indicated by the mislocation vector to the lower left - were used (filled triangles). The epicenter of the two explosions of the double event on 80/10/11 are connected with a dotted line, and the smaller of the two explosions is shown as an open octagon (after Stewart and Marshall, 1988).

36

Table 4: Explosions

Date	Time	Lat(N)	Long(E)	$m_b(ISC)$	Source*
64/10/25	07:59:57.8	73.386	54.997	5.1	JED
67/10/21	04:59:58.5	73.385	54.826	5.9	JED
68/11/07	10:02:05.5	73.388	54.873	6.1	JED
76/09/29	02:59:57.4	73.360	54.880	5.8	JED
76/10/20	07:59:57.0	73.399	54.835	4.5	JED
77/09/01	02:59:57.5	73.339	54.626	5.7	JED
77/10/09	11:00:00.3	73.414	54.935	4.5	JED
78/08/10	07:59:57.7	73.293	54.885	5.9	JED
78/09/27	02:04:58.2	73.350	54.677	5.6	JED
79/09/24	03:29:58.3	73.346	54.679	5.7	JED
79/10/18	07:09:58.3	73.318	54.821	5.8	JED
80/10/11**	07:09:57.0	73.335	54.938	5.7	JED
81/10/01	12:14:56.7	73.308	54.817	6.0	JED
82/10/11	07:14:58.2	73.348	54.601	5.6	JED
83/08/18	16:09:58.6	73.358	54.974	5.9	JED
83/09/25	13:09:57.7	73.326	54.564	5.8	JED
84/08/26	03:30:00.0	73.35	54.80	0.0	CSS
84/10/25	06:29:57.7	73.37	54.84	5.8	ISC
87/08/02	01:59:59.8	73.35	54.58	5.8	ISC
88/05/07	22:49:58.0	73.35	54.43	5.6	ISC
88/12/04	05:19:53.6	73.49	54.18	5.9	ISC

* (ISC= International Seismic Center, JED=Joint Epicenter Determination by Lilwal and Marshall, 1986, CSS= Center for Seismic Studies).
** (Double explosion according to Stewart and Marshall, 1988).

Leith *et al.*, (1990) compared a 1989 SPOT image of the Matochkin Shar with an aerial photograph from 1942 and found that the ridge area above the mouth of the Shumilikha river appeared disturbed by small circular areas with snow cover in several places. These features were interpreted as surface effects of underground nuclear tests. Figure 14, a close-up of the ridge area (around latitude 73.4N and 54.8E) shows that there is overlap between the locations of the small circular snow covered areas read from the SPOT image and JED locations of the Novaya Zemlya explosions located by Lilwal and Marshall (1986). The area, but not the orientation and lengths of the axes, of the ellipses of the 95 per cent confidence regions calculated by Lilwal and Marshall (1986) were available, so the dotted circles surrounding the JED epicenters, with $radius = \sqrt{(area/\pi)}$ in Figure 14 give some indication of the relative uncertainty in the JED locations.

Table 5 is a list of the seismic stations that recorded data for this study. Apart from sta-

Table 5: Seismic Stations

Code	Name	Lat(N)	Lon(E)	Dist. (degrees)	Max. Magnif. (k)
APA	Apatity	67.55	33.33	9.2	5.5
ARU	Arti	56.40	58.60	17.1	25
BOD	Bodaybo	57.85	114.18	27.4	52
CHS	Chusal	39.10	70.77	35.2	195
NRI	Norilsk	69.40	88.10	11.2	102
NVS	Novosibirsk	54.90	83.30	21.9	50
OBN	Obninsk	55.10	36.60	19.8	44
TLY	Talaya	51.68	103.63	29.8	36
UZH	Uzhgorod	48.63	22.30	28.7	44

tions CHS and TLY, the stations are all base stations of the Unified Seismic Observations System of the U.S.S.R. All waveforms (except four of those at APA) were recorded with the same type of seismometer, the standard vertical component SKM-3, but with different magnifications and instrument parameter settings. This resulted in somewhat different amplitude response curves for the stations, as shown in Figure 15. The four APA waveforms were recorded with a SX seismometer, supposedly older and less reliably constructed than the SKM-3. The other 16 waveforms at APA were obtained with a SKM-3 seismometer at two different gains; 14 with a low and 2 with a high gain. The frequency
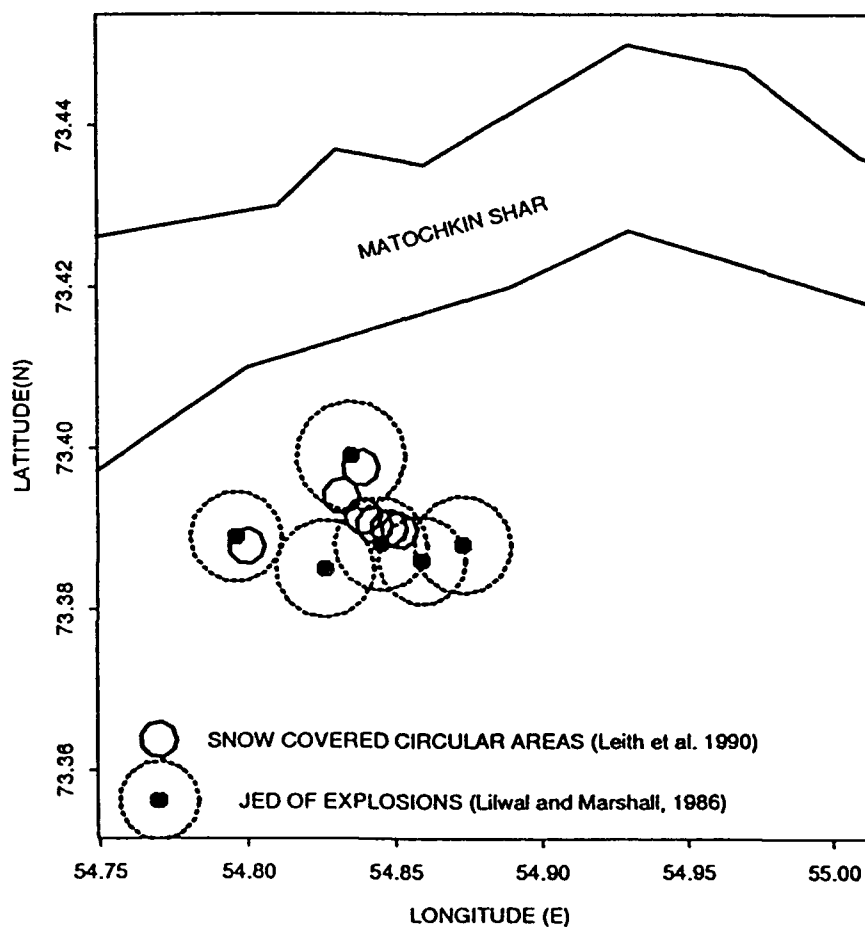
Figure 14: Comparison of explosion epicenters and snow covered circular areas read from a SPOT image analyzed by Leith *et al.* (1990) in the ridge area above the mouth of the Shumilikha river. The explosion epicenters determined by Lilwal and Marshall (1988) using the JED method are marked with filled symbols and associated 95% confidence circles. The circular snow covered areas are indicated as open octagons.

39
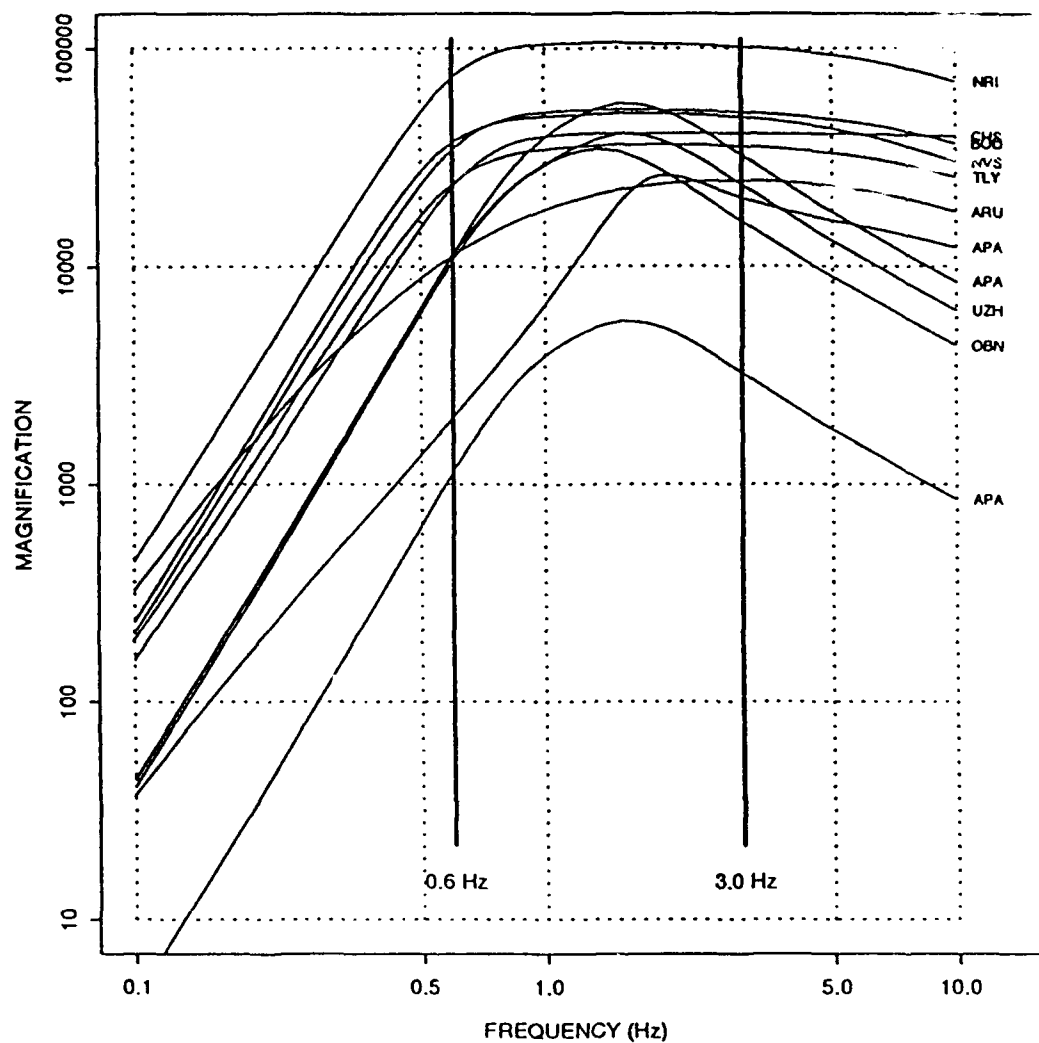
Figure 15: Typical amplitude magnification curves for the seismological stations. The three curves for APA represent those of a SKM-3 seismometer at two different gains and of a SX seismometer. The frequency band 0.6-3.0 Hz used in the calculations of RMS amplitudes is also indicated.

band from 0.6-3.0 Hz, which was used in the calculation of RMS values, is marked in the figure.

Seismograms of the explosion on 88/12/04 (and for 77/10/20 for station NRI) are shown in the record section of Figure 16. The traces are aligned on a manually picked first arrival time for the P phase and include one minute of noise window preceding the pick of the P onsets. Expected arrival times of the S and Lg phases are marked as solid lines. In addition, the limits of four time windows; initial P, P coda, S with coda, and Lg that were used for calculating RMS amplitudes (see below) are indicated with dotted lines. Although there is some variation in the waveforms from explosion to explosion, the data in Figure 16 are representative of the entire data set. Clear Lg phases with a group velocity around 3.5 km/s can be seen only at stations APA and ARU. The absence of clearly developed Lg phases at the other stations could be due to blockage by large thickness variations in the sedimentary basins of the Barents and Kara Seas as suggested by Baumgardt (1990): the Lg energy trapped in such basins is redirected and dissipated by scattering and attenuation. However, significant energy at the expected arrival time for the S phase can be seen for the nearest stations APA, NRI, and ARU. At the next distant stations, OBN and NVS, only a minor increase of the S coda level is observed. At stations BOD and UZH, which are further away, this increase of the coda level is still present but seems to be delayed about 30 s relative to the expected arrival time for S.

There were 111 waveforms available from the nine stations for the 21 explosions. The distribution of waveforms over stations and explosions is evident from the calculated magnitudes in Tables 7 through 10. There are gaps in some of the recorded waveforms in one or more of the windows for P, P coda, S with coda, or Lg phases. Magnitudes were not calculated for time windows with gaps in the data longer than one second. There were only three waveforms for the station NRI; one of them with significant gaps. The analysis was, therefore, based mainly on waveforms from the other eight stations.

Calculation of RMS Amplitudes

An RMS magnitude as a measure of explosion source size was defined by Ringdal (1983) for the Lg phase and analyzed for NORSAR recordings of explosions from the Balapan region of the Semipalatinsk test range. A time window of 120 seconds starting 40 seconds before the Lg arrival was used to calculate the RMS amplitude. If we assume that the Lg phase has a group velocity of 3.5 km/s this corresponds to a group velocity window of 3.28-3.62 km/s. A very similar definition was used by Ringdal and Hokland (1987) with a time window of 120 seconds corresponding to group velocities between 3.33 and 3.67 km/s. The time windows used in these studies were centered on a group velocity of 3.5 km/s. Hansen *et al.* (1990), calculating RMS magnitudes of Balapan explosions for stations at
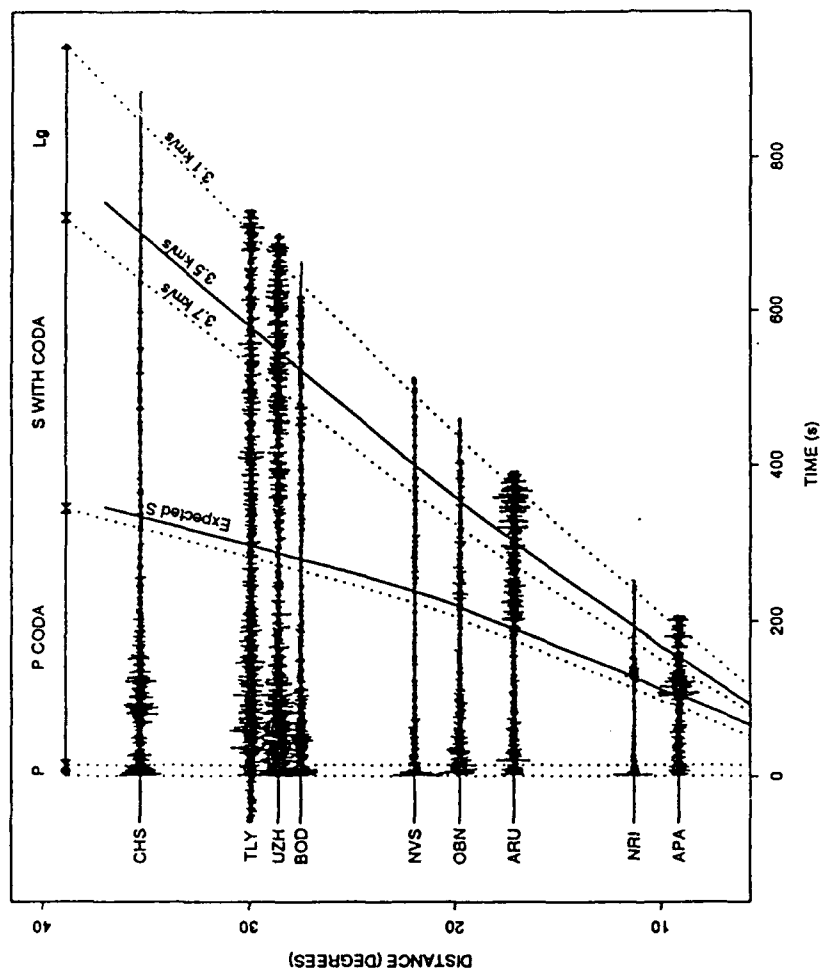
Figure 16: Waveforms of the explosions on 88/12/04 (and for 77/10/20 for station NRI) plotted as a function of epicentral distance and aligned on visually read first arrival times. Expected arrival times of the S phase and the Lg phase (group velocity 3.5 km/s) are drawn as filled lines. The windows used in the calculations of RMS amplitudes for P, P coda, S coda, and Lg are shown as dotted lines.

various epicentral distances also used a 120 second time window and chose the largest value of a RMS trace centered near the 3.5 km/s group velocity to represent the RMS amplitude. They concluded that consistent station RMS magnitudes were obtained for both a time window fixed at 120 seconds and one based on a range of Lg group velocities. A fixed time window of two minutes, however, results in a substantial variation in the range of group velocities for stations at different epicentral distances. The time window may, indeed, cover phases other than Lg. This, together with the large range in epicentral distances (9-35 degrees) of the stations analyzed here and the absence of clearly developed Lg phases at most stations for the Novaya Zemlya events, lead us to consider RMS values not only for the Lg phase, but also for other phases. Rather than using a fixed time window, we employed time windows that were related to seismic phases, which in turn lent themselves more conveniently to geophysical interpretation.

For each waveform we calculated RMS amplitudes corresponding to windows of the initial P phase (from P onset to 20 s after onset), the P coda (20 s after P onset to 15 s before the expected S arrival), the S phase with coda (15 s prior to the expected S arrival to a group velocity of 3.7 km/s), and the Lg phase (the group velocity window 3.1-3.7 km/s). The four data windows are indicated in Figure 16. The 20 s window for the initial P wave has, of course, the same length for all stations, whereas the lengths of the windows for the other phases varied with epicentral distance. In order to account for differences in instrument responses among the stations, the calculated RMS amplitudes were normalized to a common instrument: that of the SKM-3 seismometer at station OBN. As the instrument calibrations for the stations also fluctuate with time, the calibration for 1988 of the OBN seismometer was chosen as a reference. The normalization to this particular instrument was carried out in the frequency domain for computational convenience. Parseval's theorem affirms the equivalence of time and frequency domain computations.

The calculation of the RMS values was based on traces filtered between 0.6-3.0 Hz (three pole Butterworth). These frequency limits conformed to band pass filters used by Hansen *et al.* (1990), who found that consistent station RMS magnitudes were obtained as long as the band pass enhanced the main part of the Lg energy. A noise correction was also applied using the RMS amplitude of the available noise data up to five seconds preceding the manually picked P onset (usually 115 seconds of data). Noise corrected RMS values were transformed into a logarithmic scale and could be written as:

$$rms_{ij}(k) = \frac{1}{2}\log\left[\frac{1}{M_j(k)}\sum_{m_{j1}(k)}^{m_{j2}(k)} x(t)_{ij}^2 - \frac{1}{N}\sum_{n_1}^{n_2} x(t)_{ij}^2\right]$$

where $rms_{ij}(k)$ defines the RMS value of phase k at station j from explosion i, and $x_{ij}(t)$ represents the associated filtered seismic waveform (normalized to the reference OBN instrument response) sampled at times t (sampling rate 20 Hz). The lengths of the time windows of the noise sample is denoted N (115 s), and its time limits are n_1 and n_2. The limits and lengths of the windows of the fo ir phases at station j are denoted $M_j(k)$, $m_{j1}(k)$, and $m_{j2}(k)$, respectively.

The hand digitized waveforms had gaps of one second duration at minute marks. As the windows could start at any time relative to the minute mark, the number of such gaps varied from waveform to waveform. The standard deviation of this error was estimated to be 0.005 magnitude units for the shortest window used (20 s for the initial P).

The signal-to-noise ratios, SNR, of the RMS Lg amplitudes were generally high for the 15 large explosions. The average SNR value obtained as the base 10 exponent of the mean of the logarithm of the ratios, was, as one might expect, strongly dependent on distance. Apart from APA, the average SNR values decreased with distance according to the approximate relation: $\log(SNR) = 6.57 - 3.86 \log(D)$, with D being the epicentral distance in degrees. The SNR at APA was more than a factor of 10 below what would be projected from this linear relation. This low value at APA may have been due to the low magnification (only about 5.5k) for most of its waveforms and a bias may have been introduced by noise in the hand digitization process. There was fairly little variation among explosions (i.e., the suite of 15 large events) for a given station; the standard deviation of the logarithm of the SNR varied between 0.11 to 0.25. As some of this variation was due to variation in signal strength, this means that the noise levels at the stations in this frequency band were fairly stationary. One reason for expecting such stability is that many of the recordings were obtained in the early morning, local time.

RMS amplitude (uncorrected for noise) ratios for the P phase, the P coda, and the S coda relative to the Lg phase were also calculated for the 15 large explosions. The average values of these ratios (obtained like the average SNR for Lg above) varied with phase and station. For the initial P and the P coda, the ratio had a positive correlation with epicentral distance. This was expected as the amplitudes of the different phases decay at different rates with distance. There was no such correlation for the S coda ratios. The P coda and the S coda ratios were not significantly above two except for the P coda ratio at BOD and CHS. However, the RMS amplitude was somewhat larger for the S coda than for Lg for all stations except for ARU and UZH. For a given station and phase, the variation in the amplitude ratio from explosion to explosion was very small and only above 0.1 (on a logarithmic scale) for the ratios at CHS, the initial P phase at ARU and BOD, and the P coda ratio at ARU. The relatively large variation for CHS may have been due to outlying values (see following section).

44

Station Magnitudes

The calculated RMS amplitudes, rms_{ij}, normalized to the OBN instrument, band pass filtered, corrected for noise, and transformed to a logarithmic scale were then used to compute station magnitudes. As the epicentral distances between a given station and the events are almost the same, the station magnitudes, $m_{ij}(k)$, were computed by normalizing the rms_{ij} values of the $m_b(Lg)$ determined for the NORSAR array, NAO, by Ringdal (1991): $m_{ij}(k) = rms_{ij}(k) + c_j(k)$ where the normalization term was obtained in a straightforward manner: $c_j(k) = 1/n \cdot \Sigma (rms_{ij}(k) - m_{iNAO}(Lg))$. The normalization terms were determined from events with similar magnitudes, $m_{iNAO} = 5.603\text{-}5.807$ and applied to all rms_{ij} values for calculation of station magnitudes. The resulting magnitudes are listed in Tables 7 through 10, which also give network magnitudes and standard deviations for each event (denoted NET and S.D2. respectively in the tables and obtained according to the procedures below). The standard deviations of station magnitude residuals relative to network magnitudes are also included in Tables 7 through 10 (denoted S.D; their definition is given below).

Hand digitized waveforms are bound by their very nature to have limited data quality compared to modern seismic recordings. Furthermore, the data analyzed here was based on incomplete information on station seismometers and instrument calibrations. Because of these circumstances, the station magnitudes were initially searched for outlying data that was omitted in the subsequent analysis.

For this purpose, we employed a simple additive source-path model for the station magnitudes. This model assumed that the station magnitudes, $m_{ij}(k)$, at station j from event i and phase k could be written in the form:

$$m_{ij}(k) = \mu_i(k) + v_j(k) + \varepsilon_{ij}(k)$$

where m and n represent the network magnitude and station correction terms respectively. The latter terms should, of course, be close to zero, as the station magnitudes have been normalized to the same scale. The error terms, $e_{ij}(k)$, were assumed to be Gaussian and independent with zero mean and equal standard deviation, $\sigma(k)$. In addition, we imposed the condition that $\Sigma v_j = 0$. This additive model was approximately valid for the 15 large explosions, i, as they all had similar magnitudes and effects due to differences among stations in amplitude scaling with source strength were negligible.

The network magnitudes, station corrections, and the standard deviation were estimated by a least squares procedure from the over-determined system of equations. The values of

the magnitude residuals $\rho_{ij} = rms_{ij}(k) - \overline{\mu_i(k)} - \overline{v_j(k)}$, were then used as a criterion for detecting outliers ($\overline{\mu_i(k)}$ and $\overline{v_j(k)}$ network magnitudes and station corrections that were obtained from the least squares estimation). The empirical distributions of the RMS residuals are shown in Figure 17.

Outliers were identified with the least squares procedure in an iterative fashion. First, the least squares procedure was applied to all of the station magnitudes for Lg and the residual with the largest absolute value was removed, if sufficiently large. The procedure was then applied to the truncated data and so on, until no outlier remained. The same iterative procedure was applied to the station magnitudes of the other phases one at a time, S coda, P coda, and initial P. This resulted in 10 waveforms, with large residuals, being classified as outliers. The outlier data is summarized in Table 6

Table 6: Outlier Data

Date	Station	Residuals (m.u.)			
		P	P Coda	S Coda	Lg
76/09/29	CHS	-0.510	-0.436	-0.224	
76/09/29	OBN			0.248	0.293
77/09/01	UZH	-0.274		-0.216	-0.176
78/09/27	ARU		-0.267		GAP
81/10/01	CHS	-0.521	-0.421	-0.336	
83/08/18	ARU	-0.261	GAP		
84/10/25	APA			0.195	
84/10/25	UZH			0.140	
88/05/07	BOD	-0.227			
88/12/04	CHS			0.133	

and the outlying data points are also marked along with the empirical distributions in Figure 17. Four of the waveforms in Table 6 have outlying residuals for more than one type of magnitude (i.e., P, P coda, S coda, or Lg), Outlying values for these four waveforms may, therefore, be due to use of faulty instrument corrections. Possible sources of error for the other waveforms are less obvious, apart from the waveform 84/10/25 at UZH, which probably was caused by signal interference (a large impulsive signal appears in the S coda window). Whatever the reasons, the outlying data points were omitted in our subsequent

46
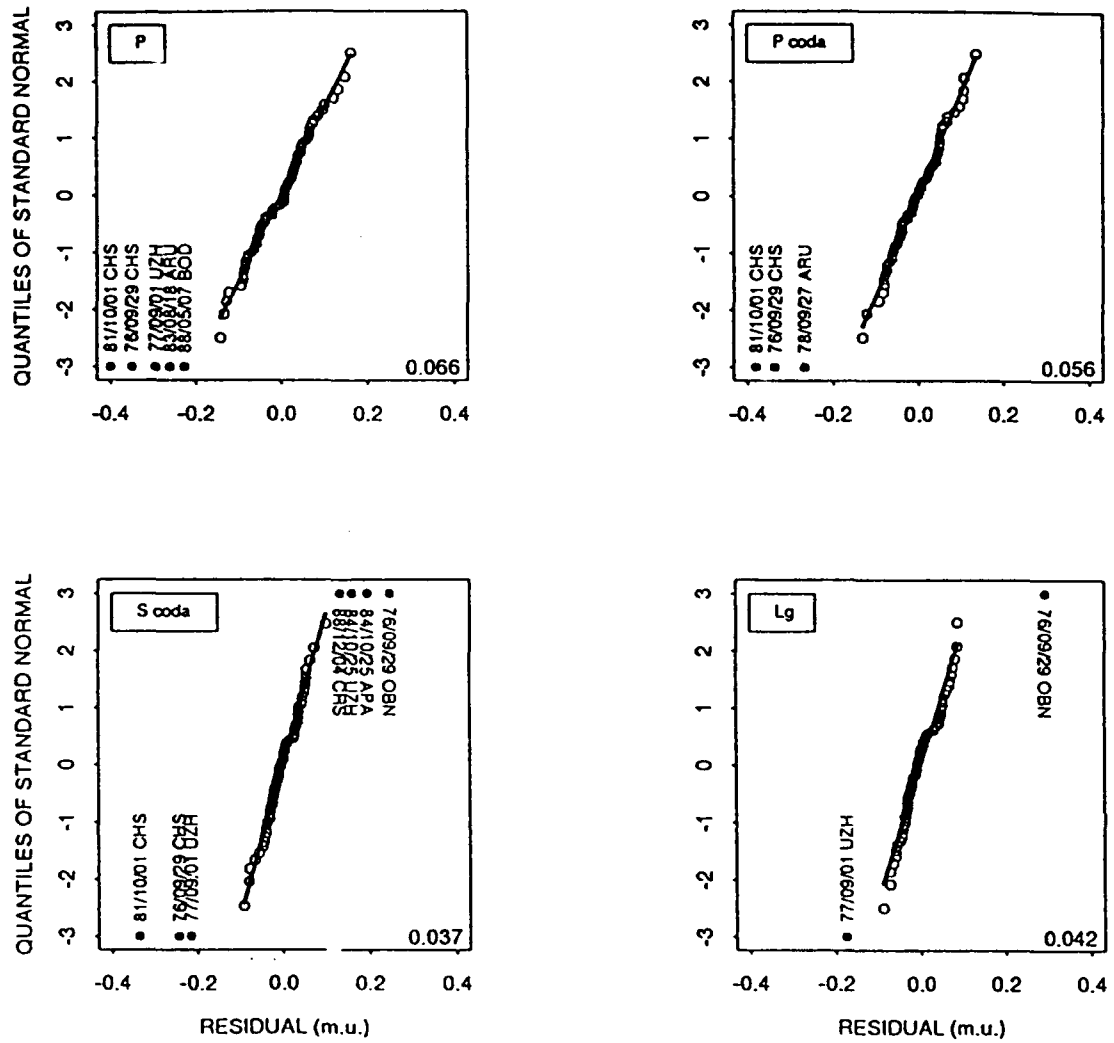
Figure 17: Empirical distributions of residuals for P, P coda, S coda, and Lg station magnitude residuals. Outlying data points are identified with explosion date and station code. In some instances these data points have been displaced for readability of the identification (see also Table 6). Standard deviations (in m.u.) are given in the lower right corner of each panel. The vertical scaling is that of a standard normal distribution, and lines inversely proportional to the standard deviations have been drawn for comparison. Apart from the outliers, the empirical distribution closely approximates that of a normal distribution.

analysis.

The standard deviations of the residuals (after removal of outliers) are also given in Figure 17. The smallest value, 0.037 (m.u.), was obtained for the RMS magnitudes of the S window. However, the difference between the values for the Lg and the S coda is hardly significant. The standard deviations in Figure 17 were based on the assumption of equal standard errors in the station magnitudes. Variations among the stations are, however, quite possible. For example, some of the scatter in station magnitudes may be contributed by the instrument corrections that were applied, and the possibility that the accuracy of the available information on instrument characteristics vary from station to station. The standard deviations of the station magnitude residuals, S.D. in Tables 7 through 10, have been summarized in Figure 18 for each phase window and station. The S.D3 values were obtained from data for the suite of 15 large events. This summary suggests that there may be differences in standard errors among station magnitudes. The small numbers of observations, however, make precise estimates of standard errors of individual station magnitudes difficult.

The S.D3 values for Lg ranged between 0.034 and 0.057 and the median value of 0.047 was somewhat higher than the standard deviation of about 0.03 at a single station for Balapan events obtained by Hansen *et al.* (1990). The station standard deviations for RMS values of Balapan events (five single stations and one array) were based on misfit errors to linear relations estimated between RMS values of station pairs. There was some variation in the misfit error among station pairs (0.022-0.038) for the Balapan data. Furthermore, for most of the station pairs only a small number (6 or less) of common observations was available and the associated misfit error might have been underestimated. Bearing in mind that there were only a small number of observations available in some cases and the apparent variation in standard deviation among stations, it is difficult to conclude, with a high degree of confidence, that the station standard deviations for the Novaya Zemlya events obtained here are generally larger than those for the Balapan events obtained by Hansen *et al.* (1990).

Network Magnitudes

In order to calculate network Lg magnitudes we solved the over determined systems of equations for the additive model, described above, after having removed all outlying data points. This was done for the 15 large events and the 3 small events separately. Although there may be differences in the standard deviations of the station magnitudes for a given phase, we assumed, for the sake of simplicity, that the standard deviations were the same, rather than employing a weighting scheme. The values of the network magnitudes spanned almost two magnitude units and their distribution is shown in Figure 19. The esti-

48
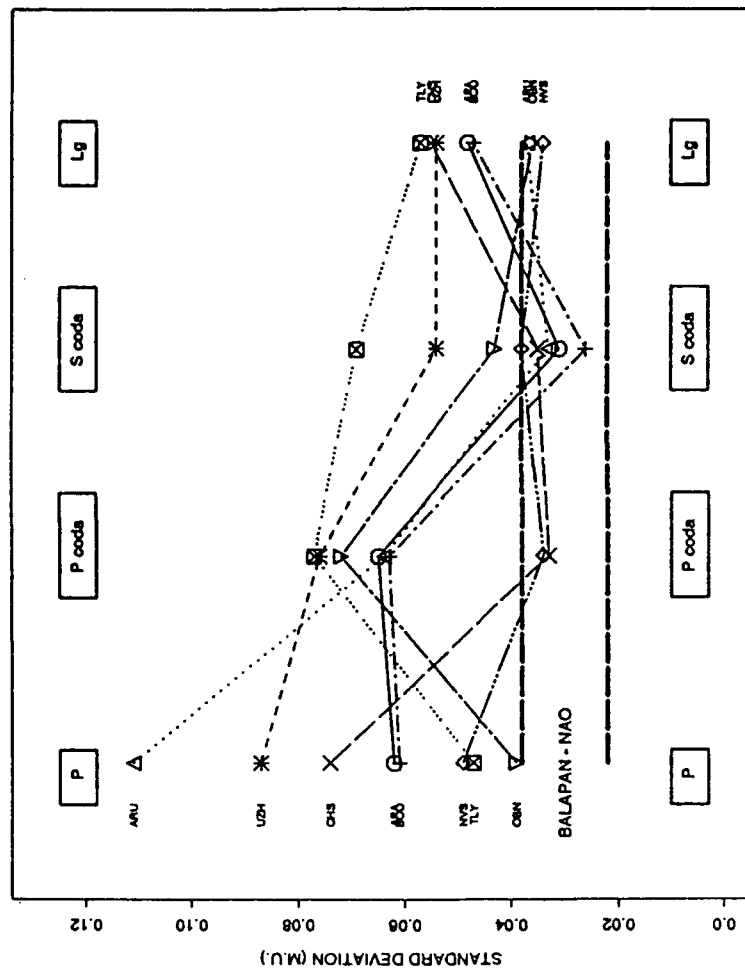
Figure 18: Standard deviations of station magnitudes obtained from the station magnitude residuals (S.D3 in Tables 7 through 10). The heavy dotted horizontal lines represent the range of variation of the standard deviations for station magnitudes for large explosions at the Balapan portion of the Semipalatinsk test range obtained by Hansen *et al.* (1990).
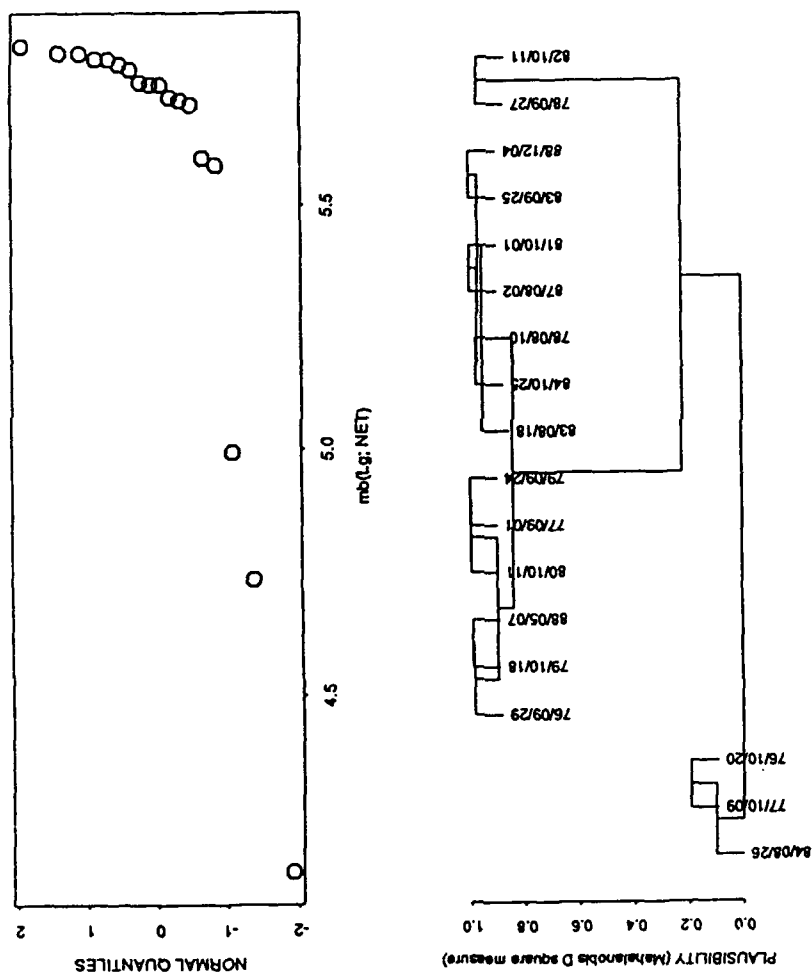
Figure 19: The upper panel shows the empirical distribution of the network Lg magnitudes, $m_b(Lg;NET)$. The lower panel is a dendogram used to formally cluster the network Lg magnitudes.

50

mated standard errors of the network Lg magnitudes (S.D2 in Table 7) depend on the number of station magnitudes and vary between 0.020 (7 stations) and 0.031 (3 stations) with a median value of 0.022 (5 stations). These standard deviations are comparable or mostly larger than the S.D1 values for the events in Table 7. The standard deviation S.D1 for an event is defined (only if more than three observations) as the standard deviation of the station magnitudes divided by the square root of the number of station magnitudes available for the event. Partly, because of the small number of observations and reduced number of degrees of freedom, the estimated standard errors (S.D2) for the three small events are comparatively large.

Due to the apparent clustering of the network Lg magnitudes in Figure 19, we attempted to group the events with a formal procedure by applying hierarchical clustering (Becker *et al.*, 1988). For this purpose we used a one-dimensional version of Mahalanobis D2 measure (Rao, 1967) as a measure of closeness between two network magnitudes, μ_i and μ_j with estimated errors, S.D2$_i$ and S.D2$_j$:

$$D_{ij}^2 = (\mu_i - \mu_j)^2 / 2 (SD2_i^2 + SD2_j^2)$$

and normalized this to "plausibility" by forming $exp(-D_{ij}^2)$. The lower panel in Figure 19 *shows the results of this hierarchical clustering* with connected linkage, as a cluster tree, or dendogram. Dates identify each event. The events are grouped into two clusters at "plausibility" levels above 0.80. The large group contains thirteen events and the small includes only two explosions. There is no obvious geographical pattern that can be related to the clustering according to network magnitude. Although the plausibility level at which we have grouped explosions with the dendogram seems reasonable (above 0.8), it is none the less somewhat arbitrary.

Figure 20 compares the network and station magnitudes for twelve of the 13 events in the large group with $m_b(P;tele)$. The data for the explosion on 76/ 09/29 is not included since it is based only on three stations. Being based on short period teleseismic body waves recorded at a world wide network, the $m_b(P;tele)$ were obtained with a maximum likelihood procedure that not only includes station corrections, but also accounts for near source focusing effects. The standard deviation of the network magnitudes, $m_b(Lg; NET)$, for these twelve events is only 0.036 m.u. On the assumption that the network magnitudes is a direct measure of actual explosion yield, it can be concluded that these twelve events had almost identical yield. As the standard deviation of the network magnitudes is about the same as the estimated standard error of an individual network magnitude, all scatter among the twelve magnitudes might be attributed to the uncertainty in the RMS measure-

51
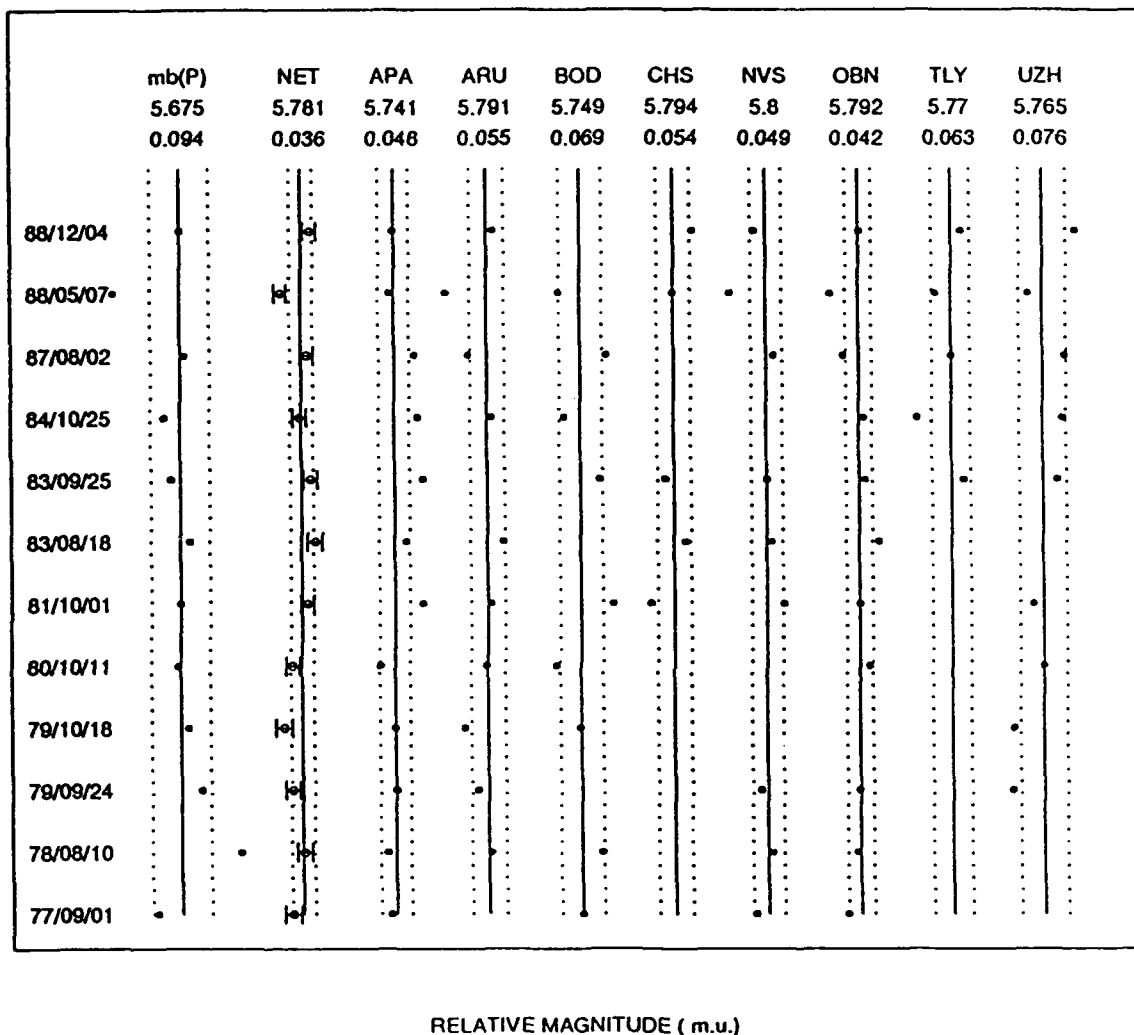
Figure 20: Comparison of magnitudes for 12 of the Novaya Zemlya explosions with dates given to the far left. The type of magnitude with associated average and standard deviation of the 12 explosions are given at the top of the diagram.

ments. The standard deviations for the station magnitudes of the twelve events are all clearly higher than 0.036. If the twelve explosions were almost identical in strength and if the station magnitudes were independent, one would, indeed, expect the standard deviation of the network magnitudes to be smaller than those of the individual station magnitudes. The comparison of magnitudes in Figure 20 show a clear difference between the $m_b(P;tele)$ and the Lg magnitudes. The standard deviation of the $m_b(P;tele)$ is about three times that of $m_b(Lg; NET)$. The large scatter for $m_b(P;tele)$ is due in particular to the data for the two explosions on 78/08/10 and 88/05/07. No similar discrepancy can be noted for the presumed double event on 80/10/11.

Although the standard deviations for the network magnitudes (S.D2 in Tables 7 through 10) of two of the small events are higher than those for many of the large events, one cannot readily attribute this to poor signal-to-noise ratios. The signal-to-noise ratios were well above 1.5, which is, according to Hansen (1990), the lower limit for reliable RMS amplitude estimates at a single site. For example, station magnitudes for NVS are generally low compared to those for BOD. This may be a result of differences in scaling of the station magnitudes with source strength. If this were the case, scatter would be introduced in the network magnitudes based on the additive model or on a straight averaging of station magnitudes. Variation in scaling with source strength among station magnitudes should therefore be accounted for when calculating network magnitudes. This was, however, not attempted here because of the limited amount of data.

The station magnitude residuals were somewhat independent among the phases. Figure 21 shows the station residuals plotted against one another for P, P coda, S coda, and Lg.In the figure a station magnitude residual for a given event is defined as the difference between the station magnitude and the average of the magnitudes of the other stations for that event. Correlation values, with standard deviations obtained from bootstrapping, are given in the scatter diagrams of Figure 21. The correlation is smallest for P and Lg values, but P coda and Lg data also show weak correlation despite the use of the same frequency band for the different phases. This independence between magnitude types may be utilized to improve magnitude estimates by combining uncorrelated magnitudes, for example, using the inverses of the variances of the magnitudes as weights. The maximum theoretical reduction in standard error for combining two independent magnitude types is about 30%. This occurs if the two types have equal standard error; if they are clearly different the reduction becomes marginal. For the purpose of illustration, we applied a weighted scheme to the group of 12 explosions with very similar Lg network magnitudes (see Figure 20). On the assumption that these events were of virtually identical strength, we expected a reduction in the standard deviation of the Lg magnitudes (0.036) of the 12 events when combining them with, for example, the P magnitudes. Using standard devia-

53
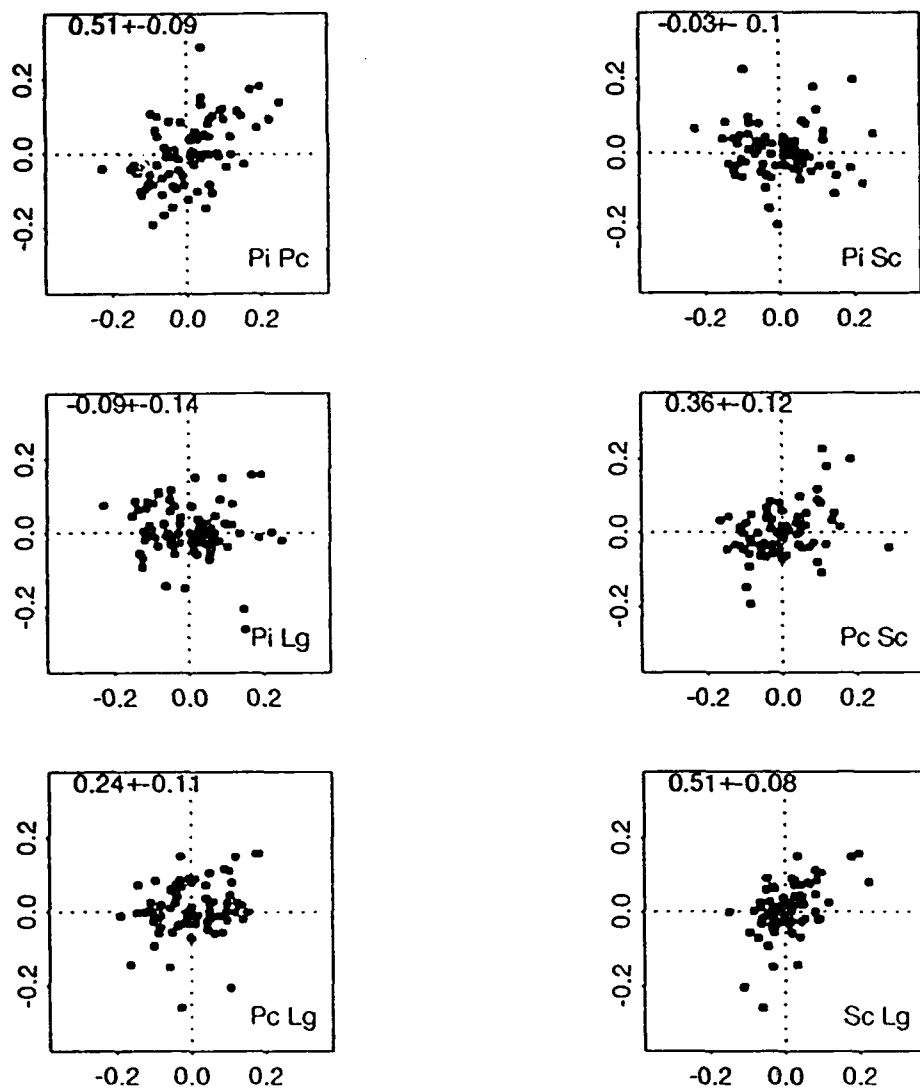
Figure 21: Pair-wise comparisons of station magnitude residuals according to phase - Pi (initial P), Pc (P coda), Sc (S coda), and Lg. The phases of the pairs are indicated in the lower right part of each panel. The correlation with associated standard deviation is given for each combination of magnitude pair.

tions $\sigma(Lg) = 0.022$ and $\sigma(P) = 0.036$ (median values for network magnitudes) in a weighted summation, the standard deviation of the magnitudes of the nine events was reduced, but only to 0.035. A combination of RMS Lg and P coda magnitudes gave an even smaller reduction, and it should be stressed that the assumption about identical strengths of the 12 events may, of course, not be correct; the marginally smaller standard deviation obtained for combined Lg and P magnitudes could well be fortuitous because of the small number of events.

The diagrams in Figure 22 compare some of the RMS magnitudes (in Tables 7 through 10) with the network magnitudes $m_b(P;tele)$ determined by Jih and Wagner (1992). The scatter diagrams in Figure 22 give slope and standard deviations of misfit errors obtained with the least squares method as adapted to seismic yield estimation by Ericsson (1971). The slopes vary somewhat suggesting differences in scaling with source strength between $m_b(P;tele)$ and the RMS magnitudes. For example, the $m_b(Lg)$ slope is larger for NVS (0.95) than for BOD (0.87). Thus, the P magnitudes, $m_b(P;tele)$ and $m_b(P;NVS)$ appear to be more sensitive to change in explosion yield than $m_b(Lg)$.

The differences in scaling with source strength among the network magnitudes, as illustrated by the slopes of the linear relationships in Figure 22, suggest that the smaller sensitivity to change in explosion yield for the RMS Lg magnitudes relative to that of $m_b(P; tele)$ might contribute to a smaller standard deviation of magnitudes for events with similar strengths. Such a "compressing" effect could contribute to the apparently small standard deviation of the RMS Lg magnitudes for the events in the group of 12 explosions (see Figure 20). The standard deviation of the magnitudes for these events is, however, still remarkably small even if this effect is accounted for. For example, if we assume that $m_b(P;tele)$ scales with explosion yield, W (logarithm of base 10 in kilotons), like $dm_b(UK)/dW = 0.75$, and that the scaling for RMS Lg is dm(RMS Lg)/dW = 0.65, then the 0.02 standard deviation of the network RMS Lg magnitudes would translate into an explosion yield uncertainty of about 15% at the two sigma level. This can be compared with the 60% uncertainty obtained by Patton (1988) for subgroups of events with uniform coupling at the Nevada Test Site using data recorded at a local network. The 15% uncertainty can, of course, be related only to relative measurements of yields of explosions with similar coupling as well as other detonation conditions. Although Lg amplitudes may be not affected by source coupling uncertainties to the extent that P waves are (Patton, 1988), it must be emphasized that the RMS Lg magnitudes of events with variations in source coupling, that cannot be corrected for by calibrations, may still be significantly biased. It may, indeed, be difficult to even estimate the uncertainty in seismic yield in such cases.

Earlier studies of explosions at the Semipalatinsk test range have revealed systematic variations in the magnitude difference, $m_b(P)-m_b(Lg)$, across the test range. For example,

55
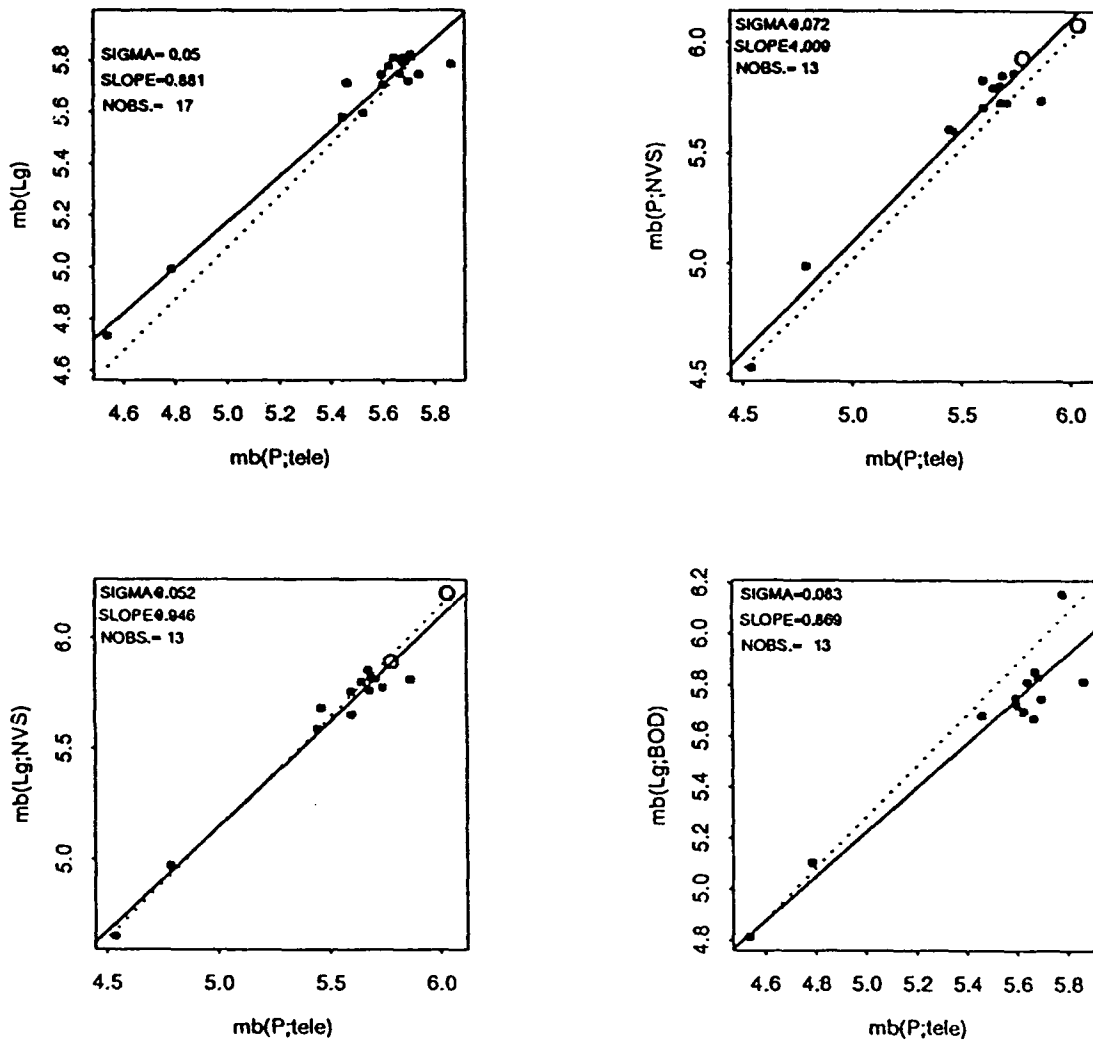
Figure 22: Pair-wise comparison of magnitudes - $m_b(P;tele)$, $m_b(Lg;NET)$, $m_b(P;NVS)$, $m_b(Lg;NVS)$, and $m_b(Lg;BOD)$. Estimated slopes, misfit errors (denoted SIGMA and give in m.u.), and number of observations are given in the upper left for each pair.

Ringdal and Marshall (1988) found that this difference was about 0.15 magnitude units higher for explosions in the Southwestern than in the Northeastern part. Ringdal and Marshall (1988) suggested that this effect is most likely a result of differences in P recordings, due to strong focusing effects in the upper mantle. As mentioned above, the explosions at Matochkin Shar are spread over an area with a diameter similar to that of the Balapan at Semipalatinsk. Because of the considerable variation in topography near Matochkin Shar - the elevation changes from 0 to about 800 m over 2-3 km in some parts - attempts have been made to evaluate the topographic effects on $m_b(P)$ and $m_b(Lg)$ with three-dimensional numerical simulations by Frankel and Leith (1991). These theoretical results, which are preliminary in nature, suggest that the azimuthal variation in teleseismic $m_b(P)$ would be less than 0.05 m.u., whereas for $m_b(Lg)$ this variation for vertical component could be up to 0.1 m.u. at close distances; the effect for Lg would diminish with increasing distance. In Figure 23 we have plotted the difference $m_b(P)$-$m_b(Lg)$ as a function of the explosion epicenter for some magnitude pairs. No consistent pattern emerges from the diagrams except for station OBN; the difference $m_b(P;OBN)$-$m_b(Lg;OBN)$ appears to be positive and negative in the western and eastern portions respectively. Also, the event 78/08/10 with the large difference $m_b(P;tele)$-$m_b(Lg;NET)$ (see Figure 20) has the southern most location of the explosions. Because of the high consistency of $m_b(Lg)$ between station pairs it appears that $m_b(Lg)$ - contrary to the theoretical results for close distances by Frankel and Leith (1991) - is not subject to strong azimuthal variation. The stability of $m_b(Lg)$ suggests that the observed variations of the magnitude difference $m_b(P)$-$m_b(Lg)$ across the Matochkin Shar test site is more likely caused by variations in $m_b(P)$. As the theoretical results of Frankel and Leith (1991) point to small azimuthal variation of $m_b(P)$ due to topography, the variation in $m_b(P)$ has to be due to other factors, such as strong focusing in the upper mantle, which seem to be in effect at Balapan.

Attenuation with Distance and Station Site Amplifications

The normalization constants $c_j(k)$, determined for each station j and phase k to bring the RMS amplitudes, rms_{ij}, on a standard magnitude scale, provide some insight into the attenuation and station site amplifications for the various phases. We normalized the $c_j(k)$ constants to path terms, $p_j(k)$: $p_j(k) = c_j(k) - c(k)$.

The eight path terms, defined in this manner, are plotted in Figure 24 for each phase as a function of epicentral distance. For the sake of comparison, amplitude attenuation curves have been drawn in the diagrams as dashed lines. A P wave attenuation curve for Western U.S.S.R. (referred to as Slunga-Kaila-Sarkar in GSE/SW/62, 1988) is drawn for the P and P coda, and the amplitude distance formula, $\Delta^{-1/3}(\sin(\Delta))^{-1/2}e^{-\gamma\Delta}$, used by Nuttli (1986), is drawn for the path terms of the S coda and Lg with $\gamma = 0.0012$ km^{-1}, typical of several
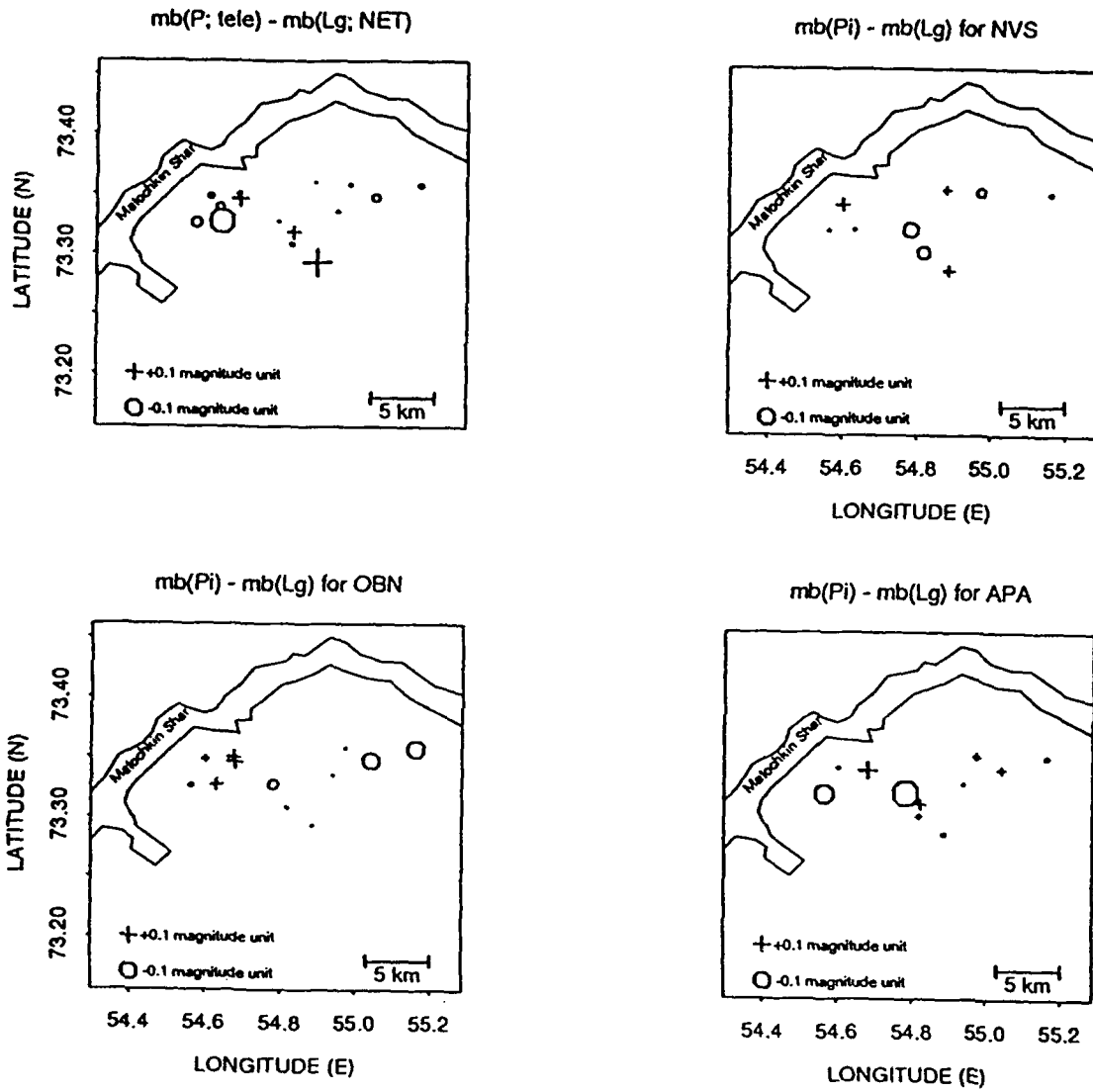
Figure 23:   The difference $m_b(P)$-$m_b(Lg)$ as a function of epicenter location for station (APA, NVS, and OBN) and network magnitudes.

58
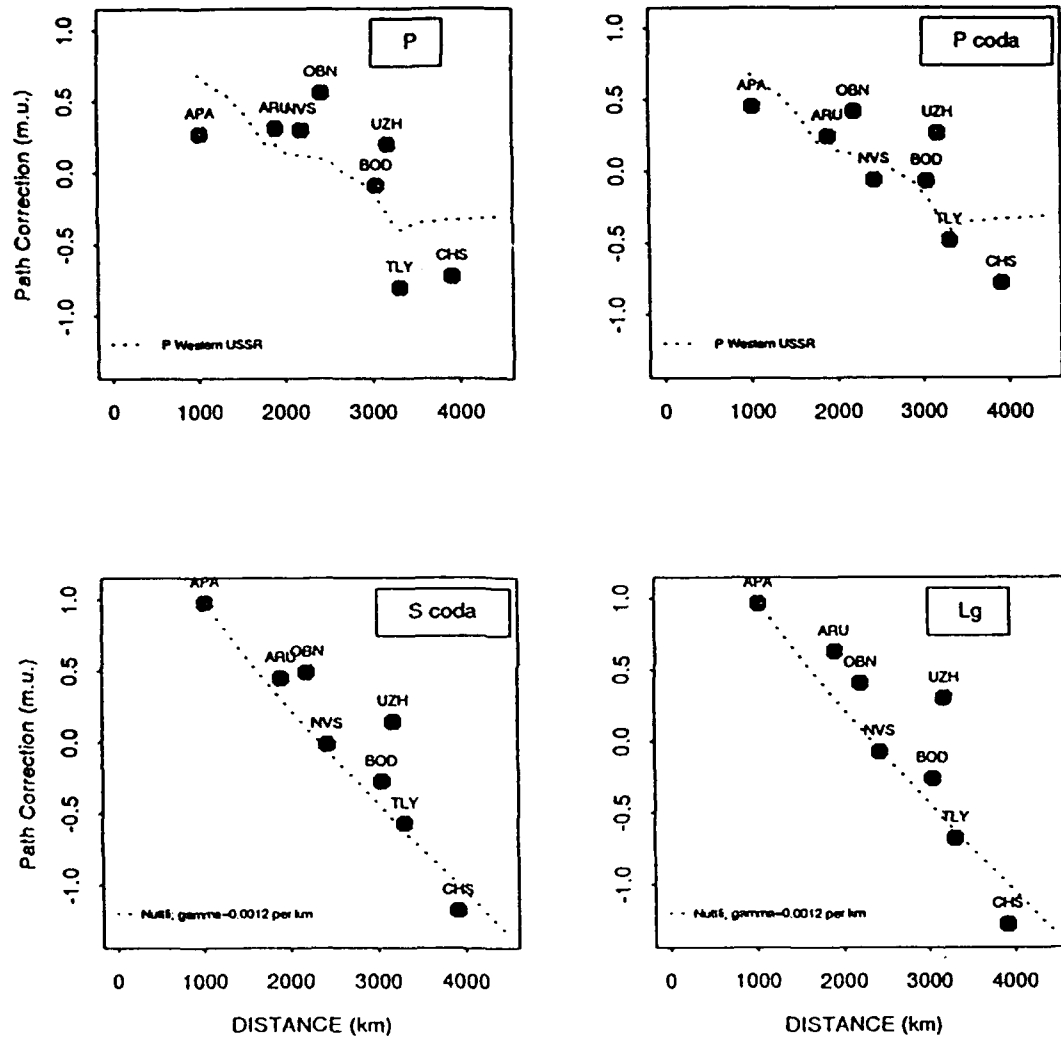
Figure 24:   Magnitude path corrections as a function of epicentral distance according to phase type. Amplitude distance curves - dotted lines defined in the text - are shown for comparison.

paths for Lg RMS amplitudes in Western and Central U.S.S.R (Israelsson, 1991). The curves, which, in particular for the S coda and Lg, are in overall agreement with the data, have been adjusted vertically in the figure to a level that approximately fits the data points.

Finally, in Figure 25 we have plotted station site amplifications defined as, $t_j(k) = p_j(k) - B_j(k)$, where the amplitude distance curve, $B_j(k)$, depends on the phase k according to the formulas described in the previous paragraph. The site amplifications for a given station are, on the whole, consistent among the phases. This is particular true for the S coda and Lg. For the P phase and P coda the amplifications at APA, CHS, and TLY are, however, strikingly different from those of the S coda and Lg.

Some Concluding Remarks

In this paper we have analyzed RMS magnitudes calculated from hand digitized recordings at nine standard seismological stations in the U.S.S.R of explosions at Novaya Zemlya including a suite of 15 large events with similar magnitudes.

Although there were clearly developed Lg phases at only two of the stations, APA and ARU, the Lg coda had sufficient signal-to-noise for calculating RMS magnitudes for the smallest explosion, with m_b around 4. Furthermore, the consistency among station RMS values based on a 3.1-3.7 km/s group velocity window is comparable to results based on modern high quality digital recordings from explosions at the Semipalatinsk test range. Estimates of the standard deviations of station RMS values vary among the stations about a median value of 0.047.

Network RMS Lg magnitudes based on the least squares method appear more robust than station magnitudes and had estimated standard errors around 0.02 (for five stations). If we account for magnitude-yield scaling, this translates to uncertainties in relative explosion yield of about 15% at the two sigma level for explosions with similar source coupling.

The Lg network magnitudes, $m_b(Lg;NET)$, for the 15 large events clustered into two distinct groups with very similar magnitudes within each group. The standard deviation of the magnitudes for the events in the largest group (twelve events) was 0.036, compared to 0.094 for body wave magnitudes, $m_b(P; tele)$ based on world wide teleseismic P wave data. Furthermore, the standard deviation of $m_b(Lg;NET)$ for the 12 events was smaller than that of any other station $m_b(Lg)$. The reduced standard deviation for the network Lg magnitude indicates independence among station Lg magnitudes. This is in contrast to the Lg amplitudes at the local network near Nevada Test Site, studied by Patton (1988), who found the they lacked independence from station to station.

RMS magnitudes based on time windows other than on that for the Lg phase, including

STATION SITE AMPLIFICATIONS
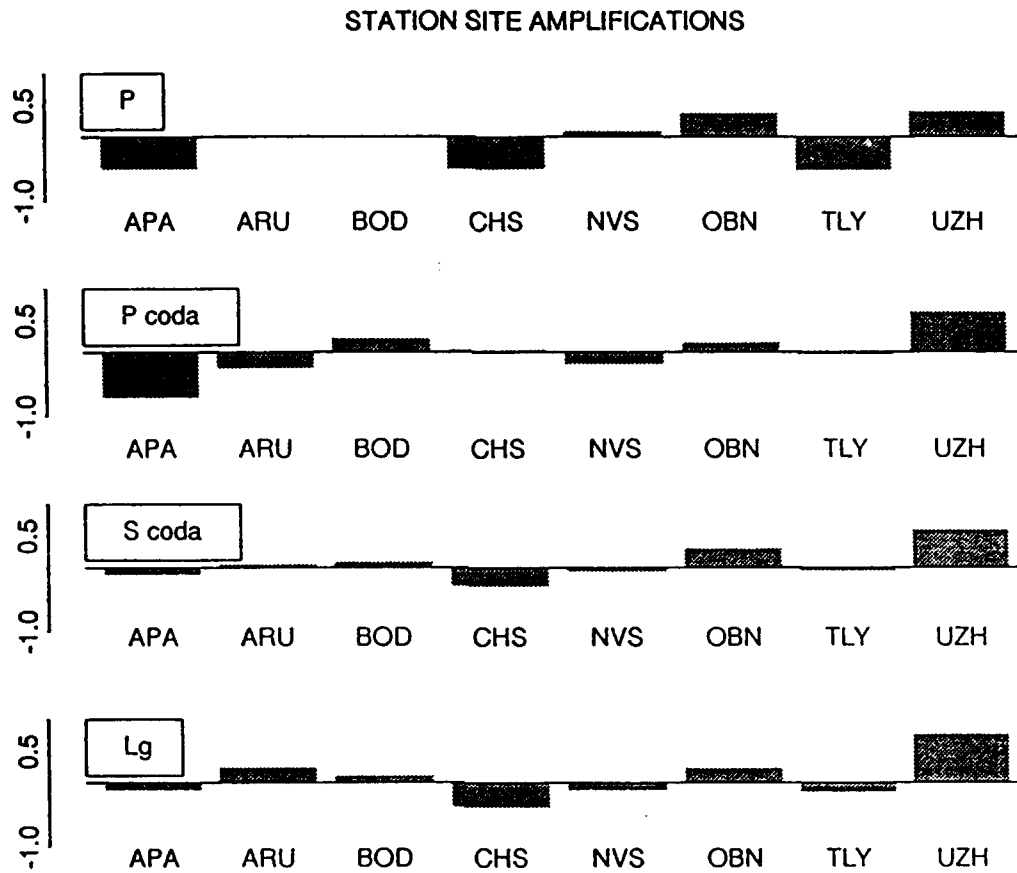
Figure 25: Station site amplifications calculated from the path corrections and the amplitude distance curves for the different phases. The vertical scaling in each bar-chart is in magnitude units.

61

the initial P phase, the P coda, and the S and its coda, were also calculated and analyzed. The results for RMS coda, with regard to consistency, were quite similar to those of RMS Lg. This implies small scatter in RMS S coda values which in turn might indicate that the high stability of the RMS Lg amplitudes obtained here and demonstrated in several other cases (see e.g., Hansen, *et al.*, 1990) could be a result of averaging amplitudes over a long time window. The necessity of this averaging involving the Lg wave is not clear. From the point of view of signal-to-noise ratio, a time window for the Lg phase is preferable for many paths. However, RMS amplitudes were generally somewhat larger for S coda than for Lg at seven of the nine stations analyzed here. One would therefore expect that magnitudes could be obtained for explosions with somewhat smaller yields using S coda than Lg at these stations, provided they have similar scaling with yield.

The standard errors for the P phase and the P coda were about 75-50% larger than those of the Lg, and the station magnitude residuals for these two types of magnitude appeared only weakly correlated with those of Lg. This may be utilized to improve the accuracy of magnitude estimates by combining magnitude types with independent residuals. As the standard errors for P and P coda are significantly larger than that for Lg, the reduction in standard error from a combination of measurements with a weighting scheme will only be marginal. The ratios of RMS amplitudes for different phases like P coda/Lg had a very small variation from explosion to explosion. The median (over stations) of the standard deviations for the ratios of P coda/Lg and S coda/Lg were 0.08 and 0.04 respectively. The stability of these ratios suggest that work on seismic discrimination problems other than yield estimation might benefit from employing RMS amplitudes rather than the standard practice of using maximum amplitudes.

Acknowledgments

Table 7: $mb(P)$

Date	APA	ARU	BOD	CHS	NRI	NVS	OBN	TLY	UZH	S.D.1	NET	S.D.2
64/10/25	+5.279+	0.000	0.000	0.000	0.000	0.000	0.000	0.000	0.000	0.000	0.000	0.000
67/10/21	+5.568+	0.000	5.769	0.000	0.000	+5.934+	0.000	0.000	0.000	0.000	0.000	0.000
68/11/07	+5.712+	0.000	0.000	6.534	0.000	+6.086+	0.000	0.000	0.000	0.000	0.000	0.000
76/09/29	0.000	0.000	5.826	(5.266)	0.000	5.709	5.754	0.000	0.000	0.000	5.780	0.059
76/10/20	4.813	0.000	4.973	0.000	0.000	4.993	4.831	0.000	4.997	0.041	5.048	0.063
77/09/01	5.717	5.839	5.791	0.000	0.000	5.834	5.756	0.000	(5.529)	0.023	5.803	0.038
77/10/09	4.582	4.711	4.730	5.498	0.000	4.533	4.728	0.000	4.736	0.122	4.788	0.048
78/08/10	5.840	5.780	5.801	0.000	0.000	5.742	5.856	0.000	0.000	0.021	5.820	0.038
78/09/27	5.725	5.602	0.000	5.590	0.000	0.000	5.640	0.000	0.000	0.031	5.640	0.042
79/09/24	5.768	5.944	0.000	0.000	0.000	5.866	5.780	0.000	5.903	0.034	5.863	0.037
79/10/18	5.784	5.737	5.737	0.000	0.000	0.000	0.000	0.000	5.965	0.054	5.813	0.042
80/10/11	5.727	5.559	5.813	0.000	0.000	0.000	5.807	0.000	5.872	0.054	5.764	0.037
81/10/01	5.889	5.803	5.774	(5.332)	0.000	5.808	5.831	0.000	5.951	0.027	5.853	0.034
82/10/11	5.572	0.000	0.000	0.000	0.000	5.610	5.547	0.000	0.000	0.000	5.586	0.048
83/08/18	5.842	(5.532)	0.000	5.793	0.000	5.729	5.828	0.000	0.000	0.025	5.792	0.042
83/09/25	5.690	0.000	5.684	5.850	0.000	5.797	5.705	5.800	5.615	0.031	5.728	0.031
84/08/26	*4.002*	0.000	0.000	0.000	0.000	3.796	0.000	0.000	0.000	0.000	4.087	0.102

Table 7: $mb(P)$

Date	APA	ARU	BOD	CHS	NRI	NVS	OBN	TLY	UZH	S.D.1	NET	S.D.2
84/10/25	5.809	5.522	5.796	0.000	0.000	0.000	5.745	5.655	5.717	0.044	5.713	0.034
87/08/02	5.806	5.920	5.761	0.000	0.000	5.854	5.811	5.831	5.806	0.019	5.835	0.032
88/05/07	5.614	5.745	(5.417)	5.733	0.000	5.604	5.590	5.644	5.587	0.025	5.644	0.032
88/12/04	5.859	5.611	5.829	5.876	0.000	5.731	5.742	5.800	5.745	0.030	5.774	0.029
S.D.	0.095	0.106	0.060	0.276	0.000	0.102	0.062	0.047	0.083	0.000	0.000	0.000

Station m_b values that are uncertain for one reason or another are indicated as follows:

[] inconsistent calibrations
() outlying data point
possible signal interference
++ instrument characteristics uncertain
** Poor SNR

64

Table 8: mb(P coda)

Date	APA	ARU	BOD	CHS	NRI	NVS	OBN	TLY	UZH	S.D.1	NET	S.D.2
64/10/25	+5.236+	0.000	0.000	0.000	0.000	0.000	0.000	0.000	0.000	0.000	0.000	0.000
67/10/21	+5.463+	0.000	5.961	0.000	0.000	+5.876+	0.000	0.000	0.000	0.000	0.000	0.000
68/11/07	+5.617+	0.000	0.000	6.463	0.000	0.000	0.000	0.000	0.000	0.000	0.000	0.000
76/09/29	0.000	0.000	0.000	(5.315)	0.000	5.665	5.800	0.000	0.000	0.000	5.695	0.074
76/10/20	4.781	0.000	5.056	0.000	0.000	4.974	4.937	0.000	4.848	0.048	5.055	0.048
77/09/01	5.700	5.851	5.910	0.000	0.000	5.796	5.775	0.000	5.625	0.042	5.821	0.033
77/10/09	4.644	4.739	4.759	5.579	0.000	4.566	4.785	0.000	4.663	0.130	4.819	0.037
78/08/10	5.781	5.789	5.794	0.000	0.000	5.787	5.897	0.000	0.000	0.022	5.825	0.033
78/09/27	5.648	(5.384)	0.000	5.673	0.000	0.000	5.672	0.000	0.000	0.000	5.568	0.043
79/09/24	5.779	5.911	0.000	0.000	0.000	5.821	5.834	0.000	5.779	0.024	5.841	0.033
79/10/18	5.748	5.693	5.747	0.000	0.000	0.000	0.000	0.000	5.787	0.019	5.756	0.037
80/10/11	5.753	5.638	5.690	0.000	0.000	0.000	5.808	0.000	5.803	0.033	5.749	0.033
81/10/01	5.843	0.000	5.761	(5.407)	0.000	5.782	5.856	0.000	5.843	0.019	5.827	0.033
82/10/11	5.623	0.000	0.000	0.000	0.000	5.566	5.533	0.000	0.000	0.000	5.587	0.043
83/08/18	5.843	0.000	0.000	5.800	0.000	5.705	5.789	0.000	0.000	0.029	5.779	0.037
83/09/25	5.760	0.000	5.910	5.850	0.000	5.861	5.701	5.892	5.738	0.031	5.811	0.028
84/08/26	*4.073*	0.000	0.000	0.000	0.000	*3.989*	0.000	0.000	0.000	0.000	4.227	0.078

Table 8: *mb(P coda)*

Date	APA	ARU	BOD	CHS	NRI	NVS	OBN	TLY	UZH	S.D.1	NET	S.D.2
84/10/25	5.826	5.636	5.629	0.000	0.000	0.000	5.730	5.611	5.736	0.034	5.700	0.030
87/08/02	5.857	5.952	5.939	0.000	0.000	5.865	5.827	0.000	5.821	0.023	5.891	0.031
88/05/07	5.665	5.719	5.708	5.769	0.000	5.669	5.574	5.755	5.658	0.022	5.690	0.026
88/12/04	5.783	5.685	5.694	5.807	0.000	5.654	5.757	5.764	5.757	0.019	5.738	0.026
S.D.	0.100	0.064	0.060	0.286	0.000	0.070	0.074	0.077	0.092	0.000	0.000	0.000

Station m_b values that are uncertain for one reason or another are indicated as follows:

[] inconsistent calibrations
() outlying data point
possible signal interference
++ instrument characteristics uncertain
** Poor SNR

Table 9: m_b(S coda)

Date	APA	ARU	BOD	CHS	NRI	NVS	OBN	TLY	UZH	S.D.1	NET	S.D.2
64/10/25	0.000	0.000	0.000	0.000	0.000	0.000	0.000	0.000	0.000	0.000	0.000	0.000
67/10/21	+5.511+	0.000	5.986	0.000	0.000	+5.773+	0.000	0.000	0.000	0.000	0.000	0.000
68/11/07	+5.619+	0.000	0.000	6.439	0.000	+6.141+	0.000	0.000	0.000	0.000	0.000	0.000
76/09/29	0.000	0.000	5.680	(5.427)	0.000	5.621	(5.899)	0.000	0.000	0.000	5.651	0.034
76/10/20	0.000	5.040	5.014	0.000	0.000	5.052	5.086	0.000	4.820	0.047	5.031	0.059
77/09/01	0.000	5.751	5.783	0.000	0.000	5.745	5.749	0.000	(5.534)	0.009	5.750	0.024
77/10/09	4.841	4.733	4.767	0.000	0.000	4.568	4.926	0.000	*4.353*	0.060	4.698	0.051
78/08/10	5.789	5.806	5.808	0.000	0.000	5.811	5.793	0.000	0.000	0.004	5.796	0.022
78/09/27	5.607	5.647	0.000	5.653	0.000	0.000	5.605	0.000	0.000	0.013	5.616	0.024
79/09/24	5.733	5.782	0.000	0.000	0.000	5.759	5.781	0.000	5.673	0.020	5.745	0.022
79/10/18	5.719	5.761	5.737	0.000	0.000	0.000	0.000	0.000	5.671	0.019	5.725	0.024
80/10/11	5.819	5.766	5.808	0.000	0.000	0.000	5.864	0.000	5.771	0.023	5.803	0.024
81/10/01	5.796	0.000	5.822	(5.462)	0.000	5.790	5.859	0.000	5.725	0.022	5.798	0.022
82/10/11	5.584	5.551	0.000	0.000	0.000	5.605	0.000	0.000	0.000	0.000	5.581	0.028
83/08/18	5.863	5.768	0.000	5.858	0.000	5.744	5.875	0.000	0.000	0.027	5.813	0.022
83/09/25	5.714	0.000	5.797	5.763	0.000	5.855	5.785	5.807	5.823	0.017	5.793	0.018
84/08/26	4.012	0.000	0.000	0.000	0.000	0.000	0.000	0.000	0.000	0.000	3.869	0.156

Table 9: $m_b(S\ coda)$

Date	APA	ARU	BOD	CHS	NRI	NVS	OBN	TLY	UZH	S.D.1	NET	S.D.2
84/10/25	(5.873)	5.727	5.646	0.000	0.000	0.000	5.794	5.548	(5.818)	0.053	5.678	0.024
87/08/02	5.821	5.806	5.841	0.000	0.000	844	5.806	5.806	5.846	0.007	5.827	0.018
88/05/07	5.684	5.735	5.682	5.753	0.000	5.719	5.694	5.764	0.000	0.013	5.716	0.018
88/12/04	5.794	5.800	5 737	(5.902)	0.000	5.709	5.784	5.709	5.831	0.018	5.769	0.018
S.D.	0.061	0.031	0.031	0.035	0.000	0.050	0.068	0.069	0.085	0.000	0.000	0.000

Station m_b values that are uncertain for one reason or another are indicated as follows:

[] inconsistent calibrations

() outlying data point

possible signal interference

++ instrument characteristics uncertain

** Poor SNR

68

Table 10: $m_b(Lg)$

Date	APA	ARU	BOD	CHS	NRI	NVS	OBN	TLY	UZH	S.D.1	NET	S.D.2
64/10/25	+5.502+	0.000	0.000	0.000	0.000	0.000	0.000	0.000	0.000	0.000	0.000	0.000
67/10/21	+5.461+	0.000	6.155	0.000	0.000	+5.892+	0.000	0.000	0.000	0.000	0.000	0.000
68/11/07	+5.525+	0.000	0.000	6.423	0.000	+6.201+	0.000	0.000	0.000	0.000	0.000	0.000
76/09/29	0.000	0.000	5.719	5.746	0.000	5.654	(5.993)	0.000	0.000	0.000	5.705	0.031
76/10/20	4.814	4.959	5.103	0.000	0.000	4.971	5.219	0.000	4.891	0.060	4.993	0.066
77/09/01	5.724	0.000	5.749	0.000	0.000	5.757	5.748	0.000	(5.565)	0.007	5.745	0.027
77/10/09	4.866	4.661	4.811	0.000	4.887	4.654	0.000	0.000	*4.455*	0.050	4.735	0.076
78/08/10	5.715	5.797	5.813	0.000	0.000	5.812	5.781	0.000	0.000	0.018	5.786	0.024
78/09/27	5.646	0.000	0.000	5.602	0.000	0.000	5.552	0.000	0.000	0.000	5.597	0.031
79/09/24	5.742	5.755	0.000	0.000	0.000	5.776	5.787	0.000	5.660	0.022	5.746	0.024
79/10/18	5.741	5.714	5.745	0.000	0.000	0.000	0.000	0.000	5.667	0.018	5.720	0.027
80/10/11	5.694	5.785	5.668	0.000	5.784	0.000	5.822	0.000	5.765	0.024	5.750	0.022
81/10/01	5.831	5.801	5.852	5.718	0.000	5.854	5.792	0.000	5.731	0.021	5.798	0.021
82/10/11	5.671	5.519	0.000	0.000	0.000	5.588	5.543	0.000	0.000	0.033	5.582	0.027
83/08/18	5.779	5.843	0.000	5.832	0.000	5.814	5.855	0.000	0.000	0.013	5.824	0.024
83/09/25	5.832	0.000	5.810	5.765	0.000	5.800	5.810	5.810	5.811	0.008	5.809	0.021
84/08/26	*4.117*	0.000	0.000	0.000	4.069	0.000	0.000	0.000	0.000	0.000	4.141	0.181

Table 10: $m_b(Lg)$

Date	APA	ARU	BOD	CHS	NRI	NVS	OBN	TLY	UZH	S.D.1	NET	S.D.2
84/10/25	5.817	5.805	5.696	0.000	0.000	0.000	5.807	5.658	5.831	0.030	5.776	0.022
87/08/02	5.806	5.729	5.831	0.000	0.000	5.821	5.741	5.770	5.836	0.017	5.797	0.021
88/05/07	5.728	5.657	5.679	5.794	0.000	5.682	5.701	5.719	5.719	0.015	5.714	0.020
88/12/04	5.740	5.811	0.000	5.856	0.000	5.762	5.795	*5.804*	5.871	0.021	5.810	0.021
S.D.	0.073	0.039	0.057	0.055	0.112	0.039	0.070	0.057	0.060	0.000	0.000	0.000

Station m_b values that are uncertain for one reason or another are indicated as follows:

[] inconsistent calibrations

() oulying data point

possible signal interference

++ instrument characteristics uncertain

** Poor SNR

References

Becker, R.A., Chambers, J.M. and A.R. Wilks (1988). The New S Language: A programming environment for data analysis and graphics, Wadsworth&Brooks/Cole Advanced Books and Software, Pacific Grove, California, pp. 702.

Baumgardt, D.R. (1990), Causes of Lg Amplitude Variations and Scattering in the Eurasian Continental Crust. in Proceedings of the Twelfth Annual DARPA/GL Seismic Research Symposium. (Eds J. Lewkowicz and J McPhetres), GL-TR-90-0212 Geophysics Laboratory, Hanscom AFB, MA. ADA226635.

GSE/SW/62 (1988), IA system - Interactive program for association and locations of seismic events. Conference of Disarmament, Working Paper, 17-Mar-1988.

Ericsson, U. (1971). Maximum likelihood linear fitting when both Variables have normal and correlated errors, National Defense Research Institute, Stockholm, Sweden, FOA 4 Report C4474-A1.

Frankel, A. and W. Leith (1991). Evaluation of Topographic Effects on $m_b(P)$ and $m_b(Lg)$ using three-dimensional numerical simulations, Manuscript Nov 5 1991, U.S. Geological Survey, Reston, VA.

Hansen, R. (1990). Analysis of data from the British station GAM near Garm, USS for Soviet nuclear explosions, in: Semiann. Tech. Summ., 1 Oct 1989-31 March 1990, NORSAR Sci. Rep. 2-89/90, Kjeller, Norway.

Hansen, R., Ringdal, F., and P.G. Richards (1990). The stability of RMS Lg measurements, and their potential for accurate estimation of the yields of Soviet underground explosions Bull. Seism. Soc. Am., 80, 2106-2126.

Israelsson, H. (1991). Analysis of historical USSR seismograms - RMS magnitudes, yields, and depths of explosions at the Semipalatinsk test range. in Proceedings of the 13th annual PL/DARPA Seismic Research Symposium, 8-10 October 1991, (Eds. J.Lewkowicz and J. McPhetres), Report PL-TR-91-2208, Phillips Laboratory, Hanscom AFB, MA. ADA241325.

Israelsson, H. (1992). Hand digitized waveforms of seismic recordings from Soviet stations for nuclear explosions in the U.S.S.R. (This Report).

Jih, R.S. and R.A. Wagner (1992) Path-corrected body wave magnitudes and yield estimates of Novaya Zemlya explosions Manuscript Feb 14 1992, Teledyne Geotech, Alexandria Labs, Alexandria VA.

Leith, W., Matzko, J.R., Unger, J. and D.W. Simpson (1990). Geology and Image Analysis of the Soviet Nuclear Test Site at Matochkin Shar, Novaya Zemlya U.S.S.R., in Proceedings of the Twelfth Annual DARPA/GL Seismic Research Symposium. (Eds J. Lewkowicz and J McPhetres), GL-TR-90-0212 Geophysics Laboratory, Hanscom AFB, MA. ADA226635.

Lilwal, R.C. and P.D. Marshall (1986). Body wave magnitudes and locations of Soviet underground explosions at the Novaya Zemlya Test Site, 'Atomic Weapons Research Establishment, AWRE Report No. O 17/86.

Nuttli, O.W. (1986). Lg magnitudes of selected East Kazakhstan underground explosions, Bull. Seism. Soc. Am., 76, 1241-1251.

Nuttli, O.W. (1988). Lg magnitudes and yield estimates for underground Novaya Zemlya nuclear explosions, Bull. Seism. Soc. Am., 78, 873-884.

Patton, H.J. (1988). Application of Nuttli's method to estimate yield of Nevada Test Site Explosions recorded on Lawrence Livermore National Laboratory's digital seismic system, Bull. Seism. Soc. Am., 78, 1759-1772.

Rao, C.R. (1967). Linear Statistical inference and its applications, John Wiley & Sons, New York, pp. 522.

Ringdal, F. (1983). Magnitudes from P coda and Lg using NORSAR data, in: Semiann. Tech. Summ., 1 Oct 82 - 31 Mar 1983, NORSAR Sci. Rep. 2-82/83, Kjeller, Norway.

Ringdal, F. (1991). RMS Lg analysis of Novaya Zemlya explosion recordings, in: Semiann. Tech. Summ., 1 Oct 90 - 31 Mar 1991, NORSAR Sci. Rep. 2-90/91, Kjeller, Norway.

Ringdal, F. and B.K. Hokland (1987). Magnitudes of Large Semipalatinsk explosions using P coda and Lg measurements at NORSAR, in: Semiann. Tech. Summ., 1 Apr-30 Sep 1987, NORSAR Sci. Rep. 1-87/88, Kjeller, Norway.

Ringdal, F. and J. Fyen (1988). Comparative analysis of NORSAR and Graefenberg Lg magnitudes of Shagan River explosions, in: Semiann. Tech. Summ., 1 Apr-30 Sep 1988, NORSAR Sci. Rep. 1-88/89, Kjeller, Norway.

Ringdal, F. and Marshall (1989). Yield determination of Soviet underground nuclear explosions at the Shagan River Test Site in: Semiann. Tech. Summ., 1 Oct 1988 -31 March 1989, NORSAR Sci. Rep. 2-88/89,

Stewart, R.C. and P.D. Marshall (1988). Seismic P-waves from Novaya Zemlya explosions: seeing double! Geophys.J., 92, 335-338

Zonenshain, L.P., J. Verhoef, R. Macnab, and H. Meyers (1991) Magnetic Imprints of Continental Accretion in the U.S.S.R, EOS, 29, 305.

Analysis of Historical Seismograms - RMS Lg Magnitudes, Yields, and Depths of Explosions at the Semipalatinsk Test Range

Hans Israelsson

Abstract

Magnitudes, $m_b(Lg)$, based on RMS amplitudes of Lg-waves recorded at 9 internal Soviet stations for 83 underground nuclear explosions at the Semipalatinsk test range were analyzed. Network magnitudes based on a combination of station magnitudes were formed as weighted averages over the station magnitudes after adjusting for variations among station magnitudes in scaling with source strength. Combining the station magnitudes into network magnitudes, although the numbers of stations were small (less than six), appeared to reduce scatter in magnitude-yield relations. The correlation between network $m_b(Lg)$ and announced explosion yields was very high and $m_b(Lg)$ closely approximated simple proportionality with the logarithm of yield throughout the yield interval 2-165 kt. The error of misfit was about 0.04 m.u. excluding data for the explosion on 72/08/16 (8 kt at 139 m), the yield of which appeared high compared to $m_b(Lg)$. The close correlation between network $m_b(Lg)$ and explosion yield together with the fact that several of the explosions were not at scaled depths, indicates that $m_b(Lg)$ may not be critically dependent on depth of burial, at least for depth ranges within a factor of two.

Introduction

Estimating the yield of underground nuclear explosions has been a central issue for seismological verification research. Seismic yield estimation has traditionally been based on magnitudes of P waves, $m_b(P)$, in spite of the sensitivity of these waves to structure. Over the last decade considerable efforts have been made to annul this disadvantage. Meanwhile, a major step forward was taken by the introduction of magnitudes from Lg waves, $m_b(Lg)$, which subsequently have established themselves as perhaps the single most precise seismic method for yield estimation. Although their first description in the seismological literature was fairly recent (Press and Ewing, 1952), what is now called Lg waves was, as Baker (1970) points out, presumably used for calculation of magnitudes on the original scale devised by Richter (1935).

Thus being employed implicitly in the very first magnitude determinations, it was not until much later that magnitudes were defined explicitly from Lg waves. For example, using data from underground nuclear explosions in the U.S., Baker (1970) developed a method

to determine Lg magnitudes and found that they had less scatter than P wave magnitudes.

In a series of papers Nuttli (1986ab, 1987, 1988) and Ringdal (1983) with co-workers (Ringdal and Hokland, 1987; Ringdal and Fyen, 1988; Ringdal and Marshall, 1989; Hansen *et al.* 1990) defined and applied Lg magnitudes directly to the yield estimation problem. Nuttli's approach was based on classical seismological measurements from standard analog recordings at local and regional distances, whereas Ringdal and co-workers drew upon modern high-quality digital array technology using data at teleseismic and regional distances.

In this note the analysis of Lg waves for yield estimation includes elements of both Nuttli's and Ringdal's approaches: Nuttli's, because the data were originally obtained by conventional analog recordings at a network of single stations, and Ringdal's, because the analog recordings were converted to digital form, albeit of limited quality, and also because we employ a quantification of Lg wave energy much along the lines of Ringdal's magnitude definition.

More specifically we calculate and analyze $m_b(Lg)$ based on hand digitized recordings at nine seismological stations in the U.S.S.R. from nuclear explosions at the Semipalatinsk Test Range, STR. The emphasis of this paper is on the precision of $m_b(Lg)$, its relationship with explosion yield, and its sensitivity to shot depth and to local geology.

Data

The map in Figure 26 shows the relative locations of the seismological stations and the STR. The major tectonic components of the area traversed by the paths between the stations and STR are also outlined (After Zonenshain *et al.* 1991). Only a few of the paths cross predominantly platform areas, whereas most of them traverse the presumably more complex Central Asiatic orogenic belt and the Kazakhstan accretionary continent. The array stations NORSAR, (NAO), and Grafenberg, (GRF), are also marked on the map in Figure 26, as $m_b(Lg)$ data from the two arrays are used as a reference and for comparisons.

Locations, times, and $m_b(P)$ for the explosions reported by ISC are listed in Table 11, which includes data for 83 explosions distributed throughout the STR: 55 at Balapan, 22 at Degelen, and 6 in the Murzhik area. Three of the explosions in Table 11, on 72/12/10, 77/10/29, and 78/08/29, were double events consisting of one explosion at Degelen and one at Balapan set off within 5 to 10 s. This means that recordings from such a double event will have interfering Lg waves. The two explosions of the double event on 77/10/29 had similar magnitudes, $m_b(P)$, whereas for the other double events the $m_b(P)$ of the Degelen explosion was much smaller than that of the Balapan event. For the sake of simplicity, the double events are considered single events in this analysis, and only the explosion at Bala-
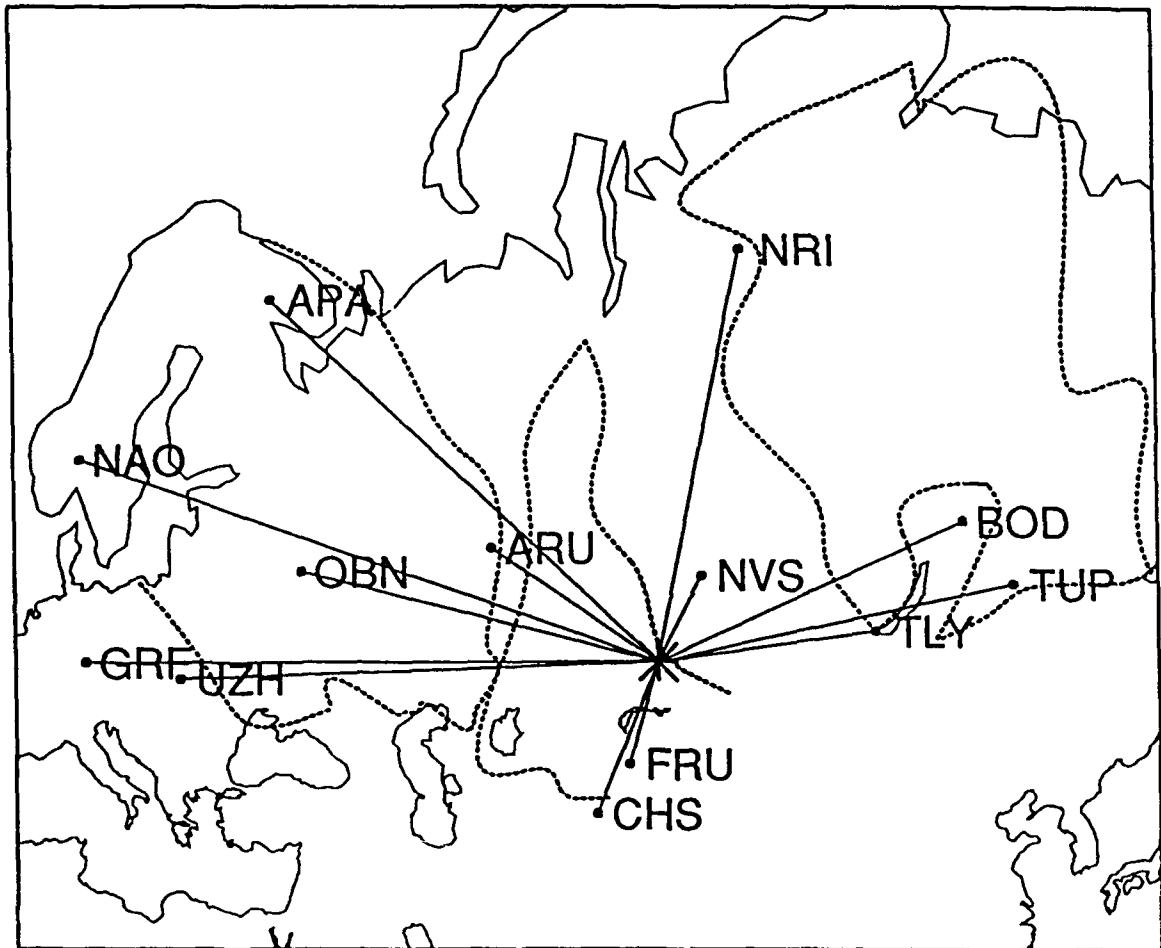
Figure 26: Map showing the relative locations of the Semipalatinsk Test Range (STR), marked with an asterisk, and the seismological stations indicated by their codes. The lines between STR and the stations correspond approximately to Lg wave paths. The dotted contours outline the boundaries of major tectonic components (After Zonenshain *et al.*, 1991).

Table 11: Explosions

Date	Time	Lat (N)	Lon (E)	m_b	Site
66/02/13	04:58:00.0	50.000	78.000		Degelen
66/03/20	05:49:57.8	49.720	78.070	6.0	Degelen
66/05/07	03:57:58.2	49.740	77.950	4.8	Degelen
68/09/29	03:42:57.8	49.820	78.180	5.8	Degelen
69/07/23	02:46:58.0	49.880	78.230	5.4	Degelen
69/11/30	03:32:57.3	49.940	78.980	6.0	Balapan SW
69/12/28	03:46:57.8	49.980	77.790	5.7	Murzhik
71/04/25	03:32:57.9	49.766	78.081	5.9	Degelen
71/06/06	04:02:57.3	49.977	77.740	5.5	Murzhik
71/06/19	04:03:57.7	49.966	77.724	5.4	Murzhik
71/10/09	06:02:57.2	49.986	77.687	5.3	Murzhik
71/10/21	06:02:57.5	50.004	77.631	5.5	Murzhik
71/12/30	06:20:57.9	49.750	78.100	5.7	Degelen
72/02/10	05:02:57.6	50.024	78.942	5.4	Balapan NE
72/03/28	04:21:57.4	49.738	78.160	5.1	Degelen
72/08/16	03:16:57.5	49.774	78.132	5.0	Degelen
72/09/02	08:56:57.3	49.884	77.603	4.9	Murzhik
72/11/02	01:26:57.8	49.914	78.848	6.1	Balapan SW
*72/12/10	04:27:07.6	49.966	78.946	6.0	Balapan NE
73/07/23	01:22:57.7	49.936	78.854	6.1	Balapan NE
73/12/14	07:46:57.1	50.026	79.016	5.8	Balapan NE
74/12/27	05:46:56.8	49.908	79.053	5.6	Balapan NE
75/02/20	05:32:57.7	49.756	78.094	5.7	Degelen
75/06/08	03:26:57.6	49.752	78.080	5.5	Degelen
75/12/25	05:16:57.2	50.018	78.863	5.7	Balapan NE

Table 11: Explosions

Date	Time	Lat (N)	Lon (E)	m_b	Site
76/08/28	02:56:57.6	49.948	78.980	5.8	Balapan NE
77/03/29	03:56:57.8	49.790	78.154	5.4	Degelen
77/09/05	03:02:57.8	50.048	78.929	5.8	Balapan NE
*77/10/29	03:07:03.0	50.056	78.866	5.6	Balapan NE
77/11/30	04:06:57.6	49.934	78.894	6.0	Balapan NE
78/03/26	03:56:57.7	49.713	78.065	5.6	Degelen
78/06/11	02:56:57.8	49.879	78.814	5.9	Balapan SW
78/07/28	02:46:57.8	49.732	78.152	5.7	Degelen
*78/08/29	02:37:06.4	49.984	79.017	5.9	Balapan NE
78/11/04	05:05:57.5	50.028	78.976	5.6	Balapan NE
79/06/23	02:56:59.0	49.886	78.916	6.2	Balapan SW
79/07/07	03:46:57.5	50.048	79.063	5.8	Palapan NE
79/08/04	03:56:57.2	49.860	78.942	6.1	Balapan SW
79/08/18	02:51:57.3	49.928	78.981	6.1	Balapan SW
79/10/28	03:16:57.0	49.961	79.068	6.0	Balapan NE
79/12/23	04:56:57.6	49.925	78.796	6.2	Balapan SW
80/05/22	03:56:57.8	49.750	78.107	5.5	Degelen
80/06/12	03:26:57.7	49.954	79.055	5.6	Balapan NE
80/09/14	02:42:39.3	49.936	78.863	6.2	Balapan SW
80/10/12	03:34:14.2	49.937	79.104	5.9	Balapan NE
80/12/14	03:47:06.5	49.867	78.967	5.9	Balapan SW
80/12/27	04:09:08.5	50.008	79.026	5.9	Balapan NE
81/03/29	04:03:50.1	49.979	79.016	5.6	Balapan NE
81/04/22	01:17:11.4	49.870	78.896	6.0	Balapan SW
81/09/13	02:17:18.4	49.890	78.976	6.1	Balapan SW

77

Table 11: Explosions

Date	Time	Lat (N)	Lon (E)	m_b	Site
81/10/18	03:57:02.7	49.876	78.885	6.1	Balapan SW
81/11/29	03:35:08.8	49.848	78.850	5.7	Balapan NE
81/12/27	03:43:14.2	49.895	78.859	6.2	Balapan SW
82/02/19	03:56:11.1	49.826	78.125	5.4	Degelen
82/04/25	03:23:05.5	49.871	78.917	6.1	Balapan SW
82/12/05	03:37:12.7	49.890	78.860	6.1	Balapan SW
82/12/26	03:35:14.4	50.061	79.049	5.7	Balapan NE
83/06/12	02:36:43.7	49.905	78.967	6.1	Balapan SW
83/10/06	01:47:06.8	49.909	78.827	6.0	Balapan SW
83/10/26	01:55:05.0	49.887	78.901	6.1	Balapan SW
83/12/26	04:29:07.0	49.835	78.205	5.6	Degelen
84/03/07	02:39:06.4	49.999	78.987	5.7	Balapan NE
84/04/15	03:17:09.3	49.686	78.141	5.7	Degelen
84/04/25	01:09:03.7	49.911	78.913	6.0	Balapan SW
84/05/26	03:13:12.5	49.925	79.030	6.1	Balapan NE
84/07/14	01:09:10.5	49.852	78.921	6.2	Balapan SW
84/10/27	01:50:10.7	49.917	78.829	6.2	Balapan SW
84/12/02	03:19:06.5	49.946	79.032	5.9	Balapan NE
84/12/16	03:55:02.8	49.884	78.824	6.1	Balapan SW
84/12/28	03:50:10.9	49.826	78.710	6.0	Balapan SW
85/02/10	03:27:07.7	49.865	78.839	5.9	Balapan SW
85/07/20	00:53:14.8	49.916	78.803	6.0	Balapan SW
87/02/26	04:58:22.1	49.800	78.104	5.4	Degelen
87/04/03	01:17:08.1	49.874	78.812	6.2	Balapan SW
87/05/06	04:02:05.8	49.803	78.110	5.6	Degelen

Table 11: Explosions

Date	Time	Lat (N)	Lon (E)	m_b	Site
87/06/06	02:37:07.1	49.803	78.089	5.4	Degelen
87/07/17	01:17:07.1	49.769	78.100	5.8	Degelen
87/12/13	03:21:04.9	49.930	78.820	6.1	Balapan SW
87/12/27	03:05:04.9	49.820	78.730	6.1	Balapan SW
88/02/13	03:05:06.0	49.930	78.910	6.1	Balapan SW
88/04/03	01:33:05.9	49.870	78.920	6.0	Balapan SW
88/05/04	00:57:06.8	49.890	78.760	6.1	Balapan SW
88/09/14	03:59:57.6	49.810	78.800	6.1	Balapan SW

pan are listed in Table 11 for each of the three double events.

Basic information about the 11 Soviet stations is given in Table 12 . The stations are located at epicentral distances ranging from about 6 to 35 degrees from the STR. Apart from CHS, TLY, and TUP, they are all part of the Unified Seismic Observation System (Kondorskaya and Aranovich., 1978). The waveforms analyzed here were recorded in general with the standard vertical component CKM-3 seismometer. However, most of the data for station NVS were obtained with a broadband instrument, SKD. Periods and damping of a given type of seismometer - SKM-3 or SKD - with associated galvanometer differ somewhat among the stations resulting in differences among the magnification curves (see Figure 27). Since the recordings were obtained over the course of more than 20 years, these parameters change with time as well. Two kinds of instrument calibrations, daily and annual, were available for the waveform data. A *daily* calibration includes the maximum magnification, V(daily), and the period range in which the magnification stays above 90% of V(daily). This is clearly not sufficient to uniquely reconstruct the magnification curve as a function of frequency. By contrast, an *annual* calibration gives instrument parameters from which the magnification curve can be constructed in its entirety. The maximum magnification can be calculated from this curve; we denote the maximum obtained in this manner, V(annual). For most of the data there is close agreement between V(daily) and V(annual), but in some instances (indicated with brackets in Table 14) the difference is larger than 10%, which corresponds to about 0.04 m.u. (magnitude unit). It is not known which type of calibration - daily or annual - is the most accurate one.

Photo copies of the analog recording were hand digitized according to a procedure
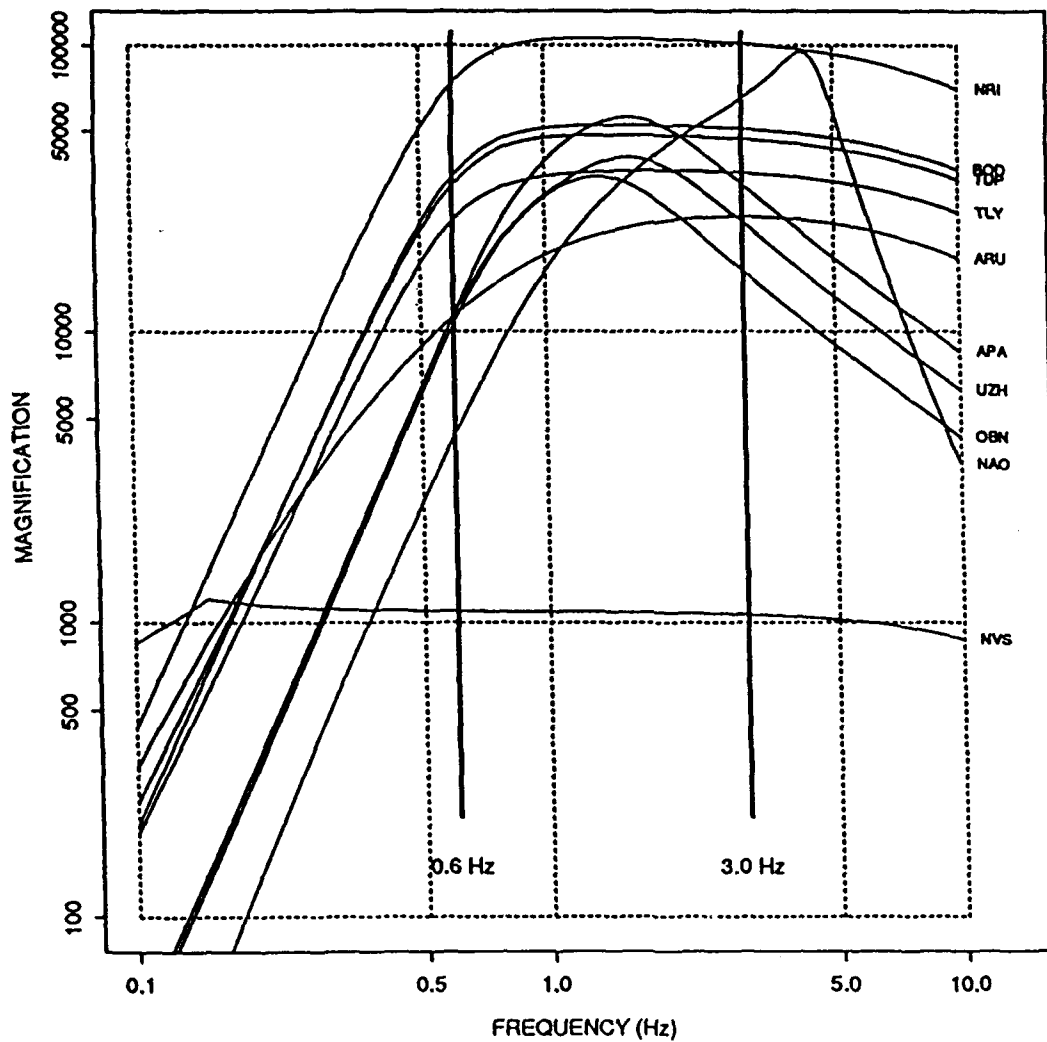
Figure 27: Magnification curves for the Soviet seismological stations. The curve for NAO (relative digital counts/micron) has been included for comparison. The frequency band 0.6-3.0 Hz, used in the calculations of RMS Lg amplitudes, is also marked.

Table 12: Stations

Code	Name	Lat.(N)	Long.(E)	Distance (degrees)
APA	Apatity	67.55	33.33	28.37
ARU	Arti	56.40	58.60	13.43
BOD	Bodaybo	57.85	114.18	22.53
CHS	Chusal	39.10	70.77	11.91
FRU	Frunze	42.83	74.62	7.38
GRF	Grafenberg	49.69	11.20	42.30
NAO	NORSAR	60.82	10.83	38.4
NRI	Norilsk	69.40	88.10	20.24
NVS	Novosibirsk	54.90	83.30	6.01
OBN	Obninsk	55.10	36.60	25.55
TLY	Talaya	51.68	103.63	16.24
TUP	Tupik	54.43	119.90	25.79
UZH	Uzhgorod	48.63	22.30	35.76

described by Chiburis *et al.* (1980). Kemerait *et al.* (1981) suggested that this procedure gives satisfactory results from 0 out to at least 3-4 Hz.

Examples of waveforms are given in Figure 28, which shows recordings typical of the 11 stations plotted as a function of epicentral distance. The group velocity window 3.1-3.7 km/s representing the low and high end of the normal range for Lg waves is also marked in the record section. Lg waves are the dominant feature of the waveforms at distances less than about 20 degrees. At greater distances most stations lack clearly developed maximum amplitudes, but the coda level in the group velocity window of Lg is still well above the ambient noise at the stations. As there are no explosions with waveforms available at all stations, the record section in Figure 28 had to be composed of data from several explosions. The distribution of waveforms over stations and over explosions is, in fact, highly variable, as can be seen in Table 14 from the distribution of calculated station magnitudes (see below). The most recordings were available for station OBN (in all 66). Because of the limited number of available waveforms and because of uncertainties about the instrument responses, data for the two stations CHS and FRU were not included in the subse-
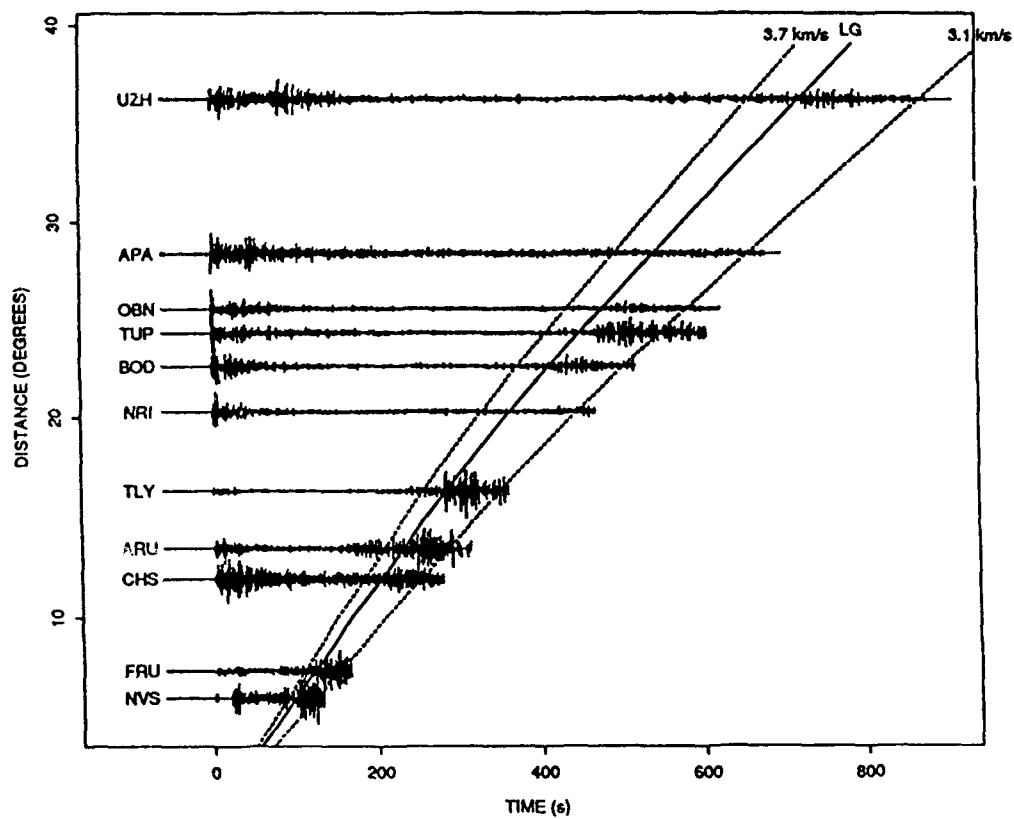
Figure 28: Typical waveforms at the Soviet stations from explosions at Semipalatinsk plotted as a function of epicentral distance. The group velocity window 3.1-3.7 km/s used in the calculations of RMS Lg amplitudes and the expected arrival time of Lg waves travelling with 3.5 km/s group velocity are also indicated.

quent analysis. Altogether 222 waveforms from 83 explosions distributed over 9 stations were used in the analysis.

RMS Lg amplitudes were computed using the group velocity window 3.1 - 3.7 km/s. In order to account for differences and temporal variations in instrument responses the calculated amplitudes had to be normalized to a common instrument: that of the SKM-3 seismometer at OBN for 1988. This normalization was carried out in the frequency domain for computational convenience.

Each calculated Lg trace amplitude was also compensated for background noise as suggested by Ringdal and Hokland (1987). The noise correction was based on a noise window of about 2 minutes immediately preceding the visually measured P onset.

The data were band pass filtered from 0.6 to 3.0 Hz (using three pole Butterworth filter) to be consistent with the definition used by Ringdal (1983) and Hansen et al. (1990). As Hansen et al. (1990) reported in their study, the choice of frequency band and time window is, not critical with regard to signal-to-noise ratio, SNR, to standard error, and to other characteristics of $m_b(Lg)$ relevant to yield estimation, as long as the main part of the Lg wave energy is captured. A group velocity window was chosen to integrate the Lg energy rather than a time window of fixed length as used by Ringdal (1983) and Hansen et al. (1990) because of the large range in epicentral distances from the STR to the stations (Cf. Table 12). With a two minute window centered around a group velocity of 3.5 km/s, there would be interference with the S phase and its coda at shorter epicentral distances.

Although RMS amplitudes and $m_b(Lg)$ were formally calculated for all available waveforms, some data were not in used in the analysis for one or more of the following reasons: poor SNR, signal interference, or uncertainties in instrument responses.

The reliability of the RMS amplitudes, although corrected for noise, depend on the signal-to-noise ratio. Hansen (1990) suggested that a SNR of 1.5 is the lower limit for reliable estimates of $m_b(Lg)$ at single stations. Here we formally calculated RMS Lg amplitudes if the SNR > 1.1, SNR defined as the RMS Lg amplitude uncorrected for noise over the noise RMS amplitude.

Interference from signals of other events may corrupt the RMS amplitudes used to measure the Lg wave energy of the explosions. Therefore, when signal interference was observed, the recordings were also removed from the analysis. Such cases included the recording for OBN 87/07/17 with a local high frequency signal interfering with the signal from the explosion and the two recordings at APA and UZH of the explosion on 87/05/06, for which large teleseismic P waves interfered with the Lg waves (from an $m_b(ISC) = 6.5$ earthquake at Andreaof Island, 51.26 N and 179.88 W).

Annual instrument calibrations were not available, or could not be inferred from comparisons with record magnification data for 10 of the waveforms. For example, the two recordings at OBN on 77/09/05 and on 77/0329 were not used as the period range of the records was 1.10-1.50 s which is significantly different from the standard range about 0.6-1.0 s for this station. It, thus, appears that they were recorded with instruments different from the standard SKM-3.

Calculation of RMS $m_b(Lg)$

The calculated RMS amplitudes, corrected for maximum magnification and converted to a logarithmic scale were used to calculate station magnitudes at station j for explosion i with the simple formula: $m_{ij}(RMS;Lg) = rms_{ij} + C_j$. The normalization term defined as $C_j = 1/n \cdot \Sigma (rms_{ij} - m_{iNAO}(RMS;Lg))$, where n is the number of stations, shifts the logarithm of the amplitude to a traditional m_b scale. The normalization was limited to Balapan events with $m_b(Lg)$ at NAO being in the range 5.75-6.10. Calculated normalization terms are listed in Table 13 and station $m_b(Lg)$ are listed in Table 14.

Table 13: Corrections Relative to mb(Lg) At NAO

Station	Correction
APA	-6.50
ARU	-5.129 0.038
BOD	-5.893 0.026
NRI	-6.122 0.085
NVS	-4.204 0.086
OBN	-5.937 0.032
TLY	-5.614 0.064
TUP	-6.288 0.092
UZH	-6.269 0.070

Table 14: $m_b(Lg)$ magnitudes

Date	APA	ARU	BOD	NRI	NVS	OBN	TLY	TUP	UZH	NET
66/02/13						6.065				6.055 0.039
66/03/20						[5.915]				5.905 0.039
66/05/07					4.697	[4.808]				4.774 0.036
68/09/29						5.729				5.719 0.039
69/07/23			5.331			5.436				5.419 0.034
69/11/30			6.043			(5.871)				6.035 0.068
69/12/28			5.806			5.684				5.712 0.034
71/04/25		[5.917]	6.007	5.851		5.957				5.934 0.025
71/06/06				5.295		(5.766)				5.378 0.097
71/06/19						5.445			5.187	5.422 0.036
71/10/09		[5.288]		5.062		[5.268]				5.215 0.027
71/10/21				5.364	5.364	[5.549]				5.526 0.036
71/12/30						[5.528]			(5.102)	5.479 0.036
72/02/10		[5.394]	5.290			[5.377]				5.338 0.026
72/03/28		5.057	4.841	4.964	4.977	[4.982]				4.952 0.024
72/08/16		5.094	4.769		4.991	[4.896]				4.925 0.025
72/09/02		4.853		4.536	4 710					4.681 0.032
72/11/02		6.153	6.133			[6.112]				6.139 0.026
72/12/10		6.095	6.100			[6.110]				6.103 0.026

Table 14: $m_b(Lg)$ magnitudes

Date	APA	ARU	BÖD	NRI	NVS	OBN	TLY	TUP	UZH	NET
73/07/23						6.237				6.227 0.039
73/12/14						5.908				5.898 0.039
74/12/27		5.840				5.784				5.798 0.028
75/02/20						5.451				5.441 0.039
75/06/08									5.076	5.262 0.086
75/12/25		5.816				5.764				5.774 0.028
76/08/28		5.829								5.806 0.037
77/03/29						+5.678+				
77/09/05		5.941				+6.219+			(5.673)	5.934 0.037
77/10/29		5.745				(6.009)			5.535	5.701 0.034
77/11/30		5.813				[5.789]			5.517	5.771 0.027
78/03/26		5.592				5.496			[5.274]	5.505 0.027
78/06/11		5.772							[5.559]	5.730 0.034
78/07/28		5.675				5.611			[5.419]	5.611 0.027

Table 14: $m_b(Lg)$ magnitudes

Date	APA	ARU	BOD	NRI	NVS	OBN	TLY	TUP	UZH	NET
78/08/29						6.028				6.018 0.039
78/11/04						5.786			[5.534]	5.755 0.036
79/06/23		6.084							6.029	6.093 0.034
79/07/07						6.006			5.924	5.994 0.036
79/08/04		6.057		6.038		6.143				6.097 0.027
79/08/18						6.122			5.950	6.094 0.036
79/10/28			5.953	6.081		6.077				6.049 0.032
79/12/23		6.025		5.986		6.037				6.030 0.027
80/05/22		5.324				5.227				5.223 0.028
80/06/12		5.682				5.620			5.531	5.627 0.027
80/09/14		6.060							5.909	6.055 0.034
80/10/12		5.938				6.010		5.912	(5.629)	5.961 0.027
80/12/14		5.923				5.917				5.910 0.028
80/12/27		5.883				5.951			5.927	5.908 0.027
81/03/29		5.678				5.508			5.551	5.571 0.028
81/04/22		5.890				5.982				5.920 0.028
81/09/13						6.106			6.127	6.106 0.036
81/10/18		5.978	5.950	(5.691)		5.972				5.967 0.026
81/11/29						5.539			5.470	5.540 0.036

Table 14: $m_b(Lg)$ magnitudes

Date	APA	ARU	BOD	NRI	NVS	OBN	TLY	TUP	UZH	NET
81/12/27		6.058				6.065				6.062 0.028
82/02/19		5.119			5.073	5.058				5.019 0.026
82/04/25						6.107			[6.124]	6.106 0.036
82/12/05									[5.883]	5.946 0.086
82/12/26		5.630				5.620			[5.463]	5.593 0.027
83/06/12		6.067				6.048		5.929	6.142	6.064 0.026
83/10/06						5.842	5.810		5.853	5.829 0.031
83/10/26						6.000	6.161			6.047 0.032
83/12/26						*5.117*	5.163		*5.109*	5.115 0.054
84/03/07							5.733			5.708 0.054
84/04/15						5.631	5.654		5.627	5.635 0.031
84/04/25		5.934				5.865	5.865		5.878	5.888 0.024
84/05/26	6.038	6.012		5.934		6.139	6.087			6.065 0.024
84/07/14						6.102	6.059	(5.780)	6.067	6.079 0.031
84/10/27					6.077	6.045			6.154	6.064 0.033
84/12/02		5.865			5.995	5.922	6.018		5.928	5.915 0.023
84/12/16		6.048				6.101	6.036	6.078		6.064 0.024
84/12/28		5.994				6.012			5.930	5.997 0.027
85/02/10		5.812				5.826	5.881	(5.909)		5.816 0.024

Table 14: $m_b(Lg)$ magnitudes

Date	APA	ARU	BOD	NRI	NVS	OBN	TLY	TUP	UZH	NET
85/07/20					5.879	5.868		5.861	5.847	5.868 0.034
87/02/26		5.121			5.114		4.999			4.988 0.029
87/04/03						6.058	6.039			6.041 0.032
87/05/06	#6.494#	5.503					5.388			5.407 0.031
87/06/06		5.197					5.094			5.070 0.031
87/07/17	5.894	5.793				#5.631#	5.808		5.727	5.776 0.029
87/12/13		6.009			5.928	6.029	6.044			6.014 0.024
87/12/27		6.014				6.027	6.069		6.037	6.029 0.024
88/02/13		6.064			6.049	6.014				6.042 0.028
88/04/03		(5.938)				6.090	6.036		6.095	6.068 0.031
88/05/04						6.071	6.123			6.080 0.032
88/09/14	5.969	6.040		6.029		5.981	6.039			6.019 0.024

Station $mb(Lg)$ magnitudes that are uncertain for one reason or another are indicated as follows:

[] inconsistent calibrations
() outlying data point
possible signal interference
++ instrument characteristics uncertain
** poor signal-to-noise ratio

89

In spite of the removal of data with poor SNR, uncertainties in instrument characteristics, or corrupted by interfering signals, there are still some $m_b(Lg)$ that appear anomalous.

In order to identify possible outliers, $m_b(Lg)$ magnitudes were compared with RMS magnitudes obtained at the NORSAR array for STR events (Ringdal and Marshall, 1989). The NAO magnitudes were in all likelihood obtained with accurate calibrations. Furthermore, as they represent average values over the NORSAR array, one would expect them to be subject to less scatter than single station magnitudes.

We applied a least median of squared regression to magnitudes at pairs of stations. This means that we estimated the slope and the intercept of the linear relation between such magnitudes by minimizing the median of the squared residuals. Furthermore, the residuals were defined as the orthogonal distances to the estimated line, rather than the standard "vertical" distance along the y-coordinate axis. That is to say, we assume errors with equal standard deviations for the two types of magnitudes in the regression. This is a generalization of the standard least median of squares regression (Rousseuw, 1984).

The median of the absolute value of a Gaussian variable with zero mean and unit standard deviation is about 0.673 (from a random number generator). Each data point with an orthogonal residual greater than 3 times the median of the absolute value of the residuals divided by 0.673 was classified as an outlier at a level of approximately 3 standard deviations.

This is illustrated by the examples in Figure 29 comparing $m_b(Lg)$ at NAO with those of ARU, OBN, TLY, and UZH. Data points that were identified as outliers by this procedure are marked as circles. The data points for 71/06/06 and 77/09/05 of OBN are clearly outliers, whereas the data point for the event 88/04/03 of ARU appears much less conspicuous.

The procedure was applied to data for stations NAO, ARU, OBN, TLY, and UZH, which all have more than 10 observations for the explosions in Table 11. In this process magnitudes for 7 waveforms, listed in Table 15, were classified as outliers. In addition, three waveforms at NRI and TUP had large station residuals and were included in Table 15. The table gives the value of the $m_b(Lg)$ residual relative to NAO. For two events with no NAO data available, 77/10/29 and 71/12/30, other stations are used as a reference. Negative and positive residuals indicate anomalously low and high $m_b(Lg)$ values, respectively. The table also includes the ratio V(daily)/V(annual) and the SNR. Both of these ratios appear within the normal range. Finally, the table also gives the ratio of the noise amplitude/median noise value. The median noise value was calculated from all available waveforms for a given station. Figure 30 compares the noise ratios with the magnitude residuals and except for OBN on 69/11/30 and UZH on 71/12/30 there seems to be a correlation in the data. This would indicate that the calibration corrections that were applied may have
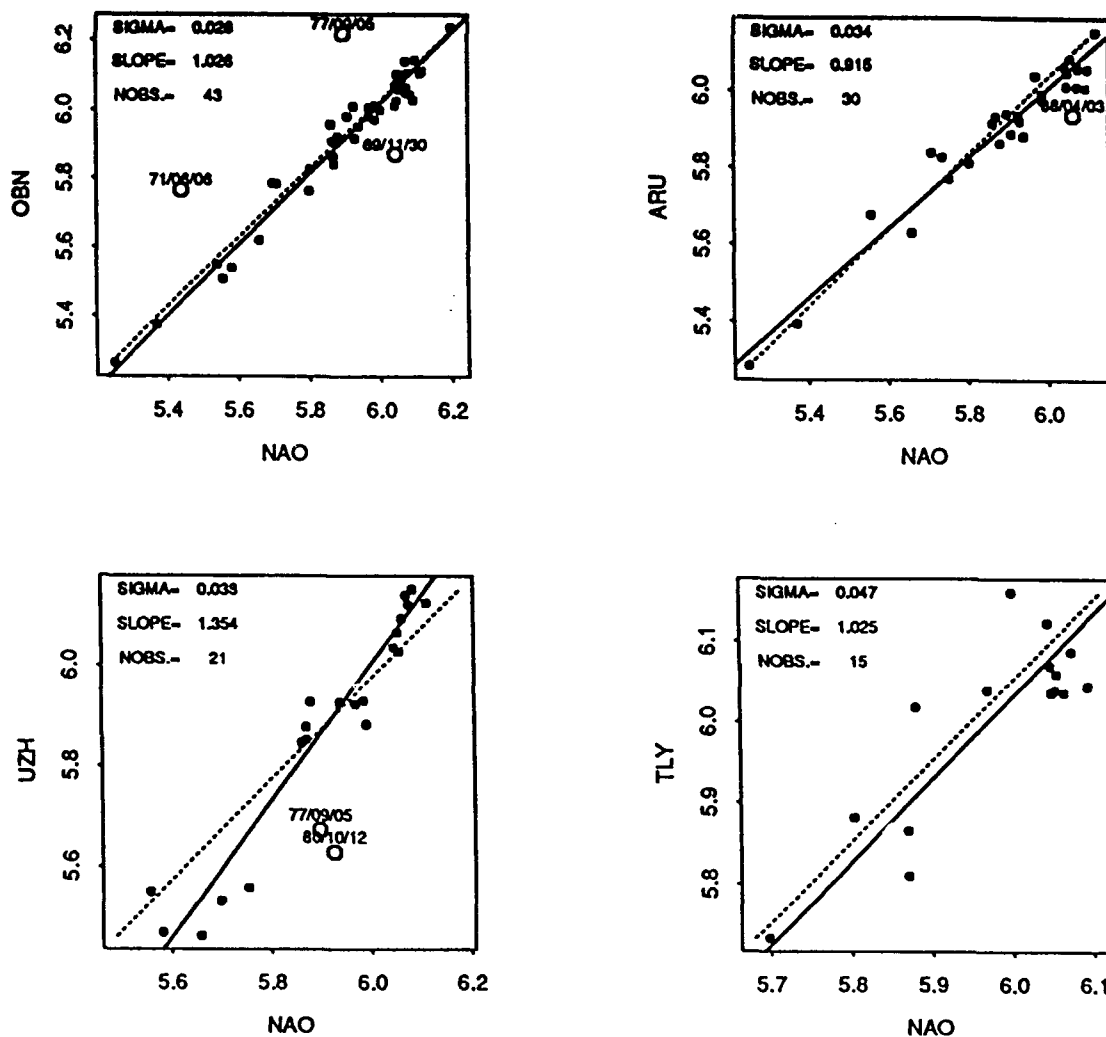
Figure 29: Comparisons of station $m_b(Lg)$ for OBN, ARU, UZH, and TLY with the reference $m_b(Lg)$ at NAO. Outlying data points are marked with circles and the associated date of the explosion. Dotted lines represent equal magnitudes, and filled lines were estimated with the Kummel-York approach introduced by Ericsson (1971) for seismic yield estimation; estimated slopes, misfit errors (SIGMA), and number of observations are also given.
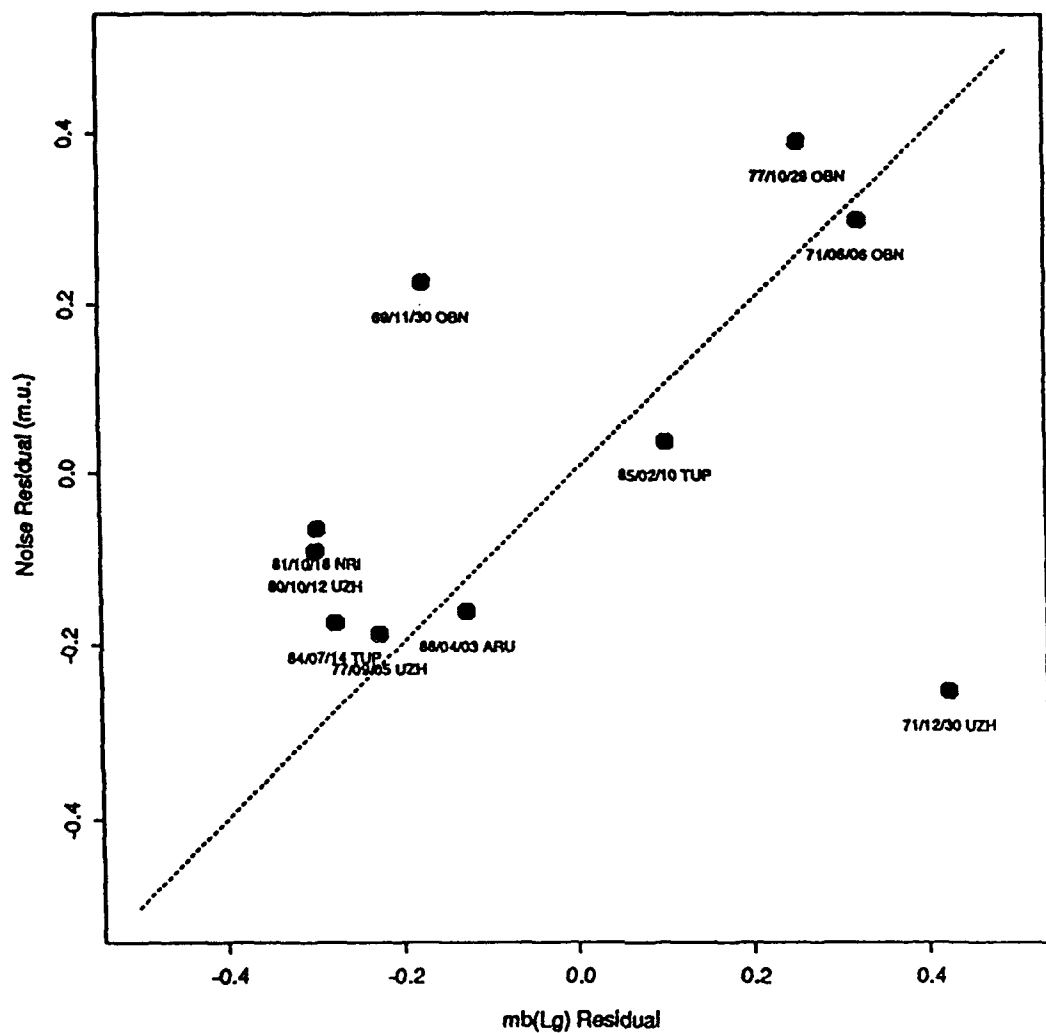
Figure 30: The scatter diagrams compare $m_b(Lg)$ residuals with noise residuals - defined as the logarithm of the ambient RMS noise divided by the median RMS noise for all waveforms - for waveforms with outlying $m_b(Lg)$ data (see Table 15). The dotted line has a slope of 1. Each outlier is identified with explosion date and station code.

Table 15: Outlier Data

Date	Sta	Resid and ref.	Seismo.	V(daily)/ V(annual)	noise/ median(noise)	SNR
69/11/30	OBN	-0.172 NAO	SKM-3	1.04	1.68	10.3
71/06/06	OBN	0.326 NAO	SKM-3	1.00	1.99	16.9
71/12/30	UZH	0.426 OBN	SKM-3	1.00	0.56	2.6
77/09/05	UZH	-0.224 NAO	SKM-3	0.93	0.65	7.8
77/10/29	OBN	0.259 ARU	SKM-3	1.03	2.46	9.6
80/10/12	UZH	-0.296 NAO	SKM-3	0.92	0.81	5.7
81/10/18	NRI	-0.294 NAO	SKM-3	1.00	0.86	24.4
84/07/14	TUP	-0.274 NAO	SKM-3	1.02	0.67	30.0
85/02/10	TUP	0.106 NAO	SKM-3	1.02	1.09	24.7
88/04/03	ARU	-0.125 NAO	SKM-32	1.00*	0.69	332.4

caused the outlying data points.

Scatter in RMS $m_b(Lg)$

Earlier studies have demonstrated the consistency and stability of station $m_b(Lg)$ by comparing magnitudes obtained at two stations from the same explosions and by estimating a linear relation between the two types of magnitudes and the associated misfit error. It is then usually assumed that the standard deviations in the two station magnitudes are equal. As we were comparing station magnitudes obtained at an array, NAO, and at single stations with possible differences in calibration accuracy, we estimated the standard deviations for the stations from station magnitude differences. As $m_b(Lg)$ may scale differently with source strength from station to station, (i.e., the $m_b(Lg)$ may not increase at the same rate with increasing source strength at all stations) we first estimate source scaling.

Figure 29 shows $m_b(Lg)$ at NAO plotted against those at ARU, OBN, TLY, and UZH and Figure 30 shows the magnitudes at OBN against those of the other stations.

The scatter diagrams in Figures 29 and 31 also give estimated slopes and misfit errors on the assumption of equal standard deviations for both types of station magnitudes, and estimated by so called Kummel-York fitting as introduced by Ericsson (1971) for seismic yield estimation. This fitting allows for differences in standard deviations of the station magnitudes, but their ratio must be known and here is assumed to be equal to 1. Estimated
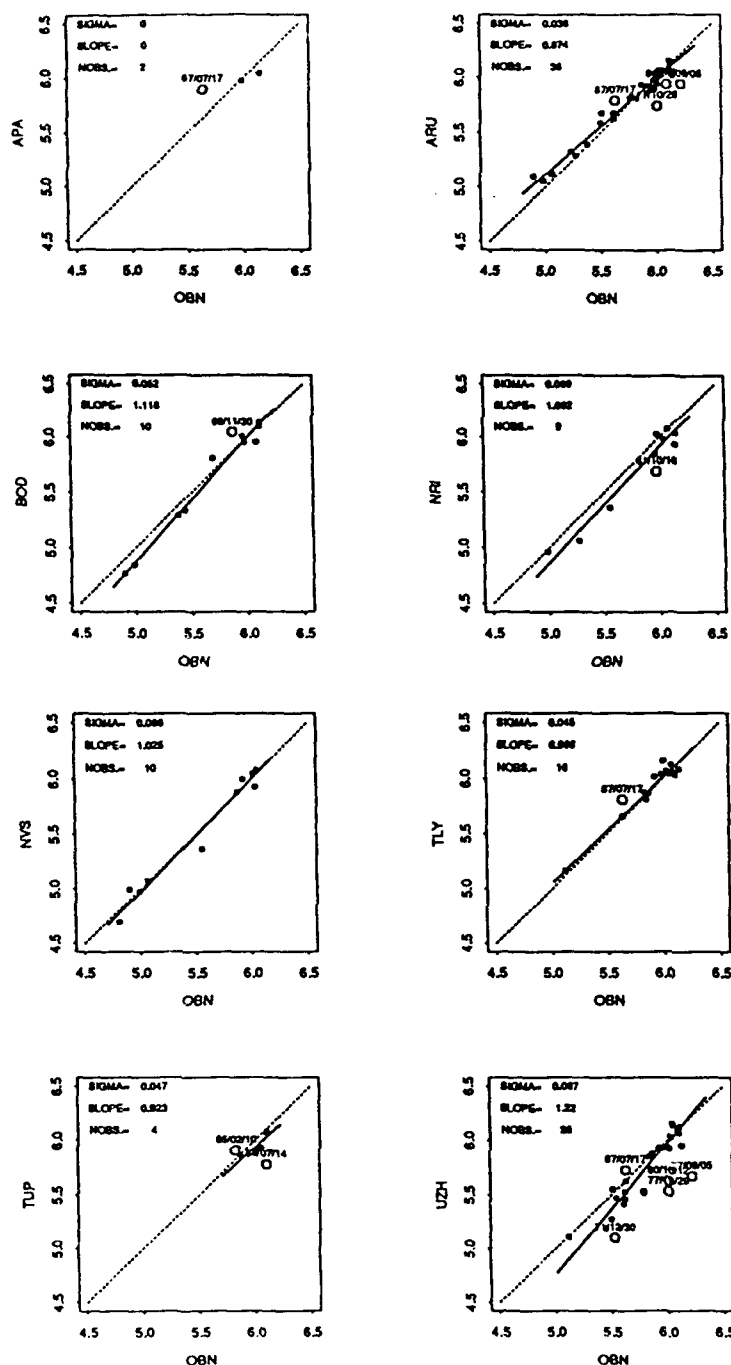
Figure 31: Comparisons of station $m_b(Lg)$ at OBN with those at other Soviet stations. Outlying data points are marked with circles and the associated date of the explosion. Dotted lines represent equal magnitudes, and filled lines were estimated with the Kummel-York approach introduced by Ericsson (1971) for seismic yield estimation; estimated slopes, misfit errors (SIGMA), and number of observations are also given.

slopes, intercepts, and standard deviations of OBN magnitudes are listed in Table 16. The

Table 16: Estimated Slopes and Intercepts Relative to OBN

Station	Slope	Intercept	Misfit Error	No. of Obs.
ARU	1.144 0.032	-0.850 0.188	0.039 0.004	36
BOD	0.898 0.045	0.617 0.255	0.043 0.015	10
NRI	0.964 0.076	0.297 0.436	0.043 0.023	9
NVS	0.982 0.058	0.111 0.320	0.048 0.019	10
TLY	1.041 0.068	-0.261 0.404	0.040 0.009	16
UZH	0.847 0.056	0.941 0.322	0.047 0.013	26

estimated standard deviations of slopes and intercepts (from Reed, 1989) are also given in the table, along with standard errors of the standard deviations estimated from simulations with a random number generator (Israelsson, 1992).

As mentioned earlier, one should expect the error in $m_b(Lg)$ for arrays to be smaller than for single stations. As the accuracy of the calibrations applied for the calculations of the $m_b(Lg)$ may also vary among the stations, this would result in differences in the scatter of the stations $m_b(Lg)$. Assuming the $m_b(Lg)$ to be independent measurements, we estimate approximate standard errors of the station $m_b(Lg)$ using the following procedure. Let m_{ij} denote the $m_b(Lg)$ at station j for explosion i, and let σ_j be the standard deviation of the station magnitudes m_{ij}. In the preceding paragraph we estimated linear relations between pairs of station magnitudes: $m_j = m_j(0) + dm_j/dm_k \, m_k$ where $m_j(0)$ denotes the intercept and dm_j/dm_k the slope, with regard to reference station k=OBN (see Table 16). From the station magnitude differences: $\Delta m_{ijk} = m_{ij} - (m_j(0) + dm_j/dm_k \, m_{ik})$ we form the over determined system of equations (for j,k= NAO, GRF, ARU, OBN, TLY, UZH):

$$\Sigma (\Delta m_{ijk} - \overline{\Delta m_{ijk}})^2 / \Sigma (\delta_{ij} \cdot \delta_{ik} - 1) = \sigma_j^2 + (dm_j/dm_k)^2 \cdot \sigma_k^2$$

where δ_{ij} and δ_{ik} denote weights equal to 1 if data available and 0 otherwise. Table 17

Table 17: Estimated Standard Errors of Station mb(Lg)

Station	σ
ARU	0.035±0.018
BOD	0.065*
GRF	0.033 0.025
NAO	0.027±0.025
NRI	0.093*
NVS	0.087*
OBN	0.038±0.022
TLY	0.052 .024
UZH	0.085±0.029

* = estimate obtained from adjusting
ratio of standard deviations in Kum-
mel-York fitting with OBN data

summarizes the standard deviations, σ, estimated from the least -squares solution of the system of equations. The standard deviations in Table 17 for stations BOD, NRI, and NVS were obtained by applying the Kummel model to data for each one of the stations to events common with station OBN and adjusting the ratio of the two standard deviations so that the estimated value for OBN agreed with that obtained from the system of equations above. There are clear differences among the σ values for the stations; NAO has the smallest standard deviation of 0.033 which is about half the estimated value for UZH. The Kummel-York results in Table 16 were based on ratios of standard deviations in Table 17 for stations OBN, ARU, TLY, and UZH.

A systematic bias between $m_b(P)$ and $m_b(Lg)$ was previously identified by Ringdal and Marshall (1989) for explosion in the Northeastern and Southwestern portions of the Bala-pan area of the STR. Ringdal and Marshall (1989) reported that the magnitude difference, $m_b(P)$ - $m_b(Lg)$, was consistently 0.15 magnitude unit larger for events in the SW portion. The $m_b(P)$ magnitudes were based on teleseismic P amplitudes recorded by a global network. Not entirely ruling out the possibility of a systematic bias in $m_b(Lg)$ between the two portions of Balapan, Ringdal and Marshall (1989) suggested that the anomaly is more likely a result of systematic differences in the P recordings due to strong focusing effects in the upper mantle.

Jih (1990) suggested, on the other hand, that the bias reflects systematic differences in the relative excitation of P and Lg waves between events in SW and NE Balapan.

In Figure 32a we have plotted $m_b(Lg)$ differences, $m_b(Lg;j)-m_b(Lg;k)$, between stations j and k for Balapan events. No systematic bias between events in the SW and NE portions can be seen from these data. In Figure 32b we have also plotted magnitude differences, $m_b(P;j) - m_b(Lg;NAO)$, for four stations, (EKA, MOX, MAT, and STU), at different azimuths from STR. The $m_b(P)$ values were obtained from station reports to ISC. The differences involving $m_b(P)$ have much larger scatter than those with $m_b(Lg)$ in Figure 32a. What is more, they are also in agreement with the observation by Ringdal and Marshall (1989) showing a bias between the SW and NE portions of Balapan. From the data in Figure 32b, this bias appears to depend on station: it is almost 0.4 m.u. for EKA and somewhat less than 0 for MAT. Variation in radiated P waves, as Ringdal and Marshall (1989) suggested, may cause the observed $m_b(P)-m_b(Lg)$ bias across Balapan. The data in Figure 32b indicate that this bias is strongly directional.

Network Magnitudes, Yield, and Depth

The station magnitudes at the Soviet stations were combined into a network $m_b(Lg)$, from the least squares solution of a standard additive model. Magnitudes at stations ARU, BOD, NRI, NVS, TLY, and UZH were converted to an "OBN" scale using the estimated linear relations in Table 16, and the equations in the over-determined system were weighted with the inverses of the estimated variances in Table 17. The resulting network magnitudes are listed in Table 14, together with estimated standard errors.

Magnitude-Yield Relationships

Figure 33 shows $m_b(Lg)$ plotted against announced explosion yields (Bocharov *et al.*, 1989) for the network, OBN, and NAO. Except for the event on 72/08/16, the data are nearly linear. Compared to a maximum likelihood $m_b(P)$ for a world-wide network, the yield of the explosion on 72/08/16 appears high. However, as pointed out earlier, there are uncertainties in the instrument calibrations which might have caused an anomalous $m_b(Lg)$ for this event. On the other hand, the methods used to determine the announced yields have not been described in the literature, nor has the yield accuracy been specified. However well the explosion yields may be determined with observations near the source, independent of seismological measurements, they are bound to have some errors. If nothing else, the numerical accuracy with which they are given seems to be limited by rounding errors; yields less than and greater than 50 kt seem to be given to the nearest kt and to the nearest 5 kt, respectively. Figure 34 shows the standard deviation (on a logarithmic scale) of such rounding errors as a function of explosion yield obtained by a random num-
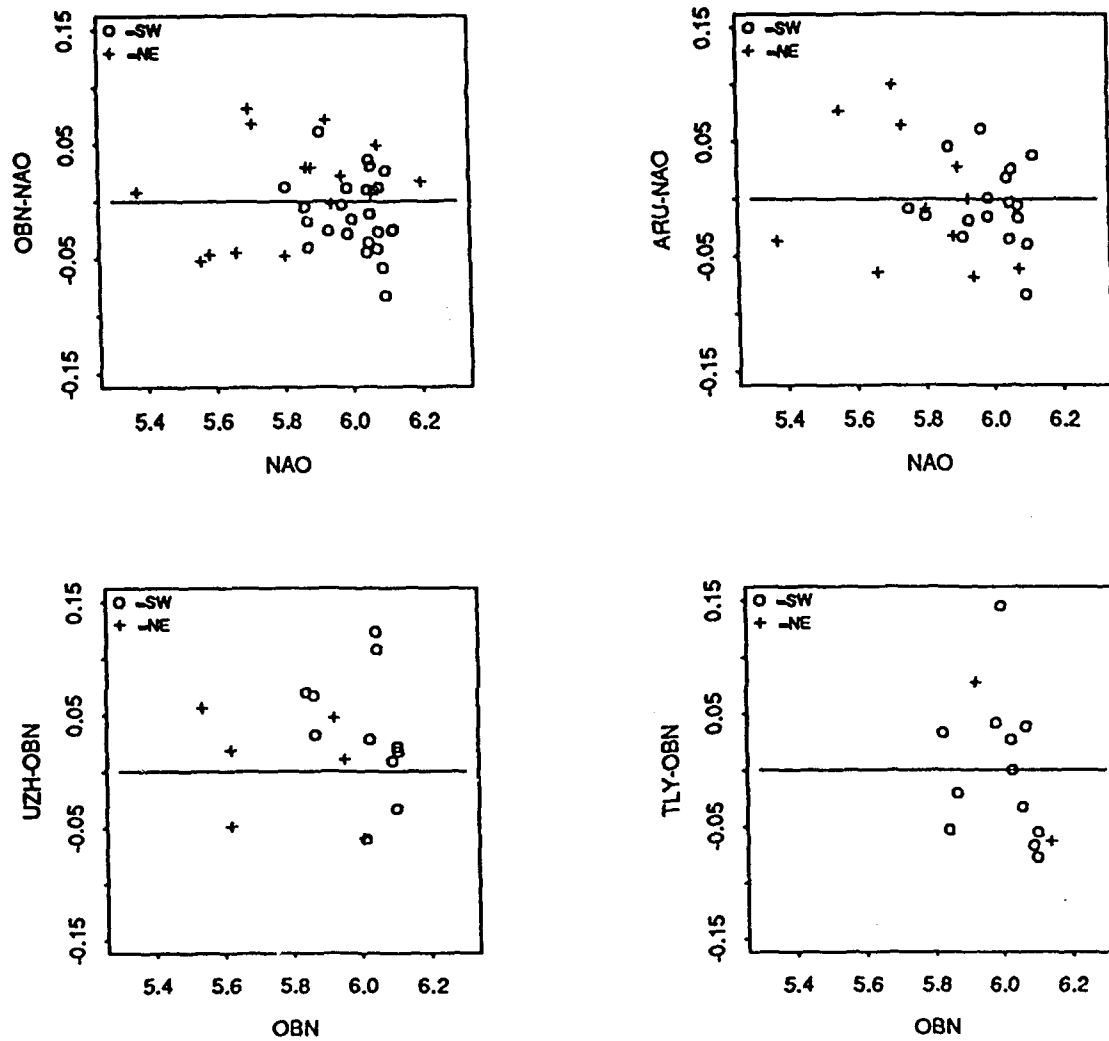
Figure 32a: A scatter diagram comparing magnitude differences $m_b(Lg;j)-m_b(Lg;k)$ for Balapan explosions for station pairs j and k= NAO, OBN, ARU, UZH, TLY. Explosions in the SW and NE parts of Balapan are indicated with circles and plus signs, respectively.
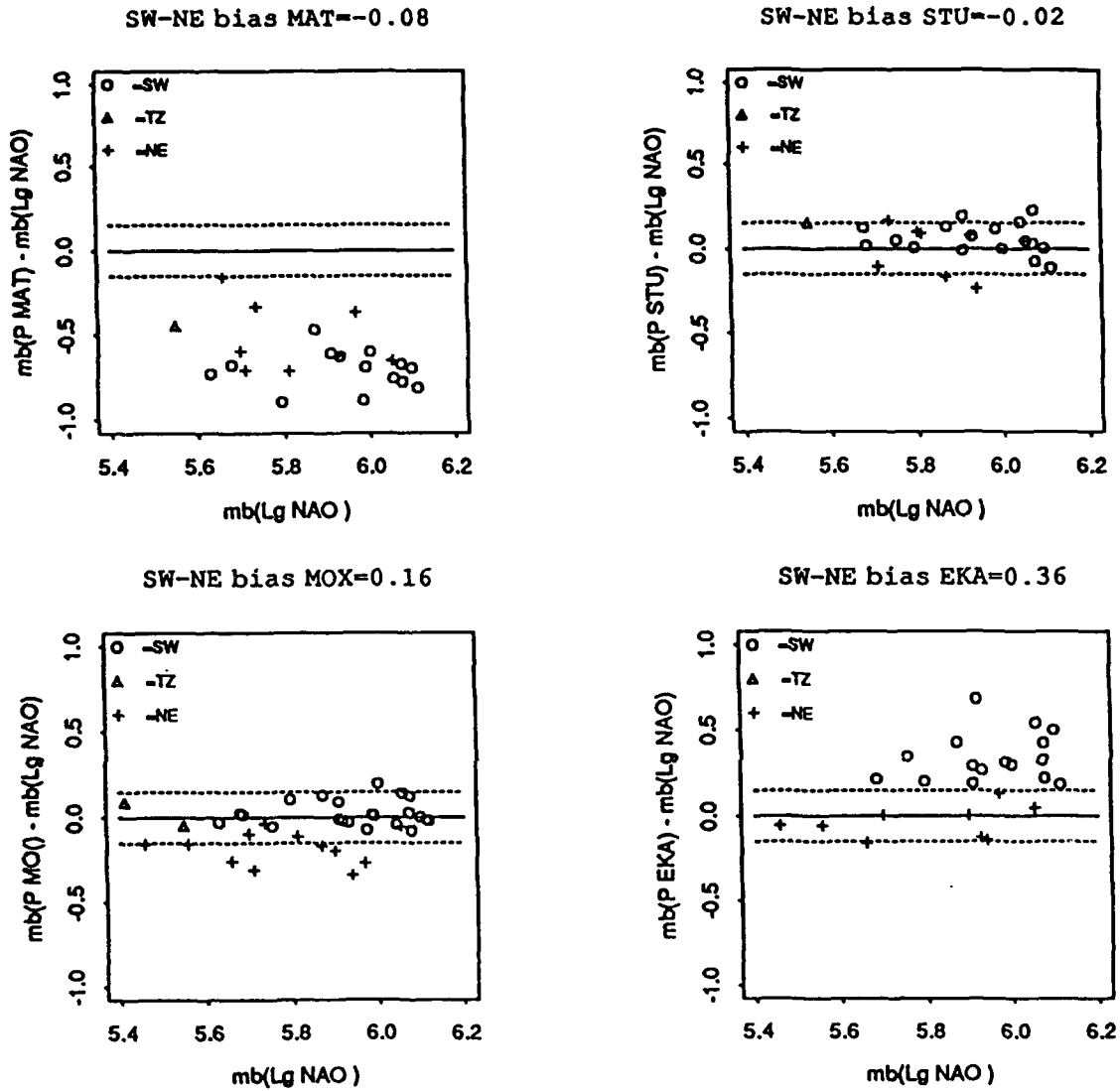
Figure 32b: Scatter diagram comparing magnitude differences $m_b(P;j)-m_b(Lg;NAO)$ for Balapan explosions for stations j=MAT, STU, MOX, EKA. Explosions in the SW and NE part of Balapan are indicated with circles and plus signs respectively. Explosions in the transition zone between NE and SW Balapan are denoted by triangles.
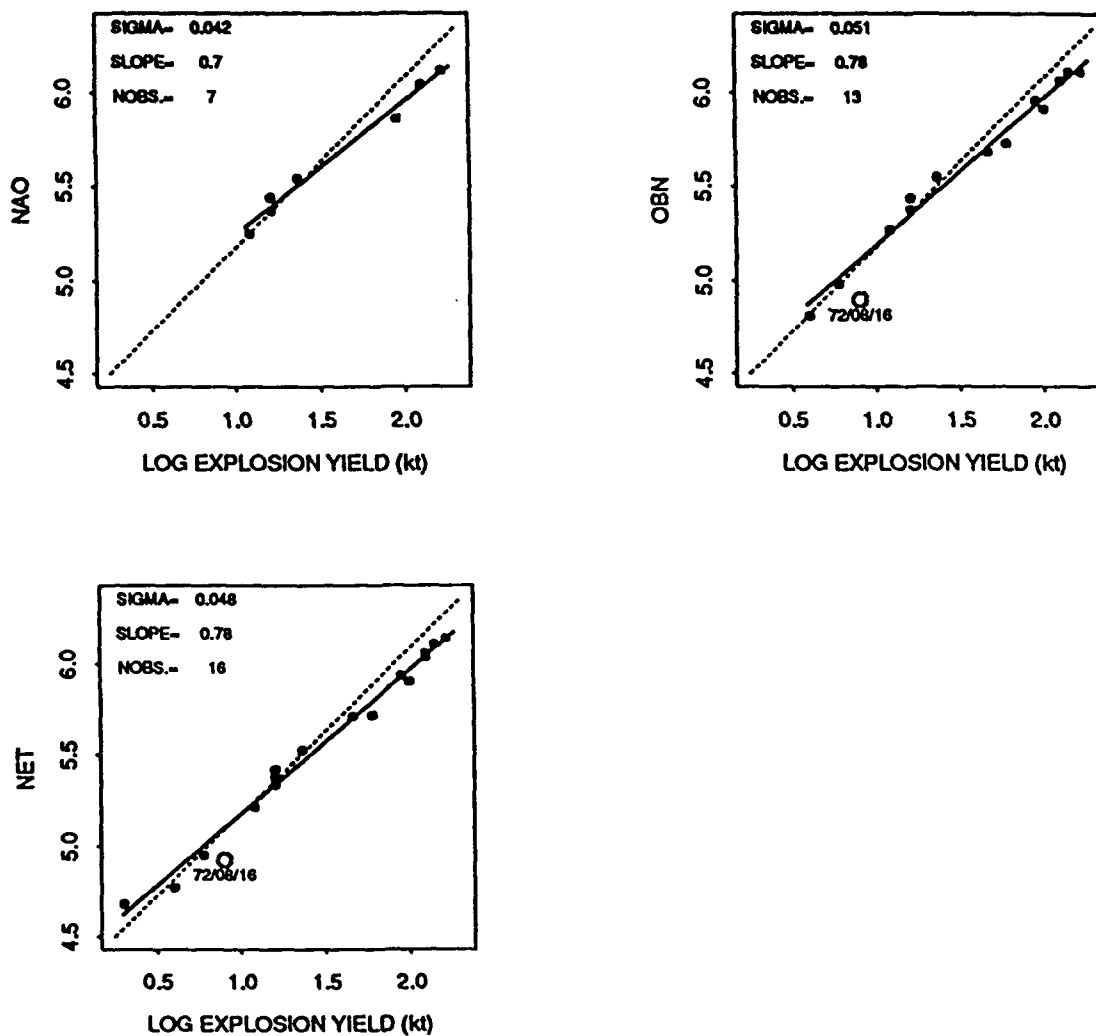
Figure 33: Comparisons of $m_b(Lg)$ and the logarithm of explosion yields (according to Bocharov *et al.*, 1989) for NAO, OBN, and the network of Soviet stations (NET). The outlying data point for the explosion on 72/08/16 is marked with an open circle. Dotted lines represent $m_b(Lg)$ source scaling of 1 with explosion yield, and filled lines were estimated with the Kummel-York approach introduced by Ericsson (1971) for seismic yield estimation; estimated slopes, misfit errors (SIGMA), and number of observations are also given.
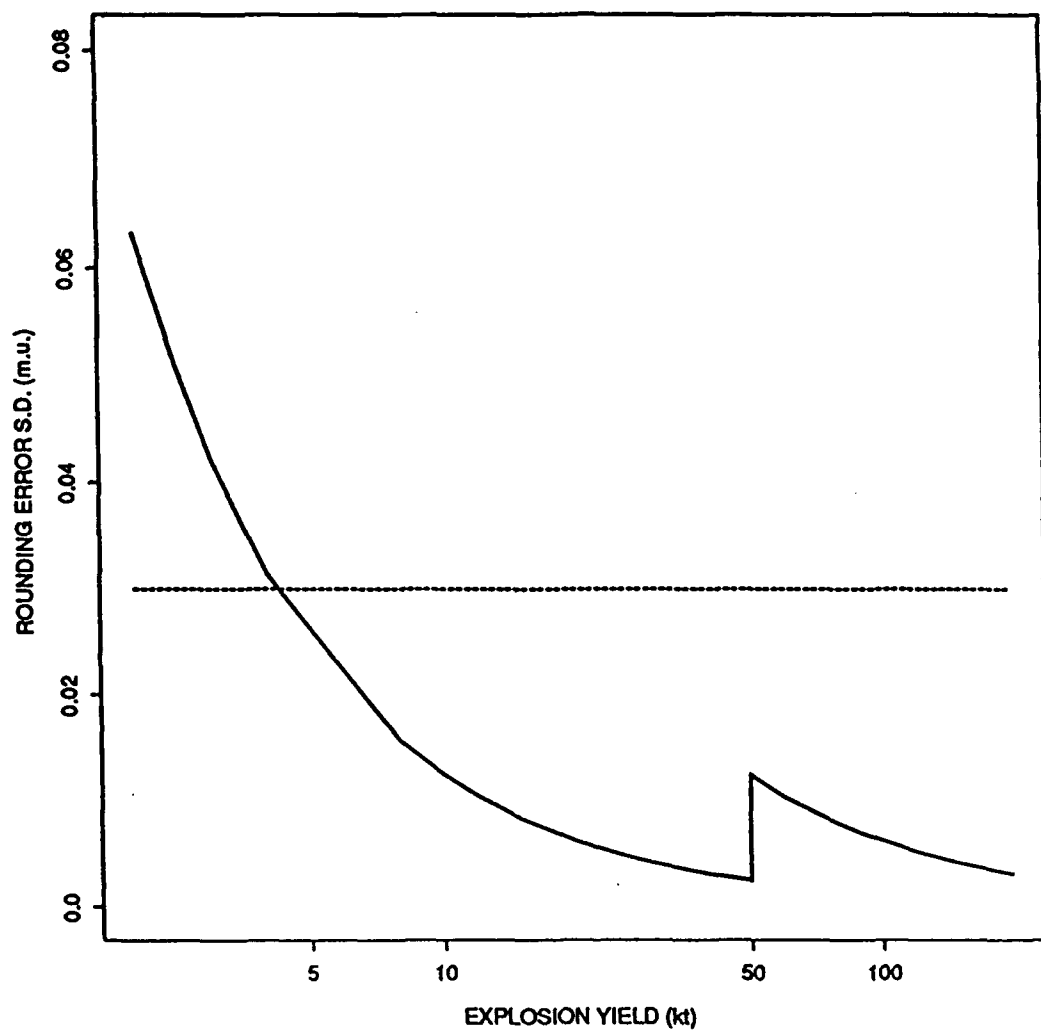
Figure 34: Estimated standard deviation of the logarithm of explosion yield as a function of explosion yield due to rounding errors; the curve was constructed with data from a random number generator.

ber generator. Below 10 kt the standard deviation is a few hundredths of a magnitude unit, which is comparable to the $m_b(Lg)$ standard errors, but still too small to account for the anomalous data of the 72/08/16 event.

Therefore, it is not obvious from the data whether this outlier is caused by instrumental errors (affecting the magnitude or the yield calculations) or is the result of seismological effects, such as anomalous coupling of yield into Lg waves at the source. In the former case, it would be reasonable to remove the data point when estimating a linear relation, while in the latter case the data point has to be included.

We assume that the errors of the announced explosion yields are small compared to magnitude errors so that linear regression can be used to estimate a linear relationship between the logarithm of the yield, W, and $m_b(Lg)$. The type of regression we choose for this purpose depends on whether the 72/08/16 event is used in the estimation or not.

Let us first look at the case where this event is omitted. Then, a standard least squares regression gives: $m_b(Lg) = 0.79\ W + 4.39$. It is reasonable to assume that the magnitude errors are Gaussian with a standard deviation of 0.049 obtained from the residuals of the estimated line. This means that the standard error of yields estimated from $m_b(Lg)$ and this linear relation is about $0.062=(0.049/0.79)$, corresponding to about 15% uncertainty. This uncertainty in yield is, however, a lower bound estimate, since we cannot ignore the uncertainties in the estimated slope and intercept (the 95% confidence intervals (0.770,0.837) and (4.278,4.593), respectively, obtained by bootstrapping; Tibshirani, 1989).

To estimate a linear relation based on all data points; i.e., including the 72/08/16 event, we employ linear regression based on the least median residual and obtain: $m_b(Lg) = 0.82\ W + 4.36$. This estimation method gives identical results regardless whether or not the outlier is included in the estimation. The magnitude errors, which can no longer be considered Gaussian, are all small, except for the outlier which has a residual from the estimated line of -0.14 m.u. If the explosion and magnitude data, including the outlier, are indeed typical of tests at Semipalatinsk, this large residual (corresponding to about 50%) would have to be considered in the assessment of $m_b(Lg)$ as a yield estimator. To these errors we need to add the uncertainties in the estimated slope and intercept with 95% confidence intervals (0.584,0.821) and (4.508,4.594) respectively.

The estimated linear relations for the two cases above are based on the assumption that the yields are error free. If we assume that errors in explosion yields and $m_b(Lg)$ are equal we can apply the Kummel-York model (Ericsson, 1971) to estimate a linear relation and the associated standard deviation. We obtained standard deviations of 0.04 and 0.05 m.u. with and without the 72/08/16 event. These errors correspond to about 12 and 15% standard deviation in the relative explosion yield at the one sigma level. This can be compared with

the 10% uncertainty often quoted for radio-chemical yield estimation methods, a standard against which seismic techniques sometimes are measured.

Effect of Shot Depth

Although it has been demonstrated that RMS Lg magnitudes from explosions are highly consistent for a variety of propagation paths and are linearly dependent on explosion yield, it has been suggested on the basis of theoretical modelling that this type of magnitude can be quite sensitive to shot depth.

Lilwal, (1988), for example, suggests that the generation of Lg waves can, under some circumstances, be strongly dependent on the shot depth. This would imply that explosions with the same yields, set off at different depths, could also have different RMS Lg magnitudes. If true, this would complicate seismic yield estimation using the Lg method.

In his theoretical modelling Lilwal (1988) obtained a substantial drop in Lg energy as the explosion source was moved from 500 to 1500 m depth. Frankel (1990) suggests that this effect is related to a change in P-wave velocity at the source rather than to a change in depth *per se*. Increasing the shot depth increases the P-wave velocity (from 4 to 5 km/s in the model). If it becomes larger than the S-wave velocity of the upper mantle, the contribution of the P-S conversion, pS, to the generation of the Lg wave is significantly reduced. Frankel (1990) also finds that as long as the source depth is varied within a single layer, (i.e., no change in the P-wave velocity), there is little change in the generated Lg energy. This is in apparent agreement with the data here, as shot depths are less than 1 km and most velocity models for and near the Semipalatinsk test range, Balapan in particular, assume a constant P-wave velocity, of about 5 km/s, in the upper 1 km of the crust (Leith, 1987; Priestley *et al.*, 1988; and Thurber *et al.* 1989). McLaughlin *et al.*(1991) modelled the generation of regional Lg phases and found that a spherically symmetric explosion in a high velocity medium of the kind at the Semipalatinsk test site is a very poor generator of Lg-wave energy. As this model was inadequate to explain observed Lg waves, they concluded that deviatoric source components would be required to model the equivalent source. Non - linear surface interaction would be responsible for this deviatoric source, which could be represented by an equivalent CLVD source. From calculations of Lg waveforms from explosions beneath flat and sloping surfaces at different scaled depths, they also found that Lg waves are a stable yield estimator in spite of the wide range of depth of burial.

The data announced by Bocharov *et al.* (1989) are summarized in Figure 35, showing explosion yield versus shot depth. The data points do not all follow the same scaling law, although it has been suggested that explosions at Balapan and Murzhik were set off
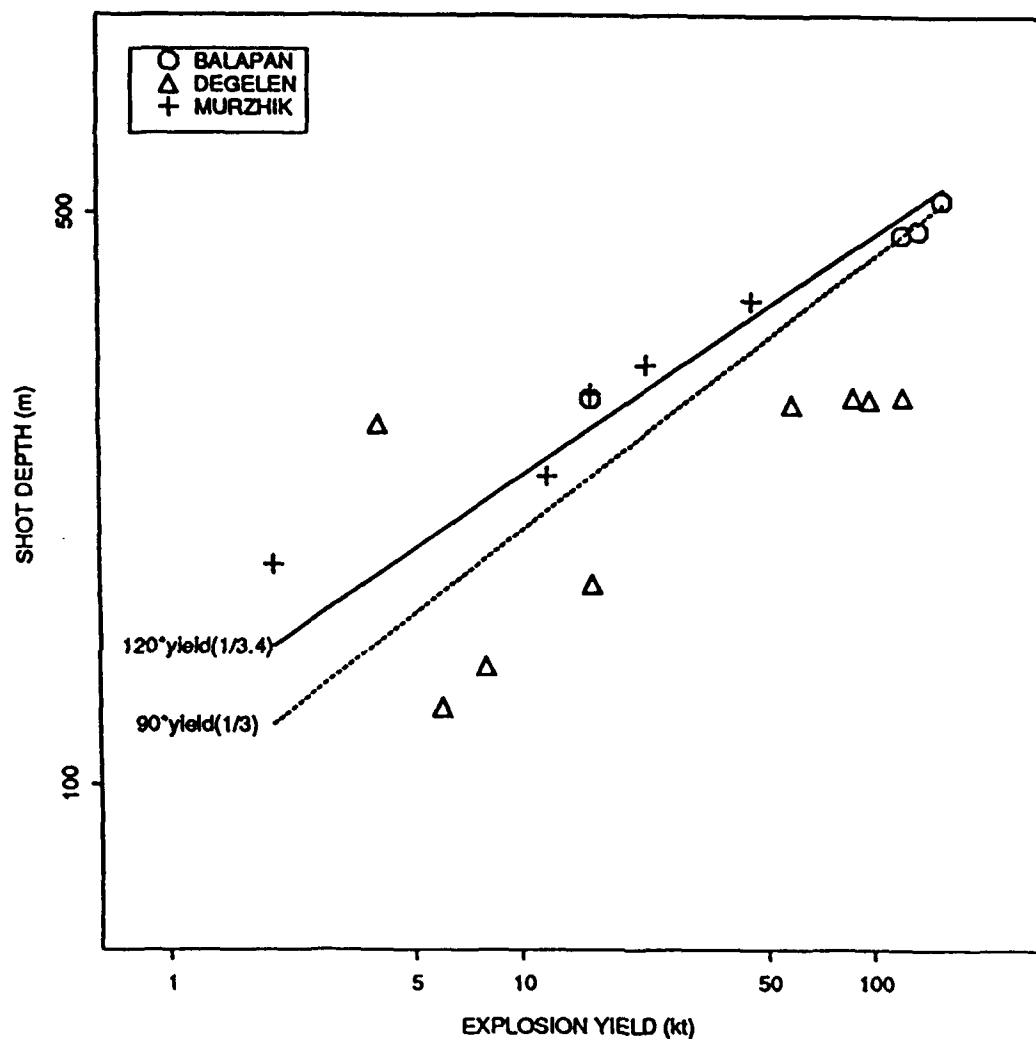
Figure 35: Explosion yield plotted against depth of burial for the data published by Bocharov *et al.* (1989) for Semipalatinsk. The dotted line was fitted to the data with an assumed slope of 1/3, and the line $120Y^{1/3.4}$ is generally considered standard depth of burial for U.S. explosions according to McLaughlin *et al.* (1991).

according to a quartic scaling law, i.e., $h = y^{1/4}$ where depth is h and Y is yield (Jih, 1990). Here, however, we assume the more conventional cubic scaling and fit a line through the data points in Figure 35, thus obtaining the relation: $h = 90Y^{1/3}$ (with least squares median regression). The relation $h = 120Y^{1/3.4}$, generally considered standard depth of burial for U.S. shots (McLaughlin *et al.*, 1991), is drawn for comparison. According to Adushkin (private communication, 1991) cube root scaling, $h0Y^{1/3}$, was applied to tests at Semipalatinsk, and that the factor h0 depended on local geology at the shot point and type of emplacement, (adit or borehole). It should be noted that the yields used to determine a suitable depth of burial based on a given depth-yield relation represent the design yields, which may be different from the actual or measured yields, such as those plotted in Figure 35.

In Figure 36 we compare the depth residuals, on a logarithmic scale, with the magnitude residuals (relative to explosion yield on a logarithmic scale). No clear correlation can be seen between the two kinds of residuals, which would suggest that the $m_b(Lg)$ may not be strongly dependent on depth at least for depth varying only by of a factor of two as here.

It should be noted that the data represents a wide range of conditions. Not only are there differences in shot medium, but there were also differences in emplacement with the explosions at Degelen being adit shots and explosions at Balapan and Murzhik set off in boreholes.

Some Concluding Comments

This note has aimed at studying the precision of $m_b(Lg)$ from underground nuclear explosions at the Semipalatinsk Test Range, their correlation with explosion yield and possible effects of shot depth. Compared to previous studies with similar objectives we have been able to use a more extensive data set, with regard both to the explosions and to the recording stations. Unlike earlier studies, which are largely confined to data from explosions at the Balapan area of the STR, several events at Degelen as well as Murzhik are included in this analysis. Also, the explosions span a large yield range, almost two orders of magnitude. The propagation paths to the nine seismological stations cover a wide interval of epicentral distances -local, regional, and teleseismic - and cross a diversity of tectonic structures.

Being hand digitized from analog recordings the data obviously have a dynamic range and frequency range smaller than those of digital recordings. Yet, they are sufficiently accurate to provide a consistent Lg RMS magnitudes comparable to that for modern high quality stations.

A few outlying station RMS Lg values were found in contrast to previous studies where
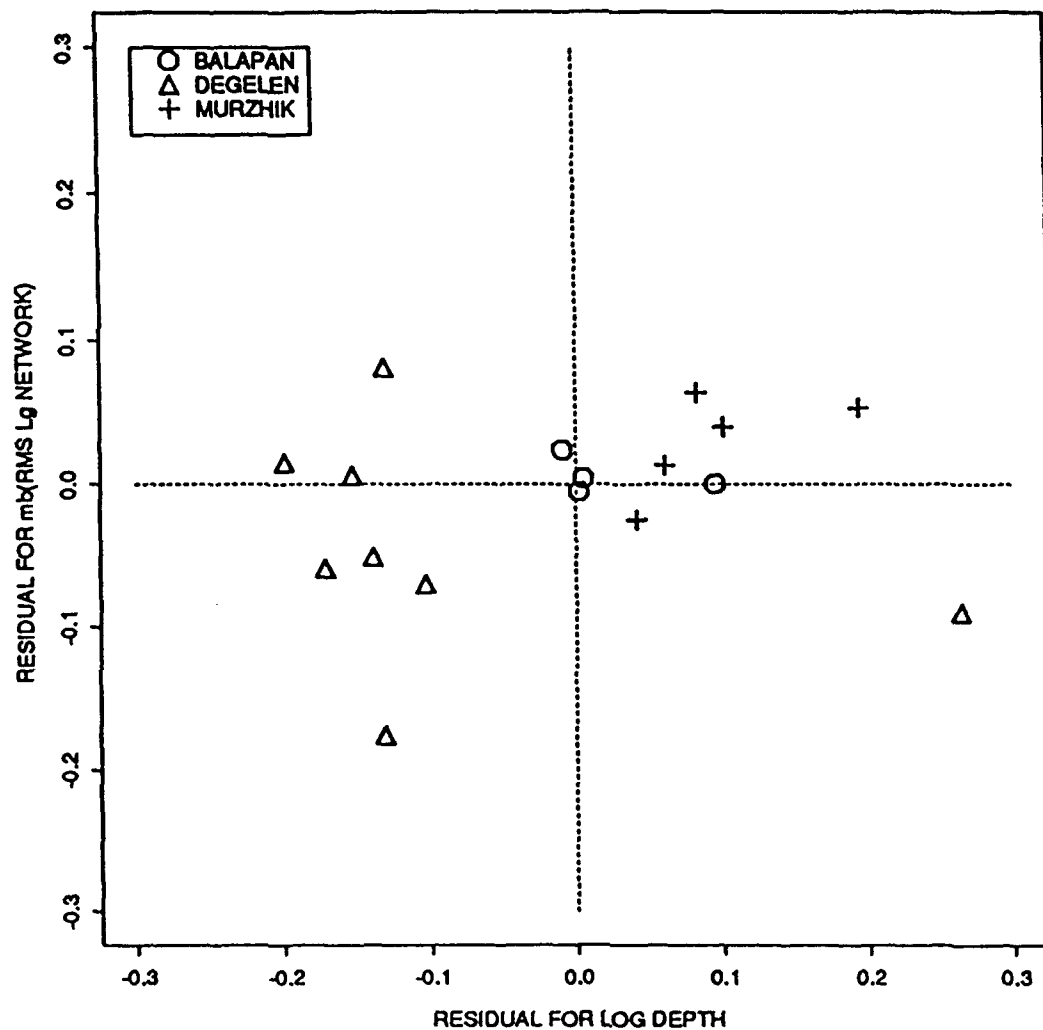
Figure 36: The residuals for the logarithm of depth from the relation $90Y^{1/3}$ based on the data by Bocharov *et al.* (1989) in Figure 35 are plotted against the $m_b(Lg;NET)$ residuals.

no outliers have been reported. Although instrument calibration errors are a probable factor, there is still the possibility that seismological effects along the propagation path caused the outliers. The fact that no outlier has been reported in earlier studies could also be a result of the limited number of propagation paths and source regions represented by the data. Whatever the reason may be, the outliers do not appear to be a problem in the calculations of network magnitudes. For a given event an outlier could usually be identified unequivocally and removed from the calculation of network magnitudes.

We found that the standard errors of the magnitudes vary somewhat among the stations. The smallest standard error (0.035 for station OBN) is only marginally larger than that of RMS Lg magnitudes at NAO, which were obtained as site-corrected averages of the magnitudes at the individual NAO sub-arrays. There was no apparent correlation between standard error and signal-to-noise ratio. It is more plausible that the variation in standard error among stations be attributed to differences in instrument characteristics at the stations. Some stations appear to have recording characteristics that change less over time than others do. The station with the largest standard error, UZH, also appeared to have the largest variation in instrument characteristics. The estimated standard errors of the station magnitudes are quite small if we consider that the uncertainty in instrument responses. Soviet seismologists state that the uncertainty is typically between 5-10%, which corresponds to 0.02-0.04 magnitude units. The contribution of uncertainties in instrument responses to the magnitude standard deviations cannot, however, be quantified. Therefore, the calculated standard deviations must be considered as upper bound estimates.

Although the small standard deviation of the RMS Lg magnitudes are encouraging the implications for yield estimation are difficult to determine exactly from the data analyzed here. This is mainly due to the fact that, as mentioned earlier, the methods used to determine the yields published by Bocharov *et al.* (1989), let alone their accuracy, are not available. What is more, it is not even clear that these announced yields are independent of seismological data.

An optimistic interpretation of the magnitude-yield data would disregard the outlier for the explosion on 72/08/16, the cause of which could not be established, and furthermore assume that the announced yields of the other explosions have errors smaller than or comparable to those of the RMS magnitudes. The close correspondence between magnitudes and yields in this case is, perhaps, somewhat unexpected, since the data represent explosions in not only three distinct, widely separated, subregions of STR but also in different types of rock - granite, siltstone, quartz porphyroid, sandstone, tuffaceous sandstone, conglomerate - and in two types of emplacement, borehole and adit. Furthermore, although the depth range is limited to a factor of two for explosions of similar yields, significant effects of shot depth on $m_b(Lg)$, as suggested by some theories for wave generation by

explosive sources, cannot be seen.

This interpretation of $m_b(Lg)$ as a highly accurate yield estimator, with its close linear relation to explosion yield and insensitivity to shot depth, to type of emplacement, and rock type, becomes untenable if we include the data for the explosion on 72/08/16. The shot characteristics of this event - adit in granite at 139 m depth - were similar to those of the explosion on 71/04/25.

Therefore, it is not until the accuracy of the announced data for the explosions becomes available and the independence of the announced yields on seismic data has been established, that it will be possible to assess, with a high degree of confidence, the $m_b(Lg)$ as a yield estimator of explosions in *different* source conditions. The uncertainty about the quality of the announced yields renders generalizations difficult even for explosions with *similar* conditions, as illustrated by the data for the explosion on 72/08/16.

Acknowledgments

References

Baker, R.G. (1970). Determining magnitude from Lg, Bull. Seism. Soc. Am., 60, 1907-1920.

Bocharov, V.S., Zelentsoz, S.A., and V.N. Michailov (1989). Characteristics of 96 underground nuclear explosions at the Semipalatinsk test site, Atomic Energy (Atomnaya Energiya), 67.

Chiburis, E.F., R.O. Ahner, E.J. Reinhart (1980). Procedures for Digitizing Seismograms ENSCO Technical Report DCS-STR-80-53

Ericsson, U. (1971). Maximum likelihood linear fitting when both variables have normal and correlated errors, National Defense Research Institute, Stockholm, Sweden, FOA 4 Report C4474-A1.

Frankel, A. (1990). Effects of source depth and Crustal structure on the spectra of regional phases determined from synthetic seismograms, in Proceedings of DARPA/AFTAC ANNUAL Review for FY89, HQ AFTAC/TTR Patrick AFB, FL 32925-6001

Hansen, R. (1990). Analysis of data from the British station GAM near Garm, USS for Soviet nuclear explosions, in: Semiann. Tech. Summ., 1 Oct 1989-31 March 1990, NORSAR Sci. Rep. 2-89/90, Kjeller, Norway.

Hansen, R., Ringdal, F., and P.G. Richards (1990). The stability of RMS Lg measurements, and their potential for accurate estimation of the yields of Soviet underground explosions Bull. Seism. Soc. Am., 80, 2106-2126.

Israelsson, H. (1992). RMS Magnitudes, yields, and depths of explosions at the Semipalatinsk Test Range. (This Report)

Jih, R.S. (1990) Geotech's Magnitude-Yield Study During 1989-1990. in Proceedings of the Twelfth Annual DARPA/GL Seismic Research Symposium. (Eds J. Lewkowicz and J McPhetres), GL-TR-90-0212 Geophysics Laboratory, Hanscom AFB, MA. ADA226635.

Kemerait, R. C., G. Kraft, J. S. Mott, and E. Dohner (1981), A study of the hand-digitizing process for digitizing short period seismic data. ENSCO Technical Report DCS-SDR-81-57

Kondorskaya, N.V. and Z.I. Aranovich (1979), The uniform system of seismic observations of the U.S.S.R.and prospects for its development, Phys. Earth and Plan. Int., 18, 78-88

Leith, W. (1987) Geology of NRDC seismic station sites in Eastern Kazakhstan, USSR.U.S. Geol. Surv. Open File Rep., 87-597.

Lilwal, R.C. (1988). Regional mb:Ms, Lg/Pg amplitude ratios and Lg spectral ratios as criteria for distinguishing between earthquakes and explosions: a theoretical study, Geophys. J. Roy. astr. Soc. 93, 137-147.

McLaughlin, K.L., J.L. Stevens, T.G. Barker, and B. Shkoller (1991). Investigations of non-linear explosions effects, in Proceedings of the 13th Annual DARPA/GL Seismic Research Symposium, 8-10 October 1991. (Eds J. Lewkowicz and J McPhetres), PL-TR-91-2208 Geophysics Laboratory, Hanscom AFB, MA. ADA241325.

Nuttli, O.W. (1986a). Lg magnitudes of selected East Kazakhstan underground explosions, Bull. Seism. Soc. Am. 76, 1241-1251

Nuttli, O.W. (1986b).Yield Estimates of Nevada Test site explosions obtained from seismic Lg waves, J. Geophys. Res., 91, 2137-2151.

Nuttli, O.W. (1987). Lg magnitudes of Degelen, Eastern Kazakhstan, Underground explosions, Bull. Seism. SOc. Am., 77, 679-681

Nuttli, O.W. (1988). Lg magnitudes and yield estimates for underground Novaya Zemlya nuclear explosions, Bull. Seism. Soc. Am. 78, 873-884.

Patton, H.J. (1988). Application of Nuttli's method to estimate yield of Nevada Test Site Explosions recorded on Lawrence Livermore National Laboratory's digital seismic system, Bull. Seism. Soc. Am. 78, 1759-1772.

Press, F. and M.W. Ewing (1952). Two slow waves across North America, Bull. Seism. Soc. Am., 42, 219-228.

Priestly, K., G. Zandt, and G.E. Randall (1988),Crustal Structure in eastern Kazakhstan, USSR from teleseismic receiver functions, Geophys. Res. Lett., 15, 613-616

Reed, C.B (1989). Linear least-squares fits with errors in both co-ordinates. Am.J.Phys. 57, 642-646. Richter, C.F. (1935). An instrumental earthquake magnitude scale, Bull. Seism. Soc. Am., 25, 1-32.

Richter, C.F. (1935).An instrument earthquake magnitude scale. Bull. Seism. Soc. Am., 25, 1-32.

Ringdal, F. (1983). Magnitudes from P coda and Lg using NORSAR data, in: Semiann. Tech. Summ., 1 Oct 82 - 31 Mar 1983, NORSAR Sci. Rep. 2-82/83, Kjeller, Norway.

Ringdal, F. (1989) NORSAR P-wave detection and yield estimation of selected Semipalatinsk explosions, in: Semiann. Tech. Summ., 1 April - 30 Sep 1989, NORSAR Sci. Rep. 1-89/90, Kjeller, Norway.

Ringdal, F. and B.K. Hokland (1987). Magnitudes of Large Semipalatinsk explosions using P coda and Lg measurements at NORSAR, in: Semiann. Tech. Summ., 1 Apr-30 Sep 1987, NORSAR Sci. Rep. 1-87/88, Kjeller, Norway.

Ringdal, F. and J. Fyen (1988). Comparative analysis of NORSAR and Grafenberg Lg magnitudes of Shagan River explosions, in: Semiann. Tech. Summ., 1 Apr-30 Sep 1988, NORSAR Sci. Rep. 1-88/89, Kjeller, Norway.

Ringdal, F. and Marshall (1989). Yield determination of Soviet underground nuclear explosions at the Shagan River Test Site in: Semiann. Tech. Summ., 1 Oct 1988 -31 March 1989,

Rousseuw, P.J. (1984). Least Median Squares Regression, Journal of the American Statistical Association, 79, 871-880.

Thurber, C., H. Given, and J. Berger (1989).Regional seismic event location with a sparse network: Application to eastern Kazakhstan, USSR,J. Geophys. Res. 94, 17,1767-17,780

Tibshirani, R. (1988).Variance stabilization and the bootstrap.Biometrika, 75, 433-444.

Zonenshain, L.P., J. Verhoef, R. Macnab, and H. Meyers (1991). Magnetic Imprints of Continental Accretion in the U.S.S.R, EOS, 29, 305.

RMS Lg Magnitudes and Path Corrections for U.S.S.R. Explosions

Hans Israelsson

Abstract

The attenuation of RMS amplitudes of Lg waves for a number of paths across the contiguous U.S.S.R were analyzed from data of hand-digitized recordings of explosions at Novaya Zemlya and Semipalatinsk. The RMS amplitudes were measured in the 0.6-3.0 Hz frequency band and the 3.1-3.7 km/s group velocity window. The log RMS Lg amplitudes for both Novaya Zemlya and Semipalatinsk events were separated into source, path, and station terms. The path term included expressions for geometrical spreading (for Airy phase) and anelastic attenuation. The decay rate of the anelastic term was found to be stable around an average of 0.0012 per km. This was somewhat surprising due to the variety of paths between the explosion sites and the stations (distances ranging from about 1000-4000 km). The station corrections correlated closely with average ambient noise at the stations. Announced explosion yields were available for events at Semipalatinsk, and the slopes of the RMS amplitude/yield curves were close to ̇.8 for the stations. The consistency of the path and station terms, combined with the assumption of similar source coupling conditions at the two test sites, make it plausible to link the log/yield curve for Semipalatinsk to the estimated source terms for Novaya Zemlya. Estimates for a suite of about 10 events with similar strengths were around 50 kt.

Introduction

The recent improved prospects for accurate seismic determinations of yields of underground nuclear explosions rely on two qualities of Lg waves: the high precision of their RMS amplitude measurements and the close correspondence of these amplitudes with explosion yield (Hansen *et al.*, 1990). The high precision has been demonstrated by a remarkable relative consistency of such amplitudes at widely distributed seismological stations for explosions at a given test site. These qualities notwithstanding, accurate yield estimates from Lg measurements are limited to calibrated explosions. For example, RMS Lg amplitudes at a given station from explosions at the same site cannot even provide accurate *relative* yields, unless the scaling of the amplitudes with yield (the rate of increase of amplitudes with increasing yield) can be estimated, i.e., *calibrated,* from data of explosions with "known" yields, determined from non-seismic methods near the sources. The calibration also provides control of the uncertain effects of the fixed path on the Lg waves between the explosions and the station, as well as possible variation from

site to site in the coupling of yield into Lg waves.

Defined uniquely for a particular explosion test site and for a fixed station network, the calibration for one site-station network configuration may, however, not be applicable to another. In order to estimate yields of explosions at any site in the *uncalibrated* case, one has to address, *inter alia,* the problem of making path corrections for the RMS Lg amplitudes since they are no longer controlled.

To get some insight into the problem of determining yields of explosions at uncalibrated sites we study, in this report, the attenuation of RMS amplitudes of Lg waves propagating along a number of paths across the contiguous U.S.S.R. For this purpose we use data that have become available as a result of the bi-lateral Nuclear Testing Talks. The data consist of hand-digitized waveforms from recordings at seismic stations located throughout the western and central parts of the U.S.S.R. of explosions at the major testing grounds near Semipalatinsk and near the Matochkin Shar at Novaya Zemlya and at four other sites in the U.S.S.R. A detailed description of these data - explosions, seismological stations, and waveforms - has been compiled by Israelsson (1991a,b). Announced yields, presumably independent of seismic information, were available at the Semipalatinsk test range, so that it could be calibrated. No such information was available for the other five sites, which were uncalibrated.

Data

The map in Figure 37 shows the relative locations of the seismological stations and the explosion sites for the data analyzed here. Lines, representing approximate wave paths, have been drawn between stations and explosion sites for which data were available. The boundaries of the major tectonic components of the area covered by the wave paths are also outlined on the map (after Zonenshain, 1991). The Siberian and East European platforms are interposed, in the central part of the map, by the Kazakhstan accretionary continent. Sandwiched between these three components are the Uralian and Central Asian orogenic belts. Most wave paths cross a mixture of tectonic structures in various combinations, and there is no wave path purely across a platform structure. For the purpose of discussion of data for explosions at Azghir (north of the Caspian Sea), the extent of the Peri-Caspian depression is also indicated on the map (after Zonenshain, 1991b).

Locations, times, and, body wave magnitudes reported by ISC for all 102 explosions, are listed in Table 18. The explosions are unevenly distributed among 6 separate sites: Semipalatinsk (81), Matochkin Shar at Novaya Zemlya (14), Azghir (4), near Krasino at Novaya Zemlya (1), near Lake Baikal (1), and in Central Siberia (1). The explosions at the Semipalatinsk test range are also unevenly distributed among its three subareas: Balapan
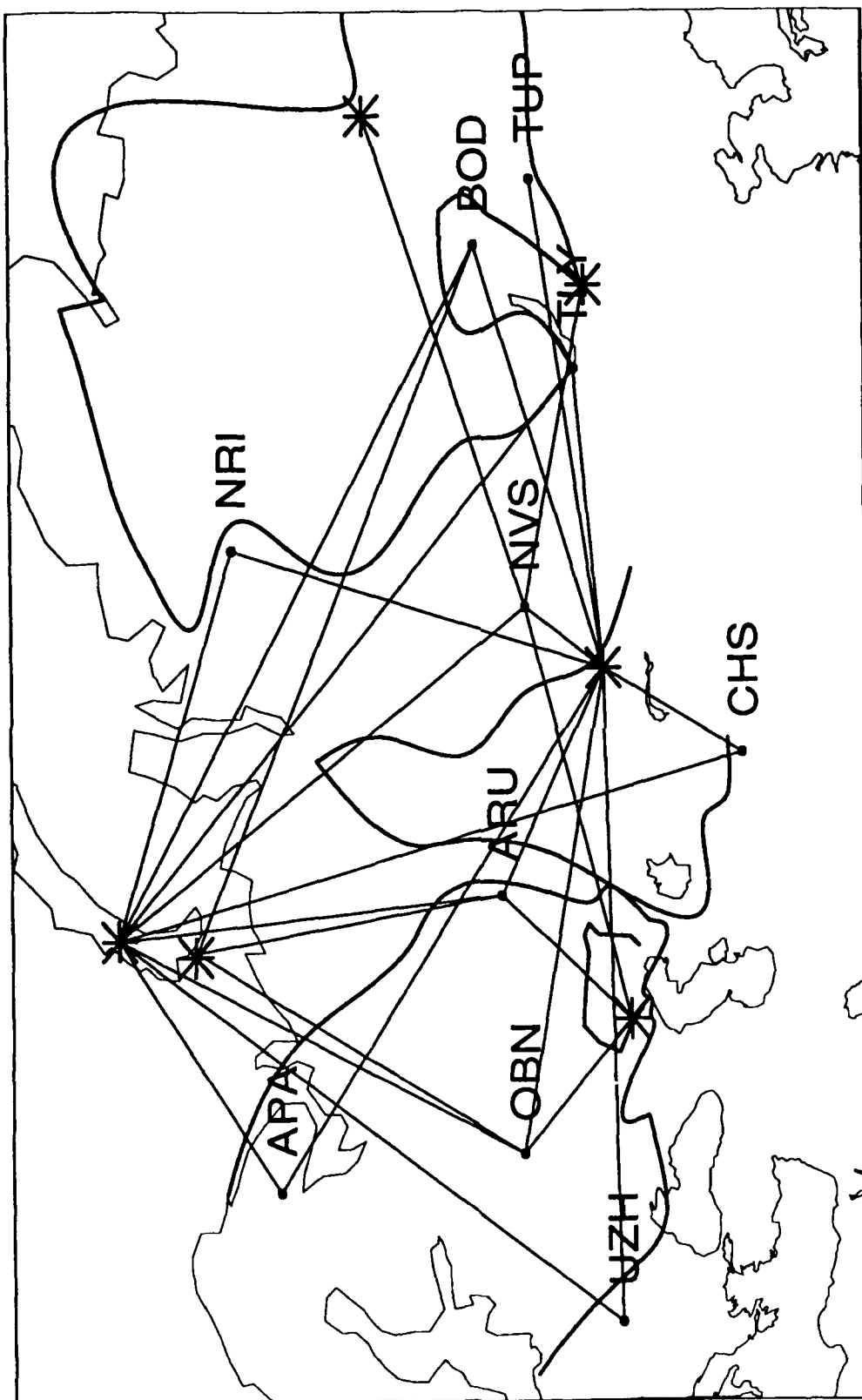
Figure 37: Map showing seismological stations, indicated with station codes, and explosion sites, marked with asterisks. A straight line has been drawn between each pair of station and explosion sites for which waveform data was available. Thick lines outline boundaries of major tectonic elements (after Zonenshain, 1991).

115

Table 18: Explosions

Date	Time	Lat.(N)	Long.(E)	$m_b(ISC)$	Site
66/03/20	05:49:57.8	49.720	78.070	6.0	Degelen
66/05/07	03:57:58.2	49.740	77.950	4.8	Degelen
68/09/29	03:42:57.8	49.820	78.180	5.8	Degelen
69/07/23	02:46:58.0	49.880	78.230	5.4	Degelen
69/11/30	03:32:57.3	49.940	78.980	6.0	Balapan SW
69/12/28	03:46:57.8	49.980	77.790	5.7	Murzhik
71/04/25	03:32:57.9	49.766	78.081	5.9	Degelen
71/06/06	04:02:57.3	49.977	77.740	5.5	Murzhik
71/06/19	04:03:57.7	49.966	77.724	5.4	Murzhik
71/10/09	06:02:57.2	49.986	77.687	5.3	Murzhik
71/10/21	06:02:57.5	50.004	77.631	5.5	Murzhik
71/12/22	06:59:56.5	47.903	48.067	6.0	Azghir
71/12/30	06:20:57.9	49.750	78.100	5.7	Degelen
72/02/10	05:02:57.6	50.024	78.942	5.4	Balapan NE
72/03/28	04:21:57.4	49.738	78.160	5.1	Degelen
72/08/16	03:16:57.5	49.774	78.132	5.0	Degelen
72/09/02	08:56:57.3	49.884	77.603	4.9	Murzhik
72/11/02	01:26:57.8	49.914	78.848	6.1	Balapan SW
72/12/10	04:27:07.6	49.966	78.946	6.0	Balapan NE
73/07/23	01:22:57.7	49.936	78.854	6.1	Balapan NE
73/09/27	06:59:58.5	70.804	53.419	5.9	Krasino
73/12/14	07:46:57.1	50.026	79.016	5.8	Balapan NE
74/12/27	05:46:56.8	49.908	79.053	5.6	Balapan NE
75/02/20	05:32:57.7	49.756	78.094	5.7	Degelen
75/06/08	03:26:57.6	49.752	78.080	5.5	Degelen
75/12/25	05:16:57.2	50.018	78.863	5.7	Balapan NE
76/07/29	04:59:58.0	47.812	48.101	5.9	Azghir

Table 18: Explosions

Date	Time	Lat.(N)	Long.(E)	$m_b(ISC)$	Site
76/08/28	02:56:57.6	49.948	78.980	5.8	Balapan
77/08/10	22:00:01.8	50.948	110.782	5.0	Lake Baikal
77/09/01	02:59:57.8	73.374	54.411	5.7	Matochkin Shar
77/09/05	03:02:57.8	50.048	78.929	5.8	Balapan NE
77/09/30	06:59:55.9	47.849	48.127	5.0	Azghir
77/10/29	03:07:03.0	50.056	78.866	5.6	Balapan NE
77/11/30	04:06:57.6	49.934	78.894	6.0	Balapan NE
78/03/26	03:56:57.7	49.713	78.065	5.6	Degelen
78/06/11	02:56:57.8	49.879	78.814	5.9	Balapan SW
78/07/28	02:46:57.8	49.732	78.152	5.7	Degelen
78/08/09	17:59:58.1	63.653	125.345	5.6	C._Siberia
78/08/10	07:59:57.7	73.314	54.697	5.9	Matochkin Shar
78/08/29	02:37:06.4	49.984	79.017	5.9	Balapan NE
78/09/27	02:04:58.4	73.382	54.441	5.6	Matochkin Shar
78/11/04	05:05:57.5	50.028	78.976	5.6	Balapan NE
79/06/23	02:56:59.0	49.886	78.916	6.2	Balapan SW
79/07/07	03:46:57.5	50.048	79.063	5.8	Balapan NE
79/07/14	04:59:55.2	47.813	48.067	5.6	Azghir
79/08/04	03:56:57.2	49.860	78.942	6.1	Balapan SW
79/08/18	02:51:57.3	49.928	78.981	6.1	Balapan SW
79/09/24	03:29:58.4	73.372	54.578	5.7	Matochkin Shar
79/10/18	07:09:58.5	73.341	54.733	5.8	Matochkin Shar
79/10/28	03:16:57.0	49.961	79.068	6.0	Balapan NE
79/12/23	04:56:57.6	49.925	78.796	6.2	Balapan SW
80/05/22	03:56:57.8	49.750	78.107	5.5	Degelen
80/06/12	03:26:57.7	49.954	79.055	5.6	Balapan NE
80/09/14	02:42:39.3	49.936	78.863	6.2	Balapan SW

Table 18: Explosions

Date	Time	Lat.(N)	Long.(E)	$m_b(ISC)$	Site
80/10/11	07:09:57.2	73.361	54.820	5.7	Matochkin Shar
80/10/12	03:34:14.2	49.937	79.104	5.9	Balapan NE
80/12/14	03:47:06.5	49.867	78.967	5.9	Balapan SW
80/12/27	04:09:08.5	50.008	79.026	5.9	Balapan NE
81/03/29	04:03:50.1	49.979	79.016	5.6	Balapan NE
81/04/22	01:17:11.4	49.870	78.896	6.0	Balapan SW
81/09/13	02:17:18.4	49.890	78.976	6.1	Balapan SW
81/10/01	12:14:56.9	73.323	54.554	6.0	Matochkin Shar
81/10/18	03:57:02.7	49.876	78.885	6.1	Balapan SW
81/11/29	03:35:08.8	49.848	78.850	5.7	Balapan NE
81/12/27	03:43:14.2	49.895	78.859	6.2	Balapan SW
82/02/19	03:56:11.1	49.826	78.125	5.4	Degelen
82/04/25	03:23:05.5	49.871	78.917	6.1	Balapan SW
82/10/11	07:14:58.4	73.371	54.342	5.6	Matochkin Shar
82/12/05	03:37:12.7	49.890	78.860	6.1	Balapan SW
82/12/26	03:35:14.4	50.061	79.049	5.7	Balapan NE
83/06/12	02:36:43.7	49.905	78.967	6.1	Balapan SW
83/08/18	16:09:58.6	73.377	54.868	5.9	Matochkin Shar
83/09/25	13:09:57.9	73.349	54.377	5.8	Matochkin Shar
83/10/06	01:47:06.8	49.909	78.827	6.0	Balapan SW
83/10/26	01:55:05.0	49.887	78.901	6.1	Balapan SW
83/12/26	04:29:07.0	49.835	78.205	5.6	Degelen
84/03/07	02:39:06.4	49.999	78.987	5.7	Balapan NE
84/04/15	03:17:09.3	49.686	78.141	5.7	Degelen
84/04/25	01:09:03.7	49.911	78.913	6.0	Balapan SW
84/05/26	03:13:12.5	49.925	79.030	6.1	Balapan NE
84/07/14	01:09:10.5	49.852	78.921	6.2	Balapan SW

118

Table 18: Explosions

Date	Time	Lat.(N)	Long.(E)	$m_b(ISC)$	Site
84/10/25	06:29:58.1	73.369	54.842	5.8	Matochkin Shar
84/10/27	01:50:10.7	49.917	78.829	6.2	Balapan SW
84/12/02	03:19:06.5	49.946	79.032	5.9	Balapan NE
84/12/16	03:55:02.8	49.884	78.824	6.1	Balapan SW
84/12/28	03:50:10.9	49.826	78.710	6.0	Balapan SW
85/02/10	03:27:07.7	49.865	78.839	5.9	Balapan SW
85/07/20	00:53:14.8	˙.916	78.803	6.0	Balapan SW
87/02/26	04:58:22.1	49.800	78.104	5.4	Degelen
87/04/03	01:17:08.1	49.874	78.812	6.2	Balapan SW
87/05/06	04:02:05.8	49.803	78.110	5.6	Degelen
87/06/06	02:37:07.1	49.803	78.089	5.4	Degelen
87/07/17	01:17:07.1	49.769	78.100	5.8	Degelen
87/08/02	02:00:00.1	73.346	54.578	5.8	Matochkin Shar
87/12/13	03:21:04.9	49.930	78.820	6.1	Balapan SW
87/12/27	03:05:04.9	49.820	78.730	6.1	Balapan SW
88/02/13	03:05:06.0	49.930	78.910	6.1	Balapan SW
88/04/03	01:33:05.9	49.870	78.920	6.0	Balapan SW
88/05/04	00:57:06.8	49.890	78.760	6.1	Balapan SW
88/05/07	22:49:58.3	73.350	54.430	5.9	Matochkin Shar
88/09/14	03:59:57.6	49.810	78.800	6.1	Balapan SW
88/12/04	05:19:53.2	73.380	54.960	5.9	Matochkin Shar

(55), Degelen (20), and Murzhik (6). Yields have been published for 17 of the Semipalatinsk explosions by Bocharov *et al.* (1989).

Table 19 lists the 10 seismological stations for which data were analyzed. The table also gives the epicentral distances between explosion sites and stations. Paths for which no data were available have their distances within parentheses. There were data available for 28 of the 60 possible paths between the 6 explosion sites and the 10 stations. The epicen-

Table 19: Seismological Stations

Code	Name	Lat. (N)	Long. (E)	DISTANCES_TO					
				Semi	Matoch kin Shar	Azghir	Krasino	Lake Baikal	C. Sibe-ria
APA	Apatity	67.55	33.33	28.4	9.2	(21.1)	(7.8)	(39.8)	(34.9)
ARU	Arti	56.40	58.60	13.4	17.1	10.7	14.6	(30.8)	32.7
BOD	Bodaybo	57.85	114.18	22.6	27.4	(39.6)	27.9	(7.2)	(8.0)
CHS	Chusal	39.10	70.77	11.9	35.2	(18.6)	(33.0)	(30.3)	(40.2)
NRI	Norilsk	69.40	88.10	20.3	11.2	(29.0)	(11.8)	(21.4)	(15.7)
NVS	Novosibirsk	54.90	83.30	6.1	21.9	(22.9)	20.6	17.0	22.8
OBN	Obninsk	55.10	36.60	25.5	19.8	10.1	17.4	(42.9)	(42.4)
TLY	Talaya	51.68	103.63	16.3	29.8	(35.3)	(29.5)	(4.5)	(16.6)
TUP	Tupik	54.43	119.90	25.8	(32.0)	(43.7)	(32.5)	(6.5)	(9.7)
UZH	Uzhgorod	48.63	22.30	35.7	28.6	(17.2)	(26.6)	(53.8)	(52.9)

tral distances of the 28 paths range from about 6 to 35 degrees. The 300 available wave-forms are distributed unevenly among the stations, from 6 at TUP to 80 at OBN. The joint detailed distribution of waveforms between stations and between explosions is evident from Table 22 that lists station magnitudes calculated according to the formula described in this report.

RMS amplitudes for the Lg phase with its coda were calculated according to the definition used by Israelsson (1991c) for each available waveform. In short, amplitudes were calculated from the group velocity window 3.1 to 3.7 km/s on traces band-pass filtered between 0.6-3.0 Hz. The trace amplitudes were also corrected for background noise and maximum instrument magnification. This means that the accuracy of the RMS amplitudes is limited by the determinations of the instrument magnifications. Although they appear to be largely consistent, the uncertainty of the magnifications is not precisely known; therefore, some scatter may be added to the RMS amplitudes by the magnification corrections applied and, in some instances, the RMS amplitudes may be off more significantly.

Path Terms

For the two test sites near Semipalatinsk and Matochkin Shar there is a comparatively large number of explosions with associated waveforms available. We take advantage of this and apply to each of the two sites separately a simple additive model that assumes that

120

the RMS amplitudes, rms_{ij}, (on a logarithmic scale) at station j, for explosion i, can be separated into a source term, s_i, and a path term, p_j: $rms_{ij} = s_i + p_j + \varepsilon_{ij}$. The error terms, ε_{ij}, are assumed to be Gaussian with zero mean and equal standard deviations, σ. In order to solve this system of over-determined equations for the unknown source and path terms we also have to impose the boundary condition: $\Sigma p_j = 0$, on the path terms. We have also made the implicit assumption that the RMS amplitudes scale in the same manner at all stations. Most of the explosions are in a limited magnitude range (see Table 18) and moreover, results by Israelsson (1991d) indicate that the stations, with the possible exception of station BOD, do scale in a similar way. Table 20 lists the estimated path terms for the two

Table 20: Path Terms

Site	Station	Path Term	S.D.	Distance (deg.)
nova	APA	0.811	0.013	9.222008
nova	ARU	0.704	0.015	17.087253
nova	BOD	-0.208	0.015	27.389851
nova	CHS	-1.189	0.021	35.191533
nova	NRI	0.456	0.000	12.233175
nova	NVS	-0.019	0.015	21.853268
nova	OBN	0.302	0.014	19.795527
nova	TLY	-0.630	0.020	29.807999
nova	UZH	0.230	0.015	28.642143
semi	APA	-0.708	0.036	28.536833
semi	ARU	0.935	0.013	13.739661
semi	BOD	0.117	0.026	22.052891
semi	NRI	-0.135	0.027	20.029040
semi	OBN	-0.043	0.012	25.921960
semi	TLY	0.450	0.017	15.734484
semi	TUP	-0.249	0.025	25.291461
semi	UZH	-0.368	0.015	36.169202

sites with associated standard errors, and they are shown graphically in Figure 38 as a
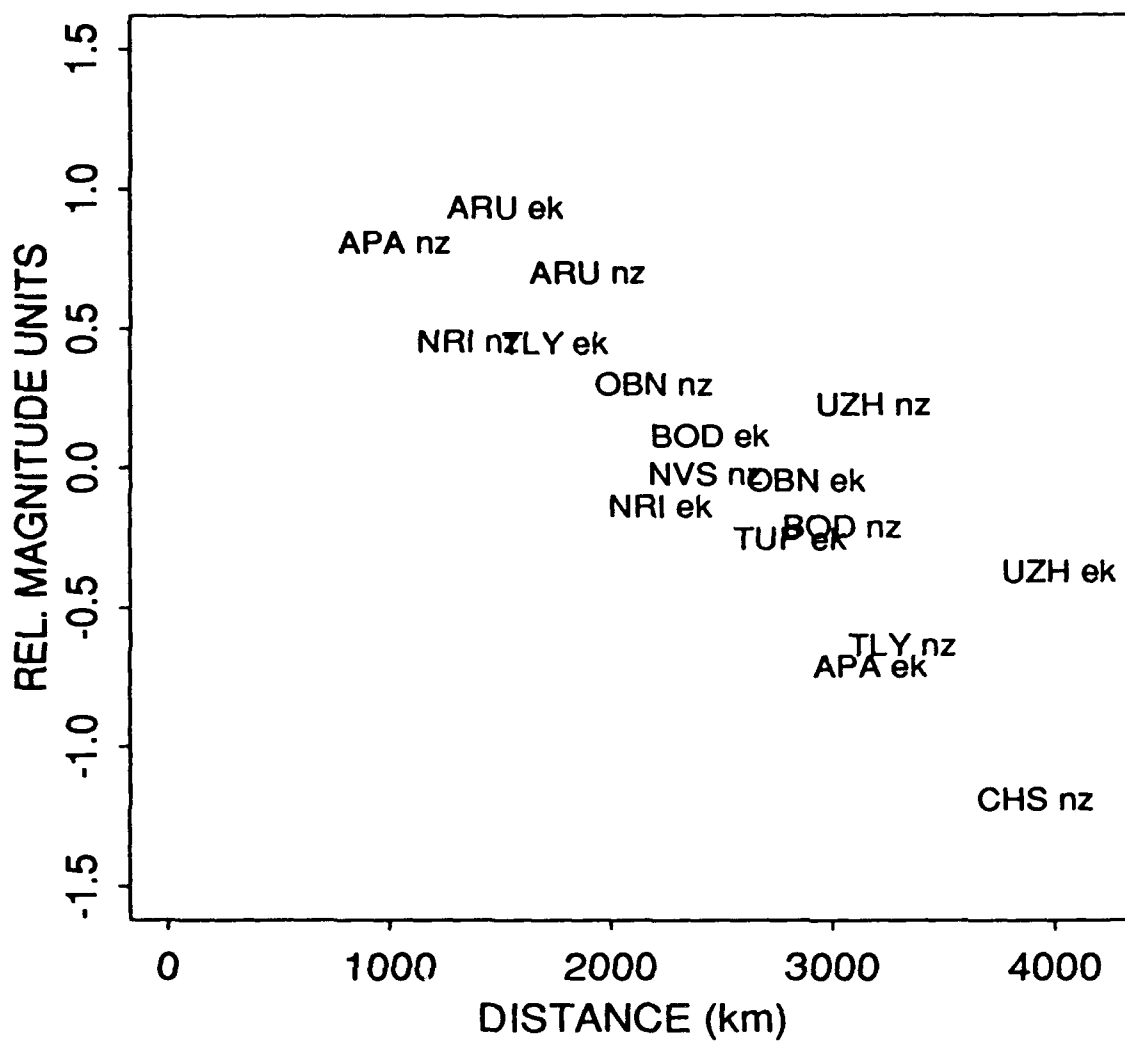
Figure 38: Estimated path corrections plotted as a function of epicentral distance. The paths are identified by station codes and by "ek" or "nz" for Semipalatinsk and Novaya Zemlya respectively.

function of epicentral distance. The estimated standard deviations of the error terms, ε_{ij}, were around 0.04. There are not enough data at the other four explosion sites to apply this additive model.

The Novaya Zemlya path term for NRI was obtained for data from the one explosion with available NRI data by comparing its RMS value to those at other stations (see Israelsson, 1991c).

The path terms decrease quite dramatically with increasing epicentral distance. There is considerable scatter around the general trend of amplitude decrease. At first glance the scatter may appear random, but some regularity can be seen, too. Provided they could both be estimated, the two path terms at a given station are either above, below, or in the central part of the general trend. This is particularly striking for station UZH.

Distance Dependence and Station Corrections

We next proceed to examine the path terms; the way they decay with distance and their dependence on the effects at the station sites.

Amplitude decay with distance

It was suggested by Nuttli (1973) that the decay of amplitudes of the Lg phase, A, as a function of epicentral distance, Δ, is proportional to: $A(\Delta) \sim \Delta^{-1/3}(sin\Delta^{-1/2})e^{-\gamma\Delta}$. This formula is based on a derivation by Ewing *et al.* (1957) for amplitudes of the Airy phase for waves from a uniform point source in a spherical earth model. According to the formula, the amplitude decay is a result of geometrical spreading (the first two factors) and non-geometrical spreading (the exponential term) characterized by one single parameter, γ (a rate decay with epicentral distance).

A model for the path terms

It is well-known, that apart from attenuation with distance, amplitudes of signals and coda at a given seismological station are also strongly dependent on the local geology at the station site. This leads us to assume that the path term can be written as the sum of the above formula for amplitude attenuation and a station correction, C_j, to account for local geology:

$$p_j = C_j + log(\Delta^{-1/3}(sin\Delta^{-1/2})e^{-\gamma\Delta}).$$

Using this expression for the path terms we go on to estimate the station corrections C_j and the γ value. In so doing we note that Nuttli (1986) obtained γ values that were similar (around 0.001 per km) for several paths from Semipalatinsk to stations in Scandinavia. Therefore, as a starting point, we assume that all paths from a given site, Semipalatinsk or

Novaya Zemlya, have the same γ value. By calculating the station corrections for seven of the stations (APA, ARU, BOD, NRI, OBN, TLY, and UZH), which have recorded explosions from both Semipalatinsk and Novaya Zemlya, using different γ values (between 0.0008 and 0.0015), we found that the station corrections obtained for the Semipalatinsk and Novaya Zemlya are quite similar for γ = 0.0012, as shown by the comparison in Figure 39. Even though quite similar, the two corrections obtained independently from the Semipalatinsk and Novaya Zemlya data for a given station are, of course, not identical. The two stations corrections show the largest disagreement for UZH having its Novaya Zemlya correction being 0.14 larger than the one for Semipalatinsk; the standard deviation obtained from the differences between the two corrections is only about 0.06 magnitude unit. This corresponds to a standard deviation of about 5 per cent of the decay rate 0.0012 per km at a distance of 20 degrees. A marginally smaller standard deviation was obtained if the data for station NRI were *not* included. As mentioned above there is only one recording from the Novaya Zemlya explosions at NRI; this is also a small explosion for which the source term may not be well constrained.

Station corrections and γ values for CHS, NVS, and TUP

For the three stations CHS, NVS, and TUP we found that the data either were insufficient to determine accurate station corrections using both Semipalatinsk and Novaya Zemlya data, or were not compatible with a common γ value for the paths from the two test sites. For CHS there were data for only three Semipalatinsk events (66/05/07, 72/03/28, and 84/05/26). For events 66/05/07 and 84/05/26 the residuals of the solution for the simple source path model applied to all station RMS values for Semipalatinsk were both large. The estimated site correction for Semipalatinsk using data for event 72/03/28 was only about two tenths of a magnitude unit smaller than that obtained for the Novaya Zemlya data. Therefore the difference between the two site corrections could either be caused by the magnification factor applied in calculating the RMS value or, perhaps more likely, by actual lateral differences in the γ values for the two paths.

The NVS station correction determined for Semipalatinsk (using data for 5 small explosions at Degelen) was about 0.5 magnitude units smaller than the one for Novaya Zemlya (based on 10 large explosions). It is unlikely that this discrepancy is due to magnification corrections because of the long time periods covered by the data for both Semipalatinsk and Novaya Zemlya. We note that the distance to NVS is only about 6 degrees and that data for all the other stations represent paths longer than 9 degrees.

Finally, for TUP there were data available only for Semipalatinsk.

STATION CORRECTIONS
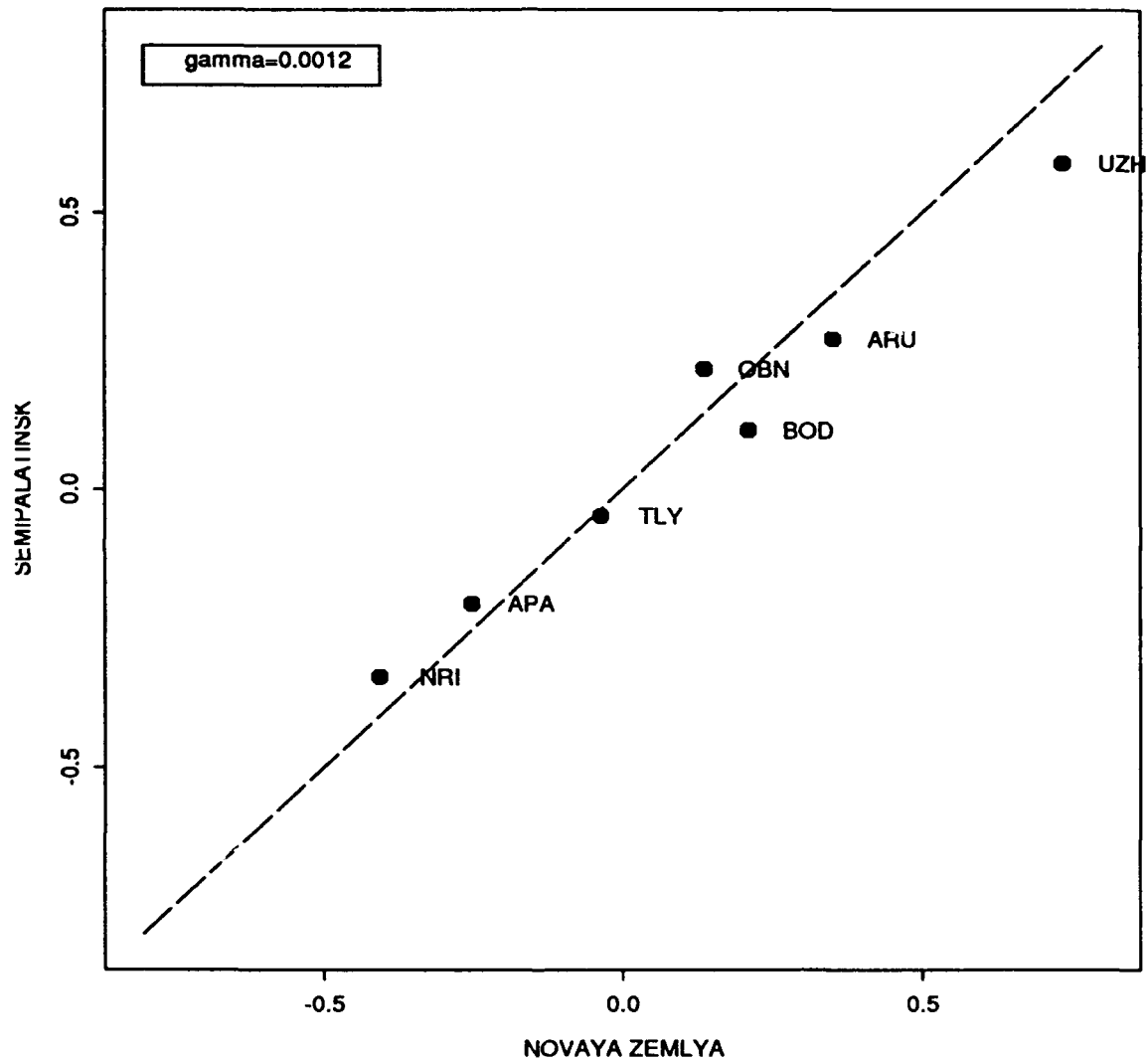
Figure 39: Station corrections estimated independently from the Semipalatinsk and Novaya Zemlya data assuming a common gamma value of 0.0012 per km.

125

With these results we estimate station corrections, C_j, by solving the additive model:

$$rms_{ij} + (1/3) \cdot \log(\Delta_{ij}) + (1/2) \cdot \log(\sin\Delta_{ij}) + \gamma \cdot \Delta_{ij} \cdot \log(e) = s_i + C_j + \varepsilon_{ij}$$

with $\gamma = 0.0012/\text{km}$, and using data for all paths (except those to Semipalatinsk for stations CHS and NVS), i.e., 17 paths. The resulting estimates are shown in Table 21 with associ-

Table 21: Station Corrections

Station	Correction	s.d.
APA	-0.227	0.018
ARU	0.324	0.013
BOD	0.185	0.018
CHS	-0.227	0.030
NRI	-0.309	0.024
NVS	0.020	0.022
OBN	0.241	0.012
TLY	-0.013	0.017
TUP	0.006	0.032
UZH	0.664	0.015

ated estimated standard errors. The estimated C_j values range over about one magnitude unit. The estimated standard deviation of the error terms were 0.06; slightly higher than the value of 0.04 obtained for the simple additive source-path model applied above to the Semipalatinsk and Novaya Zemlya data separately.

Correlation with noise

The station correction is a local amplification factor and one would expect it to be proportional to the ambient ground noise level. The estimated station corrections, C_j, show such a proportionality (within a factor of two), with the exception of station APA, as shown in Figure 40. The corrections have been plotted against the median noise RMS amplitude in the pass band 0.6-3.0 Hz. Station APA is located in the town of Apatity in a district of heavy mining industry, whereas the other stations presumably are located at rather quiet sites without strong local cultural noise sources. This might explain the outlying data point for APA with its relatively large noise amplitude.
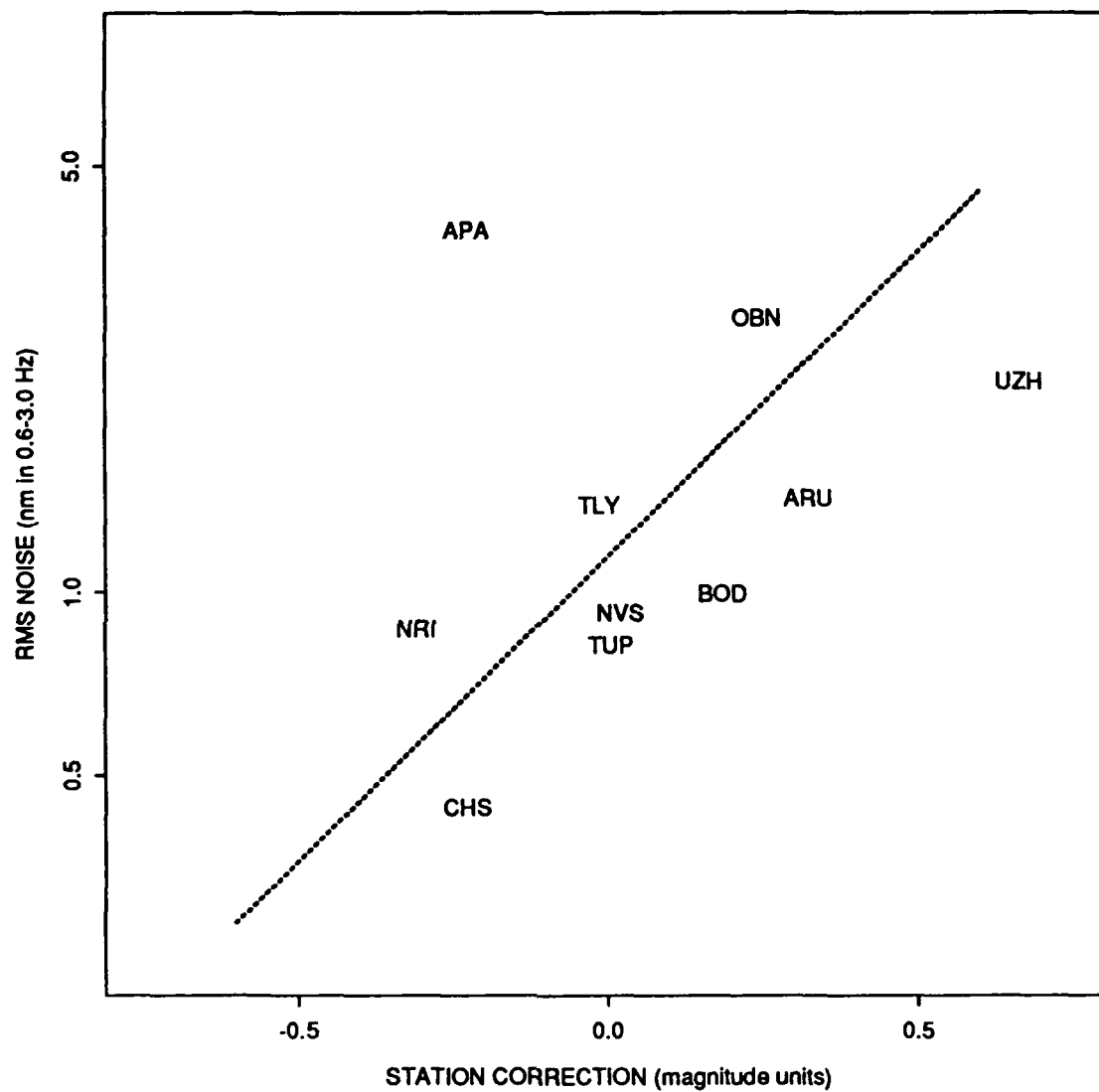
Figure 40: Comparison of station corrections and average of noise amplitudes.

We also note that the station correction for NVS is based on the Novaya Zemlya path only. If the NVS correction obtained for Semipalatinsk (Degelen), which is half a magnitude larger, were used, the NVS data point, too, would have appeared outlying in the scatter diagram. This is, of course, no evidence that the γ value for the NVS-Novaya Zemlya path is in reasonable agreement with the average value 0.0012 for the other 14 paths discussed earlier. However, the data for NVS in Figure 40 at least does not contradict this assumption.

RMS Lg Magnitude Formula

The close agreement between the pairs of independently calculated station corrections using a common γ value (0.0012) suggests that the expression for the path terms, p_j can be employed to calculate magnitudes with a simple formula common to Semipalatinsk and Novaya Zemlya explosions. This distance-dependent part of the path expression was obtained from the amplitude formula suggested by Nuttli (1973). Therefore, we start out with the magnitude formula for Lg amplitudes introduced by Nuttli (1986) and add a station correction term, C_j, (see Table 21) and a normalization constant, B:

$$ m_b (RMSLg) = 5.0 + (\log (RMS(10)/110)) - C_j + B $$

We note that the RMS amplitude is on the average almost four times smaller (0.576 in magnitude units) than the maximum amplitude in the 3.1-3.7 km/s group velocity window for the data analyzed here.

The RMS amplitude, *RMS(10)*, is extrapolated from the observed RMS value at distance Δ, to a hypothetical value at a distance of 10 km by means of the expression for the distance-dependent part of the path correction. The normalization constant B (1.273) was obtained as the median over the mean differences of station and ISC magnitudes. The resulting magnitudes, $m_b(RMS\ Lg)$, listed in Table 22 are thus normalized to the ISC body wave magnitude scale.

Table 22 also gives network magnitudes, formed as the average of station magnitudes, with associated standard deviation and number of observations. Data for the paths from Semipalatinsk to CHS and NVS were not included in the network averages.

Magnitudes for events at Azghir, Krasino, Lake Baikal, and C. Siberia

The data available to test the apparent stability of the γ value for the paths to Semipalatinsk and to Novaya Zemlya for paths to other sites are limited. There are only three events at two other sites that were recorded with some redundancy. Furthermore, there are inconsistencies of more than 0.1 magnitude unit for all three events, which are not possible to

128

Table 22: *Lg* RMS Magnitudes

Date	Network			Stations									
	mean	s.d.	N	APA	ARU	BOD	CHS	NRI	NVS	OBN	TLY	TUP	UZH
66/03/20	6.131		1							6.131			
66/05/07	4.981		1				4.844		5.159	4.981			
68/09/29	5.885		1							5.885			
69/07/23	5.443		2			5.381				5.505			
69/11/30	6.083		2			6.115				6.052			
69/12/28	5.854		2			5.918				5.791			
71/04/25	6.019	0.037	4		5.985	6.070		6.018		6.003			
71/06/06	5.451		1					5.451					
71/06/19	5.415		2							5.470			5.360
71/10/09	5.274	0.062	3		5.268			5.215		5.339			
71/10/21	5.566		2					5.514		5.619			
71/12/22	5.414		1		5.414								
71/12/30	5.629		1							5.629			
72/02/10	5.429	0.088	3		5.444	5.334				5.508			
72/03/28	5.031	0.097	4		4.966	4.934	4.841	5.138	5.437	5.087			
72/08/16	4.973	0.129	3		5.086	4.833			5.446	5.001			
72/09/02	4.747		2		4.789			4.706	5.162				
72/11/02	6.226	0.027	3		6.238	6.195				6.244			
72/12/10	6.177	0.043	3		6.131	6.185				6.215			
73/07/23	6.376		1							6.376			
73/09/27	5.692	0.138	3		5.758	5.534				5.785			
73/12/14	6.052		1							6.052			
74/12/27	5.889		2		5.892					5.885			
75/02/20	5.514		1							5.514			
75/06/08	5.489		1		5.489								
75/12/25	5.830		2		5.830					5.829			
76/07/29	5.316		1						5.316				
76/08/28	5.866		1		5.866								

129

Table 22: *Lg* RMS Magnitudes

Date	Network			Stations									
	mean	s.d.	N	APA	ARU	BOD	CHS	NRI	NVS	OBN	TLY	TUP	UZH
77/08/10	4.863		1						4.863				
77/09/01	5.795	0.071	5	5.765		5.828			5.795	5.698			5.890
77/09/05	5.944		2		5.966								5.922
77/09/30	4.625	0.180	3		4.419				4.708	4.748			
77/10/29	5.745		2		5.736								5.754
77/11/30	5.849	0.085	3		5.838					5.939			5.770
78/03/26	5.543	0.027	3		5.574					5.525			5.529
78/06/11	5.838		2		5.807								5.868
78/07/28	5.660	0.030	3		5.642					5.643			5.694
78/08/09	5.557		1						5.557				
78/08/10	5.812	0.085	5	5.713	5.886	5.892			5.838	5.730			
78/08/29	6.051		1							6.051			
78/09/27	5.604	0.087	3	5.678			5.627			5.508			
78/11/04	5.824		2							5.841			5.807
79/06/23	6.173		2		6.142								6.204
79/07/07	6.088		2							6.057			6.118
79/07/14	4.992	0.152	3		4.949				4.866	5.160			
79/08/04	6.165	0.043	3		6.116			6.181		6.197			
79/08/18	6.171		2							6.176			6.166
79/09/24	5.817	0.083	5	5.766	5.829				5.833	5.719			5.939
79/10/18	5.821	0.039	4	5.785	5.805	5.819							5.876
79/10/28	6.111	0.116	3			5.985		6.215		6.132			
79/12/23	6.094	0.028	3		6.074			6.127		6.082			
80/05/22	5.288		2		5.305					5.271			
80/06/12	5.680	0.023	3		5.693					5.693			5.654
80/09/14	6.069		2		6.109								6.029
80/10/11	5.801	0.094	6	5.732	5.859	5.755		5.721		5.775			5.966
80/10/12	6.018	0.063	3		5.983					6.090		5.980	

Table 22: *Lg* RMS Magnitudes

Date	Network			Stations									
	mean	s.d.	N	APA	ARU	BOD	CHS	NRI	NVS	OBN	TLY	TUP	UZH
80/12/14	5.976		2		5.958					5.994			
80/12/27	5.998	0.073	3		5.916					6 025			6.054
81/03/29	5.644	0.051	3		5.674					5.585			5.672
81/04/22	5.996		2		5.933					6.059			
81/09/13	6.219		2							6.187			6.251
81/10/01	5.888	0.079	6	5.862	5.921	5.980			5.921	5.746			5.900
81/10/18	5.978	0.100	4		6.034	6.000		5.831		6.049			
81/11/29	5.602		2							5.613			5.592
81/12/27	6.132		2		6.122					6.142			
82/02/19	5.090		2		5.070				5.526	5.111			
82/04/25	6.217		2							6.195			6.238
82/10/11	5.616	0.067	4	5.668	5.646				5.632	5.518			
82/12/05	6.153		1										6.153
82/12/26	5.640	0.053	3		5.643					5.692			5.586
83/06/12	6.096	0.059	4		6.105					6.132		6.010	6.137
83/08/18	5.860	0.047	5	5.876	5.935		5.828		5.838	5.824			
83/09/25	5.837	0.044	7	5.851		5.890	5.782		5.818	5.782	5.851		5.883
83/10/06	5.866	0.048	3							5.921	5.836		5.841
83/10/26	6.132		2							6.081	6.184		
83/12/26	5.156	0.074	3							5.186	5.210		5.072
84/03/07	5.742		1								5.742		
84/04/15	5.656	0.071	3							5.688	5.705		5.575
84/04/25	5.910	0.061	4		5.977					5.946	5.863		5.853
84/05/26	6.120	0.063	5	6.124	6.070		5.685	6.095		6.226	6.083		
84/07/14	6.040	0.144	4							6.187	6.085	5.844	6.043
84/10/25	5.809	0.068	5	5.855		5.803				5.760	5.732		5.897
84/10/27	6.124		2							6.124			6.124
84/12/02	5.969	0.050	4		5.922					6.007	6.017		5.930

Table 22: Lg RMS Magnitudes

Date	Network			Stations									
	mean	s.d.	N	APA	ARU	BOD	CHS	NRI	NVS	OBN	TLY	TUP	UZH
84/12/16	6.119	0.055	4		6.101					6.180	6.051	6.142	
84/12/28	6.024	0.090	3		6.063					6.088			5.922
85/02/10	5.918	0.048	4		5.871					5.907	5.910	5.986	
85/07/20	5.896	0.069	3							5.945		5.926	5.818
87/02/26	5.052		2		5.069				5.541		5.036		
87/04/03	6.097		2							6.106	6.088		
87/05/06	5.448		2		5.470						5.427		
87/06/06	5.134		2		5.133						5.135		
87/07/17	5.823	0.123	4	5.965	5.787						5.864		5.674
87/08/02	5.841	0.077	7	5.826	5.852	5.925			5.859	5.685	5.838		5.901
87/12/13	6.069	0.021	3		6.051					6.093	6.064		
87/12/27	6.066	0.041	4		6.064					6.092	6.100		6.009
88/02/13	6.089		2		6.110					6.069			
88/04/03	6.079	0.055	4		6.016					6.149	6.079		6.072
88/05/04	6.138		2							6.121	6.155		
88/05/07	5.754	0.049	8	5.776	5.770	5.752	5.804		5.715	5.651	5.783		5.777
88/09/14	6.086	0.066	5	6.056	6.052			6.200		6.036	6.085		
88/12/04	5.842	0.069	7	5.793	5.924		5.856		5.809	5.750	5.822		5.938

reconcile fully because of the unknown uncertainties in the instrument magnifications that were applied. One event near Krasino on 73/09/27, and two small Azghir events on 77/09/30 and 79/07/14 all have data for three stations. The magnitude at BOD of the Krasino event is about 0.2 magnitude unit below the values at ARU and OBN. This discrepancy could thus be due to differences in the actual γ values for these three paths or to the instrument corrections that were applied to the data.

For the two Azghir events we note that the difference between the OBN and ARU magnitudes are about 0.25 magnitude unit. For the smaller of the two events, on 77/09/30, the signal-to-noise ratio for the RMS amplitude at NVS is only 1.5, and that may explain the inconsistency in the relative magnitudes at NVS and the other two stations (ARU and OBN) for these two events.

132

Comparison with Body Wave Magnitudes

In Figure 41 we compare the Lg RMS network magnitudes, $m_b(RMS\,Lg)$, with body wave magnitudes, $m_b(P)$, reported by the ISC by plotting the difference $m_b(P) - m_b(RMS\,Lg)$ as a function of $m_b(RMS\,Lg)$. For Semipalatinsk, there is a systematic offset in the magnitude differences for events in the NE and SW portion of the Balapan area. This in agreement with a distinct bias between body wave and Lg wave magnitudes for the two portions of Balapan, identified earlier by Ringdal and Marshall (1989). They attribute this to anomalously large body wave magnitudes caused by strong focusing effects of P-waves in the upper mantle. The data in Figure 41 show that this kind of magnitude bias is not limited to the Balapan region of the Semipalatinsk test range. The $m_b(P)$ values are systematically larger than the Lg RMS magnitudes for the Degelen events, particularly for the small ones; the event on 83/12/26 had the largest difference, about 0.4 magnitude unit.

Figure 41 also shows striking differences between the two types of magnitudes for events at the Azghir site; the $m_b(P)$ is about half a magnitude or more larger than $m_b(Lg)$. Without additional information it is difficult to explain whether this anomaly is caused by bias in $m_b(P)$, $m_b(RMS\,Lg)$ or both. As for Balapan, it might be due to strong focusing of P waves in the upper mantle. However, since the bias for Azghir appears to be clearly larger than for Balapan, we indulge in the speculation of anomalously low $m_b(RMS\,Lg)$ values being caused by blockage of the Lg waves by the Peri-Caspian depression (indicated in Figure 37), since its central part lacks a granitic layer (Zonenshain, 1990). Underneath the 20 to 25 km thick sedimentary cover, there is instead a thin high-velocity layer. The depth to Moho is comparatively shallow, about 35 km at its lowest in the Peri-Caspian depression, and there are also indications of a paleo-oceanic floor. Some support to the hypothesis of blockage is also lent by the differences in station magnitudes $m_b(RMS\,Lg)$ at OBN and ARU for the Azghir events. The somewhat smaller ARU values (0.2-0.3 magnitude unit) might be caused by added blockage effects along the apparently more extensive wave path across the Peri-Caspian depression for ARU. The path between the station UZH and Semi-palatinsk also crosses the Persi-Caspian depression (see Figure 37). In the calculations of station corrections for a fixed γ value (0.0012), the Semipalatinsk correction came out about 0.14 magnitude units smaller than the Novaya Zemlya one for UZH (see Figure 39). Translated into path attenuation, this difference means a larger attenuation for the Semi-palatinsk than for the Novaya Zemlya path to UZH. This difference, however, may well be coincidental and constitute no direct evidence of blockage of Lg across the Peri-Caspian depression in this case for UZH.

For the events at the sites near Krasino, in Central Siberia, and near Lake Baikal (marked as Central Siberia in Figure 41) we find that the two types of magnitudes are in reasonable agreement. The $m_b(RMS\,Lg)$ values for Central Siberia and Lake Baikal (only one explo-
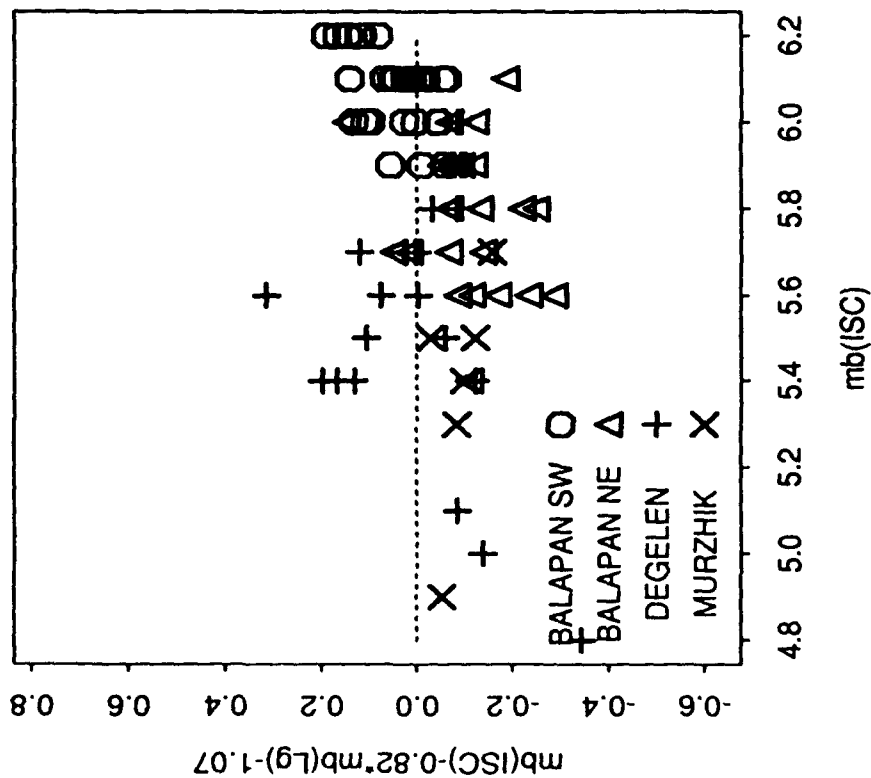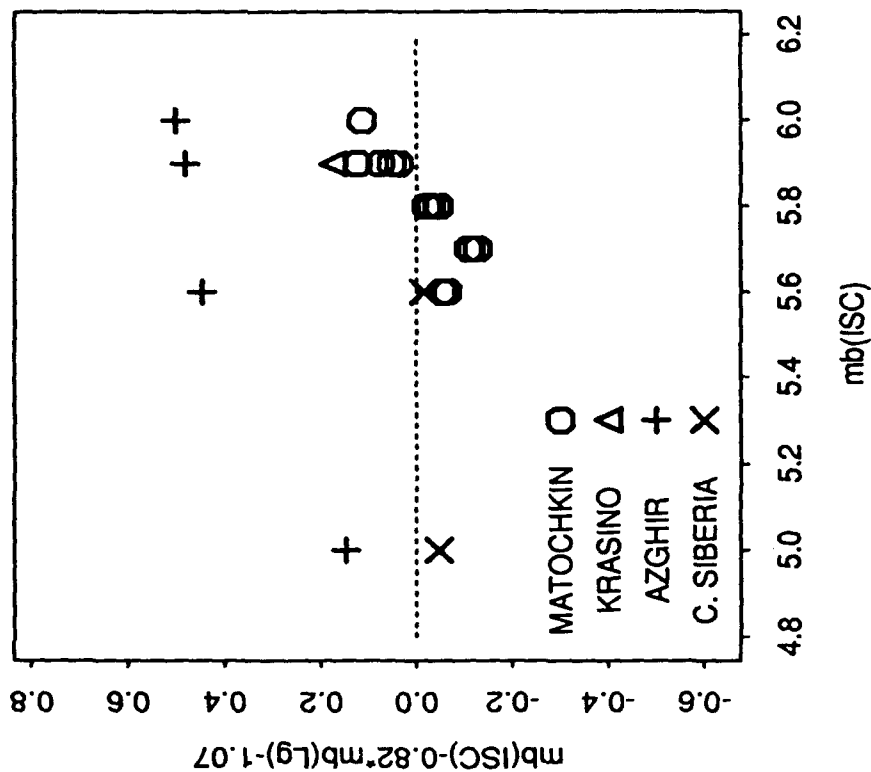
Figure 41: The diagrams compare $m_b(ISC)$ with $m_b(Lg)$ for the various explosion sites. The magnitude difference, $m_b(ISC)$ - $0.82*m_b(Lg)$ - 1.07, from the estimated linear relation is plotted against $m_b(ISC)$.

sion at each site) are based solely on data at station NVS, whose station correction is based on the Novaya Zemlya path. The agreement between $m_b(P)$ and $m_b(RMS\ Lg)$ for NVS is again no evidence for a γ value of about 0.0012 for the NVS-Novaya Zemlya path. However, this value is not contradicted by the Lg RMS magnitudes for the two Siberian explosions. They indicate that the γ values for the paths from the Central Siberia and Lake Baikal events to NVS are compatible with the average value of 0.0012.

Calibration with Announced Explosion Yields

Owing to the stability of the γ value, we proceed to estimate a linear relationship between explosion yield and $m_b(RMS\ Lg)$ using events at Semipalatinsk with announced yields, and apply this relation to estimate yields of other explosions at Semipalatinsk and elsewhere in a straightforward manner.

Figure 42 shows the announced yields plotted against the $m_b(RMS\ Lg)$. A linear relation: $m_b(RMS\ Lg) = 0.793\ log(Yield) + 4.47$ was obtained with standard linear regression of $m_b(RMS\ Lg)$ on $log(Yield)$. The standard deviation of the magnitude residuals from the linear relation was 0.038. The outlying data point for the explosion on 72/08/16 was not used in the regression.

Figure 43 shows the distribution of the explosion yields for all explosions at the three subregions of the Semipalatinsk test range and Matochkin Shar. The linear relation between magnitude and yield was based on data for explosions throughout the Semipalatinsk test range, at Balapan, Degelen, and Murzhik. Therefore, yields of Semipalatinsk events not included in the estimation of the linear relationship between magnitude and yield can be considered as calibrated *directly*, assuming that variation in seismic coupling is negligible. The yields of the explosions in SW Balapan are largely confined to the range 50-150 kt, with a suite of some 10 explosions having very similar yields around 100 kt. The yields of the Degelen explosions cover almost the full range of all explosions. The estimated yield for one of the explosions at NE Balapan, 73/07/23, is clearly above 150 kt. Apart from this event, the yields of NE Balapan events are generally smaller than those of SW Balapan events, and cover a range from about 25 to 100 kt. NE Balapan events also include a suite (five events) with similar yields, around 50 kt.

Yields calculated with the linear formula for explosions at sites other than Semipalatinsk are calibrated only *indirectly*. They are, of course, more uncertain than yields based on calibrated data, not only because the magnitude formula describes the actual path effects only approximately, but also because of the possibility of systematic differences in seismic coupling. Therefore, we refer to them as indirectly estimated yields. The distribution of the indirectly estimated yields for Matochkin Shar explosions, shown in Figure 43, has little

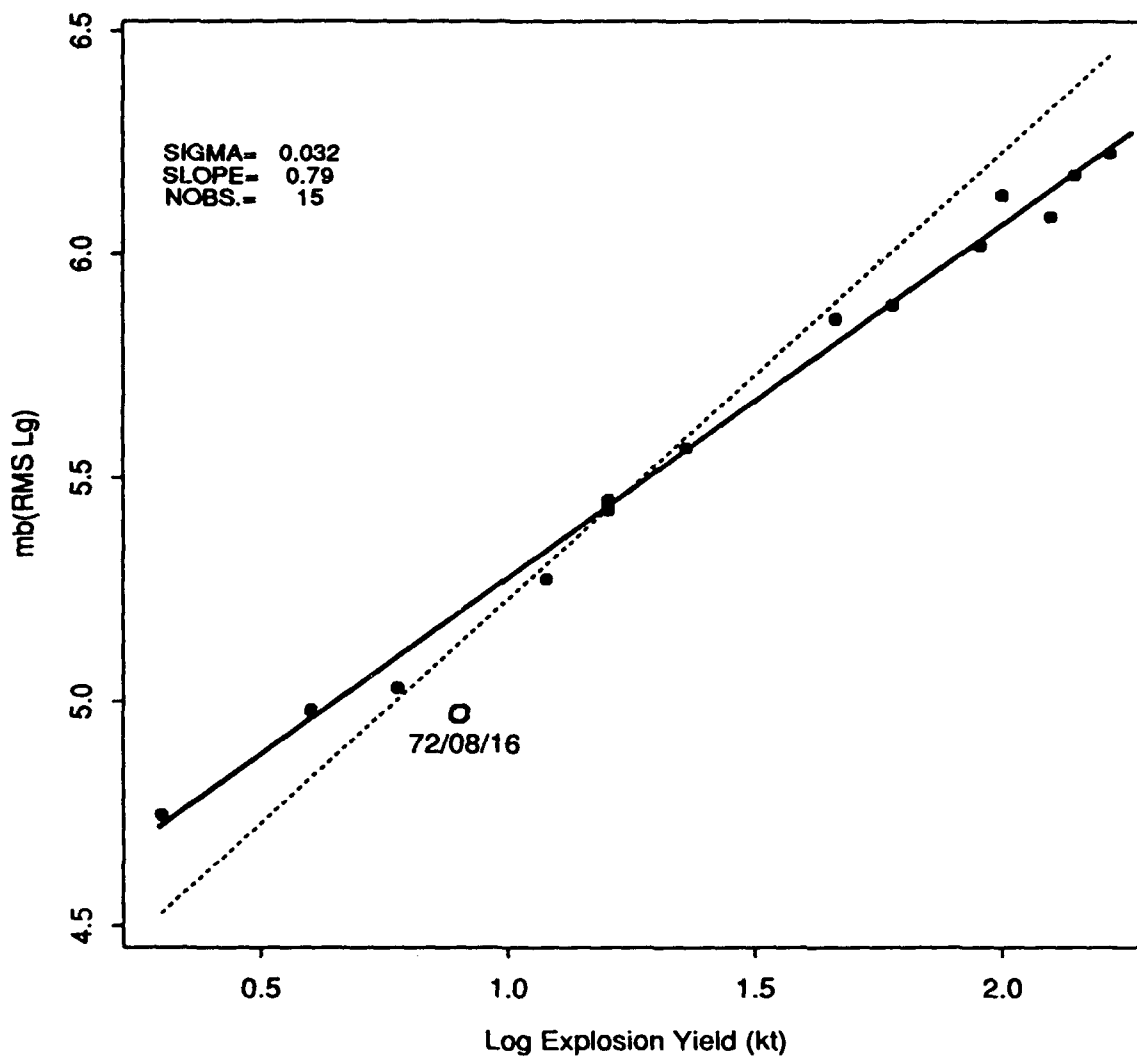Figure 42: Network $m_b(Lg)$ plotted against yields published by Bocharov *et al.* (1989). The heavy line was estimated with standard least squares regression giving a slope of 0.79 and a misfit error of 0.032 magnitude units omitting the data for the explosion on 72/08/16, marked with an open circle. The dotted line represents a slope of 1.
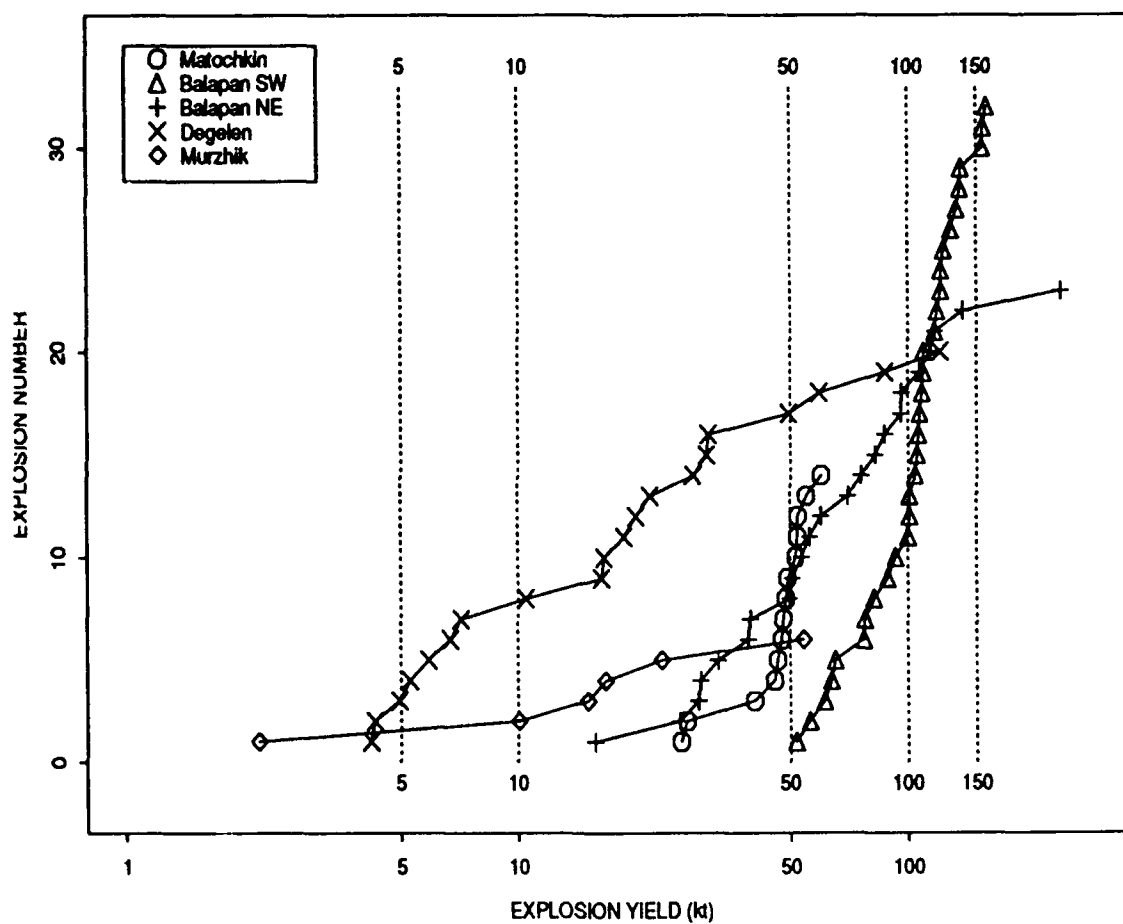
136

Figure 43: Distribution of explosion yields estimated from network $m_b(L_g)$.

scatter, with 12 of the 14 explosions close to 50 kt. The other two Matochkin Shar explosions are around 25 kt.

The Lg RMS measurements available for explosions at other sites are insufficient and, in some instances, too inconsistent to obtain indirect yield estimates with some confidence. Only for the sake of completeness do we formally calculate such yields from the linear relation above. For the explosion near Krasino (in the Southern part of Novaya Zemlya), indirect yields obtained from the three station magnitudes vary between 21 (BOD) and 44 kt (ARU and OBN). The indirect yields of the two explosions near Lake Baikal (77/08/10) and in Central Siberia (78/08/09) were 5 and 23 kt respectively, but were based only on data from station NVS. Because of the large discrepancy between the $m_b(P)$ and $m_b(RMS Lg)$ for the Azghir events, their indirect yield estimates (71/12/22 15, 76/07/29 11, 77/09/ 30 2, and 76/07/14 4 kt) may well be significantly biased.

Concluding Remarks

In this analysis we have found that the attenuation of RMS amplitudes of Lg waves appear, perhaps somewhat unexpectedly, to be fairly stable for a variety of propagation paths across large parts of Western and Central U.S.S.R. The attenuation along these paths, varying in length from 9 to 35 degrees and crossing a mixture of major tectonic components, is described by a simple formula. According to this formula the RMS amplitudes decay as the product of two terms, one for geometrical spreading of surface waves on a sphere, and one decaying exponentially with distance. The rate of decay of the exponent of the latter term is found to be close to $0.0012 \ km^{-1}$ for paths to seven stations from the test sites at Semipalatinsk and Novaya Zemlya.

This implies that a magnitude-yield relation obtained for one test site with calibrated data may be applicable, in the first approximation, to another site at a different location. This is exemplified in this note by calculating indirect yield estimates for explosions at Novaya Zemlya and two other sites using a magnitude-yield relation based on data announced for explosions at Semipalatinsk. The practical value of this approach to indirect yield estimation depends not only on the premise that path effects can be controlled, but also on the assumption that coupling of yield into Lg waves is on the whole similar for calibrated and uncalibrated sites. For this to be truly useful, this latter assumption should be verified.

The analysis of the Lg RMS amplitudes for the three paths from Azghir suggests that one should not hastily assume that the simple magnitude formula, obtained for many paths from Semipalatinsk and Novaya Zemlya, is invariably applicable in the Western and Central U.S.S.R. Indeed, the data for station NVS show that the formula is not even valid for all paths from these two sites, although the apparent discrepancy for the NVS data may be

due to the short distance, about 6 degrees, between this station and the Semipalatinsk testing grounds.

References

Bocharov, V.S., S.A. Zelentsoz, and V. Mikhailov (1989). Characteristics of 96 underground nuclear explosions at the Semipalatinsk test site, *Atomic Energy,* **67,** 210-214.

Hansen, R., Ringdal, F., and P.G. Richards (1990). The stability of RMS Lg measurements, and their potential for accurate estimation of the yields of Soviet underground explosions *Bull. Seism. Soc. Am.,* **80,** 2106-2126

Israelsson, H. (1991a). Hand digitized waveforms from recordings at Soviet stations from nuclear explosions in the U.S.S.R. - Description of data set I (*Manuscript in preparation*)

Israelsson, H. (1991b). Hand digitized waveforms from recordings at Soviet stations from nuclear explosions in the U.S.S.R. - Description of data set II (*Manuscript in preparation*)

Israelsson, H. (1991c). RMS magnitudes for explosions at Novaya Zemlya based on recordings at Soviet Stations (*This Report*)

Israelsson, H. (1991d) Consistency of Lg RMS magnitudes for explosions based on hand digitized data at internal Soviet Stations (*Manuscript in preparation*)

Nuttli, O.W. (1973). Seismic wave attenuation and magnitude relations for eastern North America *J. Geophys. Res.* **78,** 876-885

Nuttli, O.W. (1986). Lg magnitudes of selected East Kazakhstan underground explosions, *Bull. Seism. Soc. Am.* **76,** 1241-1251.

Nuttli, O.W. (1988). Lg magnitudes and yield estimates for underground Novaya Zemlya nuclear explosions, *Bull. Seism. Soc. Am.* **78,** 873-884.

Patton, H.J. (1988). Application of Nuttli's method to estimate yield of Nevada Test Site Explosions recorded on Lawrence Livermore National Laboratory's digital seismic system, *Bull. Seism. Soc. Am.* **78,** 1759-1772.

Ringdal, F. (1983). Magnitudes from P coda and Lg using NORSAR data, in: *Semiann. Tech. Summ., 1 Oct 82 - 31 Mar 1983,* NORSAR Sci. Rep. 2-82/83, Kjeller, Norway.

Ringdal, F. and B.K. Hokland (1987). Magnitudes of Large Semipalatinsk explosions using P coda and Lg measurements at NORSAR, in: *Semiann. Tech. Summ., 1 Apr-30 Sep 1987,* NORSAR Sci. Rep. 1-87/88, Kjeller, Norway.

Ringdal, F. and J. Fyen (1988). Comparative analysis of NORSAR and Grafenberg Lg magnitudes of Shagan River explosions, in: *Semiann. Tech. Summ., 1 Apr-30 Sep 1988,* NORSAR Sci. Rep. 1-88/89, Kjeller, Norway.

Ringdal, F. and P. D. Marshall (1989). Yield determination of Soviet underground nuclear explosions at the Shagan River Test Site, in: *NORSAR Semiannual Tech. Summary, 1 Oct 1988 -- 31 March 1989,* NORSAR Sci. Rep. 2 - 88/89, Kjeller, Norway.

Zonenshain, L.P., J. Verhoef, R. Macnab, and H. Meyers (1991a). Magnetic Imprints of

Continental Accretion in the U.S.S.R. *EOS*, **72,**

Zonenshain, L.P, M. I. Kuzmin, and L.M. Napatov (1991b). Geology of the USSR: A Plate-Tectonic Synthesis, *Geodynamics Series Volume 21*, American Geophysical Union, Washington D.C., pp. 242

Zonenshain, L. P., M. I. Kuzmin, and L. M. Natapov (1990). Geology of the USSR: A Plate-Tectonic Synthesis, *Geodynamics Series Volume 21*, American Geophysical Union, Washington, D.C., pp. 242

Zonenshain L. P., J Verhoef, R. Macnab, and H. Meyers (1991). Magnetic Imprints of Continental Accretion in the U.S.S.R. *Eos*, **72**, 305.

A Spectral Decomposition of *Lg* Waves from Explosions and Scaling of RMS Magnitudes

Hans Israelsson

Abstract

We attempt to study the variation of $m_b(Lg)$ scaling using estimates of the frequency dependence of *Lg* source and path spectra. For this purpose, we draw upon a unique set of *Lg* wave recordings at six internal Soviet stations for explosions at Semipalatinsk and Novaya Zemlya. The analysis suggests that the frequency components of the estimated *Lg* source spectra, for yields in the range 50-150 kt, scale differently with yield. At low frequencies, (0.2-0.7 Hz) the spectral amplitudes are more or less directly proportional to explosion yield. At frequencies above 0.7 Hz the scaling factor decays sharply to about 0.6 at about 1.0 Hz, above which the scaling stays fairly constant. Furthermore, although the attenuation coefficient of the non-geometrical spreading was fairly stable (misfit error within 5-10% of the model) for the 12 paths and varied in a systematic manner with frequency, the resulting path spectra will differ in shape depending on epicentral distance. Finally, the frequency dependent site amplifications vary significantly both in overall level (with about one m.u.) and in shape (largest range of variation for given station is about 0.4 m.u.). Therefore the frequency scaling of the *Lg* source spectrum in combination with differences among the frequency responses of the non-geometric attenuation (due to different distances) and among the site amplifications appear to give rise to variation in station $m_b(Lg)$ scaling.

Introduction

Magnitudes based on RMS amplitudes of *Lg* waves, $m_b(Lg)$, are perhaps the most promising seismic estimators of yields of underground nuclear explosions. Such magnitudes determined for a fixed *Lg* wave path (that is to say a path between a given seismic station and explosion site) have shown a precision remarkable to seismic magnitudes. A close linear relationship with explosion yield has also been demonstrated, at least over a limited range (Ringdal, 1989). However, the slope of the linear relation (that is the rate with which the *Lg* wave amplitude increases with increasing source strength) may vary from one path to another. This variation in scaling of $m_b(Lg)$ has been reported for paths in different distance ranges - local, regional, and teleseismic - in North America as well as in Eurasia by Ringdal and Fyen (1988), Patton (1988), and Hansen *et al.* (1990).

The physical reasons for this variability have not yet been sufficiently explored. Analyzing data from Semipalatinsk explosions recorded at the two arrays NORSAR and GRF,

Ringdal and Fyen (1988) suggested that frequency scaling of the Lg source spectrum together with differences in instrument responses between the two arrays may account for the observed difference in $m_b(Lg)$ scaling between the two arrays. They were, however, unable to substantiate this explanation due to insufficient signal-to-noise ratio for the GRF data. Patton (1988), studying data for NTS explosions, found that the variability was seen for explosions below the water table and not for explosions above. As the locations of explosions below the water table were closely spaced in an area separate from the more widely spread above-water-table explosions, he suggested that this precluded propagation effects, except possibly near the source, explaining the variability in $m_b(Lg)$ scaling. Finally, Hansen *et al.* (1990) did not go into any detailed discussion of the physical reasons underlying their observations. Whatever the reasons maybe, the variation in $m_b(Lg)$ scaling has to be taken into account for the purpose of yield estimation. In many instances, this can be carried out empirically from the data at hand in a straightforward manner.

In this note we attempt to study the variation of $m_b(Lg)$ scaling as functions of the frequency dependence of Lg source and path spectra. For this purpose, we draw upon a unique set of Lg wave recordings at six internal Soviet stations for explosions at Semipalatinsk and Novaya Zemlya. The analysis assumes that the Lg waves are attenuated in a similar fashion between explosion sites and stations regardless of the tectonic differences of their paths. Justification for this assumption is rendered by the apparently stable and simple Lg attenuation observed in a previous study of these data (Israelsson, 1992). While the analysis herein is aimed primarily at the implications for estimation of explosion yield, its results also have bearing upon the generation and propagation of Lg waves generally.

Data

The map in Figure 44 shows the Semipalatinsk and Novaya Zemlya explosion sites and the seismic stations with Lg wave data. There are data from 61 explosions, 14 near Matochkin Shar at Novaya Zemlya ($m_b(ISC)$=5.6-6.0) and 47 at the Balapan area (18 in the NE and 29 in the SW part) of the Semipalatinsk test range ($m_b(ISC)$=5.4-6.1).

The stations are listed in Table 23. They all belong to the Uniform System of Seismic Observations of the U.S.S.R. (Kondorskaya and Aranovich, 1979) and are broadly distributed in Eastern and Central U.S.S.R. with epicentral distances to the two explosion sites varying between 9 and 36 degrees. Four of the stations, APA, ARU, OBN, and UZH, are located on or near the rim of the East-European platform, whereas the two remaining stations, BOD and TLY, are close to the boundaries of the Siberian platforms (see Figure 44). Although the stations are located on or near platforms, the 12 wave paths (approximated as straight lines in the map) traverse tectonic structures that are predominantly non-platforms: the Central Asiatic and Uralian orogenic belts and the Kazakhstan accretionary
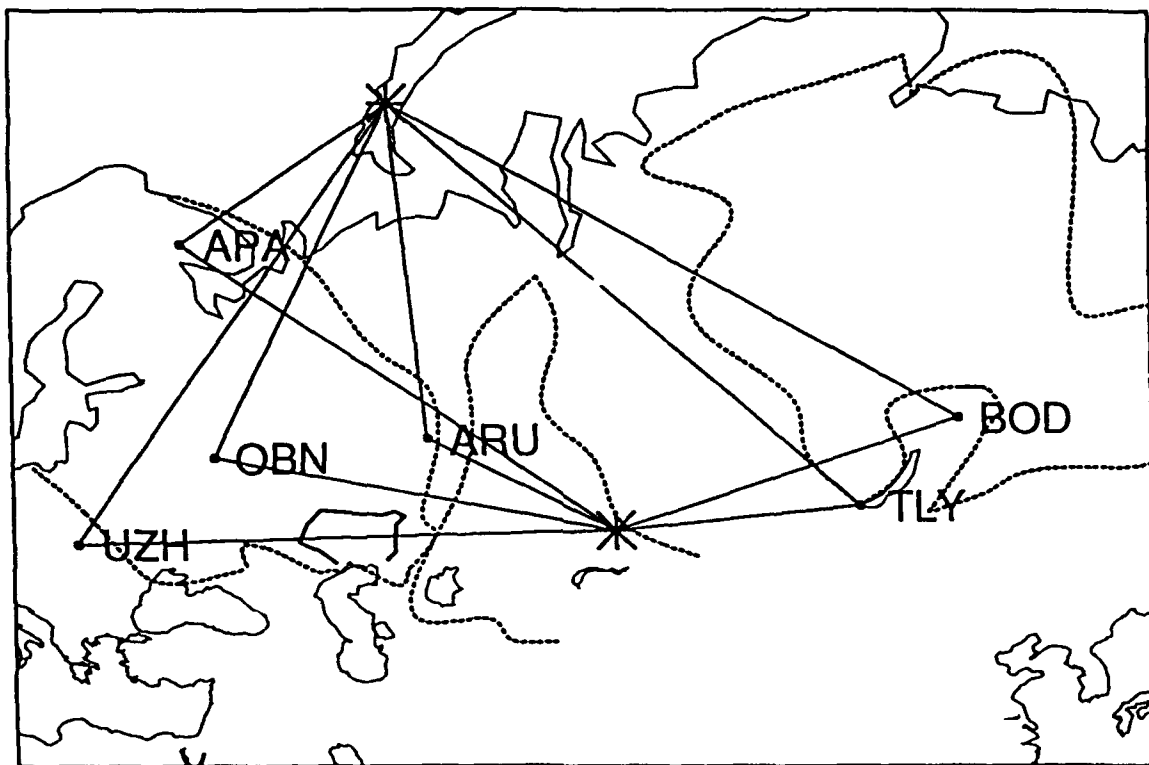
144

Figure 44: Map showing the relative locations of the explosion sites near Semipalatinsk and at Novaya Zemlya (marked with asterisks) and the seismological stations (indicated with station codes). The dotted lines represent the boundaries of the major tectonic elements, the East-European and the Siberian platforms on either side of the Kazakhstan accretionary continent in the central part of the map (after Zonenshain, 1991). Wedged in between the accretionary continent and the two platforms are the Uralian and the Central Asiatic orogenic belts. The depression to the north of the Caspian sea is also outlined in the map as a heavy full line. The straight lines between stations and explosion sites represent only approximate great circle paths along the earth's surface.

Table 23: Seismological Stations

Code	Name	Lat(N)	Lon(E)
APA	Apatity	67.55	33.33
ARU	Arti	56.40	58.60
BOD	Bodaybo	57.85	114.18
CHS	Chusal	39.10	70.77
OBN	Obninsk	55.10	36.60
UZH	Uzhgorod	48.63	22.30

continent.

Typical instrument magnification curves for the six seismic stations are compared in Figure 45. Although the recordings were obtained with the same type of seismometer, SKM-3, at all stations, there are some differences among the magnification curves. These affect the frequency band 0.6-3.0 Hz (indicated in Figure 45), commonly used for $m_b(Lg)$ calculations. Some curves in Figure 45 have a pronounced peak around 2 Hz, whereas others stay almost constant above 1 Hz. The instrument responses for most stations also change with time due to instrumental drift and/or to deliberate alterations. Because of the temporal variations, computed spectral amplitudes were normalized to a reference response curve: the calibration of 1988 for the station OBN (drawn in Figure 45).

The recorded waveforms, all vertical components, were hand digitized (sampling rate 20 Hz) from copies of the original analog records and are believed to be accurate up to 2-4 Hz (Kemerait *et al.* 1981).

RMS amplitudes were calculated after narrow bandpass filtering the waveforms for a suite of center frequencies between 0.2 and 2.6 Hz; in steps of 0.05 Hz from 0.2 to 0.80 Hz and in steps of 0.1 Hz from 0.8 to 2.6 Hz. The Lg amplitudes were calculated over a time window corresponding to group velocities between 3.1-3.7 km/s, representing the low and high ends of the normal range. An example of the frequency response of the narrow band filters (center frequency 0.3 Hz) is given in Figure 45. As a final step, each Lg amplitude was compensated for the ambient noise level, in a standard manner, by forming the square root of the difference between the squared RMS Lg and noise amplitudes. The RMS noise amplitude was calculated from a 2 minute window prior to the P onset.

Model

For a given center frequency, f, we assume that the logarithm of the RMS amplitude, $A(f)$,
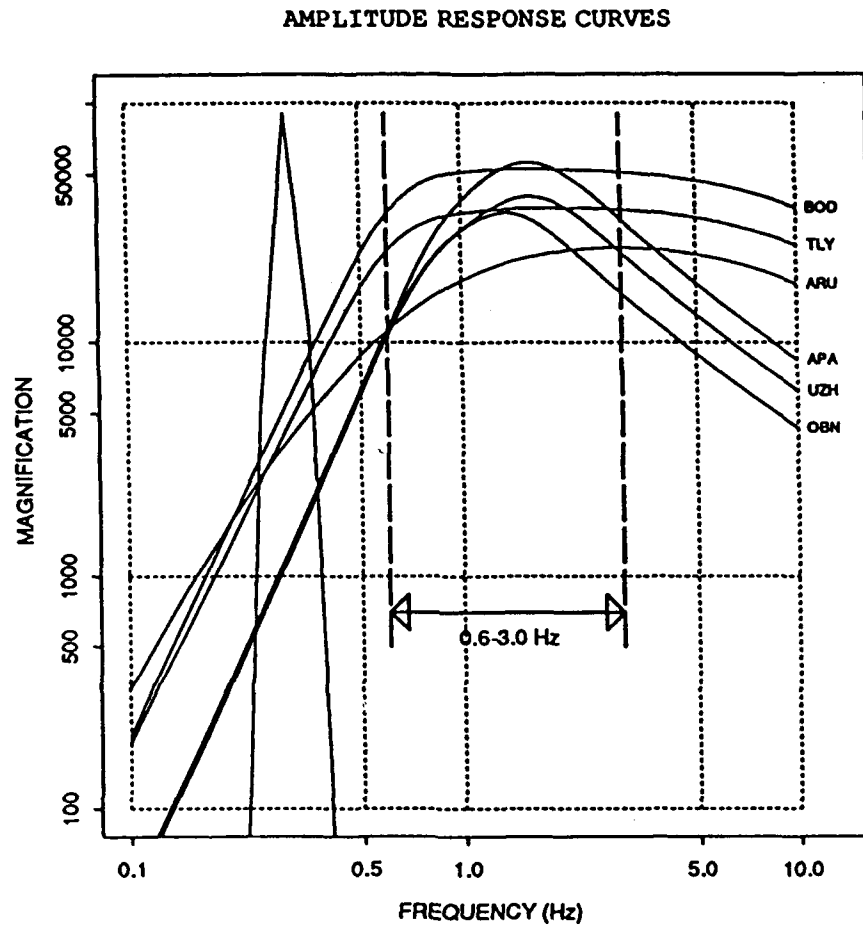
146

AMPLITUDE RESPONSE CURVES

Figure 45: Typical amplitude magnification curves for the six seismic stations. The frequency band 0.6-3.0 Hz, commonly employed for RMS *Lg* magnitude calculations, is also marked. The narrow passband centered at 0.3 Hz is also drawn as an example of the filtering used in the spectral analysis

147

can be separated into a source term, $S(f)$, and path term, $P(f)$, i.e., $A(f)=S(f)+P(f)+\varepsilon$; where the error term ε is assumed to be Gaussian with zero mean. Furthermore, we assume that the path term can be resolved into geometrical spreading, G, (the standard formula for Airy phase derived by Ewing *et al.*, 1957 and widely used for Lg, see e.g., Nuttli, 1973), non-geometric attenuation, characterized by a frequency dependent attenuation coefficient γ, and a station correction, $T(f)$, reflecting the local site amplification. $P(f)=G(\Delta) - \gamma(f) \Delta log(e)+T(f)$, where Δ denotes epicentral distance. The unknowns, $S(f)$, $\gamma(f)$, and $T(f)$, are thus all functions of frequency. Estimates for each frequency of these unknowns were obtained in two steps: first we obtained the γ values, and then the source terms and stations corrections were estimated.

The γ-values were obtained in the following manner. With the γ-value varying between 0.0 to 0.003 km^{-1}, in steps of 0.00005, the unknowns, $S_i(f)$ and $T_j(f)$, were estimated tentatively (subsequently revised once a γ-value was arrived at, see below) from two independent systems of equations, one for Novaya Zemlya and one for Semipalatinsk data. The γ-value, for which the two solutions of station corrections, $T_j(f)$, were in closest agreement, according to the criterion described below, was then used as an estimate. The system of equations for each site could, thus, be written as:

$$A_{ij}(f) - G(\Delta_{ij}) + \gamma(f) \cdot \Delta_{ij} \cdot \log(e) = S_i(f) + T_j(f) + \varepsilon_{ij}$$

$A_{ij}(f)$ denotes the amplitude at station j for explosion i. In these equations, the attenuation coefficient is not treated as an unknown, but as a parameter. For each system of equations we also imposed the restriction that the average value of the station corrections be zero.

Figure 46 shows examples of station corrections obtained in this manner from data at the two test sites independently. The two corrections estimated for each station are plotted against one another and the straight line represents equal values, which would be obtained if the data were in complete agreement with the model. The two examples in Figure 46 represent extreme cases with regard to goodness of fit. The best and worst fits were thus obtained for frequencies 1.1 and at 0.5 Hz, respectively, the misfit error of the station corrections being 0.035 and 0.121, respectively. The median of this standard error for all frequency bands was 0.068. Translated into non-geometrical attenuation, this corresponds to a spread in the attenuation coefficient of about 5 percent at an epicentral distance of 20 degrees, a distance typical of the Lg paths. This comparatively small scatter lends support to the assumption that a frequency dependent non-geometric attenuation common to all 12 paths can be used as a first approximation for these data.
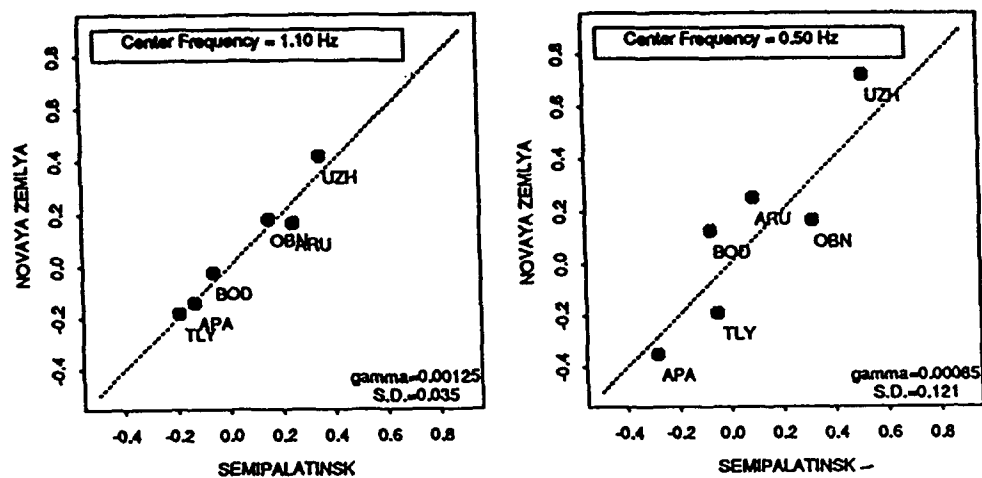
148

Figure 46: Comparison of station corrections estimated from Semipalatinsk and Novaya Zemlya data, for frequencies 1.1 Hz, to the left, and 0.5 Hz, to the right. The misfit errors are also given in the diagram.

Once the attenuation coefficient had been determined for a given frequency, according to the procedure outlined above, station corrections, $T_j(f)$, and source functions, $S_i(f)$, were estimated from a system of equations based on data at both test sites simultaneously.

Attenuation Coefficient and Station Corrections

Figure 47 shows the estimated attenuation coefficient as a function of frequency. In the frequency range 0.45 to 1.5 Hz it increases almost monotonically. Below this range it seems to decrease slightly and above 1.5 Hz it stays almost constant. It is often assumed that the attenuation coefficient can be written as: $\gamma(f) = 2\pi f / QU$ where U represents the group velocity and Q the temporal quality factor, which in turn is assumed to have a frequency dependence of the form $Q = Q_0 \cdot f^n$ with Q_0 representing the temporal quality factor at 1 Hz. With a group velocity of 3.5 km/s the temporal quality factor, in the range 0.45-1.5 Hz, can be written approximately as: $Q=731f^{0.42}$ for our data.

A number of estimates of the temporal quality factor for propagation paths in different parts of the world have been published. In Figure 48 we compare our results with those for some other paths across or near shield areas in North America, Australia, and Eurasia. The upper frame shows the Q values as a function of frequency and in the lower frame we have used η-Q plots as introduced by Mitchell (1991). The shaded areas in the lower frame summarize the compilation of *Lg* coda Q by Mitchell (1991) for the Basin and Range province, to the left, and for cratonic regions of Africa and the E.United States, to the right.

The values obtained here for West-Central U.S.S.R are similar to those of E. United States and the Canadian Shield. Somewhat inconsistently, however, they are also higher than those obtained for Eastern Kazakh (Given *et al.*, 1990, and Sereno, 1990). This apparent discrepancy can be due to differences in the propagation distances. For the data here the average distance is about 2000 km, while the data for Eastern Kazakh did not extend beyond 700 km.

The comparisons have to be made with some care, as there are differences in the types of data used in these studies. Furthermore, there are fundamental differences in methodologies used to estimate the Q values. For example, Bowman and Kennett (1991), who obtain clearly different Q values for the North Australian Craton, attributed to gradients of crustal velocity, assume that the station corrections are frequency - independent and equal for all stations. Here and in the studies by Chun *et al.* (1987) and Gupta and McLaughlin (1987) the station corrections are found to be highly variable both with station and with frequency (see below).

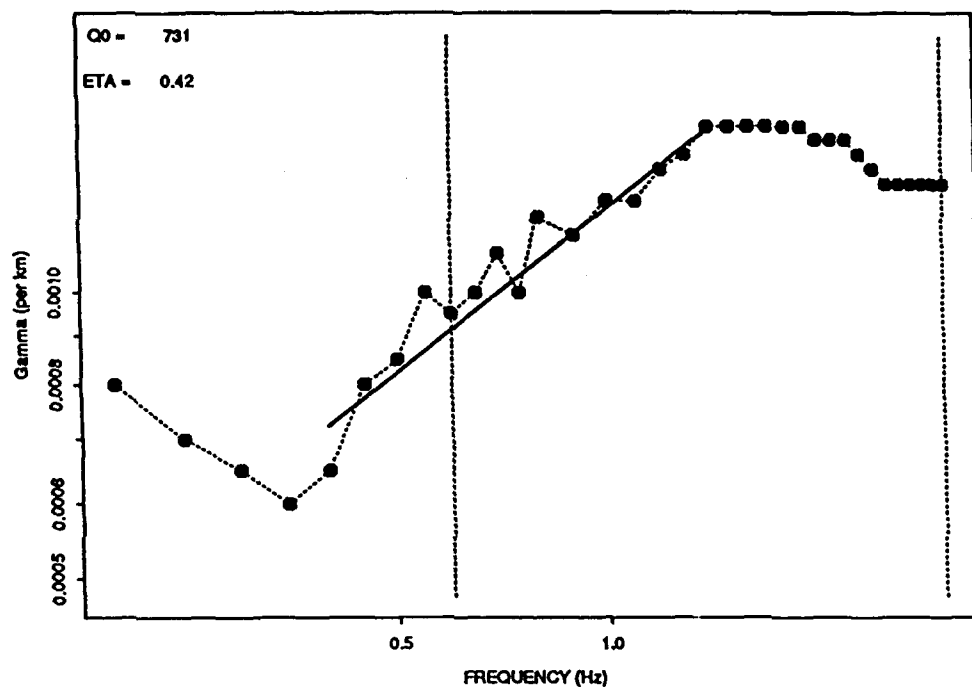Figure 49 shows the station corrections as a function of frequency. The most striking dif-

Figure 47: Estimated g-values as a function of frequency. The solid line represent was obtained with weighted linear regression; the weights being the squared inverse of the misfit errors of the station corrections as illustrated in Figure 46. The estimated linear relation can be translated into frequency of the temporal quality factor, with Q0=731 and e=0.42.
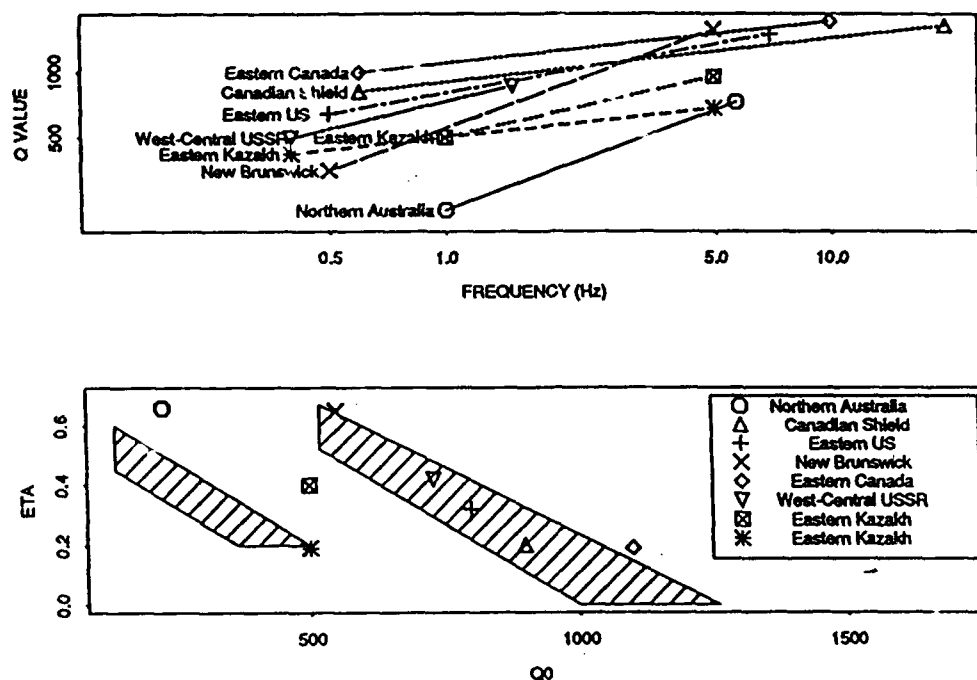
Figure 48: Comparison of the frequency dependence of the temporal quality factor esti-
mated for the data here, i.e., Wes:-Central U.S.S.R., with estimates for other
regi ns in the world: N. Australia (Bowman and Kennett, 1991), the Cana-
dian Shield (Hasegawa, 1985), Eastern U.S. (Mitchell, 1991), New Brun-
swick (Shien and Hermann, 1987), E. Canada (Chun *et al.*, 1987), and
E.Kazkh (Given *et al.*, 1990; Sereno, 1990). The top diagram shows Q as a
function of frequency and in the bottom diagram the estimates are given in a
Q0-e plot. The shaded areas in the lower diagram summarizes the compila-
tion of *Lg* Q coda values by Mitchell (1991) for the Basin and Range prov-
ince and Cratonic regions of Africa and E. United States.
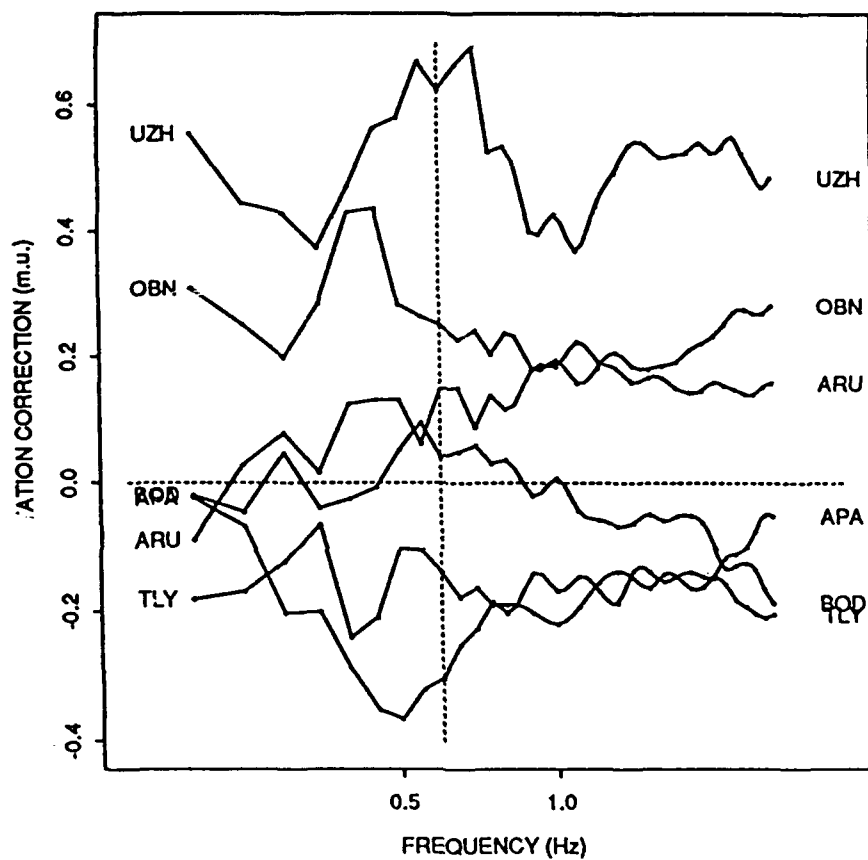
152

Figure 49: Estimated station corrections as a function of frequency.

ference among these functions is the range of almost one magnitude unit in the overall level; the local site amplification at UZH being the highest and those of APA and TLY being the lowest. Furthermore, the functions vary with frequency both in shape and in degree among the stations. The curves for UZH and OBN have pronounced peaks around near 0.6 and 0.4 Hz respectively, whereas for ARU the function steadily increases with frequency. For a given station the range of variation is, at its largest, about 0.4 magnitude units (for APA). This large variation and frequency dependence in station corrections is in broad agreement with results for seismic stations in N. America obtained by Chun *et al.* (1987) and Gupta *et al.* (1987). According to Chun *et al.* (1987) station site effects can even cause frequency dependent fluctuations that completely dominate the effect due to non-elastic attenuation. In earlier studies Gupta and McLaughlin (1987) and Chun *et al.* (1987) have also demonstrated that *Lg* wave station corrections, although complex, are *stable characteristics of the individual recording station.* Thus, Gupta and McLaughlin (1987) found that the *Lg* site effects are strongly correlated with local station geologies; amplitudes recorded in hard rock and soft rock being below and above average values, respectively.

The information regarding station geologies for the stations analyzed here (ARU and, OBN, loam and limestone respectively; see Given, 1990) is, however, too incomplete to even attempt such correlations.

Source Terms

Figure 50 shows source terms, S(f), for different frequencies plotted as a function of explosion yield. The yields have been estimated from $m_b(Lg)$ magnitudes that were calibrated for Semipalatinsk explosions (Israelsson, 1992). The data follow linear trends with slopes that differ markedly with frequency.

Figure 51 shows the estimated slopes as a function of frequency for all the data with error bars representing estimated standard deviations. The slope is close to or slightly above 1 for frequencies below 0.7 Hz and decreases rapidly between 0.7 and 1 Hz. Above 1 Hz, it stays fairly constant around 0.6.

Figure 51 also shows the misfit error of the linear relations - between source terms and yields - as a function of frequency, and the misfit error divided by the estimated slope. The latter ratio would represent the standard deviation of yields (on a logarithmic scale) determined from the estimated linear relation. This standard error has a pronounced minimum for frequencies around 0.5-0.7 Hz. This is primarily due to differences in slope values.

Figure 52 shows empirical source spectra as a function of frequency for 20, 50, 100, and 200 kt - derived from the source terms and corrected for seismic instrument response. The
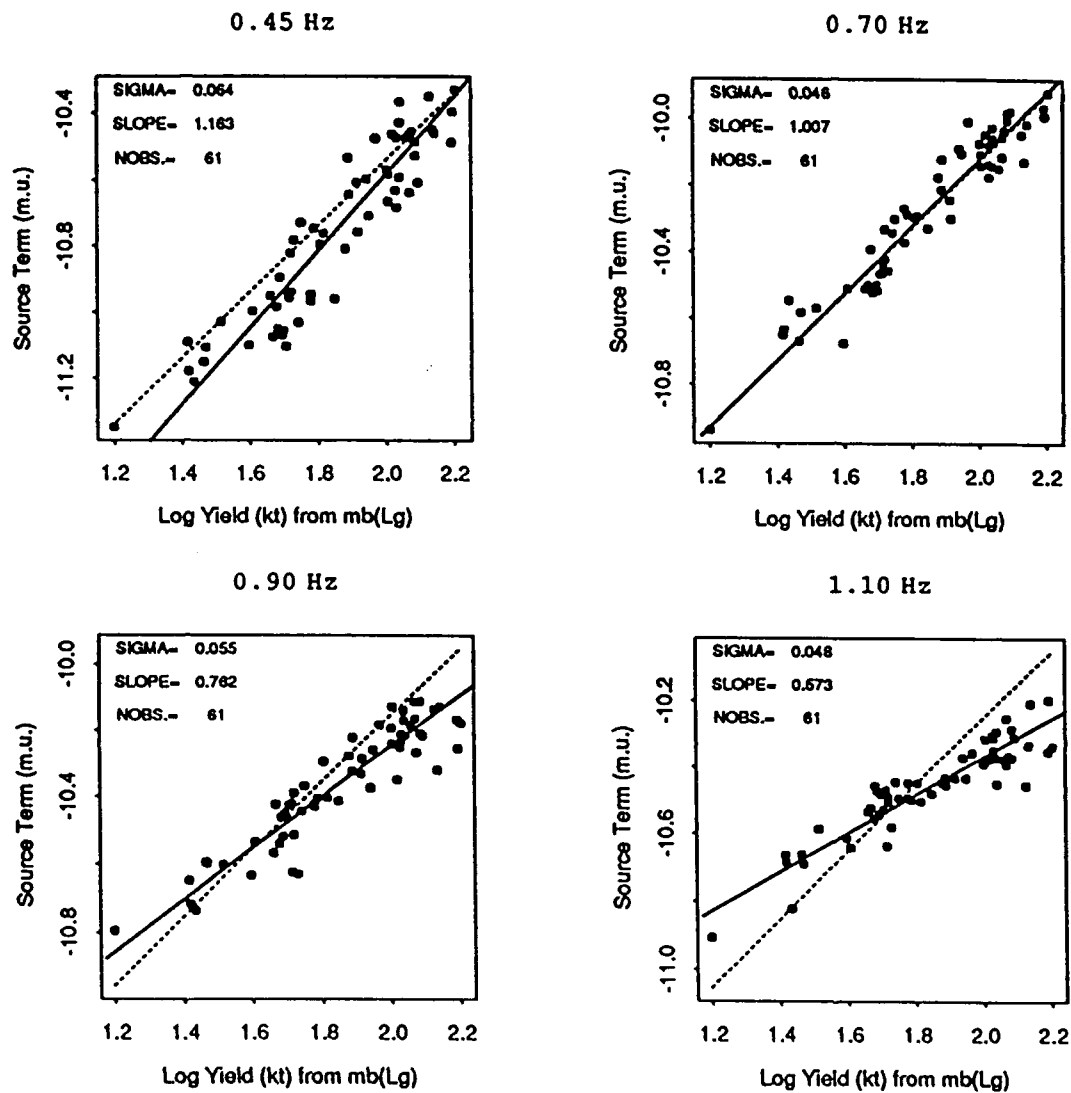
Figure 50: Estimated source terms for different frequencies plotted against estimated explosion yields of Semipalatinsk events. Estimated slopes and misfit errors (SIGMA) and number of observations are also given for each diagram.
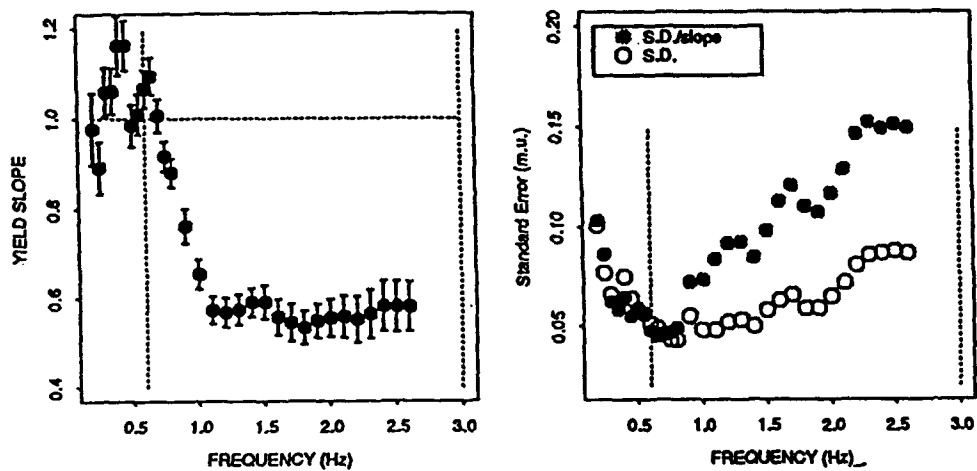
Figure 51: Estimated source term - yield slopes as a function of frequency with error bars for estimated standard errors, in the left frame, and misfit errors (S.D.) and S.D. divided by slope estimates, to the right, also as a function of frequency.
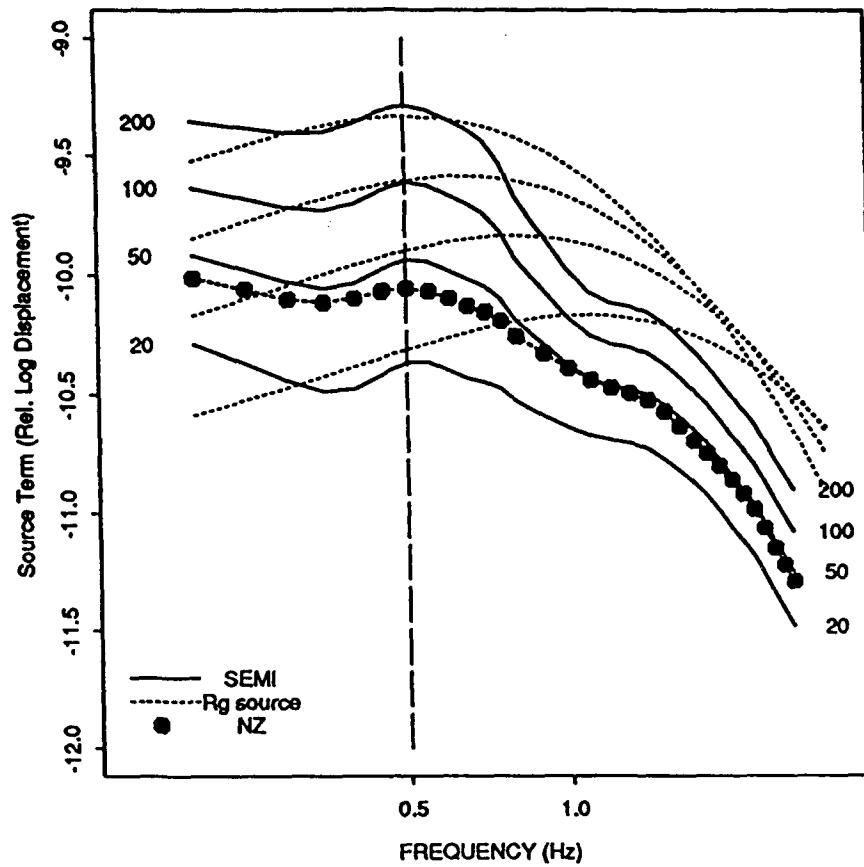
156

Figure 52: Estimated source terms as a function of frequency normalized to different yields (given in kt in the diagram), for Semipalatinsk (SEMI) and Novaya Zemlya (NZ). Dotted lines (Rg) show source functions for fundamental mode Rayleigh waves.

source spectra were based on an average spectrum and a frequency dependent relation for the yield slope. The average spectrum was obtained from the frequency dependent source terms for 8 Semipalatinsk explosions with very similar magnitudes corresponding to yields close to 100 kt. The relation for yield slope was obtained by smoothing the estimated slope data in Figure 50 and was used to scale the average spectrum for 100 kt to lower and higher yields (20, 50 and 200 kt respectively in Figure 52). The source term spectrum for Novaya Zemlya explosions represents an average spectrum of 9 explosions with very similar magnitudes within 0.04 magnitude unit; it is close to the Semipalatinsk source spectrum for 50 kt.

Although the Lg wave has commanded a great deal of attention in studies on yield estimation, there is no widely accepted function for the explosion source. For the sake of comparison with the empirical source spectra in Figure 52, we use an Lg source spectrum proposed by Gupta and et al. (1992). This assumes that low frequency Lg is largely dominated by near-source scattering of the fundamental mode Rayleigh waves into S waves. The amplitude spectrum of fundamental mode Rayleigh wave can be written as: $R(f) \sim \Phi(f) f^{.5} 10^{-4.4(d/v)f}$, F is the reduced displacement potential, d the shot depth, and v the P velocity in the source region (see formula by Gupta et al. 1992 based on derivation by Hudson and Douglas, 1975). In Figure 52 we have calculated $R(f)$ for different yields using the F suggested by VonSeggern and Blandford (1971), with parameters for granite and $v=5.0$ km/s. The scaling of shot depth with explosion yield from Gupta et al. (1992) was also used in the calculations. The $R(f)$ curves in Figure 52 become increasingly different from the empirical curves with increasing frequency. However, Gupta et al. (1992) assume that low frequency Lg is produced only by some of the fundamental mode Rayleigh waves. This portion, called scattering function by Gupta et al. (1992), varies with frequency.

In Figure 53 we have displayed the ratios of the spectra of the empirical Lg sources and the Rayleigh source functions. The four ratio curves, representing four yields; 20, 50, 100, and 200 kt, are quite similar for frequencies below about 1 Hz, and represent the spectrum of the 'scattering' function defined by Gupta et al. (1992), which is assumed to be a function of frequency only and not shot depth. The ratios fall off with frequency approximately as f^{-1} in the band 0.2-1.0 Hz.

Scaling of $m_b(Lg)$ Magnitudes

Using the frequency dependent attenuation coefficient, source terms, and station corrections, and we can now model the $m_b(Lg)$ scaling and compare it with observations. As the estimates for the source terms, station corrections, and the attenuation coefficient all were obtained from the data, this comparison is clearly not an independent test of their validity.
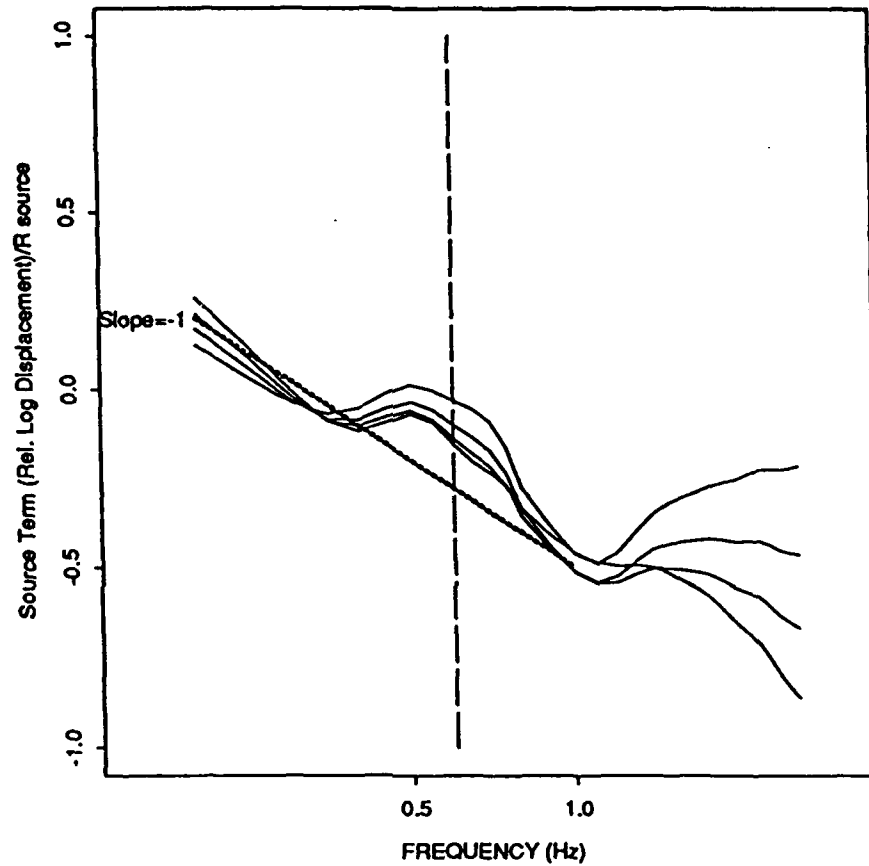
Figure 53: Ratio of source terms and Rg source functions for yields 20, 50, 100, and 200 kt (see Figure 52) as a function of frequency. The dotted line represent a frequency decay of f^{-1}.

159

It only serves to verify the consistency with the data, i.e with the observed variation in $m_b(Lg)$ scaling.

The *observed* $m_b(Lg)$ values for each station were based on RMS amplitudes for waveforms, bandpass filtered between 0.6-3.0 Hz (three pole Butterworth), in time segments corresponding to the group velocity window 3.1-3.7 km/s. The response for each station was also been normalized to that of the 1988 calibration for station OBN.

The *modelled* $m_b(Lg)$ values were calculated in the frequency domain from the spectral functions of the source (Figure 52), a non-elastic attenuation function with a temporal quality factor $Q0f^{0.42}$, the station corrections (Figure 49), the OBN 1988 instrument response, and a 0.6-3.0 Hz bandpass filter.

First we compare the $m_b(Lg)$ scaling with yield. Figure 54 shows $m_b(Lg)$ observed and modelled for the station OBN for a set of a suite of explosions with yield in the range from 4 to 150 kt. The yields of the observed data were those reported by Bocharov *et al.* (1989), and they are supposedly independent of seismic information. The comparison between modelled and observed data is confined to station OBN, as it is the only station, for which a substantial number of $m_b(Lg)$ are available for explosions with yields reported by Bocharov *et al.* (1989). The slopes estimated from the two cases are in reasonable agreement and both significantly less than 1.0. We also note that the modeled $m_b(Lg)$ data are not exactly proportional to yield. The estimated standard error is, however, quite small, 0.015 magnitude units.

Finally, we turn to pair-wise comparisons of station magnitudes for explosions at a given site. Such comparisons have previously been used to demonstrate the high precision in estimated relative station $m_b(Lg)$. The comparisons here are confined to the stations ARU, OBN, and UZH, as data for only a relatively small number of common events were available for other station pairs. Figure 55 shows $m_b(Lg)$ values, observed and modelled, for the station pairs OBN-ARU, and OBN-UZH. There is reasonable agreement between observed and modelled data. The estimated slopes (given in Figure 55) are greater than and less than one for OBN-ARU and OBN-UZH respectively. ARU is closer and UZH father from the Semipalatinsk test site, respectively, than OBN. Modelled data for which the station corrections were all equal to one and independent of frequency had estimated slopes different from those in Figure 55, which are based on the frequency dependent station corrections in Figure 49. This would indicate that the slope is determined by the combined effects of source spectral scaling, frequency dependence of non-elastic attenuation, and the station corrections. Finally, calculations of modelled and observed $m_b(Lg)$ for the three stations based on the frequency band 0.3-0.75 Hz (for which the source spectra seem to scale close to 1) still resulted in differences - although smaller - in the estimated slopes
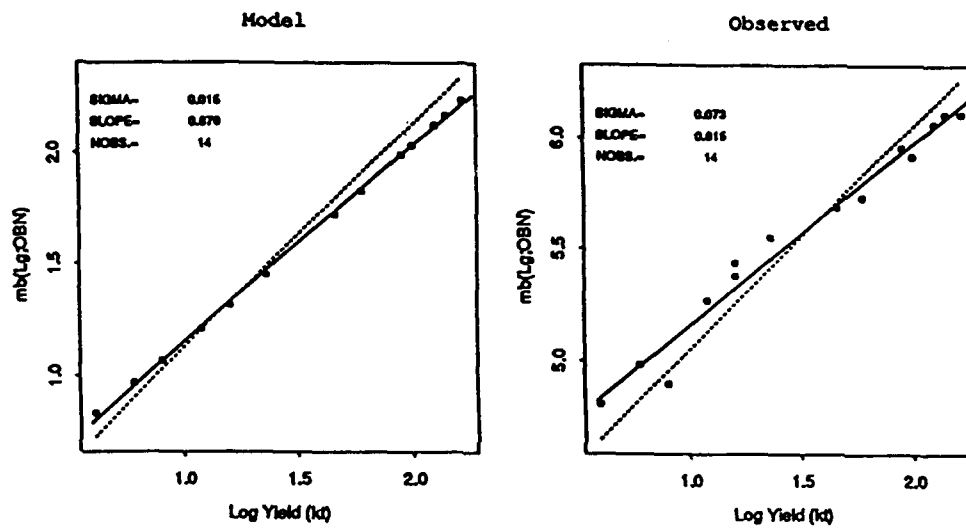
Figure 54: Comparison of modelled and observed $m_b(Lg)$ and yield data for OBN. The $m_b(Lg)$ is based on the commonly used 0.6-3.0 frequency band. Estimated slopes and misfit errors and the number of observations are also indicated in the diagrams.

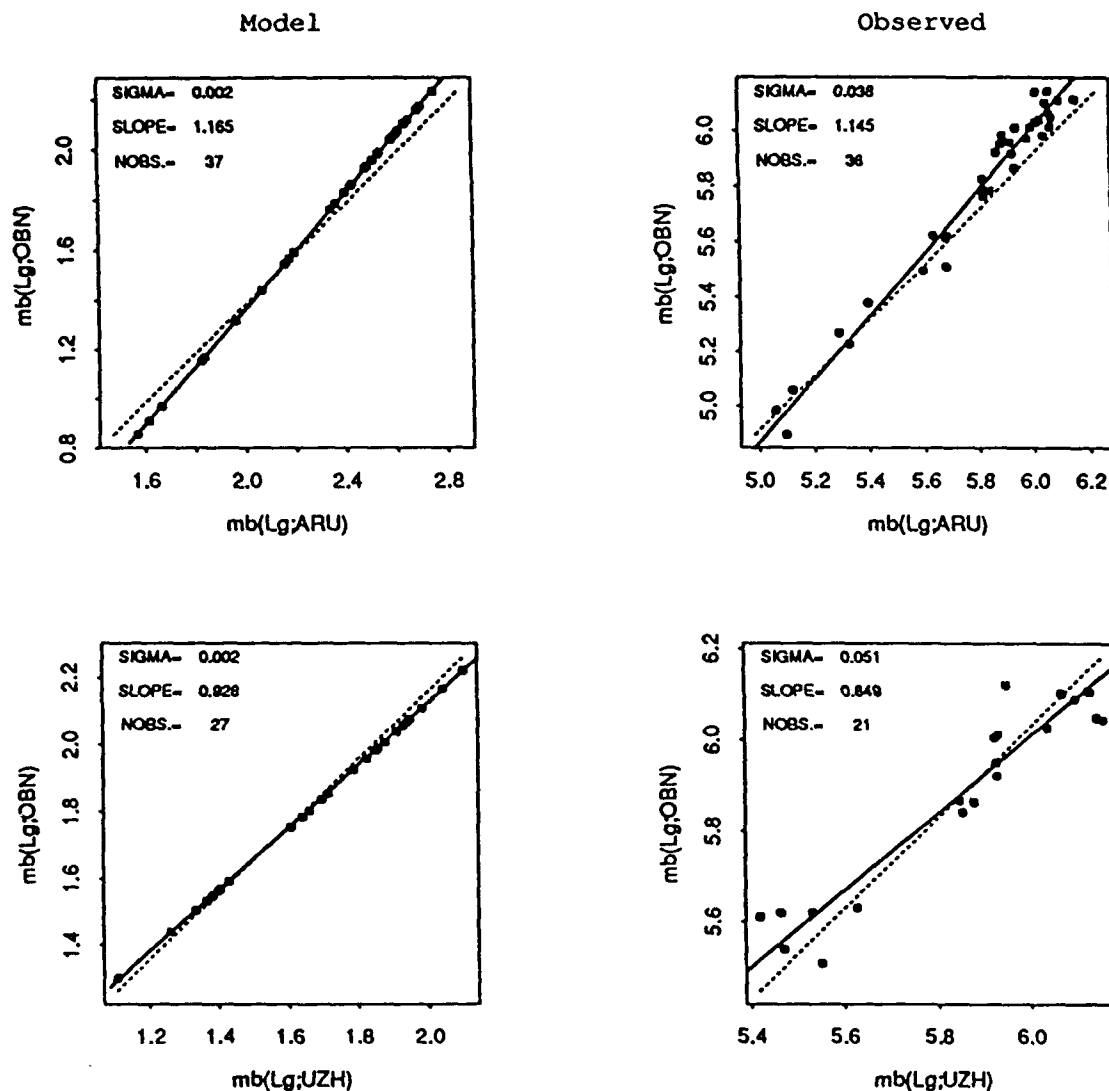Model   Observed

Figure 55:   Comparison of modelled and observed $m_b(Lg)$ data at ARU, OBN, and
              UZH. The $m_b(Lg)$ is based on the commonly used 0.6-3.0 frequency band.
              Estimated slopes and misfit errors and the number of observations are also
              indicated in the diagrams.

for the station pairs OBN-ARU and OBN-UZH.

Concluding Comments

In this note we have attempted to separate Lg wave spectra, obtained from narrow band pass filtering, into source and path terms with the intention of getting some insight into the variability of $m_b(Lg)$ scaling (i.e., the observation that the rate of increase in station $m_b(Lg)$ with increasing yield of explosions may vary with station).

The analysis suggests that the frequency components of the estimated Lg source spectra, for yields in the range 50-150 kt, scale differently with yield. At low frequencies, (0.2-0.7 Hz) the spectral amplitudes are more or less directly proportional to explosion yield. At frequencies above 0.7 Hz the scaling factor decays sharply to about 0.6 at about 1.0 Hz, above which the scaling stays fairly constant. Furthermore, although the attenuation coefficient of the non-geometrical spreading was fairly stable (misfit error within 5-10% of the model) for the 12 paths and varied in a systematic manner with frequency, the resulting path spectra will differ in shape depending on epicentral distance. Finally, the frequency dependent site amplifications vary significantly both in overall level (with about one m.u.) and in shape (largest range of variation for given station is about 0.4 m.u.).

Therefore, the frequency scaling of the Lg source spectrum in combination with differences among the frequency responses of the non-geometric attenuation (due to different distances) and among the site amplifications appear to give rise to variation in station $m_b(Lg)$ scaling. We have analyzed data from 6 stations and compared $m_b(Lg)$ scaling for 3 of them (due to limited amount of data) and have found that there are variations in the $m_b(Lg)$ scaling, even if a low frequency band is utilized.

If one considers the high relative precision of $m_b(Lg)$, (within a few hundredths of a m.u.), this variation mainly implies that each station $m_b(Lg)$ may, in fact, represent a different magnitude scale. This is because a difference in yield slope for two stations may introduce a systematic bias between their station magnitude values. Let us assume, for example, that $m_b(Lg)$ are available at two stations for two explosions with yields differing by about one order of magnitude and that the $m_b(Lg)$-yield slopes for the two stations differ by 15 percent, being say 1.00 and 0.85. This difference in slope would introduce a bias of about 0.06 m.u. between the two station magnitudes for one of the explosions. This should be compared with the standard deviation of 0.03 m.u.; often quoted as the relative precision of station $m_b(Lg)$.

For a network larger than the one studied here, the possibility of the attenuation coefficient being strongly dependent on path exists as well, and variability in $m_b(Lg)$ scaling is likely. In order to combine *station* $m_b(Lg)$ values into an optimum *network* $m_b(Lg)$, variation in

scaling, therefore, has to be considered.

The spectral decomposition of the recorded Lg waves obtained here can also be related to results from studies on generation and propagation of Lg waves generally. For example, the source spectra and their scaling are consistent with the hypothesis advanced by Gupta *et al.* (1992) that low frequency Lg waves are produced from scattering of explosion generated Rg into S waves. The so called 'scattering' function, defined by Gupta *et al.* (1992) as the portion of the Rg that is converted into S waves, was formally calculated as the ratio of the obtained empirical source functions and source functions for fundamental mode Rayleigh waves. This ratio was fairly consistent for explosions of different yields at low frequencies, where it is approximately inversely proportional to frequency. The apparent stability of the attenuation coefficient is, perhaps, somewhat surprising considering the variety in tectonic structures traversed by the wave paths. The temporal quality factor representing these paths is similar to estimates for cratonic regions of Africa and the Eastern United States, but is also higher than estimates obtained for shorter paths across Kazakhstan.

Acknowledgments

References

Bocharov, V.S., Zelentsoz, S.A., and V.N. Michailov (1989). Characteristics of 96 underground nuclear explosions at the Semipalatinsk test site, Atomic Energy (Atomnaya Energiya), 67.

Bowman, J.R. and B.L.N. Kennett (1991). Propagation of *Lg* waves in the North Australian Craton: Influence of Crustal Velocity Gradients, Bull. Seism. Soc. Am., 81, 592-610. Chun, K.-Y., G.F. West, R.J. Kokoski and C. Sampson (1987). A novel technique for measuring *Lg* attenuation: results from eastern Canada between 1 and 10 Hz, Bull. Seism. Soc. Am., 77, 398-419.

Ewing, W.M., Jardetsky, W.S., and F. Press (1957). Elastic waves in layered media. McGraw Hill, New York, NY, 380 pp.

Given, H.K. (1990), Variations in broad band Seismic noise at IRIS/IDA stations in the USSR with implications for event detection. Bull. Seism. Soc. Am., 80, 2072-2105.

Given, H.K., N.T. Tarasov, V. Zhuraavle, F.L. Vernon, J.Berger, and I.L. Nerserov (1990).

High Frequency Observations in Eastern Kazakhstan, USSR, with emphasis on chemical explosion experiments, J. Geophys. Res, 95, 295-307.

Gupta, I.N. and K.L. McLaughlin (1987). Attenuation of ground motion in the eastern United States, Bull. Seism. Soc. Am., 77, 366-383.

Gupta, I.N., W.W. Chan, and R.A. Wagner (1992) A comparison of regional phases from underground nuclear explosions at East Kazakh and Nevada test sites, Bull. Seism. Soc. Am., 82, 352-382.

Hansen, R., Ringdal, F., and P.G. Richards (1990). The stability of RMS *Lg* measurements, and their potential for accurate estimation of the yields of Soviet underground explosions, Bull. Seism. Soc. Am., 80, 2106-2126.

Hasegawa, H.S. (1985). Attenuation of *Lg* waves in the Canadian Shield, Bull. Seism. Soc. Am., 75, 1569-1582.

Hudson, J.A. and A. Douglas (1975). On the amplitudes of seismic waves, Geophys. J., 42, 1039-1044.

Israelsson, H. (1992). Path corrections for U.S.S.R. explosions and RMS *Lg* magnitudes (Manuscript in preparation)

Kemerait, R. C., G. Kraft, J. S. Mott, and E. Dohner (1981), A study of the hand-digitizing process for digitizing short period seismic data. ENSCO Technical Report DCS-SDR-81-57

Kondorskaya, N.V. and Z.I. Aranovich (1979), The uniform system of seismic observations of the U.S.S.R.and prospects for its development, Phys. Earth and Plan. Int., 18, 78-88.

Mitcł ·ll, B.J. (1991), Regional variation of Q *Lg* and its frequency dependence: implications for crustal structure and evolution. in Proceedings of the 13th Annual DARPA/GL Seismic Research Symposium, 8-10 October 1991. (Eds J. Lewkowicz and J McPhetres), PL-TR-91-2208 Geophysics Laboratory, Hanscom AFB, MA, ADA241325.

Nuttli, O.W. (1973). Seismic wave attenuation and magnitude relations for Eastern North America J. Geophys. Res. 78, 876-885.

Patton, H.J. (1988). Application of Nuttli's method to estimate yield of Nevada Test Site Explosions recorded on Lawrence Livermore National Laboratory's digital seismic system, Bull. Seism. Soc. Am. 78, 1759-1772.

Ringdal, F. (1989) NORSAR P-wave detection and yield estimation of selected Semipalatinsk explosions, in: Semiann. Tech. Summ., 1 April - 30 Sep 1989, NORSAR Sci. Rep. 1-89/90, Kjeller, Norway.

Ringdal, F. and J. Fyen (1988). Comparative analysis of NORSAR and Grafenberg *Lg* magnitudes of Shagan River explosions, in: Semiann. Tech. Summ., 1 Apr-30 Sep 1988, NORSAR Sci. Rep. 1-88/89, Kjeller, Norway.

Sereno, T.J., Jr., (1990). Frequency dependent attenuation in Eastern Kazakhstan and implications for seismic detection thresholds in the Soviet Union, Bull. Seism. Sc. Am., 80, 2089-2105.

Shin, T.C. and R.B. Hermann (1987). *Lg* attenuation and source studies using 1982 Miramichi data, Bull. Seism. Soc. Am., 7ⁱ, 384-397.

VonSeggern, D. and R. Blandford (1972). Source Time Functions and Spectra for Underground Nuclear Explosions, Geophys. J. Astr. Soc., 31, 83-97.

Zonenshain, L.P., J. Verhoef, R. Macnab, and H. Meyers (1991). Magnetic Imprints of Continental Accretion in the U.S.S.R, EOS, 29, 305.

DISTRIBUTION LIST

Prof. Thomas Ahrens
Seismological Lab, 252-21
Division of Geological & Planetary Sciences
California Institute of Technology
Pasadena, CA 91125

Prof. Keiiti Aki
Center for Earth Sciences
University of Southern California
University Park
Los Angeles, CA 90089-0741

Prof. Shelton Alexander
Geosciences Department
403 Deike Building
The Pennsylvania State University
University Park, PA 16802

Dr. Ralph Alewine, III
DARPA/NMRO
3701 North Fairfax Drive
Arlington, VA 22203-1714

Prof. Charles B. Archambeau
CIRES
University of Colorado
Boulder, CO 80309

Dr. Thomas C. Bache, Jr.
Science Applications Int'l Corp.
10260 Campus Point Drive
San Diego, CA 92121 (2 copies)

Prof. Muawia Barazangi
Institute for the Study of the Continent
Cornell University
Ithaca, NY 14853

Dr. Jeff Barker
Department of Geological Sciences
State University of New York
 at Binghamton
Vestal, NY 13901

Dr. Douglas R. Baumgardt
ENSCO, Inc
5400 Port Royal Road
Springfield, VA 22151-2388

Dr. Susan Beck
Department of Geosciences
Building #77
University of Arizona
Tuscon, AZ 85721

Dr. T.J. Bennett
S-CUBED
A Division of Maxwell Laboratories
11800 Sunrise Valley Drive, Suite 1212
Reston, VA 22091

Dr. Robert Blandford
AFTAC/TT, Center for Seismic Studies
1300 North 17th Street
Suite 1450
Arlington, VA 22209-2308

Dr. G.A. Bollinger
Department of Geological Sciences
Virginia Polytechnical Institute
21044 Derring Hall
Blacksburg, VA 24061

Dr. Stephen Bratt
Center for Seismic Studies
1300 North 17th Street
Suite 1450
Arlington, VA 22209-2308

Dr. Lawrence Burdick
Woodward-Clyde Consultants
566 El Dorado Street
Pasadena, CA 91109-3245

Dr. Robert Burridge
Schlumberger-Doll Research Center
Old Quarry Road
Ridgefield, CT 06877

Dr. Jerry Carter
Center for Seismic Studies
1300 North 17th Street
Suite 1450
Arlington, VA 22209-2308

Dr. Eric Chael
Division 9241
Sandia Laboratory
Albuquerque, NM 87185

Prof. Vernon F. Cormier
Department of Geology & Geophysics
U-45, Room 207
University of Connecticut
Storrs, CT 06268

Prof. Steven Day
Department of Geological Sciences
San Diego State University
San Diego, CA 92182

1

Marvin Denny
U.S. Department of Energy
Office of Arms Control
Washington, DC 20585

Dr. Cliff Frolich
Institute of Geophysics
8701 North Mopac
Austin, TX 78759

Dr. Zoltan Der
ENSCO, Inc.
5400 Port Royal Road
Springfield, VA 22151-2388

Dr. Holly Given
IGPP, A-025
Scripps Institute of Oceanography
University of California, San Diego
La Jolla, CA 92093

Prof. Adam Dziewonski
Hoffman Laboratory, Harvard University
Dept. of Earth Atmos. & Planetary Sciences
20 Oxford Street
Cambridge, MA 02138

Dr. Jeffrey W. Given
SAIC
10260 Campus Point Drive
San Diego, CA 92121

Prof. John Ebel
Department of Geology & Geophysics
Boston College
Chestnut Hill, MA 02167

Dr. Dale Glover
Defense Intelligence Agency
ATTN: ODT-1B
Washington, DC 20301

Eric Fielding
SNEE Hall
INSTOC
Cornell University
Ithaca, NY 14853

Dr. Indra Gupta
Teledyne Geotech
314 Montgomery Street
Alexanderia, VA 22314

Dr. Mark D. Fisk
Mission Research Corporation
735 State Street
P.O. Drawer 719
Santa Barbara, CA 93102

Dan N. Hagedon
Pacific Northwest Laboratories
Battelle Boulevard
Richland, WA 99352

Prof Stanley Flatte
Applied Sciences Building
University of California, Santa Cruz
Santa Cruz, CA 95064

Dr. James Hannon
Lawrence Livermore National Laboratory
P.O. Box 808
L-205
Livermore, CA 94550

Dr. John Foley
NER-Geo Sciences
1100 Crown Colony Drive
Quincy, MA 02169

Dr. Roger Hansen
HQ AFTAC/TTR
Patrick AFB, FL 32925-6001

Prof. Donald Forsyth
Department of Geological Sciences
Brown University
Providence, RI 02912

Prof. David G. Harkrider
Seismological Laboratory
Division of Geological & Planetary Sciences
California Institute of Technology
Pasadena, CA 91125

Dr. Art Frankel
U.S. Geological Survey
922 National Center
Reston, VA 22092

Prof. Danny Harvey
CIRES
University of Colorado
Boulder, CO 80309

Prof. Donald V. Helmberger
Seismological Laboratory
Division of Geological & Planetary Sciences
California Institute of Technology
Pasadena, CA 91125

Prof. Eugene Herrin
Institute for the Study of Earth and Man
Geophysical Laboratory
Southern Methodist University
Dallas, TX 75275

Prof. Robert B. Herrmann
Department of Earth & Atmospheric Sciences
St. Louis University
St. Louis, MO 63156

Prof. Lane R. Johnson
Seismographic Station
University of California
Berkeley, CA 94720

Prof. Thomas H. Jordan
Department of Earth, Atmospheric &
 Planetary Sciences
Massachusetts Institute of Technology
Cambridge, MA 02139

Prof. Alan Kafka
Department of Geology & Geophysics
Boston College
Chestnut Hill, MA 02167

Robert C. Kemerait
ENSCO, Inc.
445 Pineda Court
Melbourne, FL 32940

Dr. Max Koontz
U.S. Dept. of Energy/DP 5
Forrestal Building
1000 Independence Avenue
Washington, DC 20585

Dr. Richard LaCoss
MIT Lincoln Laboratory, M-200B
P.O. Box 73
Lexington, MA 02173-0073

Dr. Fred K. Lamb
University of Illinois at Urbana-Champaign
Department of Physics
1110 West Green Street
Urbana, IL 61801

Prof. Charles A. Langston
Geosciences Department
403 Deike Building
The Pennsylvania State University
University Park, PA 16802

Jim Lawson, Chief Geophysicist
Oklahoma Geological Survey
Oklahoma Geophysical Observatory
P.O. Box 8
Leonard, OK 74043-0008

Prof. Thorne Lay
Institute of Tectonics
Earth Science Board
University of California, Santa Cruz
Santa Cruz, CA 95064

Dr. William Leith
U.S. Geological Survey
Mail Stop 928
Reston, VA 22092

Mr. James F. Lewkowicz
Phillips Laboratory/GPEH
Hanscom AFB, MA 01731-5000(2 copies)

Mr. Alfred Lieberman
ACDA/VI-OA State Department Building
Room 5726
320-21st Street, NW
Washington, DC 20451

Prof. L. Timothy Long
School of Geophysical Sciences
Georgia Institute of Technology
Atlanta, GA 30332

Dr. Randolph Martin, III
New England Research, Inc.
76 Olcott Drive
White River Junction, VT 05001

Dr. Robert Masse
Denver Federal Building
Box 25046, Mail Stop 967
Denver, CO 80225

Dr. Gary McCartor
Department of Physics
Southern Methodist University
Dallas, TX 75275

3

Prof. Thomas V. McEvilly
Seismographic Station
University of California
Berkeley, CA 94720

Prof. John A. Orcutt
IGPP, A-025
Scripps Institute of Oceanography
University of California, San Diego
La Jolla, CA 92093

Dr. Art McGarr
U.S. Geological Survey
Mail Stop 977
U.S. Geological Survey
Menlo Park, CA 94025

Prof. Jeffrey Park
Kline Geology Laboratory
P.O. Box 6666
New Haven, CT 06511-8130

Dr. Keith L. McLaughlin
S-CUBED
A Division of Maxwell Laboratory
P.O. Box 1620
La Jolla, CA 92038-1620

Dr. Howard Patton
Lawrence Livermore National Laboratory
L-025
P.O. Box 808
Livermore, CA 94550

Stephen Miller & Dr. Alexander Florence
SRI International
333 Ravenswood Avenue
Box AF 116
Menlo Park, CA 94025-3493

Dr. Frank Pilotte
HQ AFTAC/TT
Patrick AFB, FL 32925-6001

Prof. Bernard Minster
IGPP, A-025
Scripps Institute of Oceanography
University of California, San Diego
La Jolla, CA 92093

Dr. Jay J. Pulli
Radix Systems, Inc.
2 Taft Court, Suite 203
Rockville, MD 20850

Prof. Brian J. Mitchell
Department of Earth & Atmospheric Sciences
St. Louis University
St. Louis, MO 63156

Dr. Robert Reinke
ATTN: FCTVTD
Field Command
Defense Nuclear Agency
Kirtland AFB, NM 87115

Mr. Jack Murphy
S-CUBED
A Division of Maxwell Laboratory
11800 Sunrise Valley Drive, Suite 1212
Reston, VA 22091 (2 Copies)

Prof. Paul G. Richards
Lamont-Doherty Geological Observatory
 of Columbia University
Palisades, NY 10964

Dr. Keith K. Nakanishi
Lawrence Livermore National Laboratory
L-025
P.O. Box 808
Livermore, CA 94550

Mr. Wilmer Rivers
Teledyne Geotech
314 Montgomery Street
Alexandria, VA 22314

Dr. Carl Newton
Los Alamos National Laboratory
P.O. Box 1663
Mail Stop C335, Group ESS-3
Los Alamos, NM 87545

Dr. George Rothe
HQ AFTAC/TTR
Patrick AFB, FL 32925-6001

Dr. Bao Nguyen
HQ AFTAC/TTR
Patrick AFB, FL 32925-6001

Dr. Alan S. Ryall, Jr.
DARPA/NMRO
3701 North Fairfax Drive
Arlington, VA 22209-1714

Dr. Richard Sailor
TASC, Inc.
55 Walkers Brook Drive
Reading, MA 01867

Prof. Charles G. Sammis
Center for Earth Sciences
University of Southern California
University Park
Los Angeles, CA 90089-0741

Prof. Christopher H. Scholz
Lamont-Doherty Geological Observatory
 of Columbia University
Palisades, CA 10964

Dr. Susan Schwartz
Institute of Tectonics
1156 High Street
Santa Cruz, CA 95064

Secretary of the Air Force
(SAFRD)
Washington, DC 20330

Office of the Secretary of Defense
DDR&E
Washington, DC 20330

Thomas J. Sereno, Jr.
Science Application Int'l Corp.
10260 Campus Point Drive
San Diego, CA 92121

Dr. Michael Shore
Defense Nuclear Agency/SPSS
6801 Telegraph Road
Alexandria, VA 22310

Dr. Matthew Sibol
Virginia Tech
Seismological Observatory
4044 Derring Hall
Blacksburg, VA 24061-0420

Prof. David G. Simpson
IRIS, Inc.
1616 North Fort Myer Drive
Suite 1440
Arlington, VA 22209

Donald L. Springer
Lawrence Livermore National Laboratory
L-025
P.O. Box 808
Livermore, CA 94550

Dr. Jeffrey Stevens
S-CUBED
A Division of Maxwell Laboratory
P.O. Box 1620
La Jolla, CA 92038-1620

Lt. Col. Jim Stobie
ATTN: AFOSR/NL
Bolling AFB
Washington, DC 20332-6448

Prof. Brian Stump
Institute for the Study of Earth & Man
Geophysical Laboratory
Southern Methodist University
Dallas, TX 75275

Prof. Jeremiah Sullivan
University of Illinois at Urbana-Champaign
Department of Physics
1110 West Green Street
Urbana, IL 61801

Prof. L. Sykes
Lamont-Doherty Geological Observatory
 of Columbia University
Palisades, NY 10964

Dr. David Taylor
ENSCO, Inc.
445 Pineda Court
Melbourne, FL 32940

Dr. Steven R. Taylor
Los Alamos National Laboratory
P.O. Box 1663
Mail Stop C335
Los Alamos, NM 87545

Prof. Clifford Thurber
University of Wisconsin-Madison
Department of Geology & Geophysics
1215 West Dayton Street
Madison, WS 53706

Prof. M. Nafi Toksoz
Earth Resources Lab
Massachusetts Institute of Technology
42 Carleton Street
Cambridge, MA 02142

5

Dr. Larry Turnbull
CIA-OSWR/NED
Washington, DC 20505

DARPA/RMO/SECURITY OFFICE
3701 North Fairfax Drive
Arlington, VA 22203-1714

Dr. Gregory van der Vink
IRIS, Inc.
1616 North Fort Myer Drive
Suite 1440
Arlington, VA 22209

HQ DNA
ATTN: Technical Library
Washington, DC 20305

Dr. Karl Veith
EG&G
5211 Auth Road
Suite 240
Suitland, MD 20746

Defense Intelligence Agency
Directorate for Scientific & Technical Intelligence
ATTN: DTIB
Washington, DC 20340-6158

Prof. Terry C. Wallace
Department of Geosciences
Building #77
University of Arizona
Tuscon, AZ 85721

Defense Technical Information Center
Cameron Station
Alexandria, VA 22314 (2 Copies)

Dr. Thomas Weaver
Los Alamos National Laboratory
P.O. Box 1663
Mail Stop C335
Los Alamos, NM 87545

TACTEC
Battelle Memorial Institute
505 King Avenue
Columbus, OH 43201 (Final Report)

Dr. William Wortman
Mission Research Corporation
8560 Cinderbed Road
Suite 700
Newington, VA 22122

Phillips Laboratory
ATTN: XPG
Hanscom AFB, MA 01731-5000

Prof. Francis T. Wu
Department of Geological Sciences
State University of New York
 at Binghamton
Vestal, NY 13901

Phillips Laboratory
ATTN: GPE
Hanscom AFB, MA 01731-5000

AFTAC/CA
(STINFO)
Patrick AFB, FL 32925-6001

Phillips Laboratory
ATTN: TSML
Hanscom AFB, MA 01731-5000

DARPA/PM
3701 North Fairfax Drive
Arlington, VA 22203-1714

Phillips Laboratory
ATTN: SUL
Kirtland, NM 87117 (2 copies)

DARPA/RMO/RETRIEVAL
3701 North Fairfax Drive
Arlington, VA 22203-1714

Dr. Michel Bouchon
I.R.I.G.M.-B.P. 68
38402 St. Martin D'Heres
Cedex, FRANCE

6

Dr. Michel Campillo
Observatoire de Grenoble
I.R.I.G.M.-B.P. 53
38041 Grenoble, FRANCE

Dr. Jorg Schlittenhardt
Federal Institute for Geosciences & Nat'l Res.
Postfach 510153
D-3000 Hannover 51, GERMANY

Dr. Kin Yip Chun
Geophysics Division
Physics Department
University of Toronto
Ontario, CANADA

Dr. Johannes Schweitzer
Institute of Geophysics
Ruhr University/Bochum
P.O. Box 1102148
4360 Bochum 1, GERMANY

Prof. Hans-Peter Harjes
Institute for Geophysic
Ruhr University/Bochum
P.O. Box 102148
4630 Bochum 1, GERMANY

Prof. Eystein Husebye
NTNF/NORSAR
P.O. Box 51
N-2007 Kjeller, NORWAY

David Jepsen
Acting Head, Nuclear Monitoring Section
Bureau of Mineral Resources
Geology and Geophysics
G.P.O. Box 378, Canberra, AUSTRALIA

Ms. Eva Johannisson
Senior Research Officer
National Defense Research Inst.
P.O. Box 27322
S-102 54 Stockholm, SWEDEN

Dr. Peter Marshall
Procurement Executive
Ministry of Defense
Blacknest, Brimpton
Reading FG7-FRS, UNITED KINGDOM

Dr. Bernard Massinon, Dr. Pierre Mechler
Societe Radiomana
27 rue Claude Bernard
75005 Paris, FRANCE (2 Copies)

Dr. Svein Mykkeltveit
NTNT/NORSAR
P.O. Box 51
N-2007 Kjeller, NORWAY (3 Copies)

Prof. Keith Priestley
University of Cambridge
Bullard Labs, Dept. of Earth Sciences
Madingley Rise, Madingley Road
Cambridge CB3 OEZ, ENGLAND